

# **Functional development of prefrontal- hippocampal networks in mouse models of neuropsychiatric disorders**

## **DISSERTATION**

with the aim of achieving a doctoral degree (Dr. rer. nat.)  
at the Faculty of Mathematics, Informatics and Natural Sciences  
Department of Biology  
University of Hamburg

Submitted by

**Marilena Hnida**

(born in Stade, Germany)

2024

Hamburg, Germany

This work has been carried out at the Institute of Developmental Neurophysiology, Center for Molecular Neurobiology Hamburg (ZMNH), University Medical Center Hamburg-Eppendorf (UKE).

Director: Prof. Dr. Ileana L. Hanganu-Opatz

**Date of disputation:** 12.07.2024

**First evaluator: Prof. Dr. Ileana L. Hanganu-Opatz**

Institute of Developmental Neurophysiology

Center for Molecular Neurobiology Hamburg (ZMNH)

University Medical Center Hamburg-Eppendorf (UKE)

**Second evaluator: Prof. Dr. Thomas G. Oertner**

Institute of Synaptic Physiology

Center for Molecular Neurobiology Hamburg (ZMNH)

University Medical Center Hamburg-Eppendorf (UKE)

**Chair of examination committee: Prof. Dr. Christian Lohr**

Neurophysiology - Institute of Cell and Systems Biology of Animals

Department of Biology - Faculty of Mathematics, Informatics and Natural Sciences

University of Hamburg

**Examination committee member: Dr. Esther Diekhof**

Neuroendocrinology - Institute of Cell and Systems Biology of Animals

Department of Biology - Faculty of Mathematics, Informatics and Natural Sciences

University of Hamburg

## **Eidesstattliche Versicherung / Declaration on oath**

### **Eidesstattliche Versicherung**

Hiermit erkläre ich, Marilena Hnida, an Eides statt, dass ich die vorliegende Dissertationsschrift selbst verfasst und keine anderen als die angegebenen Quellen und Hilfsmittel benutzt habe.

---

Ort, Datum

---

Unterschrift

### **Declaration on oath**

I, Marilena Hnida, hereby declare on oath that I wrote the present dissertation myself and used no other resources and aids than those listed.

---

City, Date

---

Signature

# Contents

|  |             |
|--|-------------|
| <b>Eidesstattliche Versicherung / Declaration on oath .....</b>  | <b>i</b>    |
| <b>Contents.....</b>   | <b>ii</b>   |
| <b>Summary .....</b>   | <b>iv</b>   |
| <b>Zusammenfassung.....</b>  | <b>vi</b>   |
| <b>Abbreviations.....</b>  | <b>viii</b> |
| <b>1 Introduction .....</b>  | <b>1</b>    |
| 1.1 Prefrontal cortex and its network interactions with the hippocampus .....  | 1           |
| 1.1.1 Anatomy of the prefrontal cortex .....   | 1           |
| 1.1.2 Prefrontal-hippocampal communication .....   | 4           |
| 1.1.3 Oscillatory activity in the prefrontal-hippocampal network .....   | 5           |
| 1.1.4 Functional development of the prefrontal cortex and the prefrontal-hippocampal network.....                    | 7           |
| 1.2 Neurodevelopmental disorders through the example of schizophrenia .....  | 10          |
| 1.2.1 Multiple-hit hypothesis .....  | 11          |
| 1.2.2 Cognitive dysfunctions and an underlying aberrant prefrontal-hippocampal network as fundamental symptoms ..... | 13          |
| 1.2.3 Adolescence is a vulnerable developmental period .....   | 15          |
| 1.3 Objectives and aims of the thesis .....  | 17          |
| <b>2 Methods .....</b>   | <b>19</b>   |
| 2.1 Experimental animals .....   | 19          |
| 2.2 Behavioral experiments with freely moving mice - Object recognition tasks .....                                  | 20          |
| 2.3 In vivo electrophysiology in anesthetized mice .....   | 21          |
| 2.3.1 Surgical procedure.....  | 21          |
| 2.3.2 Recording procedure .....  | 21          |
| 2.4 In vivo electrophysiology in awake mice .....  | 21          |
| 2.4.1 Surgical procedure.....  | 21          |
| 2.4.2 Recording procedure .....  | 22          |
| 2.5 Establishment of behavioral experiments with head-fixed mice – delayed non-match to sample T-Maze task.....      | 23          |
| 2.6 Histology .....  | 24          |
| 2.6.1 Perfusion.....   | 24          |
| 2.6.2 Immunohistochemistry .....   | 24          |
| 2.6.3 Imaging.....   | 25          |
| 2.6.4 Image analysis .....   | 25          |
| 2.7 Data analysis of electrophysiological recordings .....   | 26          |
| 2.7.1 Head-fixed movement and open-field behavior .....  | 26          |
| 2.7.2 LFP analysis .....   | 26          |
| 2.7.3 Spike analysis .....   | 28          |
| 2.8 Statistical analysis .....   | 29          |
| 2.8.1 Object recognition tasks .....   | 29          |
| 2.8.2 Microglia inclusions .....   | 29          |
| 2.8.3 Anesthetized electrophysiological recordings.....  | 29          |
| 2.8.4 Awake electrophysiological recordings .....  | 30          |
| <b>3 Results .....</b>   | <b>31</b>   |
| 3.1 Transient minocycline treatment in GE mice.....  | 31          |
| 3.1.1 Transient minocycline treatment in GE mice can rescue enhanced microglia function.....                         | 31          |
| 3.1.2 Transient minocycline treatment during later development cannot rescue abnormal recognition memory .....       | 33          |

---

|          |   |            |
|----------|---|------------|
| 3.2      | Prefrontal-hippocampal-entorhinal network activity during prejuvenile development in anesthetized dual-hit GE mice.....   | 36         |
| 3.2.1    | LFP and MUA in PFC, HP and LEC are not different in prejuvenile GE mice compared to WT mice.....  | 36         |
| 3.2.2    | Synchrony between prefrontal cortex and hippocampal formation is augmented in prejuvenile GE mice.....  | 38         |
| 3.3      | Establishment of delayed non-match to sample working memory task on the MobileHomeCage.....   | 40         |
| 3.4      | Prefrontal-hippocampal network activity patterns across late development in <i>Df(16)A<sup>+/-</sup></i> and WT mice.....   | 46         |
| 3.4.1    | <i>Df(16)A<sup>+/-</sup></i> mice show a similar weight increase to WT with implanted headplates.....   | 46         |
| 3.4.2    | <i>Df(16)A<sup>+/-</sup></i> mice show minor alterations in locomotor behavior.....   | 47         |
| 3.4.3    | Developmental trajectories of prefrontal local field potential are disturbed in <i>Df(16)A<sup>+/-</sup></i> mice.....  | 49         |
| 3.4.4    | Prefrontal spiking activity is altered in a behavioral state-dependent manner in adolescent <i>Df(16)A<sup>+/-</sup></i> mice.....  | 53         |
| 3.4.5    | Developmental trajectories of hippocampal theta power are abnormal in adolescent <i>Df(16)A<sup>+/-</sup></i> mice.....   | 58         |
| 3.4.6    | LFP-synchrony in <i>Df(16)A<sup>+/-</sup></i> mice is disturbed throughout and in late adolescence.....   | 61         |
| 3.4.7    | Synchronization of prefrontal and hippocampal units develops abnormally across adolescence in <i>Df(16)A<sup>+/-</sup></i> mice.....  | 64         |
| <b>4</b> | <b>Discussion.....</b>  | <b>68</b>  |
| 4.1      | Considerations of the dual-hit GE and the <i>Df(16)A<sup>+/-</sup></i> mouse models in schizophrenia research.....  | 69         |
| 4.2      | Rescue function of transient minocycline treatment in neonatal dual-hit GE mice.....  | 72         |
| 4.2.1    | Rescue of microglial function in the prefrontal cortex during neonatal development.....   | 72         |
| 4.2.2    | Partial rescue of recognition memory functions in prejuvenile dual-hit GE mice.....   | 73         |
| 4.3      | Prefrontal-hippocampal-entorhinal network activity in anesthetized prejuvenile dual-hit GE mice.....  | 76         |
| 4.4      | Establishment of awake head-fixed recordings on the MobileHomeCage in an open field movement paradigm and a working memory task.....  | 77         |
| 4.5      | Late developmental patterns of prefrontal-hippocampal network activity across adolescence in a 22q11.2 deletion syndrome mouse model.....   | 81         |
| 4.5.1    | Developmental trajectories of prefrontal-hippocampal network activity in the 22q11.2ds mouse model.....   | 81         |
| 4.5.2    | Translational considerations of disturbed prefrontal-hippocampal network communication throughout adolescence between the <i>Df(16)A<sup>+/-</sup></i> model and the 22q11.2 deletion syndrome..... | 88         |
| 4.6      | Concluding remarks and future directions.....   | 91         |
|          | <b>References.....</b>  | <b>95</b>  |
|          | <b>List of Figures.....</b>   | <b>111</b> |
|          | <b>List of Tables.....</b>  | <b>112</b> |
|          | <b>Appendix.....</b>  | <b>113</b> |
|          | List of materials, equipment and software.....  | 113        |
|          | Detailed statistics for Results 3.4.....  | 115        |
|          | List of Publications.....   | 121        |
|          | <b>Acknowledgements.....</b>  | <b>122</b> |

---

## Summary

Neurons in our brain are organized in functional networks, giving rise to synchronized oscillatory activity, enabling flexible and efficient information processing and communication between brain areas. The development of these networks is influenced by early life patterns of neuronal activity. Perturbations in the development of these patterns have been put in context with mental disorders, giving them the epithet neurodevelopmental disorders. A core symptom of these disorders is dysfunctions in cognition. Cognitive abilities emerge and mature during the late developmental period of adolescence. These abilities rely on functional local and long-range networks of the prefrontal cortex (PFC). The PFC shows a prolonged period of development and matures in parallel with cognitive abilities during adolescence. Although several studies have placed the PFC in context with neurodevelopmental disorders, in-depth insight into the developmental trajectories of the prefrontal networks, especially in their connectivity with the hippocampus (HP), is still lacking. The HP is already a main input area to the PFC during early development and this network is involved in various cognitive functions, including memory processing. Therefore, the work presented in this thesis aimed to identify and analyze underlying mechanisms of prefrontal development in the context of neurodevelopmental disorders, with a focus on connectivity with the HP and emphasis on late development.

In a first step, a dual-hit mouse model, combining a genetic and an environmental risk factor (GE), was utilized. Histological investigation showed that microglia already play a key role in the perturbations in the PFC in early development. These detrimental effects could be rescued through microglial inhibition of antibiotic minocycline during a very specific time window of neonatal development. The neonatal period in rodents roughly translates to the second to third trimester of gestation in humans. Later administration of minocycline did not lead to similar rescue properties. In addition, it had no beneficial effect on object recognition tasks, which are behavioral abilities depending on prefrontal-hippocampal-entorhinal interactions in prejuvenile development.

An electrophysiological investigation of this network during prejuvenile age in anesthetized mice revealed a hypersynchronization of prefrontal-entorhinal and prefrontal-hippocampal interactions in the dual-hit GE mice. As these perturbations were different from those observed at neonatal age, it can be argued that the prejuvenile period in rodents, roughly translating to early childhood in humans, is also critical for the maturation of cognitive abilities.

To deepen the investigation in this direction, further electrophysiological investigations of the prefrontal-hippocampal network were to be performed in awake mice. To this end, a recording method on a movable underground, the MobileHomeCage, was established based on a previously published protocol. This method allowed for investigation of innate behaviors in an open field, but the implementation of a complex working memory task relying on learned and rewarded behavior was not possible.

The established method allowed for electrophysiological recordings during voluntary movement and resting periods in the prefrontal-hippocampal network across adolescent development. These investigations were carried out in a genetic 22q11.2 deletion syndrome (ds)

---

mouse model (*Df(16)A<sup>+/-</sup>*), with a similar etiology to late onset neurodevelopmental disorders, such as schizophrenia. The prefrontal gamma rhythm developed abnormally in the *Df(16)A<sup>+/-</sup>* mice, alongside perturbed firing synchronies of pyramidal neurons and PV interneurons in a behavioral state-dependent manner. This implies an abnormal fine-tuning of the excitation/inhibition balance in the local prefrontal circuits. Similarly, the hippocampal theta rhythm, which synchronizes PFC and HP during working memory tasks, developed abnormally in the *Df(16)A<sup>+/-</sup>* mice. This disturbed hippocampal theta rhythm could have implications for network synchronization. Here, it was shown that the precise timing of prefrontal pyramidal neurons as well as PV interneurons to hippocampal spike timing matured in a perturbed, behaviorally state-dependent manner. This could imply that prefrontal spikes are interacting with hippocampal firing, but that the modulation of prefrontal oscillatory rhythms cannot be generated in the same way as in healthy development. These results suggest that the imprecise timing of firing, the less coherent oscillatory rhythm and the abnormal prefrontal gamma rhythm might be underlying causes of the insufficient maturation of cognitive abilities in 22q11.2ds mouse models and possibly patients.

Together, the findings presented in this thesis provide a contribution to the identification of mechanisms and time windows for possible biomarkers or interventions in neurodevelopmental disorders already before and especially during adolescence. Adolescence is a period of refinement and fine-tuning of preset circuits, and the disturbances seen in this time are less prominent than those observed during the neonatal period. However, adolescence is a vulnerable time of development. Hence, elucidating mechanisms and dysfunctions of prefrontal networks during later maturation is critical for a more profound understanding of neurodevelopmental disorders. Even though several open questions remain, the work presented here establishes a foundation for follow-up research. It potentially opens up pathways for investigations into early identification of neurodevelopmental disorders and intervention strategies on specific mechanisms, precisely-timed during development.

## Zusammenfassung

Neurone sind in unserem Gehirn in funktionalen Netzwerken organisiert, die das Entstehen synchronisierter Oszillationen ermöglichen, welche wiederum eine flexible und effiziente Informationsverarbeitung und Kommunikation zwischen Gehirnbereichen bedingen. Die Entwicklung dieser Netzwerke wird bereits im frühen Leben durch Muster neuronaler Aktivität beeinflusst. Nachteilige Beeinträchtigungen in der Ausbildung dieser Muster werden mit bestimmten psychiatrischen Erkrankungen, auch als neurologische Entwicklungsstörungen bezeichnet, in Verbindung gebracht. Ein Kernsymptom dieser Erkrankungen sind Fehlfunktionen in der Kognition. Kognitive Fähigkeiten reifen während der späteren Entwicklung vom Kindesalter über die Adoleszenz zum Erwachsenenalter und beruhen auf funktionalen lokalen und weitreichenden Netzwerken des präfrontalen Kortex (PFC). Der PFC weist im Vergleich zu sensorischen und subkortikalen Gehirnarealen eine verzögerte Entwicklung auf und reift parallel zu den kognitiven Fähigkeiten erst während der Adoleszenz vollständig. Obwohl der PFC oft in Zusammenhang mit neurologischen Entwicklungsstörungen gebracht wurde, liegt noch keine vollständige Aufklärung der Entwicklungsverläufe der präfrontalen Netzwerke, insbesondere in Bezug auf die Konnektivität mit dem Hippokampus (HP), vor. Der HP zeigt bereits in der frühen Entwicklung Projektionen zum PFC und treibt diesen an. Das präfrontale-hippokampale Netzwerk ist an verschiedenen kognitiven Funktionen, wie z.B. der Gedächtnisverarbeitung, beteiligt. Die in dieser Dissertation vorgestellte Arbeit zielte darauf ab, die zugrundeliegenden Mechanismen der präfrontalen Entwicklung hinsichtlich neurologischer Entwicklungsstörungen zu untersuchen, mit einem Schwerpunkt auf der Konnektivität mit dem HP und der späten Entwicklung.

In einem ersten Schritt wird ein ‚*dual-hit*‘ Mausmodell verwendet, das einen genetischen (‚*genetic*‘ (G)) und einen umweltbedingten (‚*environmental*‘, (E)) Risikofaktor (GE) kombiniert. Histologische Untersuchungen zeigten, dass Mikroglia bereits in der frühen Entwicklung eine Schlüsselrolle bei den Störungen im präfrontalen Kortex spielen. Diese schädlichen Effekte konnten durch eine Verabreichung des mikrogliahemmenden Antibiotikum Minocyclin während eines bestimmten Zeitfensters der neonatalen Entwicklung behoben werden. Eine spätere Verabreichung von Minocyclin zeigte keine ähnlichen Anzeichen einer Wiederherstellung der normalen Entwicklung des präfrontalen Kortex. Ebenso hatte die spätere Verabreichung keine positive Wirkung auf Objekterkennungsaufgaben in präjuvenilen Tieren. Diese testen Verhaltensfähigkeiten, die von präfrontalen-hippokampalen-entorhinalen Interaktionen abhängen.

Elektrophysiologische Untersuchungen dieses Netzwerks im präjuvenilen Alter an anästhesierten Mäusen ergab eine Hypersynchronisation der präfrontal-entorhinalen und präfrontal-hippocampalen Interaktionen bei den ‚*dual-hit*‘ GE-Mäusen in dieser Entwicklungsphase. Da sich diese Störungen von denen im Neugeborenenalter unterscheiden, wird argumentiert, dass die präjuvenile Phase in Mäusen, welche im Menschen grob der Kindheit (ca. 2-7 Jahre) entspricht, zusätzlich entscheidend für die Reifung der kognitiven Fähigkeiten ist.

Um die Untersuchungen in dieser Richtung zu vertiefen, wurden weitere elektrophysiologische Analysen des präfrontalen-hippokampalen Netzwerks bei wachen Mäusen durchgeführt. Dafür

---

wurde auf Basis eines zuvor veröffentlichten Protokolls eine Aufnahmemethode auf einem beweglichen Untergrund, dem MobileHomeCage, etabliert. Diese Methode ermöglichte die Untersuchung angeborener Verhaltensweisen im ‚Open-Field‘. Die Umsetzung einer komplexen Arbeitsgedächtnisaufgabe, die auf erlerntem und belohntem Verhalten beruhte, war jedoch nicht möglich.

Diese kopffixierte Methode ermöglichte elektrophysiologische Aufnahmen oszillatorischer Aktivität während Bewegungen und in Ruhephasen im präfrontal-hippokampalen Netzwerk über die gesamte adoleszente Entwicklung. Die folgenden Untersuchungen wurden in einem genetischen Deletionssyndrom (DS) 22q11.2 -Mausmodell (*Df(16)A<sup>+/-</sup>*) durchgeführt. Das DS 22q11.2 weist einen hohen genetischen Risikofaktor für Schizophrenie auf, wodurch sich dieses Modell besser auf diese spät einsetzende Erkrankung bezieht. Der präfrontale Gammarrhythmus entwickelte sich bei *Df(16)A<sup>+/-</sup>*-Mäusen abnormal, zusammen mit gestörten Synchronisationen des Feuerrhythmus der Neurone in einer vom Verhaltenszustand abhängigen Weise. Dies impliziert eine gestörte Feinabstimmung des exzitatorischen/inhibitorischen Gleichgewichts im präfrontalen lokalen Netzwerk. In ähnlicher Weise entwickelte sich der hippocampale Thetarhythmus, der PFC und HP während Arbeitsgedächtnisaufgaben synchronisiert, bei *Df(16)A<sup>+/-</sup>*-Mäusen anders als in gesunden Tieren. Dieser gestörte Rhythmus könnte Auswirkungen auf die Netzwerksynchronisation haben. Bezüglich dieser wurde gezeigt, dass das genaue Timing des Feuerns präfrontaler pyramidal Neurone, sowie parvalbumin-exprimierender Interneurone zum Feuerrhythmus hippocampaler Neurone in einer vom Verhaltenszustand abhängigen Weise gestört reifte. Dies könnte darauf hindeuten, dass die präfrontalen Neurone mit dem Feuern der hippocampalen Neurone zwar interagieren, die kohärenten Oszillationsrhythmen jedoch nicht auf die gleiche Weise wie bei einer gesunden Entwicklung erzeugt werden können. Diese Ergebnisse legen nahe, dass der ungenaue Zeitpunkt des Feuerns der präfrontalen und hippocampalen Neurone, der weniger kohärente Oszillationsrhythmus und der abnormale präfrontale Gammarrhythmus die Ursachen für die unzureichende Reifung der kognitiven Fähigkeiten in DS 22q11.2-Mausmodellen und möglicherweise auch bei Patienten neurologischer Entwicklungsstörungen sein könnten.

Die in dieser Arbeit präsentierten Erkenntnisse leisten einen Beitrag zur Identifizierung von Mechanismen und Zeitfenstern für mögliche Biomarker oder Interventionen bei neurologischen Entwicklungsstörungen vor und während der Adoleszenz. Die Adoleszenz ist eine Zeit der Verfeinerung und Feinabstimmungen voreingestellter Schaltkreise im Gehirn und insbesondere im präfrontalen Kortex. Die in dieser Zeit observierten entwicklungsbedingten Veränderungen und Störungen in den präfrontalen Netzwerken sind weniger stark ausgeprägt als die in der neonatalen Entwicklung stattfindenden. Dennoch ist die Adoleszenz eine anfällige Zeit der Entwicklung, und die Aufklärung der Mechanismen und Funktionsstörungen präfrontaler Netzwerke während dieser ist für ein besseres Verständnis neurologischer Entwicklungsstörungen von entscheidender Bedeutung. Trotz weiterhin bestehender offener Fragen, bildet die hier vorgestellte Arbeit eine Grundlage für die Folgeforschung und könnte zukünftige Arbeiten zu Identifikationsmethoden neurologischer Entwicklungserkrankungen und Interventionsstrategien, die gezielt auf spezielle Mechanismen und Zeitpunkte abgestimmt sind, ermöglichen.

## Abbreviations

|           |  |          |  |
|-----------|--|----------|--|
| 22q11.2ds | 22q11.2 deletion syndrome                                    | LEC      | lateral entorhinal cortex                    |
| 5HT3aR    | 5-hydroxytryptamine 3a receptor                              | LFP      | local field potential                        |
| ACC       | anterior cingulate cortex                                    | LME      | linear mixed-effect model                    |
| ADHD      | attention deficit hyperactivity disorders                    | MEC      | medial entorhinal cortex                     |
| AMPA      | $\alpha$ -amino-3-hydroxy-5-methyl-4-isoxazolepropionic acid | MIA      | maternal immune activation                   |
| ASD       | autism spectrum disorders                                    | mino     | minocycline                                  |
| CA1       | cornu ammonis 1  | MUA      | multi-unit activity                          |
| dCA1      | dorsal cornu ammonis 1                                       | NMDA     | N-Methyl-D-aspartic acid                     |
| DG        | dentate gyrus  | NOR      | novel object recognition task                |
| Disc1     | <i>disrupted-in-schizophrenia 1</i>                          | NR       | nucleus reuniens                             |
| DNMS      | delayed non-match to sample                                  | OB       | olfactory bulb                               |
| DR        | discrimination ratio   | P        | postnatal day                                |
| E         | embryonic  | PAC      | phase-amplitude coupling                     |
| early ado | early adolescent   | (m)PFC   | (medial) prefrontal cortex                   |
| EC        | entorhinal cortex  | PL       | prelimbic area                               |
| EE        | environmental enrichment                                     | poly I:C | polyinosinic:polycytidylic acid              |
| EEG       | electroencephalogram   | PPC      | pairwise phase consistency                   |
| eSPW      | early sharp waves complexes                                  | PSD      | power spectral density                       |
| fMRI      | functional magnetic resonance imaging                        | PT       | pyramidal tract neurons                      |
| FR        | firing rate  | PV       | parvalbumin                                  |
| Fs        | fast spiking   | RR       | recency recognition task                     |
| GABA      | $\gamma$ -Aminobutyric acid                                  | Rs       | regular spiking                              |
| GDD       | global developmental delay                                   | SDR      | spectral dependency ratio                    |
| GDPs      | giant depolarizing potentials                                | SOM      | somatostatin                                 |
| GE        | genetic-environmental  | SPAs     | synchronous plateau assemblies               |
| HP        | hippocampus  | SPW      | sharp waves                                  |
| i/vCA1    | intermediate/ventral cornu ammonis 1                         | STTC     | spike time tiling coefficient                |
| IBA-1     | ionized calcium binding adaptor molecule 1                   | SUA      | single-unit activity                         |
| IL        | infralimbic area   | VGLUT1   | vesicular glutamate transporter 1            |
| ISI       | inter-spike interval   | VIP      | vasoactive intestinal polypeptide-expressing |
| IT        | intratelencephalic neurons                                   | VMT      | ventromedial thalamus                        |
| late ado  | late adolescent  | WT       | wildtype, controls                           |

# 1 Introduction

The ancient Greek physician Hippocrates already considered the brain particularly significant as the key to our emotions, thoughts, and behavior (Walshe, 2016). Today, we know that the brain serves as a control center within our body. It receives, stores and processes sensory inputs from our environment and coordinates an adequate response (Thiebaut de Schotten and Forkel, 2022). This complex function is enabled by the organization of neurons into functional networks (Engel et al., 2001; Fries, 2015). The coordinated neuronal activity gives rise to synchronized oscillations, which in turn enable and support flexible and efficient information processing between brain areas (Buzsáki et al., 2012; Buzsáki and Draguhn, 2004; Buzsáki and Watson, 2012). These activity patterns already arise during early life stages and a disruption of their development can result in tremendous changes and abnormalities later in life, such as mental disorders (Chini and Hanganu-Opatz, 2021). A fundamental symptom of these disorders is dysfunctions in cognition. Cognitive abilities rely on healthy and functional networks of the prefrontal cortex, the brain area involved in many higher-order processes (Miller, 2000; Miller and Cohen, 2001).

## 1.1 Prefrontal cortex and its network interactions with the hippocampus

### 1.1.1 *Anatomy of the prefrontal cortex*

The prefrontal cortex (PFC) is considered a hub of cognitive processing (Miller and Cohen, 2001). It is one of the most advanced brain areas, being involved in numerous higher functions such as attention, flexibility, social interactions, language production and working memory (Miller, 2000). Within the brain, the PFC is located in the frontal lobe. In the evolutionary viewpoint it is one of the last brain regions to develop (Fuster, 2001). It is highly interconnected with several other brain areas including other cortical regions but also subcortical structures and notably the limbic formation (Fuster, 2001). Over the course of the past century, the PFC has been anatomically defined in various ways, all of which has been deemed problematic in some regard. In 1890, David Ferrier defined the PFC as the brain area which does not evoke movement when electrically stimulated (Ferrier, 1890). However, in this definition the PFC includes structurally dissimilar brain areas, comprising granular and non-granular ones (Preuss, 1995). The presence of the cortical granular layer 4 is the basis for a second definition of the PFC. It is used to distinguish between the granular prefrontal areas and the agranular motor and premotor areas (Preuss, 1995). This definition is problematic because it only holds true for primates, as other mammals lack a granular layer 4 in the frontal areas. Despite the fact that higher cognitive abilities are exclusively restricted to humans and non-human primates, some cognitive abilities, such as attention and working memory, are also present in other mammals (Carlén, 2017; Fuster, 2000). Additionally, the Brodmann areas comprising the PFC include some non-granular areas (Uylings et al., 2003). The third and newest theory defining the PFC

---

relies on it being the projection zone of the mediodorsal nucleus (MD) of the thalamus (Rose and Woolsey, 1948). In an updated version, the PFC is defined as the brain area showing the strongest interconnectivity with this thalamic nucleus (Uylings et al., 2003). This definition allows the identification of homologous areas of the granular brain region of primates in other mammals, including rodents (Uylings et al., 2003). Even though the cerebral cortex of primates, and especially of humans, is magnitudes larger than that of rodents, it has been argued that rats and mice also possess a PFC (Carlén, 2017; Preuss, 1995; Preuss and Wise, 2022; Uylings et al., 2003). The primate PFC is commonly divided into the dorsolateral, dorsomedial, ventromedial and orbital prefrontal cortex. In rodents, the PFC consists of fewer subdivisions, which are agranular and therefore argued to be more primitive, than the granular cortex of primates (Preuss and Wise, 2022). One division of rodent PFC is the medial prefrontal cortex (mPFC) which is roughly homologous to the dorsolateral prefrontal cortex in primates and subdivided into the infralimbic (IL) area, prelimbic (PL) area and anterior cingulate cortex (ACC) (Carlén, 2017; Van De Werd et al., 2010). The present thesis focuses mostly on the PL of the mPFC.

The mPFC in rodents is organized in a laminar structure and consists of the layers 1, 2/3 (superficial layers) and 5/6 (deep layers). The PFC follows an inside-out migration pattern during development, with early-born neurons forming the deep layers and late-born neurons forming the superficial layers (Nadarajah and Parnavelas, 2002). In sensory areas, layer 4 is the typical input layer from the thalamus. The mPFC receives inputs from subcortical regions in layers 2/3 as well as in layers 5/6, forms local circuits and propagates the signals within the PFC and to other brain structures (Anastasiades and Carter, 2021). Local microcircuits in the PFC are formed between pyramidal neurons and interneurons (Anastasiades and Carter, 2021). Pyramidal neurons, also termed principal cells, are glutamatergic excitatory projection neurons and make up approximately 80 % of the cortical neurons (Han and Sestan, 2013). Pyramidal neurons constitute the main output system of the cortex and the largest input system (Han and Sestan, 2013). In contrast, inhibitory interneurons only make up roughly 20 % of cortical neurons and comprise the backbone of local circuitry (Harris and Shepherd, 2015). Excitatory neurons of the cortex have been classified into three classes based on their axonal projection patterns (Harris and Shepherd, 2015). One class comprises the intratelencephalic (IT) neurons, found in layers 2 to 6, which only project to structures within the telencephalon as well as to the contralateral cortex. Another class consists of the pyramidal tract neurons (PT), which are located in layer 5B and project to subcortical structures, such as the brainstem, midbrain and spinal cord. The corticothalamic neurons make up the third class. Those are located in layer 6, and primarily project to the ipsilateral thalamus (Harris and Shepherd, 2015).

The  $\gamma$ -Aminobutyric acid (GABA)ergic interneurons are divided into several subtypes with diverse phenotypes, with three main subclasses based on their expression of specific molecular markers. These are the parvalbumin (PV), the somatostatin (SOM) and the 5-hydroxytryptamine 3a receptor (5HT3aR)-expressing interneurons (Harris and Shepherd, 2015). In addition, a major subpopulation of the 5HT3aR interneurons is the vasoactive intestinal polypeptide (VIP)-expressing interneurons. These subclasses each show specific morphological properties, partially overlapping between subclasses, with which they target distinct regions of pyramidal neurons (Benes and Berretta, 2001). SOM and PV interneurons mostly target dendrites of

---

excitatory neurons, with SOM and PV basket cells primarily targeting apical dendrites close to the soma and therefore showing potent inhibition of excitatory neurons. Regarding excitatory neurons, VIP interneurons preferentially target basal dendrites and side branches of apical dendrites. However, they mostly target interneurons and are therefore involved in disinhibitory circuits (Benes and Berretta, 2001; Harris and Shepherd, 2015). All classes of interneurons receive intrinsic excitatory input from cortical pyramidal neurons. However, the thalamus also provides extrinsic excitatory input. The thalamic input mainly targets the fast-spiking PV interneurons (Benes and Berretta, 2001; Harris and Shepherd, 2015). This interplay between excitatory and inhibitory neurons leads to the formation of complex circuits, with the interneurons being involved in feedback and feedforward inhibitory mechanisms, which stabilize the activity of excitatory neurons. In the feedback circuit, an activated excitatory neuron activates an interneuron, which in turn inhibits excitatory neurons including those that activated it. In a feedforward inhibitory system, an extrinsic excitatory input activates local excitatory neurons, but also targets interneurons, which in turn inhibit the local excitatory neurons (Benes and Berretta, 2001; Harris and Shepherd, 2015).

In addition to the neuronal cell classes, the brain also encompasses non-neuronal cells, the glia cells. The main types of glia cells are oligodendrocytes, astrocytes, ependymal cells and microglia (Fields et al., 2014). Microglia are the macrophages of the brain and are involved in removing pathogens and apoptosis (Mosser et al., 2017). Microglia can exist in different activation states with associated morphological traits. Ramified microglia monitor their surroundings in the brain for potential danger signals. In their amoeboid state, microglial cells are phagocytically active (Crews and Vetreno, 2016; Mosser et al., 2017). Microglia activity is controlled by ‘on’ and ‘off’ signals. Appearance of ‘on’ signals as well as disappearance of ‘off’ signals can trigger an immediate microglial activation (Biber et al., 2007). Activated microglia act through phagocytosis, removing apoptotic cells, nonfunctional structures and toxic cellular waste (Biber et al., 2007). Abnormal functioning in microglia can cause reductions in gray matter, spine density and dendritic branching and be neurotoxic (Howes and McCutcheon, 2017). In addition to their functions as part of the immune system of the brain, microglial cells also shape neuronal circuits. Neurons release various ‘on’ and ‘off’ signals and hence can actively trigger microglial activity. In addition, microglia can sense neuronal activity and maintain brain homeostasis through dynamic interaction with the neurons. During development, microglial cells interact with various other cell types. They phagocytose neurons as well as neuronal and oligodendrocyte precursors, thereby shaping neuronal circuits and influencing myelination. Furthermore, they are active on smaller scales and refine and sculpt existing circuits through synaptic pruning (Mehl et al., 2022). In the adult brain, microglial cells modulate neuronal activity, neurogenesis and synaptic plasticity (Biber et al., 2007; Zhao et al., 2024). For example, they eliminate synapses between neurons showing asynchronous activity, thereby shaping neuronal circuits in the PFC, among other regions (Hammond et al., 2018). This modulation also affects widespread networks, which is of particular significance given the extensive connections the PFC has with other brain regions, including the hippocampus.

### *1.1.2 Prefrontal-hippocampal communication*

In addition to being one of the most advanced brain areas, the PFC is highly interconnected with almost all neocortical areas but also with subcortical structures such as the amygdala, claustrum, hippocampus (HP) and thalamus (Miller, 2000; Miller and Cohen, 2001). Most connectivity of the PFC is reciprocal and pyramidal neurons of the PFC project back to the contralateral PFC, amygdala, claustrum and thalamus (Anastasiades et al., 2019; Collins et al., 2018; McGarry and Carter, 2017). The connectivity within the PFC is organized layer-wise. The MD projects to the superficial layers 2/3 and the deep layers 5/6, but with a significant bias towards the superficial layers (Anastasiades and Carter, 2021). The superficial layers of PFC in turn project to the deep layers, constituting the main output region of the PFC (Anastasiades and Carter, 2021).

In addition, the deep layers receive strong input from monosynaptic projections from the hippocampal area cornu ammonis 1 (CA1) (Ferino et al., 1987; Jay and Witter, 1991). The HP, which received its name from the seahorse-shape it takes in humans and non-human primates, is a subcortical brain structure within the medial temporal lobe. The main functions of the HP include memory and spatial processing (Sigurdsson and Duvarci, 2016). It comprises the four areas of the cornu ammonis (CA1-4), the dentate gyrus (DG) and the subiculum (Amaral and Witter, 1989). Most cortical projections from the HP originate in the CA1. In contrast to the dense projections from CA1 to the mPFC, there are only very sparse excitatory projections from the ACC to the HP (Rajasethupathy et al., 2015). Due to its numerous bidirectional connections, it is postulated that the PFC functions as a top-down control hub. This means that the PFC monitors and gates behavior and brain activity (Miller, 2000; Miller and Cohen, 2001). Regarding the HP, top-down control is exerted via indirect pathways, crossing the entorhinal cortex (EC), or most prominently the Nucleus reuniens (NR) of the thalamus and via direct long-range GABAergic projections, which inhibit disinhibitory microcircuits within the HP (Malik et al., 2022; Xu and Südhof, 2013).

In its interplay, the prefrontal-hippocampal network is involved in various cognitive functions (Sigurdsson and Duvarci, 2016). In humans, it has been shown that this network is active during contextual information processing, in a fear extinction paradigm and spatial working memory tasks (Bähner et al., 2015; Eichenbaum, 2017). Studies in rodents have shown a contribution of the network in similar domains, namely reward learning, anxiety and avoidance as well as working memory (Godsil et al., 2013). The CA1 of the HP can be further divided along the dorsal-ventral axis, into a dorsal hippocampal part (dCA1) and an intermediate/ventral part (i/vCA1). Both of these demonstrate distinct functional relevance in relation to the PFC, with the dCA1 being more involved in spatial coding and object location, whereas the i/vCA1 is involved in context representation. In contrast to the dCA1, the i/vCA1 has monosynaptic projections to the mPFC areas, including the PL (Ghoshal and Conn, 2015; Wirt and Hyman, 2017). The prominent flow of information in this network is directed from the HP to the PFC via monosynaptic projections from i/vCA1 but also via polysynaptic connections from dCA1 over the i/vCA1 or NR (Hallock et al., 2016; O'Neill et al., 2013). For a spatial working memory task it was shown that the dCA1 synchronizes with the mPFC, but the i/vCA1 is essential for the synchronization of these areas (O'Neill et al., 2013).

One main input-output area of the HP is the EC. In humans it consists of the anterior-lateral and posterior-medial subregions. In rodents the EC is usually divided into the lateral entorhinal cortex (LEC) and the medial entorhinal cortex (MEC) (Witter et al., 2000). The EC is considered a relay station between the hippocampal formation and the cortex (Fyhn et al., 2004). The MEC is involved in spatial navigation and includes grid and head-direction cells in its neuronal build. In contrast, the LEC receives sensory information through the perirhinal cortex as well as the olfactory bulb (OB) and is critical for decoding context and temporal information in associative recognition memory and stimulus features (Dickerson and Eichenbaum, 2010). Layers 2/3 of the LEC project to all subregions of the HP, with strong connectivity to the CA1 region. CA1 receives direct projections from the LEC, but also indirect projections via DG, which projects mossy fibers to CA3, which in turn projects via the Schaffer collaterals to pyramidal neurons of CA1 (van Strien et al., 2009). Besides the excitatory pathways, the LEC also shows long-range inhibitory connections with CA1, which inhibit inhibitory microcircuits, thereby disinhibiting excitatory CA1 neurons (Basu et al., 2016). The LEC receives input from CA1 via layer 5, which is forwarded to its layers 2/3 (van Strien et al., 2009). Layer 2 of the LEC projects to the deep layers (5/6) of the PFC (Agster and Burwell, 2009; Jones and Witter, 2007).

The anatomical connectivity of the three areas can have implications for the communication between these brain areas. The interconnectivity of the areas functionally results in network communication through coherent oscillatory rhythms (Fries, 2015).

### *1.1.3 Oscillatory activity in the prefrontal-hippocampal network*

The primary electrical active cells of the brain, the neurons, are organized in an infinite number of networks. The coordinated and synchronized activity arising from these networks, the oscillations, are fundamental for information processing within and between brain areas. This information flow underlies higher cognitive abilities (Buzsáki et al., 2012; Buzsáki and Draguhn, 2004; Buzsáki and Watson, 2012).

Oscillatory brain activity is dependent on the timed interplay between inhibitory interneurons and excitatory pyramidal neurons (Cardin, 2016). The inhibitory input onto other interneurons or excitatory neurons alters the excitability. This can result in excitatory input onto target neurons, which can then in turn either propagate inhibitory or excitatory signals (Buzsáki and Draguhn, 2004; Buzsáki et al., 2013). The changes in these excitatory and inhibitory signals induce voltage fluctuations in the brain. These voltage fluctuations can be measured with non-invasive and invasive methods. A non-invasive method is the electroencephalogram (EEG), which is recorded on top of the skull and often used in humans. A more invasive method is the electrocorticogram, with electrodes placed on the cortex. For recordings of the local field potential (LFP), electrodes are placed in the brain tissue in close proximity to the oscillatory active cells (Buzsáki et al., 2012).

Oscillatory brain activity occurs in various rhythms. In the prefrontal-hippocampal network three rhythms are of special interest. These are the slow theta rhythm, the fast gamma rhythm and the sharp waves-ripples complexes (SPWRs) (Buzsáki et al., 1983). Slow rhythms arise

---

from large networks and can therefore coordinate neuronal activity across long distances and brain areas. Theta rhythms mainly occur during active exploration and rapid eye movement (REM) sleep (Buzsáki, 2002). It has been proposed that they modulate synaptic strength and are involved in the spatio-temporal encoding of memory engrams. One core generator of theta rhythms is the medial septum (MS) (Buzsáki, 2002). Inhibitory neurons located in the MS project to inhibitory neurons in hippocampal areas, thereby disinhibiting them, leading to the generation of theta oscillations (Freund and Antal, 1988; Robinson et al., 2016). However, it has been proposed, that the HP can facilitate theta rhythms intrinsically in the absence of the MS, suggesting the presence of several types of theta rhythm in the HP (Goutagny et al., 2009). Theta rhythms can also be observed in the EC and PFC. However, the PFC does not generate them intrinsically (Buzsáki, 2002). The delay of signal transmission from the monosynaptic projections from i/vCA1 to the mPFC, as well as from the polysynaptic projections from dCA1, are short enough to fit into a single theta cycle (Colgin, 2011). Various studies have reported a coherent theta rhythm in the HP and PFC when both are recorded simultaneously (Adhikari et al., 2010; Jones and Wilson, 2005; O'Neill et al., 2013). Taking this together, the theta rhythm is capable of coordinating direct interactions between the two brain areas. Likewise, the hippocampal theta rhythm influences prefrontal activity through two additional mechanisms, namely the entrainment of prefrontal spike timing and the modulation of prefrontal gamma activity. It has been shown that around 40% of prefrontal neurons are active phase-locked to the hippocampal theta rhythm and that this synchrony is important for spatial navigation and working memory (Siapas et al., 2005). The modulation of prefrontal gamma activity through hippocampal theta rhythm is an example of a cross-frequency coupling (Sirota et al., 2008). One other one can be found between the HP and LEC. The oscillatory coupling at ~20-40 Hz and phase-locking of LEC and CA1 neurons to a ~20-40 Hz rhythm is proposed to involve components of theta and slow gamma and is needed for memory function (Colgin et al., 2009).

The fast gamma oscillations are put into context with rhythms evoked by locally synchronized networks (Buzsáki and Wang, 2012). Gamma oscillations are often transmitted via cross-frequency coupling (Buzsáki and Wang, 2012). However, gamma oscillations can be transmitted directly via long-range GABAergic interneurons or via fast conducting excitatory neurons (Buzsáki et al., 2013; Melzer and Monyer, 2020). The prefrontal gamma rhythm might be coupled with hippocampal gamma rhythm as well as with LEC gamma rhythm. This information flow across the three areas might be related to underlying information processing related to external environments (Hafting et al., 2005).

Sharp waves (SPW) are large amplitude events occurring in the HP during sleep and immobility (Buzsáki, 1986). They typically last about 40-100 ms and are often accompanied by high-frequency ripple events (100-250 Hz). SPW are generated by a synchronous discharge of neurons in the CA3 that causes a depolarization in the CA1 via Schaffer collaterals. At the same time, CA1 pyramidal and interneurons are activated simultaneously, resulting in the high-frequency ripple (Buzsáki, 2015; Buzsáki and Silva, 2012). In the PFC, sleep spindles and increased firing rates have been observed shortly after SPW (Mölle et al., 2006; Siapas and Wilson, 1998). This mechanism is hypothesized to be critical for transfer of short-term memory from the HP to long-term storage in the cortex (Maingret et al., 2016; Wierzynski et al., 2009).

Oscillatory activity in the prefrontal-hippocampal network is essential for cognitive abilities in the adult brain. A synchronous network activity is already present in early development and shows perturbations in mouse models of neurodevelopmental disorders (Chini and Hanganu-Opatz, 2021).

### *1.1.4 Functional development of the prefrontal cortex and the prefrontal-hippocampal network*

Although mental disorders comprise a broad variety of diseases, a common aspect is that they are caused by abnormal developmental processes of the brain. Therefore, they are also termed neurodevelopmental disorders (Davis et al., 2016). Key symptoms of mental disorders are dysfunctions in cognition, which heavily relies on the PFC and the prefrontal-hippocampal network (Miller, 2000; Miller and Cohen, 2001). The foundations for adult cognition are already built during very early development with neurulation, proliferation, migration and differentiation in the embryonic phase, followed by synaptogenesis, myelination and synaptic pruning in later developmental stages, and circuit refinement taking place until late adolescence (Chini and Hanganu-Opatz, 2021; Delevich et al., 2018; Stiles and Jernigan, 2010).

#### *1.1.4.1 Early functional development of the prefrontal-hippocampal network activity*

Even in early developmental stages, the immature brain shows oscillatory electrical activity, which is distinctly different from the oscillatory activity seen in the adult brain (Antón-Bolaños et al., 2019). The observed discontinuity of electrical activity, namely the alternation between oscillatory activity and periods of network silence, is observed across the whole brain and across evolutionarily distant species (Hanganu-Opatz, 2010; Khazipov et al., 2004; Vanhatalo and Kaila, 2006; Workman et al., 2013). In neonatal rodents, the spontaneous bursts of activity have been termed spindle bursts (Khazipov and Luhmann, 2006). The developmental stage of neonatal rodents corresponds to the second/ third gestational trimester in humans (Clancy et al., 2001). In prematurely born humans, comparable oscillatory activity patterns to spindle bursts have been observed, here called delta brushes (Vanhatalo and Kaila, 2006). Despite the different names, spindle bursts and delta brushes share similar features, occurring at an infraslow frequency (<1 Hz) and travelling in occipito-frontal direction (Colonnese and Khazipov, 2012; Vanhatalo et al., 2005).

Rodent spindle bursts mainly comprise theta frequency and can occasionally be accompanied by beta-gamma activity. They are found in various cortical areas, including sensory, motor and somatosensory areas (An et al., 2014; Khazipov et al., 2004). In visual and auditory cortices spindle bursts are present before the retina or cochlea are sensitive to peripheral input, but spontaneous discharges of retina or cochlea trigger the activity (Ackman et al., 2012; Wang et al., 2015). In motor and somatosensory cortices, spontaneous limb movements can evoke the spindle bursts (An et al., 2014; Khazipov et al., 2004). Blocking input from the sensory periphery reduces the occurrence of spindle bursts, but does not eliminate them completely (Hanganu et al., 2006). This indicates that the cortex can evoke spindle bursts intrinsically. One important structure for the generation of this early activity entraining the brain is the subplate (Luhmann et al., 2009; Tolner et al., 2012). This structure is located under the cortical plate and

contains neurons that initially receive inputs from the thalamus (McConnell et al., 1989). Abolishment of this neuronal ensemble eliminates spindle burst activity, highlighting the impact of the thalamocortical circuit in this early activity (Luhmann et al., 2009; Tolner et al., 2012). Spindle burst activity in the sensory systems, by synchronizing cortical and subcortical networks, drives maturation of sensory systems by refining cell migration, differentiation and synaptic plasticity (Katz and Shatz, 1996; Khazipov and Luhmann, 2006).

In contrast to the developmental activity in the sensory system, early activity in brain circuits underlying higher cognitive functioning is less well understood. Similar to oscillatory activity in sensory areas, early activity in the PFC has been described as discontinuous bouts of electrical discharge (Brockmann et al., 2011). The activity in PFC ranges in theta frequency and is superimposed by beta-gamma activity (Brockmann et al., 2011). In contrast to the activity observed in sensory areas, the emergence of the discontinuous activity in PFC is delayed and only arises shortly after birth in rodents. In parallel with an increase in firing rate and power of the oscillatory activity, it becomes continuous by about postnatal day (P) 11-12 (Chini and Hanganu-Opatz, 2021). Excitatory pyramidal neurons from the superficial layers underlie the generation of the fast component of these rhythms in the PFC (Bitzenhofer et al., 2017).

Even during these early developmental stages the HP and PFC are already connected by monosynaptic projections from i/v HP to the PFC. Excitatory input from the CA1 drives the early activity patterns in the PFC (Ahlbeck et al., 2018).

The HP shows characteristic activity patterns during early development. Around birth, HP activity is dominated by synchronous plateau assemblies (SPAs), which are patterns of coordinated firing mediated by gap-junctions and proposed to be GABA-dependent (Egorov and Draguhn, 2013). They vanish in the first postnatal weeks, when giant depolarizing potentials (GDPs) occur (Crépel et al., 2007; Egorov and Draguhn, 2013). GDPs are also GABA-dependent. However, they recruit a larger number of neurons than SPAs and are mediated through chemical synapses (Crépel et al., 2007). SPAs and GDPs have been observed in *in vitro* slices, but hypothesized counterparts to GDPs, the so called early sharp waves complexes (eSPW) have been described *in vivo* (Leinekugel et al., 2002). An underlying feature of eSPW is an increased firing rate of numerous neurons in the CA1, which is proposed to be driven by CA3 and EC input (Valeeva et al., 2018). Entorhinal-hippocampal projections are already present before birth, with the EC placed upstream of the HP as its main source of sensory input at a neonatal age (Hartung et al., 2016a; Supèr and Soriano, 1994). eSPW are often embedded in bursts of oscillatory activity in the frequency range of theta to beta/low gamma. eSPW show a strong modulation of prefrontal LFP and increase the firing rate in this brain area (Ahlbeck et al., 2018; Xu et al., 2021a). The monosynaptic projections from CA1 target the deep layers of the PFC, where the signal is transmitted to the superficial layers (Anastasiades and Carter, 2021).

The hippocampal drive to the PFC is already strong in neonatal mice and with it also the synchrony between the two areas (Brockmann et al., 2011; Krüger et al., 2012). It remains unclear which kind of information the early prefrontal activity processes, but it has been shown to be relevant for circuit refinement and later behavior (Chini and Hanganu-Opatz, 2021). An abnormally increased prefrontal activity during the neonatal age period in rodents results in

---

long-term functional and behavioral disturbances (Bitzenhofer et al., 2021). Moreover, studies in mouse models of mental illnesses showed disturbances in the prefrontal-hippocampal network already in neonatal age along with behavioral disabilities in prejuvenile age (Hartung et al., 2016b; Xu et al., 2019). In children it was shown, that delayed maturation of prefrontal activity might predict impaired behavioral disturbances (McLaughlin et al., 2010). Alongside the electrical activity in the PFC, several other developmental processes are ongoing in the first postnatal weeks in rodents, such as neuronal migration, apoptosis, myelination, dendritic development and synaptogenesis and synaptic pruning. With some of the processes reaching well into adolescence, the PFC shows a prolonged development in comparison to sensory and subcortical areas and matures fully in later developmental stages (Chini and Hanganu-Opatz, 2021).

### *1.1.4.2 Late development of the prefrontal-hippocampal network*

Adolescence is the transitional period from childhood to adulthood, associated with physical and psychological maturation. In humans, adolescence is typically regarded as the time spanning the teenage years. The World Health Organization (WHO) defines individuals between 10 and 19 years of age as adolescents, although the physical growth and cognitive enhancement can take place over a longer period extending from before 10 years of age to later than 19 years (WorldHealthOrganisation, 2024). Physical changes, such as enhanced body growth and increased secretion of sex hormones, are accompanied by changes in the central nervous system (Sisk and Foster, 2004). During adolescence, the amount of white matter in the brain increases, while the amount of gray matter increases before subsequently decreasing (Giedd, 2004). The occurrence of this inverted U-shape pattern is attributed to enhanced synaptic pruning during adolescence (Gogtay et al., 2004). Microglia eliminate unnecessary synaptic connections and thus refine neuronal circuits (Mallya et al., 2019). An increased myelination enhances efficiency of communication within the PFC and with interconnected areas throughout adolescence. These processes increase information processing and might underlie the maturation and enhancement of cognitive abilities during adolescence (Giedd et al., 1999). In addition to the morphological changes in dendritic lengths and through synaptic pruning, several neurotransmitter systems also undergo developmental changes during adolescence. In the glutamatergic system, more synapses are pruned than in the inhibitory system, resulting in a changing excitatory/inhibitory balance (Weinberger et al., 2005). Within the limbic system, dopamine and serotonin levels change, which can lead to an emotional imbalance along with higher responsiveness to stress and rewards and more risk-taking behaviors (Shoval et al., 2014; Spear, 2000). In addition to the changes reported above, functional changes have also been reported. EEG recordings during resting states show an increase in 7-30 Hz oscillations and a decrease in slow oscillations (0-7 Hz) (Marek et al., 2018).

Similar developmental changes during adolescence have also been shown in rodents. Mice attain puberty at about postnatal day (P) 42. Adolescence roughly ranges from P20 to P60, when early adulthood starts (Dutta and Sengupta, 2016). In this species rapid growth and hormonal changes during adolescence are accompanied by maturation of brain circuits and function (Bitzenhofer et al., 2021; Bitzenhofer et al., 2020; Drzewiecki et al., 2016; Pöplau et al., 2023).

In addition to the aforementioned changes, it has been shown that oscillatory activity is refined in adolescence. Gamma oscillations in particular increase in power and accelerate from around 15 Hz in the second postnatal week to around 30-80 Hz in the fourth postnatal week. In addition entrainment of firing of excitatory and inhibitory neurons to the prefrontal gamma rhythm changes during adolescence (Bitzenhofer et al., 2020; Chini and Hanganu-Opatz, 2021; de Almeida et al., 2013). Likewise, PV expression increases and GABA as well as N-Methyl-D-aspartic acid (NMDA) receptors are altered (Caballero et al., 2014a; Datta et al., 2014; Konstantoudaki et al., 2018). Along with these changes in the prefrontal local circuitry, prefrontal synchrony and inhibition linearly increase, while gamma power and spiking peak during adolescence. These changes are caused by microglia-mediated synaptic pruning and therefore a breakdown and rewiring of prefrontal local circuitry during adolescence (Pöppelau et al., 2023). Like the local circuitry in the PFC, the input from the HP still exhibits plasticity in adolescence through functional remodeling of NMDA transmission (Flores-Barrera et al., 2014). Similarly, the still developing GABAergic transmission in the PFC influences the hippocampal dependent long-term depression in the PFC (Caballero et al., 2014b). This highlights plasticity in the prefrontal-hippocampal network during adolescence. In contrast, it has been hypothesized that for example the basolateral amygdala-prefrontal pathway is already mature before the onset of adolescence (Flores-Barrera et al., 2014). Together, this underlies the refinement of local prefrontal circuits, but also of the prefrontal-hippocampal network in adolescence (Chini and Hanganu-Opatz, 2021).

The neonatal period and adolescence are vulnerable life times for developmental processes. Perturbations of these developmental processes during this times can have detrimental effects and possibly result in the manifestation of neurodevelopmental disorders (Chini and Hanganu-Opatz, 2021; Davis et al., 2016).

## **1.2 Neurodevelopmental disorders through the example of schizophrenia**

In the 5<sup>th</sup> edition of the ‘Diagnostic and Statistical Manual of Mental Disorders’ (DSM-5), neurodevelopmental disorders are defined as a group of conditions with their onset in the developmental period. This group of conditions comprises intellectual disability, autism spectrum disorder (ASD) and attention deficit hyperactivity disorder (ADHD) among others (Morris-Rosendahl and Crocq, 2020). These disorders show a high comorbidity with each other, hence there is a recent trend to move away from a strict classification into the discrete conditions, but instead to place them on a spectrum (Morris-Rosendahl and Crocq, 2020; Sokolova et al., 2017). In the past years, adult neuropsychiatric disorders, such as bipolar disorder and schizophrenia, have been added to this group of conditions as they share genetic risk genes with the childhood onset neurodevelopmental disorders (Khodosevich and Sellgren, 2023; Owen et al., 2011). Along with the shared genetic etiology, there is also emerging evidence for environmental factors as shared pathogenic mechanisms in these disorders (Morris-Rosendahl and Crocq, 2020). Neurodevelopmental disorders share perturbed

---

neurological functions, such as problems with language and speech, motor skills, behavior as well as memory and learning (Bourgeron, 2015). Working memory dysfunctions in particular and cognitive disabilities in general are core symptoms in schizophrenia (Arguello and Gogos, 2009; MacKenzie et al., 2018; Panov et al., 2023). Schizophrenia is an example of a neurodevelopmental disorder with a late onset, typically during adolescence or early adulthood (Gogtay et al., 2011). As previously described, during adolescence the brain, specifically the PFC and in parallel cognitive abilities, undergo maturational and refinement processes (Chini and Hanganu-Opatz, 2021; Delevich et al., 2018; Klune et al., 2021; Pöplau et al., 2023). Here, emphasis is put on schizophrenia for the aforementioned reasons and in order to link the developmental period of adolescence with late onset neurodevelopmental disorders.

### 1.2.1 Multiple-hit hypothesis

Several decades ago, it was hypothesized (Neurodevelopmental Hypothesis (NDH)) that psychiatric disorders are neurodevelopmental disorders and that one hit disrupting normal brain maturation is sufficient to trigger these diseases (Weinberger, 1987). However, the one-hit hypothesis is insufficient to explain the prodromal phase of the disease as well as the ongoing progression throughout the course of the disorders (McGrath et al., 2003). Consequently, the NDH was extended to include an additional second hit. It has been proposed that one hit occurs prenatally in the embryonic phase and the second one occurs later in life during another vulnerable developmental time window (Davis et al., 2016; Gogtay et al., 2011). However, this two-hit hypothesis is also inadequate to explain the heterogeneity of symptoms and neuroanatomical alterations found in neurodevelopmental disorders. Therefore, a newer model, the multiple-hit hypothesis, was introduced. According to this model, multiple hits of different risk and etiology act together on a genetically primed individual during specific periods of neurodevelopment, causing the disorders (Davis et al., 2016).

Two genetic risk factors that are an integral part of this thesis are the *disrupted-in-schizophrenia 1* (*Disc1*) mutation and the 22q11.2 microdeletion, which will be briefly introduced in the following paragraphs.

The *Disc1* mutation was first identified in a Scottish family showing an increased occurrence of schizophrenia cases, and was subsequently also found in other populations (Millar et al., 2000; Sachs et al., 2005). Since then, *Disc1* as a sole risk factor for schizophrenia has been revised, as it was found to be disrupted also in many other mental illnesses, including ASD and bipolar disorders. It is now considered a generalized risk factor for neuropsychiatric diseases and abnormal development (Brandon et al., 2009). The *Disc1* gene codes for the *Disc1* protein, which shows functions in neural developmental processes and brain maturation (Soares et al., 2011). The *Disc1* protein is involved in neuronal proliferation, differentiation, migration, cAMP signaling and cytoskeletal modulation. As it is expressed in especially high amounts during critical developmental periods and in close proximity to neuronal progenitors, it has been suggested that it plays an important role in the regulation of embryonic and adult neurogenesis (Brandon et al., 2009; Le Strat et al., 2009).

The DiGeorge or 22q11.2 deletion syndrome (ds), caused by the 22q11.2 microdeletion is a severe and highly prevalent genetic disorder that occurs in approximately 1 in 4000 live births

---

(Karayiorgou et al., 2010). It is regarded as a genuine genetic risk factor for schizophrenia, as it is estimated that it accounts for 1-2 % of sporadic schizophrenia cases, is a recurrent genetic mutation that causes sporadic schizophrenia cases, and up to one-third of carriers develop schizophrenia during adolescence and early adulthood (Karayiorgou et al., 2010). The genetic mutation of 22q11.2ds typically has a length of 3.0 Mb or 1.5 Mb, with a higher prevalence of the 3.0 Mb-sized mutation and is located on chromosome 22q11.2 (Karayiorgou et al., 2010). This mutation affects approximately 30-50 protein-coding genes. Some better characterized genes are *T-Box 1 Transcription Factor (TBX1)*, *DiGeorge Syndrome Critical Region 8 (DGCR8)*, *Crk-like Adaptor Protein L (CRKL)*, *Proline Dehydrogenase (PRODH)*, *Reticulon 4 Receptor (RTN4R)*, *Zinc-finger DHHC-type Containing 8 (ZDHHC8)*, *Catechol-O-Methyl Transferase (COMT)*, *Guanine Nucleotide Binding Protein b-polypeptide 1-Like (GNB1L)*, *Septin 5 (SEP5)* and *Glycoprotein Ib Platelet Subunit Beta (GP1BB)* (Du et al., 2020). These genes contribute to the variety of symptoms in the 22q11.2ds, such as congenital malformations, immune system complications and neurological issues. Several genes included in this deletion impact the brain and behavior as well as the development of both. These include the *COMT*, which is critical for dopamine metabolism, and *PRODH*, which is involved in glutamate synthesis. In mouse models, *ZDHHC8*, *Dgcr8*, *Ranbp1* and *Rtn4r* have been put in the context of brain function and development (Karayiorgou and Gogos, 2004; Morrow et al., 2018; Stark et al., 2008).

The etiology of schizophrenia encompasses not only genetic factors, which render an individual susceptible to schizophrenia from conception onwards, but also environmental risk factors (Murlanova and Pletnikov, 2023). Environmental risks usually occur pre- or perinatal, during childhood or adolescence, hence generally during critical developmental periods. During the prenatal and perinatal period, risk factors include maternal traumas, vitamin D insufficiency and infections (Stephenson and Craig, 2022). During early childhood, parental separation, head injuries and trauma can increase the susceptibility to develop schizophrenia (Scattolin et al., 2022). In the later vulnerable period of adolescence and early adulthood, risk factors comprise drug abuse, social stress and reduced social connectedness (Mäki et al., 2005). According to the multiple-hit hypothesis, genetic susceptibility in combination with one or several events of environmental risk factors can manifest in symptoms of neurodevelopmental disorders.

One major prenatal environmental risk factor is maternal infection during pregnancy (Massrali et al., 2022). Maternal immune activation (MIA) can induce the activation of inflammatory pathways, which in turn lead to the secretion of cytokines and chemokines that can cross the placenta, affecting the fetus. As some of these molecules can also cross the blood-brain barrier, MIA can disrupt fetal brain development and lead to a higher susceptibility of developing neurodevelopmental disorders in the offspring (Massrali et al., 2022). MIA can be mimicked in animal models, often with an injection of the bacterial cell wall component lipopolysaccharide (LPS) or the artificial viral mimetic polyinosinic:polycytidylic acid (poly I:C) (Reisinger et al., 2015). In part of the experiments conducted in the scope of this thesis, the genetic predisposition of the *Disc1* mutation is combined with an MIA through poly I:C injection (Boksa, 2010).

The focus of this doctoral thesis is to investigate the development of the prefrontal-hippocampal network in the background of neurodevelopmental disorders during vulnerable time windows

---

of development. To achieve this, the work focuses on a combination of the weaker genetic predisposition, the *Disc1* mutation with an environmental hit, namely a MIA, and on the sole, stronger genetic risk factor, the 22q11.2 microdeletion, both modelled in mice (Karayiorgou et al., 2010; Oberlander et al., 2019). Some neurodevelopmental disorders, for example schizophrenia, typically show an onset during adolescence and early adulthood, when the first psychotic episodes occur (Gogtay et al., 2011). This acute phase of the disease is often preceded by a prodromal phase, which includes diminishing cognitive abilities (George et al., 2017).

### *1.2.2 Cognitive dysfunctions and an underlying aberrant prefrontal-hippocampal network as fundamental symptoms*

Cognitive dysfunctions, which have the potential to adversely affect the quality of life for patients, are core symptoms of neurodevelopmental disorders such as schizophrenia. These cognitive dysfunctions interfere with patients' personal and professional lives and do not show a significant response to the conventional treatment of mental disorders with antipsychotics (Arguello and Gogos, 2009; MacKenzie et al., 2018; Panov et al., 2023).

Symptomatology of neurodevelopmental disorders is remarkably diverse and, for example in the case of schizophrenia, symptoms are typically divided into three categories: positive, negative and cognitive symptoms (Jauhar et al., 2022; Tandon et al., 2009). Positive symptoms of schizophrenia are often reality distortions, such as delusions and hallucinations. These typically manifest during adolescence and early adulthood and hence mark the onset of the disorder (Tandon et al., 2009). Negative symptoms comprise reduced social drive, blunting/loss of affective functions, loss of motivation and interest and an inability to experience pleasure (Carpenter et al., 1988; Marder and Umbricht, 2023). The third class of symptoms, the cognitive symptoms, constitute intellectual deficits, perturbed processing speed, speech impairments, as well as deficits in executive functioning, episodic and working memory (Carbon and Correll, 2014; Tandon et al., 2009). These symptoms are highly prevalent in schizophrenia, are usually already present in the prodromal phase and persist throughout the course of the disorder (Häfner et al., 1998). Cognitive deficits adversely influence an individual's life, as they can lead to social withdrawal and an inability to carry out a profession or job (Arguello and Gogos, 2009). In addition, the classical treatment of this disorder with antipsychotics has good efficiency on positive symptoms, but less so on negative and does not affect cognitive symptoms (Haddad and Correll, 2018; MacKenzie et al., 2018; Panov et al., 2023). Thus, cognitive symptoms of this disease are a tremendous burden on patients' lives but also on healthcare systems and societies (Kadokia et al., 2022).

Cognitive abilities in general rely on the PFC, one of the functionally most advanced and interconnected brain regions (Miller, 2000; Miller and Cohen, 2001; Spencer-Smith and Anderson, 2009). Within the domain of cognitive abilities, working memory is of specific interest as it is essential for several behavioral patterns, but a disrupted working memory is also argued to be a core symptom of schizophrenia (Eryilmaz et al., 2016; Gold et al., 2018). Working memory is a component of higher cognitive functioning and essential for goal-directed behaviors, reasoning, and decision-making (Baddeley, 1992). Historically, working memory was put in context with the 'magical number 7', as it was attributed to store seven bits of

information for processing (Miller, 1956). Today, working memory is defined as the capacity to store information for a brief period of time and promptly retrieve it with the opportunity of manipulating it towards a goal-directed behavior (Baddeley, 1992). Working memory functioning relies on prefrontal activity in interplay with the HP (Backus et al., 2016; Hyman et al., 2010). It has been proposed that a dysfunctional prefrontal-hippocampal network underlies the manifestation of working memory deficits in neurodevelopmental disorders (Sigurdsson and Duvarci, 2016).

Several studies have shown working memory impairments in schizophrenic patients, but impairments have also been demonstrated in schizoaffective and bipolar disorder (Gold et al., 2018; Sigurdsson and Duvarci, 2016). In addition, various abnormalities in brain anatomy, neurotransmitter systems and connectivity have been described in neurodevelopmental disorders (Keshavan et al., 2008). Regarding the prefrontal-hippocampal network, both areas individually show impairments in these disorders, but the connectivity and synchrony between the two areas is also disrupted (Meyer-Lindenberg et al., 2005; Rasetti et al., 2011). The HP shows a reduced volume and abnormal activity during memory tasks, with a hyperactivity in baseline activity proposed to be a possible underlying reason for the abnormal dopaminergic system observed in patients (Modinos et al., 2015; Small et al., 2011). The PFC is a focus for research into the pathophysiology of neurodevelopmental disorders, as the HP shows an abnormal recruitment of the PFC during cognitive tasks, such as working memory or executive control tasks (Meyer-Lindenberg et al., 2005; Rasetti et al., 2011). In addition, it has been shown that excitatory pyramidal neurons as well as inhibitory interneurons within the PFC exhibit altered morphology and connectivity (Chao et al., 2010; Spratt et al., 2019). In particular, the role of PV interneurons has been put in the focus of research, as they play a key role in the generation of the gamma oscillatory rhythm, which is perturbed in schizophrenic patients (Buzsáki and Wang, 2012).

Various studies also directly investigated the synchronous activity between the PFC and HP. It has been shown that the prefrontal-hippocampal network has a reduced connectivity during working memory tasks in schizophrenic patients compared to healthy controls (Henseler et al., 2010). Sibling studies have shown that even in healthy individuals with potentially higher susceptibility for neurodevelopmental disorders, the hippocampal-prefrontal network activity is already perturbed, highlighting a possible genetic contribution (Benetti et al., 2009). Similar to the discoveries in patients with neurodevelopmental disorders, the prefrontal-hippocampal pathway is impaired in rodent models of those illnesses (Sigurdsson and Duvarci, 2016; Sigurdsson et al., 2010). Enhanced synchrony in the oscillatory theta rhythm between the PFC and HP was found in healthy humans performing a memory task, underlining the role of this rhythm in the integration of memory (Backus et al., 2016). Hippocampal theta rhythm entrains prefrontal local gamma rhythm and spiking patterns (Siapas et al., 2005; Sirota et al., 2008). In a rodent model of neurodevelopmental disorders, theta coherence between the two areas and entrainment of prefrontal spikes to the hippocampal theta rhythm during a working memory task were shown to be perturbed (Sigurdsson et al., 2010).

Considering these results in the context of the neurodevelopmental hypothesis of psychiatric disorders, the question arises as to how the prefrontal-hippocampal network matures and if

perturbations in more prone individuals are already present during development. The identification of critical or vulnerable developmental periods could lead to novel and more advanced therapeutic interventions for these disorders.

### *1.2.3 Adolescence is a vulnerable developmental period*

Throughout early life, the brain develops from a bunch of migrating progenitor cells into highly specific, functional neuronal circuits integrated into well-connected brain areas, enabling complex behaviors. Subcortical as well as sensory brain areas mature during earlier life development, while the PFC shows a prolonged maturation period (Chini and Hanganu-Opatz, 2021; Delevich et al., 2018). The PFC only fully matures later in life during adolescence and early adulthood, giving rise to the behavioral abilities that depend on it. In particular, cognitive abilities such as working memory only emerge and mature during childhood, adolescence and early adulthood (Klune et al., 2021).

On the flip side, the onset of neurodevelopmental disorders typically becomes apparent during childhood and adolescence. Several neurodevelopmental disorders, such as ASD, ADHD and global developmental delay (GDD) are diagnosed in childhood (Mintz Hemed and Melosh, 2023). However, late onset neurodevelopmental disorders, such as schizophrenia, typically begin to show during adolescence and early adulthood (Khodosevich and Sellgren, 2023). As the onset of schizophrenia is often diagnosed with the first psychotic event, this later developmental period is considered of high relevance in the background of schizophrenia (Gogtay et al., 2011). According to the multiple-hit hypothesis of the etiology of neurodevelopmental disorders, one or multiple hits causing perturbations during vulnerable time windows can cause these disorders to manifest (Davis et al., 2016). Adolescence is a period of physical and psychological growth, accompanied by maturation processes in the central nervous system, especially in the PFC (Giedd et al., 1999; Sisk and Foster, 2004; WorldHealthOrganisation, 2024). Perturbations in the developmental processes during this time of life can result in the manifestation of neuropsychiatric disorders. These perturbations can include large-scale abnormalities, such as increased weight gain, which has been shown to potentially influence cognitive abilities and increase the risk for neurodevelopmental disorders, but can also include less obvious abnormalities in the maturation of the brain (Miller et al., 2015; Wentz et al., 2017).

As mentioned previously, during adolescence, gray and white matter volumes change in specific patterns (Giedd, 2004). Other studies of cohorts of childhood onset patients and individuals with an ultra-high risk to develop schizophrenia show that the processes of gray and white matter maturation in the PFC are disrupted during adolescence and are more widespread in patients with an onset in adolescence than in adult-onset patients (Douaud et al., 2009; Gogtay et al., 2011). The inverted U-shape pattern of gray matter volume change has been attributed to microglial pruning, most prominently on excitatory neurons (Gogtay et al., 2004; Weinberger et al., 2005). In adolescent mice, it was shown that depleting microglia disrupts this pruning process and with it the normal development of prefrontal activity and cognitive abilities (Pöpplau et al., 2023). Moreover, during adolescence, functional connectivity among brain areas is refined through altered synaptic plasticity and interneurons in the circuitries, which

results in reduced information processing of environmental stimuli. Dysfunctional oligodendrocytes, and with them abnormal myelination, may affect local and long-range circuits as well (Nave and Ehrenreich, 2014; Sakurai and Gamo, 2019). These abnormal changes in pruning and neuronal circuits can cause an imbalance in the excitation/inhibition ratio, which has been hypothesized to underlie cognitive disabilities in schizophrenia (Gonzalez-Burgos and Lewis, 2008; O'Donnell, 2011). The fine-tuned interplay of excitatory and inhibitory interneurons, causing the excitation/inhibition ratio, underlies the local gamma rhythm in several areas of the brain, including the PFC. A disturbed gamma rhythm in the PFC was associated with impaired cognitive abilities (Cho et al., 2015; Guan et al., 2022; Williams and Boksa, 2010). Furthermore, a weaker gamma band oscillation was found to occur in the prodromal phase of schizophrenia in high-risk individuals (Andreou et al., 2015).

Alongside the glutamatergic and GABAergic neurotransmitter systems, the dopamine levels within the limbic system undergo tremendous changes during adolescence. The subsequent imbalance in this system causes adolescents to become more prone to risk-taking and reward-seeking behavior and more susceptible to stress (Shoval et al., 2014; Spear, 2000). In turn, this leads to a higher risk for drug abuse and vulnerability to addiction (Chambers et al., 2003). In the context of neurodevelopmental disorders and the multiple-hit hypothesis, drug abuse or addiction during adolescence can be an additional hit to enhance the risk for these diseases (Davis et al., 2016). Epidemiological studies show that cannabis misuse during adolescence can result in a higher risk for psychotic episodes resembling schizophrenia (Rubino and Parolaro, 2014; Rubino et al., 2015).

Taken together, this highlights adolescence as a vulnerable period, especially considering the maturation of the PFC and its circuitries, e.g. the HP, which is still undergoing development during adolescence (Flores-Barrera et al., 2014).

From studies in mouse models of neurodevelopmental disorders, we know that the prefrontal-hippocampal network is already disrupted at a neonatal age. This manifests as an impaired synchrony in theta activity in the PFC and HP (Hartung et al., 2016b; Xu et al., 2021a). This reduced synchrony early in life switches to an overshoot of synchrony during early adolescence in the dual-hit mouse model, combining a genetic and an environmental risk factor (Hartung et al., 2016b; Xu et al., 2021a). In a 22q11.2ds model, the early adulthood period (postnatal day (P) 60 to 70) was reported to be a critical period for the PFC and ventral HP, with the PFC already showing abnormal gamma power at P40 and P60 (Mukherjee et al., 2019). However, the period of adolescence in mice ranges from around weaning (~P21) to early adulthood (~P60) (Brust et al., 2015; Laviola et al., 2003). Adolescence and early adulthood are the developmental periods in which schizophrenia typically shows its onset with the first psychotic episodes (Selemon and Zecevic, 2015). Consequently, the maturation of the prefrontal-hippocampal network in the context of neurodevelopmental disorders during this time is of particular interest, but the developmental trajectories of the network activity have not yet been fully elucidated.

### 1.3 Objectives and aims of the thesis

In a rough framework, the experiments performed in the scope of this thesis aimed at identifying and analyzing underlying mechanisms of prefrontal development with a specific focus on three main points:

1. Prefrontal development in the context of neurodevelopmental disorders
2. Prefrontal development during adolescence
3. Prefrontal development in the as a result of the interplay with the hippocampus

The first part of the thesis focuses on prefrontal activity in a mouse model of mental illness and is published in Chini et al. (2020). One part of the experiments performed in the scope of this thesis identifies the role of microglial pruning in the PFC during neonatal development in mice of the dual-hit model, combining a genetic predisposition (*Disc1*) and an environmental hit (GE), and in GE mice receiving a therapeutic intervention during a hypothetical critical period, functioning as a possible rescue mechanism. The results of these experiments show that synaptic pruning is enhanced in neonatal GE mice in the PFC, with the microglia showing a hypermature phenotype. Therefore, it is hypothesized that the microglia in the model of neurodevelopmental disorder bypass the normal maturation period. This is rescued by administration of minocycline during the critical developmental period.

The second set of experiments constituted behavioral experiments comparing healthy controls to GE mice during early juvenile age, receiving the medical intervention during a hypothetical non-critical developmental period. The results show that GE mice receiving the intervention during this time, similar to untreated GE mice, have poorer recognition memory in the context of timeliness.

The second part of this thesis focuses on investigating activity patterns in the prefrontal-hippocampal-entorhinal network in prejuvenile mice of the dual-hit GE model of neurodevelopmental disorders. To this end, electrophysiological recordings of LFP and multi-unit activity (MUA) were performed simultaneously in the PFC, HP and LEC of early juvenile GE and control mice. Prejuvenile GE mice exhibited an enhanced synchrony not only between the PFC and HP, but also between the PFC and LEC compared to controls. These results showed that the prefrontal-hippocampal network activity is perturbed in mouse models of neurodevelopmental disorders at a pre-adolescent age.

However, these results leave an open question as to the functional relevance of the network during adolescence.

The third part of this thesis follows up and aims at connecting electrophysiological recordings with a behavioral task testing the working memory performance of adolescent mice and identifying underlying activity patterns. To achieve this, awake recordings enabling movement mimicking free spatial orientation and locomotion were established on a system called MobileHomeCage. Subsequently, a delayed non-match to sample (DNMS) T-Maze task (in short: T-Maze task) was planned to be established on the MobileHomeCage and combined with electrophysiological recordings. However, several trials showed that juvenile and adult

wildtype mice are incapable of performing this complex task under head-fixed conditions on the MobileHomeCage.

The fourth part of this thesis focuses on elucidating the late developmental maturation process of the prefrontal-hippocampal network in the context of neurodevelopmental disorders. To this end, electrophysiological recordings of LFP and MUA were performed simultaneously in the PFC and HP of adolescent mice of a genetic model of neurodevelopmental disorders ( $Df(16)A^{+/-}$ ) and wildtype (WT) controls ranging from P20 to P60. The recordings were performed in awake, behaving mice under head-fixed conditions on the MobileHomeCage system (Neurotar, Helsinki, Finland) and the signal was divided into resting and movement periods (Au - Kislin et al., 2014). The prefrontal single-unit spiking activity acquired in WT mice was additionally used in a project deciphering how the extreme distributions of structural and functional parameters in the adult brain unfold during development ((Chini et al., 2023), currently under revision at *Cell Reports*). In this thesis, it is shown that prefrontal activity in the broad-band gamma range and hippocampal activity in the theta range exhibited perturbed movement-dependent developmental trajectories throughout adolescence in  $Df(16)A^{+/-}$ . However, this did not result in altered activity in late adolescent/early adult mice. In the HP the spike correlations developed in similar patterns, but with a steeper rise in the  $Df(16)A^{+/-}$  mice, while in the PFC the correlated maturation of putative pyramidal neurons and PV interneurons was disturbed. On the network level, there was lower synchrony in late adolescent  $Df(16)A^{+/-}$  mice in LFP and from hippocampal neurons to PV interneurons, but a higher correlation of hippocampal neurons with putative pyramidal neurons.

---

## 2 Methods

The experimental models, primers, software, laboratory and technical equipment as well as chemicals and consumables, which have been used in the experiments and analysis, are listed in Table 1 in the Appendix.

### 2.1 Experimental animals

All experiments were performed in compliance with German laws and the guidelines of the European community for the use of animals in research. In addition, all experiments were approved by the local ethical committee (N18/015, N19/121). Experiments were carried out on C57BL/6J (control, wildtype (WT)), heterozygous *Disc1* (B6.129S6-Disc1tm1Kara, MGI: 3623218 (<http://www.informatics.jax.org/>)) and heterozygous *Df(16)A<sup>+/-</sup>* (Del(16Dgcr2-Hira)3Aam) (MGI:3798957 (<http://www.informatics.jax.org/>), (Stark et al., 2008)) mice. The *Disc1* as well as the *Df(16)A<sup>+/-</sup>* line were bred on C57BL/6J background.

To generate dual-hit mice, timed pregnant dams were injected with the viral mimetic poly I:C (5 mg/kg body weight (bw)) at embryonic day (E) 9 (Hartung et al., 2016b). Heterozygous *Disc1* mice were generated by mating homozygous *Disc1* mice with C57BL/6J mice. The *Disc1* mutation carries two termination codons and results in a truncated transcript (Koike et al., 2006; Kvajo et al., 2008). Genotypes were assessed using genomic DNA (tail biopsies) and the primers: forward primer 5'-TAGCCACTCTCATTGTCAGC-3' and reverse primer 5'-CCTCATCCCTTCCACTCAGC-3'. Offspring from *Disc1* females mated with WT males and from WT females mated with *Disc1* males were pooled together because no difference was found between the groups (Chini et al., 2020). Minocycline treatment was undertaken over the lactating dams. For this, minocycline (daily dosage 30 mg/kg bw) in combination with sucrose was added to the drinking water of the dam from postnatal day (P) 1 to P8 or P9 to P16. The dams pass the antibiotic on to the pups via lactation (Dansie et al., 2013; Luzi et al., 2009). They did not show a reduced intake of drinking water when the water was supplemented with minocycline.

The *Df(16)A<sup>+/-</sup>* mice show a heterozygous deletion on chromosome 16 spanning 27 genes (Chr16:17658219-18789059 bp). Genotypes were determined using genomic DNA (tail biopsies) and the following primer sequence: forward primer 5'-ATCCCCATGGACTAATTATGGACAGG-3', reverse primer 5'-GGTATCTCCATAAGACAGAATGCTATGC-3'. WT females were bred with heterozygous *Df(16)A<sup>+/-</sup>* males. Before weaning, the mice were housed with the dam and their littermates. After weaning, the offspring were housed with at least two cage-mates. All mice were kept in a 12h light / 12h dark cycle. Humidity and temperature were kept constant (40% relative humidity; 22 °C), and fodder and water were provided *ad libitum*. The day of birth was considered P0.

## 2.2 Behavioral experiments with freely moving mice - Object recognition tasks

The object recognition tasks were carried out in prejuvenile WT and GE mice treated with minocycline during the later period of P9 to P16. The behavioral tests were conducted in a white circular arena with a diameter of 34 cm and a height of 30 cm. This size maximizes explorative behavior while also minimizing incidental contact with the objects. The utilized objects were smaller than twice the size of the prejuvenile mice (height: 3 cm, diameter 1.5-3 cm) and did not resemble living stimuli as they did not exhibit eye spots and were not predator-shaped. They consisted of five differently shaped and colored objects that were easy to clean to remove odors from previous trials (cleaning solution: 0.1 % acetic acid). The objects were fixed to the arena with magnets attached to their bottoms. Objects and arena were cleaned after each trial. The interaction of the animal with the objects was captured with a black-and-white CCD camera (VIDEOR TECHNICAL E. Hartig GmbH), mounted 100 cm above the arena, which was connected to a PC to let the video tracking software (Video Mot2 software, TSE Systems GmbH) run.

Both novelty recognition paradigms consisted of familiarization and test trials. Before each task, the mice were placed in the arena to habituate to it for 10 min. In the familiarization trials, the mouse was allowed to explore two identical objects in the test arena. After 10 min of free exploration of the objects, the mice were placed back in a temporary holding cage.

For the novel object recognition task (NOR) the mice were kept in the holding cage for 5 min and then placed in the same arena as before, now containing one object from the familiarization trial and one novel object. The mice were allowed to explore the different objects for 5 min. The NOR was conducted with P17-P18 mice.

In the recency recognition task (RR), the first familiarization phase was followed by a second familiarization phase with a new identical object pair after a delay of 30 min in the holding cage. This phase was followed by the test phase after a break of 5 min with one object from the first familiarization and one object from the second familiarization phase. In the test phase, the mouse could explore the objects for 5 min. The RR was conducted with P19-P22 mice.

In both paradigms, object interaction during the first five minutes and length of single interactions was assessed. The trials were tracked for the Video Mot2 analysis software. For analysis, the object recognition module was used. The mouse was identified by a 3-point tracking method identifying the head, tail base and center of gravity. To assess object interactions, a square zone was created around the objects digitally and each entry of the head was counted as an interaction. An overlay of head and center of gravity in the object zone was counted as climbing and sitting on the object and was discarded. The data were imported into Matlab (MATLAB2017b, Mathworks, MA, USA) and analyzed offline with custom-written algorithms.

Discrimination ratios (DR) and single interaction time ratios were calculated as:

$$DR = \frac{Time_{Object2} - Time_{Object1}}{Time_{Object2} + Time_{Object1}}$$

## 2.3 In vivo electrophysiology in anesthetized mice

### 2.3.1 Surgical procedure

The extracellular recordings of local field potential (LFP) and multi-unit activity (MUA) were performed in the prelimbic area (PL) of the medial prefrontal cortex (mPFC), the cornu ammonis (CA) 1 of the hippocampus (HP) and superficial and deep layers of the lateral entorhinal cortex (LEC) of P16-26 GE and WT mice. The recordings were conducted under urethane anesthesia. Before the surgical procedure, mice were injected with 1 mg/g body weight of urethane (Sigma-Aldrich, St Louis, MO, USA) in 0.9 NaCl solution (*i.p.*). The surgery was carried out under additional isoflurane anesthesia (induction: 5 %, maintenance 2 %). To reduce muscle artifacts, neck muscles were cut and locally treated with a mixture of bupivacaine and lidocaine (0.5% bupivacaine / 1% lidocaine) for analgesia. The scalp and connective tissue were removed, and dental cement was applied, enclosing two plastic bars used to fix the head of the mouse in a stereotactic frame, leaving the skull open above the target areas. Craniotomies were performed by carefully thinning the skull and then removing the remaining bone with a motorized drill above the mPFC (bregma + 1 mm, midline + 0.5 mm), the intermediate HP (lambda + 1 mm, midline + 4.5 mm), LEC (lambda + 0 mm, midline + 6 mm) and the cerebellum. Throughout the whole surgical procedure the mice were kept on a heating mat at 37°C and eyes were kept moist with an eye ointment (Bepanthen, Bayer, Leverkusen, Germany).

### 2.3.2 Recording procedure

After the surgical procedure, the mouse was placed in a stereotactic frame and fixated with the bars mounted to the skull. Electrodes (NeuroNexus, MI, USA) were carefully and slowly inserted into the PL (A1x16 recording sites, 100 µm spacing, 2 mm depth), the CA1 (A1x16 recording sites, 50 µm spacing, 1.8-2.3 mm depth, 25° angle), and LEC (A1x16 recording sites, 100 µm spacing, 2 mm, horizontally). A silver wire was inserted into the cerebellum, to serve as a ground and reference electrode. Before starting signal acquisition, a recovery period of 15 min was provided to improve signal quality and stability of unit activity. The electrical signal of the brain areas was acquired for 30 -40 min. Extracellular signals were band-pass filtered (0.1–9000 Hz) and digitized (32 kHz) with a multichannel extracellular amplifier and its accompanying software ‘Cheetah’ (Digital Lynx SX; Neuralynx, Bozeman, MO, USA). The recording sites were stained with DiI coating of the electrodes and confirmed post-mortem.

## 2.4 In vivo electrophysiology in awake mice

### 2.4.1 Surgical procedure

Acute multisite extracellular recordings of LFP and MUA in the mPFC and HP were performed in P20 to P60 awake mice of both sexes. For head fixation during the recordings, a metal

---

headplate (Neurotar, Helsinki, Finland) was implanted beforehand. This surgery was performed at least 2 days before the first recording. 30 min before the surgical procedure, buprenorphine (0.5 mg/kg bw) was injected subcutaneously. Throughout the entire procedure, the animals were anesthetized with isoflurane (5 % induction, 2.5 % maintenance) and placed on a heating mat to maintain body temperature. Anesthesia depth was confirmed by checking the paw withdrawal reflex by pinching the toe. Their eyes were coated with an eye ointment (Bepanthen, Bayer, Leverkusen, Germany) to prevent them from drying out. After disinfection with Betaisodona (MundiPharma, Frankfurt a.M., Germany), the scalp was removed from the top of the head and the edges were additionally treated for analgesia through application of a Lidocaine/Bupivacaine mixture (1 % L / 0.5 % B).

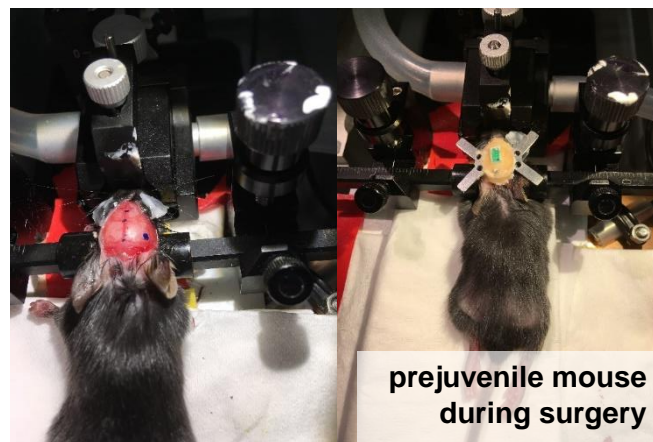


**Figure 1: Surgical procedure of headplate implantation for head fixation during recordings.** Left, photograph of a prejuvenile mouse undergoing surgery. Right, photograph of prejuvenile mouse after completion of surgery.

Two craniotomies made the mPFC (0.5–2.0 mm anterior to bregma, 0.1–0.5 mm right to the midline) and HP (0–0.7 mm anterior to lambda, 4.5–5.5 mm right to the midline) accessible for recordings. To protect the open tissue with Kwik-Cast sealant (World Precision Instruments, Friedberg, Germany) throughout the complete experimental time window, synthetic windows were fixed to the skull around the craniotomy. A silver wire, serving as a ground and reference electrode, was inserted between the skull and cerebellum after an additional craniotomy posterior to lambda. The metal head-plate was attached to the skull with dental cement. To prevent dehydration, saline (10 ml / kg bw) was injected subcutaneously at the end of the surgical procedure. For recovery from anesthesia, mice were placed in a cage on a heating mat and were put back into their home cage with their cage mates after fully awakening. For further analgesia, Metacam (0.5 mg/ml, Boehringer-Ingelheim, Germany) was mixed into soft food and provided for 48 h after the surgery.

### 2.4.2 Recording procedure

After full recovery from the surgery, the mice were acclimatized to the head fixation system and trained to move the air-lifted carbon cage from the MobileHomeCage system (Neurotar, Helsinki, Finland) at least twice for 30 min. For multisite, simultaneous recordings, the craniotomies were uncovered and electrodes (NeuroNexus, MI, USA) were stereotactically inserted into the mPFC (one-shank, A1x16-channel, 100  $\mu$ m-spaced, 2.0 mm deep) and the HP

---

(one shank, A1x16-channel, 50  $\mu\text{m}$  spaced, 30° angle, 2.0-2.7 mm deep until reaching the reversal potential) with the help of a motorized arm (Scientifica IVM Triple, Scientifica, UK). After settling of the electrodes, the electrical signal of the brain areas was acquired for 30 - 40 min. Extracellular signals were band-pass filtered (0.1–9000 Hz) and digitized (32 kHz) with a multichannel extracellular amplifier (Digital Lynx SX; Neuralynx, Bozeman, MO, USA). For prefrontal LFP, a channel within the PL area was selected. For hippocampal LFP, a channel in the pyramidal layer was chosen (reversal  $\pm$  100  $\mu\text{m}$ ). Simultaneously to the recording, the movement of the mice was tracked with the MobileHomeCage Lomotion tracking software v.2.2.1 (Neurotar, Helsinki, Finland). After finishing the acquisition, the electrodes were stereotactically removed, the craniotomies covered up again and the mice returned to their home cages. Mice were not kept away from their cage mates and home cages for longer than 1.5 h at a time. The same mice were recorded several times, leaving at least two days in between recordings to allow the tissue to recover. The location of the electrode was confirmed *postmortem*. For this, the recording sites were stained by inserting DiI-coated electrodes after the last recording.

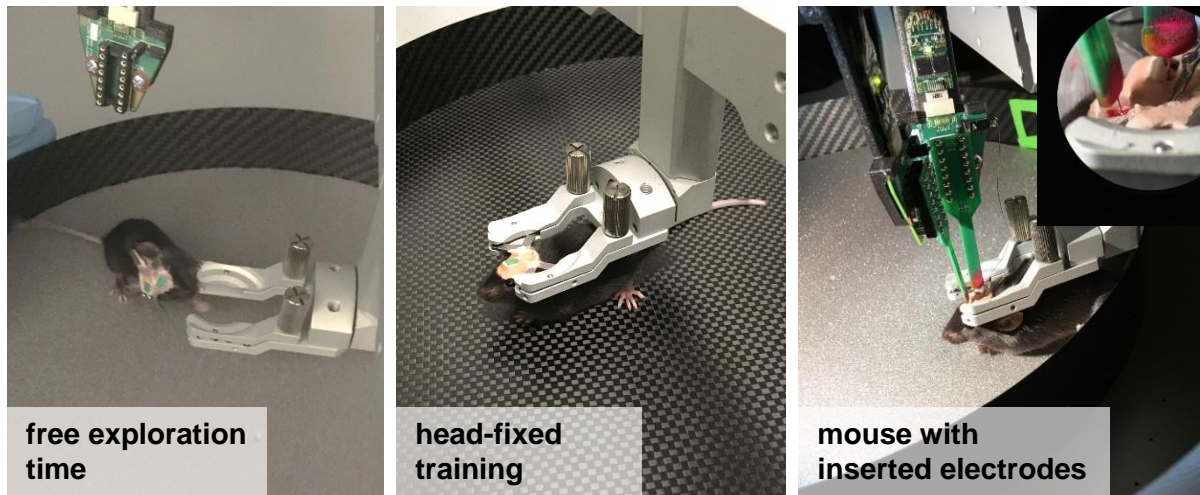


**Figure 2: Training and recording procedure on the MobileHomeCage setup.** Left, photograph of a mouse freely exploring the carbon cage and head fixation system during the familiarization phase. Middle, photograph of a mouse during the head-fixed training. Right, photograph of a mouse during a recording with inserted electrodes and inset showing the electrode insertion in more detail.

## 2.5 Establishment of behavioral experiments with head-fixed mice – delayed non-match to sample T-Maze task

The experiments to establish the delayed non-match to sample (DNMS) T-Maze task in head-fixed animals were carried out with headplate-implanted adolescent and early adult mice (P30-60). In the classical DNMS task, a subject has to choose a stimulus that does not match the stimulus presented before the recall delay (Rodriguez and Paule, 2009). Transferred to rodents, working memory can be assessed with the DNMS task in a Y-/ or T-Maze. In such a maze, rodents tend to alternate between visited arms if allowed to explore the maze freely (d’Isa et al.,

2021). For the assessment of working memory, the test is divided into several phases. In the sample phase, the subject visits one arm and receives a reward there. Entry in this arm can be by choice or forced due to closure of the second arm. Subsequently, the subject is transferred back to the start zone and, after a delay period, is allowed to choose an arm to explore. Only the previously unvisited arm is rewarded. Typically, correct completion of 8 out of 10 consecutive trials is counted as successful learning of the task. The task phases were performed in the head-fixed mice on the MobileHomeCage in the same manner. For this, a round T-Maze from Neurotar (Helsinki, Finland) was used. Various modifications were made to this T-Maze, which are described in detail in Results 3.3. Before the start of the test, mice were allowed to first habituate to the head fixation in the open carbon cage, then were transferred to the round T-Maze and allowed to explore this carbon cage as well. In the sample phase, the mice could enter one arm and received a liquid reward delivered by a manually triggered syringe pump there. Afterward, they were transferred to the start zone for a 30 sec delay phase. In the test phase, both arms were opened and mice were allowed to choose an arm. A reward was delivered in the previously unrewarded arm. Mice were then transferred back to the start zone for a 90 sec inter-trial interval. Movement in the carbon T-Maze was tracked with the tracking capability software of the MobileHomeCage Lomotion tracking software v.2.2.1 (Neurotar, Helsinki, Finland). Correct visiting of arms was manually assessed. The exact protocols are described in Results 3.3, as they vary between the different approaches and experimental groups used. The information provided there includes: the reward used, how many trials were performed per day, how many training days were needed and the time of day the experiments were performed.

## 2.6 Histology

### 2.6.1 Perfusion

Following the electrophysiological recordings and to extract brains for morphological investigation, the mice were anesthetized with 10 % ketamine (aniMedica, Germany) and 2 % xylazine (WDT eG, Germany) in physiological saline solution (0.9 % NaCl) (10 µg/g body weight, *i.p.*). Tail and toe pinch reflexes were checked for depth of anesthesia. After complete fade-out of reflexes, the animals were transcardially perfused with a 0.9 % saline solution to wash out blood, followed by Histofix (Carl Roth, Germany) containing 4 % paraformaldehyde to fixate the tissue. The brains were extracted and post-fixed in the same solution for 24 hours. Afterward, the brains were sectioned coronally in 100 µm slices and Dapi-stained with mounting medium for reconstruction of the electrode positioning or in 50 µm sections for immunohistochemistry.

### 2.6.2 Immunohistochemistry

For morphological investigation of microglial cells and their overlay with engulfed puncta, 50 µm thick slices of the PFC of P8-10 WT, GE and GE mino treated mice, were stained for ionized calcium-binding adapter molecule 1 (IBA-1) and Vesicular glutamate transporter 1

(VGLUT1). The slices were permeabilized and blocked with PBS with 0.3 % Triton X-100 (Sigma-Aldrich, MO, USA) and 3 % bovine serum albumin (BSA) (Jackson Immuno Research, PA, USA). Hereafter, they were incubated with rabbit monoclonal primary antibody against IBA-1 (1:500, catalog #019-19741, Wako, Germany) and polyclonal guinea-pig antibody against VGLUT1 (1:1000, Synaptic Systems, Germany). After subsequent washing with PBS, the slices were stained with the secondary antibodies Alexa Fluor-568 donkey anti-rabbit (1:500, Life Technologies, CA, USA) and Alexa Fluor-488 goat anti-guinea pig (1:500, Molecular Probes, OR, USA). In a final step, the slices were transferred to glass slides and covered with Vecta-Shield (Vector Laboratories, Newark, CA, USA).

### 2.6.3 Imaging

For reconstruction of the electrode positioning, wide-field fluorescence imaging with a binocular microscope (Olympus SZ51, Hamburg, Germany) was performed. For microglia morphology and engulfment of puncta, slices were imaged with a confocal microscope (Olympus FX-100, Olympus, Hamburg, Germany). Images of IBA-1-positive cells and VGLUT vesicle overlay, were acquired as microscopic stacks with an objective with 60x magnification (numerical aperture 1.35). The images had a pixel resolution of 1024 x 1024 pixels, with a pixel size of 103 nm and a Z-step size of 750 nm. The number of images depended on the span of the microglial cell on the z-axis. For each mouse, 5 images of microglial cells per slice from 3 slices were acquired.

### 2.6.4 Image analysis

To analyze the microglial engulfment of synaptic material, the overlay of IBA-1 positive cells and VGLUT1 puncta was assessed. The preprocessing of the images was performed in ImageJ and Matlab (MATLAB2017b, Mathworks, MA, USA). For the reconstruction of microglial cells from the IBA-1, images underwent background subtraction (*imopen*, with a ‘disk’ of radius 50), 3D double-threshold binarization (*hysteresis3d* function; lower threshold = 0.1, upper threshold = 0.5, connectivity = 26) and 3D median filtering (*ordfilt3D*). The 3D hysteresis step consisted of the identification of regions with high intensity and a following step to identify connected regions of lower intensity. As terminals of microglial cells are often less bright than the cell soma, this allows for a better binarization including the terminals. The preprocessing of the VGLUT1 images was done by background subtraction (*rolling ball* radius = 2 pixels), median filtering (*despeckle*), maximum filtering (radius = 2 pixels), binarization (auto threshold) and segmentation (*watershed*). Further processing was performed in Matlab. Here, the volume of the VGLUT1 areas was quantified in 3D (*bwlabeln*, connectivity = 8) and used if the ROI was between 100 and 500 pixels in size. The 3D tensors of reconstructed microglial cells and VGLUT1 stacks were multiplied, and VGLUT1 puncta that showed a complete 3D overlay with the microglial cell were considered ‘engulfed’.

---

## 2.7 Data analysis of electrophysiological recordings

### 2.7.1 Head-fixed movement and open-field behavior

The movement of the mice in the 290 mm diameter carbon cage of the MobileHomeCage system was recorded with the MobileHomeCage Locomotion tracking software v.2.2.1 (Neurotar, Helsinki, Finland). The running speed as well as the coordinates for each sampling time point, were extracted from the output of the software and analyzed with custom-written algorithms in Matlab. For behavioral movement pattern analysis, movement that exceeded 5 mm/s was averaged across the first 5 min and 30 min of recording time. For movement ratio, the sampling points in which speed exceeded the threshold were summed for either the first 5 min or 30 min of recording time and divided by all sampling points of these times:

$$\text{Movement ratio} = \frac{\text{Time mouse was moving}}{\text{Total time}}$$

Similarly, the time in the center was assessed for the first 5 min or 30 min by summing the sampling points for which the coordinates lay within a distance of 65 mm from the center. For alignment with the electrophysiological recordings and the possibility to divide this signal into movement and resting periods, a continuous TTL was sent to the amplifier when the movement of the mouse exceeded the speed threshold.

### 2.7.2 LFP analysis

#### 2.7.2.1 Power spectral density

In vivo data were analyzed with custom-written algorithms in Matlab (MATLAB2017b, Mathworks, MA, USA) environment. The electrophysiological signals were band-pass filtered (0.5-100 Hz) with a third-order Butterworth filter forward and backward in order to preserve phase information. The power spectral density (PSD) in each area was calculated on 1 s long windows of the down-filtered LFP signal using Welch's method with non-overlapping windows. For data acquired from anesthetized mice, the whole signal was used. For analysis of data from awake mice, the 30-45 min long signal was divided into periods of 10 sec length. Subsequently, this LFP signal was down-sampled for PSD analysis. PSD was calculated on 1 sec long segments of the 10 sec long signal, followed by median averaging for resting and running periods respectively.

#### 2.7.2.2 Phase-amplitude coupling

The phase-amplitude coupling (PAC) was assessed for data acquired from awake head-fixed mice. The PAC between the PFC theta phase (1-12 Hz) and the gamma amplitude (20-100 Hz) as well as between the HP theta phase and the PFC gamma amplitude was calculated on 10 sec long segments, which were classified into resting and movement periods. The PAC was calculated using the normalized modulation index method as described previously (Onslow et al., 2011). Two raw signals,  $x_{ph}$  (signal containing the lower frequency modulating signal) and

$x_{amp}$  (signal containing the higher frequency modulated signal) were band-pass filtered with a third-order Butterworth filter for the desired frequency band. From the analytical signal obtained through convolution with complex Morlet wavelet, the amplitude envelope of the higher-frequency oscillation  $A_{famp}$  and the instantaneous phase of the lower frequency signal  $\theta_{fph}$  were calculated as absolute values and phase angle of the signal. For the MI, a complex valued composite signal was generated in which the amplitude comprised  $A_{famp}$  values and the phase was composed of  $\theta_{fph}$ .

$$Z_{fph,famp(t)} = A_{famp}(t) \cdot e^{i\theta_{fph}(t)}$$

The MI was calculated as the absolute value of this composite signal:

$$MI_{fph,famp} = |average(Z_{fph,famp}(t))|$$

To assess significance, values were compared to a shuffled dataset and not significant values were rejected. The PAC was median averaged for resting and movement periods separately.

### 2.7.2.3 Coherence

Imaginary coherence was assessed for data obtained from anesthetized mice as well as for data acquired from awake mice. For anesthetized recordings, the imaginary coherence was calculated for PFC-HP, PFC-LEC and HP-LEC on the full signal. Imaginary coherence for awake recordings between PFC and HP was calculated on 10 sec long segments that were classified into resting and movement periods. The imaginary part of coherence is insensitive of volume conduction (Nolte et al., 2004) and was calculated by taking the absolute value of the imaginary component of cross-spectral density ( $P_{XY}(f)$ ) of the two signals normalized by the power spectral density ( $P_{XX}(f)$  and  $P_{YY}(f)$ ) of each:

$$C_{XY} = |Im(\frac{P_{XY}(f)}{\sqrt{P_{XX}(f)P_{YY}(f)}})|$$

### 2.7.2.4 Spectral dependency ratio

The spectral dependency ratio (SDR) was assessed for awake recordings for the resting and movement power spectral densities (PSD) of PFC and HP. It was calculated according to a previously published protocol (Shajarisales et al., 2015), by taking the mean of the PSD of signal X ( $P_{XX}(f)$ ) and dividing it by the mean of the PSD of signal Y ( $P_{YY}(f)$ ) times the mean of the normalized PSDs:

$$SDR_{X \rightarrow Y} = \frac{mean(P_{YY}(f))}{mean(P_{XX}(f)) * mean(\frac{P_{YY}(f)}{P_{XX}(f)})}$$

$$SDR_{Y \rightarrow X} = \frac{mean(P_{XX}(f))}{mean(P_{YY}(f)) * mean(\frac{P_{XX}(f)}{P_{YY}(f)})}$$

Significantly higher SDR values give the most likely direction of causation.

---

### 2.7.3 *Spike analysis*

#### 2.7.3.1 *Multi-unit analysis*

For the detection of MUA in anesthetized and awake recordings, the signal was band-pass filtered using a third-order Butterworth filter forward and backward to preserve phase information to 500-5000 Hz frequencies. MUA was detected with a threshold of 3.5x the standard deviation of the signal. For anesthetized recordings, the firing rates (FR) of each area were calculated on the MUA signal, by dividing the total number of spikes by the signal length.

#### 2.7.3.2 *Single-unit analysis*

In order to sort the MUA into activity arising from single units spikes were detected, clustered with klusta (Rossant et al., 2016) (<https://github.com/kwikteam/klusta>) and afterwards manually curated in phy environment (<https://github.com/cortex-lab/phy>). The data were then imported into Matlab and analyzed using custom-written algorithms. For awake recordings prefrontal units were classified into fast spiking (Fs) and regular spiking (Rs) units based on their waveform and a previously set-up threshold (halfwidth < 0.31 ms, trough to peak latency < 0.64 ms) (Bitzenhofer et al., 2020). FR and inter-spike interval (ISI) were calculated for resting and movement periods respectively and for prefrontal spiking activity for Rs and Fs units separately.

#### 2.7.3.3 *Spike-LFP coupling*

To assess phase locking of spikes, it was first tested whether the spikes are significantly locked towards the LFP rhythm of interest. For anesthetized recordings, the LFP rhythms were theta rhythms of the HP and LEC. For awake recordings, the spike-LFP coupling was assessed for prefrontal spiking to prefrontal gamma rhythm (30-80 Hz), for hippocampal spiking to hippocampal theta rhythm (2-12 Hz) and for prefrontal spiking to hippocampal theta rhythm (2-12 Hz). To assess significance of locking, a previously published algorithm was used (Siapas et al., 2005). The LFP signal was filtered using a third-order Butterworth filter forward and backward to preserve phase information to the desired frequency band. The instantaneous phase was extracted using the Hilbert transform on this signal. Significance of locking was tested with the Rayleigh test for non-uniformity.

The strength of locking was assessed through the pairwise phase consistency (PPC) and calculated exclusively on the significantly locked units based on a previously published protocol (Vinck et al., 2010). The PPC is a firing rate bias free method. Like before, the LFP signal was filtered with a third-order Butterworth filter to the desired frequency bands and the instantaneous phase was extracted with a Hilbert transform. The PPC was calculated by taking the mean of the cosine of the absolute angular distance (dot product) among all pairs of phases.

#### 2.7.3.4 *Spike time tiling coefficient*

The spike time tiling coefficient (STTC) was analyzed for awake recordings according to a previously published protocol (Cutts and Eglén, 2014). The calculation of the STTC was performed as follows:

$$STTC = \frac{1}{2} \left( \frac{P_A - T_B}{1 - P_A T_B} + \frac{P_B - T_A}{1 - P_B T_A} \right)$$

$P_A$  is the proportion of spikes of a spike train A that fall within a latency of a spike of spike train B.  $T_A$  is the proportion of time that occurs within the latency from spikes of spike train A. The same applies for  $P_B$  and  $T_B$ . The latency was set to 10 ms for PFC and 100 ms for HP and interaction between the two brain areas.

## 2.8 Statistical analysis

### 2.8.1 Object recognition tasks

The statistical analyses were carried out in R Statistical Software (R Project for Statistical Computing, Austria) and Matlab environments. The data for RR were analyzed with a bootstrapped ( $n = 5000$  repetitions) heteroscedastic one way ANOVA for trimmed means and a bootstrap posthoc test (*yuenbt*, *yuend*, *t1waybt*, *mcppb20*, *glht*, *lsmeans* functions of the *WRS2*, *multcomp* and *lsmeans* R package). A standard 20% level of trimming for the mean was selected for these tests. The RR data were included in a manuscript and compared to other experimental groups (Chini et al., 2020). The NOR data were analyzed with a non-parametric Mann-Whitney-U test equivalent in Matlab (ranksum test).

### 2.8.2 Microglia inclusions

The statistical analyses were carried out in R Statistical Software (R Project for Statistical Computing, Austria) environments. Since several microglial cells were imaged in slices obtained from the same mouse, data were considered nested and analyzed with a linear mixed-effect model (LME) with animal as a random effect. Parameter estimation was performed with the *lmer* function of the *lme4* R package (Bates et al., 2014). The *summary* function (*lmerTest* R package (Kuznetsova et al., 2017)) was used to assess a significant effect between control, GE and GE<sub>mino</sub> mice. Post-hoc analysis was performed with the *emmeans* R package (Searle et al., 1980).

### 2.8.3 Anesthetized electrophysiological recordings

The statistical analyses were carried out in the Matlab environment. The data were acquired from independent samples. However, due to the low number of samples, a non-parametric test was performed. Data obtained from GE mice were directly compared to data from WT mice, making an ANOVA equivalent redundant. Therefore, the data were analyzed with a non-parametrical t-test equivalent, the Mann-Whitney-U test in Matlab (ranksum).

#### 2.8.4 Awake electrophysiological recordings

The statistical analyses were carried out in Matlab and R Statistical Software (R Project for Statistical Computing, Austria) environments. The data are considered nested and were therefore analyzed with a linear mixed-effect model (LME) with condition ( $Df(16)A^{+/-}$  / WT) and age as fixed effects and animal, sex and recording number of the animal as random effects. The parameters were estimated with the *lmer* function of the *lme4* R package (Bates et al., 2014). The *summary* function of the *lme* was used to assess a significant effect of condition (*lmerTest* R package) (Kuznetsova et al., 2017). To test for a difference between the slopes of the predicted values for each condition, the *emtrends* function of the *emmeans* R package was used (Searle et al., 1980). Differences between  $Df(16)A^{+/-}$  early adolescent (ado) and late ado mice and WT early ado and late ado mice were tested with a posthoc Tukey's t-test. Circular data were tested for significance in Matlab using the *circ\_cmtest* function.

The details for each statistical method applied as well as the results are summarized in Table 2: Detailed statistics for Figures 23-42. In scatter plots, the average is visualized as the predicted values from the linear model for  $Df(16)A^{+/-}$  and WT mice separately and with 95 % confidence interval as the shaded area. In violin plots, the data average is displayed as the median with 25- and 75-percentiles.

## 3 Results

### 3.1 Transient minocycline treatment in GE mice

The results presented in this part of the thesis (3.1) are published in Chini et al. (2020) (doi: <https://doi.org/10.1016/j.neuron.2019.09.042>). The work in this publication aimed to elucidate the circuit dysfunctions of the prefrontal cortex (PFC) in the neonatal development that might underlie disturbed gamma activity, which has been connected to neurodevelopmental disorders (Cho et al., 2015; Uhlhaas and Singer, 2015). Previous research has demonstrated that prefrontal activity already exhibits abnormalities in neonatal development in dual-hit mice combining a genetic (G) and an environmental hit (E), as a maternal immune activation (MIA) (Hartung et al., 2016b). Other experiments carried out within the scope of the study by Chini et al. (2020) revealed an inability of prefrontal neurons to organize the beta-gamma entrainment of prelimbic (PL) circuits. Furthermore, reduced dendritic branching and numbers of synapses in prefrontal pyramidal neurons was shown. This resulted in the supposition that microglial activity was involved in the abnormal development of the prefrontal circuits in this mouse model.

#### *3.1.1 Transient minocycline treatment in GE mice can rescue enhanced microglia function*

Microglial cells are the active macrophages of the brain and hence the foundation of its immune system (Mosser et al., 2017). Besides this function, microglia shape neural networks by removing synapses between neurons that are not active together (Hammond et al., 2018). During development, they play a key role not only in the remodeling and engulfing of synapses, but also by regulating synapse formation in the developing brain. Abnormal development of microglial cells, which can be induced by MIA, can have effects into adulthood and has been linked to mental illness. Minocycline a tetracyclic antibiotic with anti-inflammatory properties, has shown promising results in the treatment of mental disorders, reducing the stress-induced inflammatory response of microglia (Garrido-Mesa et al., 2013; Sellgren et al., 2019; Zhang et al., 2018).

The number and morphology of microglial cells in the PL of dual-hit GE mice were shown to be severely abnormal. Accordingly, their number and size are enhanced in GE mice, while roundness is reduced, which was rescued by the administration of minocycline (Chini et al., 2020).

In order to gain further insights into the functional implications of microglial cells in the context of neurodevelopmental disorders, experiments were conducted to evaluate the engulfment of synaptic material by microglia. To accomplish this objective, the staining of brain slices of GE, control and GE<sub>mino</sub> mice with the microglia-specific ionized calcium-binding adapter molecule 1 (IBA-1), which is located in the cytoplasm of microglial cells, was conducted (Deininger et al., 2002). In the same brain slices, Vesicular glutamate transporter 1 (VGLUT1), a protein

---

associated with the membrane of synaptic vesicles, was stained (Oni-Orisan et al., 2008). The images acquired from both stainings (IBA-1 staining in red, VGLUT1 staining in green) were merged and an overlay was created (Figure 3, A). The microglia cells and VGLUT1 puncta were reconstructed in each image plane of the acquired z-stack, as depicted in Figure 3, B. In the subsequent step of the 2D reconstruction, 3D reconstructions of microglial cells and VGLUT1 puncta that were completely overlaid were extracted (Figure 3, C). This reconstruction was performed for all microglial cells obtained for each of the three groups to compare distal cell volume and engulfment in control, GE and GE<sub>mino</sub> mice.

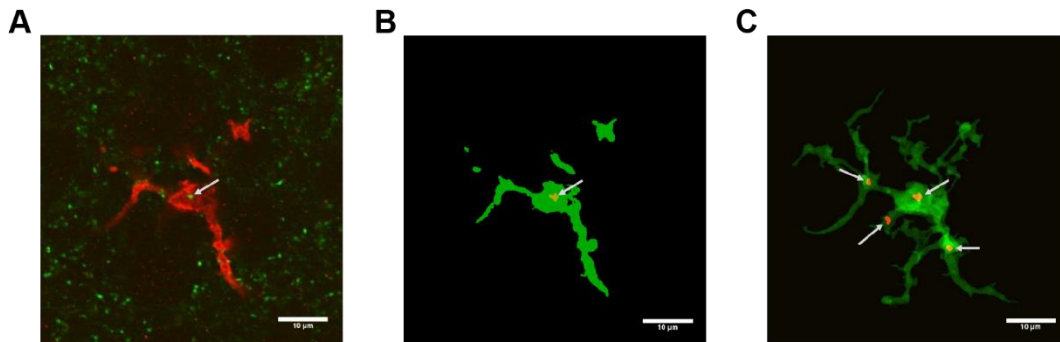


**Figure 3: Representation of microglia engulfment analysis.** (A) Acquisition of an Iba1-stained microglial cell (red) and VGlut-stained synaptic puncta (green). (B) Reconstruction of microglia (green) and engulfed puncta (yellow-red) in one image plane. (C) 3D reconstruction of a microglia (green) and engulfed puncta (yellow-red) used to calculate microglial cell volume, as well as number and volume of inclusions.

Examples of microglial cells detected in each of the three groups are shown in Figure 4. The 3D reconstruction of the microglial cells allowed for the analysis of the distal cell volume of the microglial cells, which serves as a proxy for the protrusions of the cells. Furthermore, the number and volume of inclusions of VGLUT1 puncta, as proxies for synaptic pruning, could be evaluated in neonatal mice of the three groups.

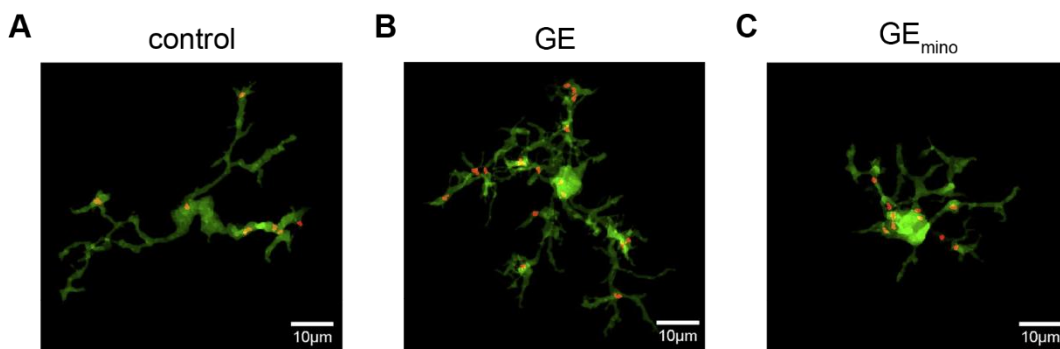


**Figure 4: Examples of 3D reconstructed microglial cells with inclusions of VGLUT puncta in the three conditions.** (A) Example of a microglia in the PFC of a neonatal control mouse. (B) Microglia in the PFC of a neonatal GE mouse. (C) Example of a 3D reconstructed microglia in the PFC of a neonatal GE mouse, treated with minocycline from postnatal day (P) 1 to P8. Microglia are illustrated in green, VGLUT puncta in yellow-red.

The distal cell volume of microglia in GE mice (n=52 cells) is significantly higher than in GE<sub>mino</sub> mice (n = 55 cells, p = 0.008) and, to a lesser extent, also higher than in control mice (n

= 53 cells,  $p = 0.072$ ) (Figure 5, C). The microglial cells of controls and GE<sub>mino</sub> mice show no difference in the volume of inclusions ( $p = 0.323$ ) (Figure 5, B). The number of inclusions is also higher in GE mice than in controls ( $p = 0.006$ ) and in GE<sub>mino</sub> mice ( $p = 0.08$ ). In addition, the volume of inclusions is increased in GE mice compared to controls ( $p = 0.006$ ) and GE<sub>mino</sub> mice ( $p = 0.08$ ) (Figure 5, A).

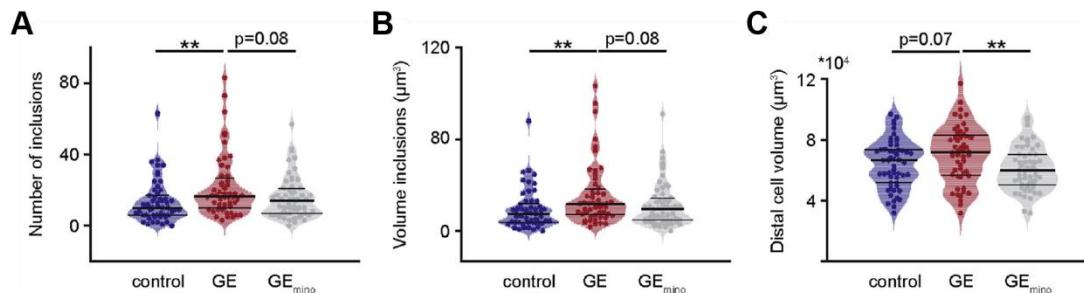


**Figure 5: Phagocytic activity of microglial cells in GE mice, GE mice treated with minocycline and control mice.** (A) Violin plot displaying the number of inclusions per microglial cell in the PFC of control (blue;  $n = 53$  cells from 4 mice), GE (red;  $n = 52$  cells from 4 mice), and GE<sub>mino</sub> mice (gray;  $n = 55$  cells from 4 mice). (B) + (C) Same as (A) but for the volume of inclusions per microglia and the distal volume of microglial cells. Data are presented as median with 25<sup>th</sup> and 75<sup>th</sup> percentiles. Individual data points are shown as asterisks. The shaded area represents the probability distribution of the variable. \*  $p < 0.05$ , \*\*  $p < 0.01$ , \*\*\*  $p < 0.001$ , linear mixed-effect model.

These findings indicate that minocycline administration during the proposed critical period of P1–8 partially restores the functional alterations microglial cells exhibit in the neonatal dual-hit GE mice.

### 3.1.2 Transient minocycline treatment during later development cannot rescue abnormal recognition memory

In previous investigations, and in accordance with the aforementioned publication, it had been demonstrated that prejuvenile GE mice exhibit altered behavioral abilities (Chini et al., 2020; Hartung et al., 2016b). This was evaluated using novelty recognition paradigms (Figure 6). These tasks are based on the innate drive of mice to explore novel stimuli over familiar ones, and have been shown to rely on a functional prefrontal-hippocampal network (Barker and Warburton, 2011; Krüger et al., 2012; Warburton and Brown, 2015). The tasks are divided into familiarization and testing phases. In the novel object recognition test (NOR), the interaction time with one familiar object is compared to the interaction time with one novel object (Figure 6, A). In the recency recognition test (RR), the interaction time with a less recent object is compared to the interaction time with a more recently familiarized object (Figure 6, B). These paradigms do not require prior training or rely on food or water deprivation, and therefore are suitable for prejuvenile mice still undergoing development (Krüger et al., 2012). In this study, control mice and GE mice treated with minocycline during the later period (P9-16) were tested. In previous experiments, it had been demonstrated that minocycline treatment during the P1-8 period rescued behavioral deficits the GE mice showed in the RR test (Chini et al., 2020). Chini et al. (2020) also reported that mice spent the same amount of time examining the two identical objects during the familiarization phases.

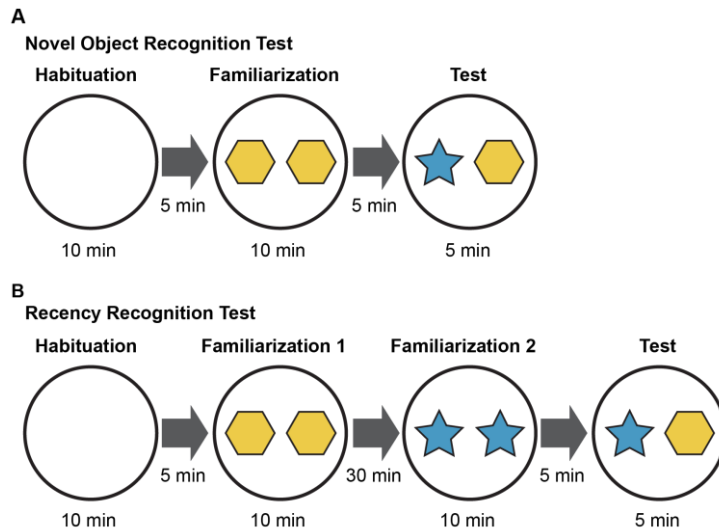


**Figure 6: Object Recognition Paradigms.** (A) Schematic representation of the Novel Object Recognition Test (NOR). (B) Schematic representation of the Recency Recognition Test (RR).

In the NOR, mice were presented with two identical objects to freely explore for 10 min. The heatmaps depicting the mean of all mice within a group illustrate the duration of interaction with each object.

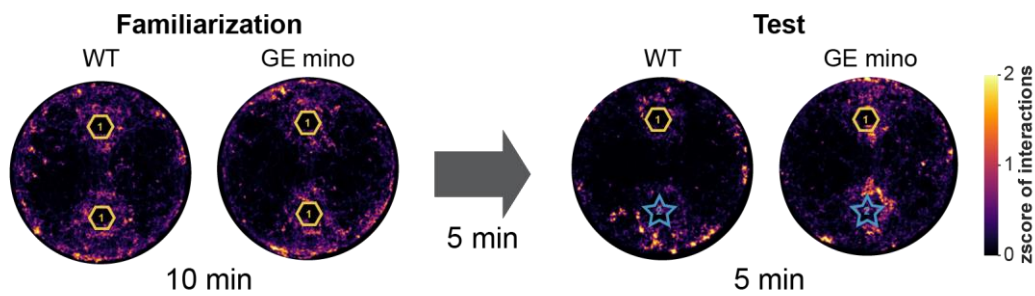


**Figure 7: Interaction with the objects in the NOR.** Heatmaps of the time spent in each position of the arena as mean of all mice of one condition. Left, during the familiarization phase of the task and right, during the test phase with one familiar and one novel object.

During the familiarization phase, both WT control mice and  $GE_{\text{mino late}}$  mice spent a comparable amount of time exploring both objects, whereas control mice devoted more time to the novel object during the test phase (Figure 7).

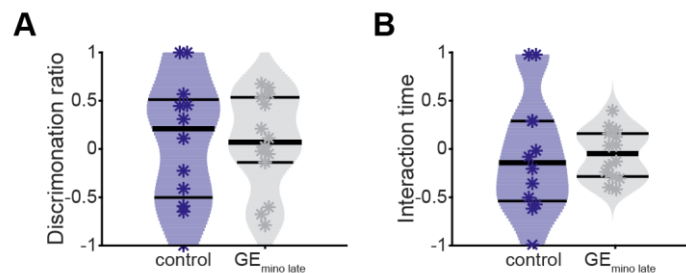


**Figure 8: NOR in WT and GE mice treated with minocycline during P9 to P16.** (A) Violin plot displaying the DR of WT (blue;  $n = 16$ ), and  $GE_{\text{mino late}}$  mice (gray;  $n = 15$ ). (B) Violin plot displaying the interaction time of WT and  $GE_{\text{mino late}}$  mice.

## Results

Data are presented as median with 25<sup>th</sup> and 75<sup>th</sup> percentiles. Individual data points are shown as asterisks. The shaded area represents the probability distribution of the variable. \*  $p < 0.05$ , \*\*  $p < 0.01$ , \*\*\*  $p < 0.001$ , Mann-Whitney-U test.

The quantitative comparison of the time spent with the novel object and the time spent with both objects, interpreted as the discrimination ratio (DR), did not reveal any significant differences between the two groups (Figure 8, A). The same hold true for the length of single interaction times (Figure 8, B).

These findings are in line with previous results, as no differences in the NOR were reported between WT and untreated GE mice either (Chini et al., 2020).

The picture appears to be different for the RR. In this task, GE mice exhibit a significantly lower DR, which is rescued by treatment with minocycline during P1-8 (Chini et al., 2020). To determine whether minocycline treatment at a later stage also alleviates behavioral deficits, the RR was evaluated in both control and GE mice treated with minocycline from P9 to P16. The heatmaps depicting the mean of all mice within a group illustrate the duration of interaction with each object, indicating a similar interaction time during the familiarization trials but not in the test trial in the control mice (Figure 9).

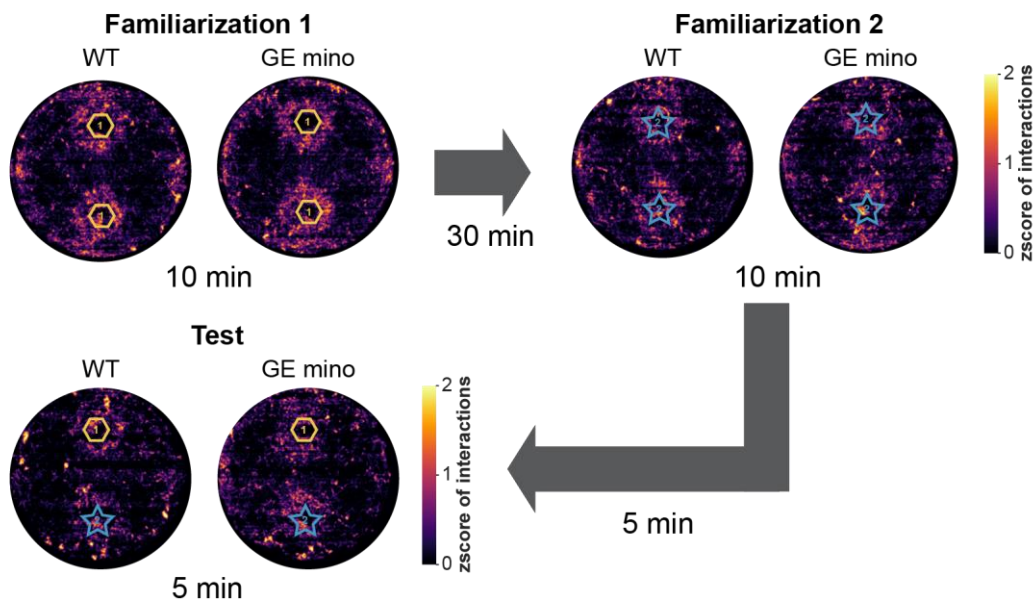


**Figure 9: Interaction with the objects in the RR.** Heatmaps of the time spent in each position of the arena as mean of all mice in one condition. Upper left, during the first familiarization phase of the task, upper right, during the second familiarization phase of the task and lower left, during the test phase with one object from each familiarization phase.

A quantitative analysis of the DR and single interaction time showed that the  $GE_{\text{mino late}}$  mice ( $n=16$ ) had a significantly lower DR of the less recently familiarized object than the control mice ( $n = 15$ ,  $p = 0.037$ ) (Figure 10, A). The single interaction time was not significantly different between the two groups (Figure 10, B). The results obtained with the  $GE_{\text{mino late}}$  mice are comparable to those obtained with the untreated GE mice.

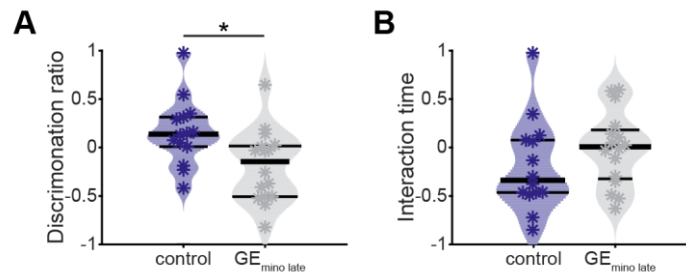


**Figure 10: RR in WT and GE minocycline treated mice during P9 to P16.** (A) Violin plot displaying the DR of WT (blue;  $n = 16$ ), and GE<sub>minocycline</sub> mice (gray;  $n = 15$ ). (B) Violin plot displaying the interaction time of WT and GE<sub>minocycline</sub> mice.

Data are presented as median with 25<sup>th</sup> and 75<sup>th</sup> percentiles. Individual data points are shown as asterisks. The shaded area represents the probability distribution of the variable. \*  $p < 0.05$ , \*\*  $p < 0.01$ , \*\*\*  $p < 0.001$ , robust, bootstrapped ANOVA.

Together with previously described effects, these results indicate that the timing of minocycline treatment is crucial for the rescue of novelty recognition memory in dual-hit GE mice (Chini et al., 2020).

### 3.2 Prefrontal-hippocampal-entorhinal network activity during prejuvenile development in anesthetized dual-hit GE mice

The prefrontal-hippocampal network is crucial for cognitive abilities (Miller, 2000; Miller and Cohen, 2001). Previous research has shown that the prefrontal-hippocampal network is disturbed in neonatal and juvenile dual-hit GE mice (Hartung et al., 2016b; Oberlander et al., 2019; Xu et al., 2019; Xu et al., 2021a). During neonatal development, the lateral entorhinal cortex (LEC) influences this network, projecting to the PFC as well as to the HP and facilitating their oscillatory entrainment (Hartung et al., 2016a). To investigate the prefrontal-hippocampal-entorhinal network during prejuvenile development, electrophysiological recordings of local field potential (LFP) and multi-unit activity (MUA) were performed simultaneously in the PL, cornu ammonis 1 (CA1) and LEC in P16-26 WT and GE mice under urethane anesthesia.

#### 3.2.1 LFP and MUA in PFC, HP and LEC are not different in prejuvenile GE mice compared to WT mice

Previous investigations showed altered oscillatory and firing activity within the PL of neonatal GE mice (Chini et al., 2020). To determine whether the abnormal electrophysiological activity patterns persist into subsequent developmental phases and are present in the HP or LEC during prejuvenile development, power and firing rate (FR) were assessed in each brain region. The observed oscillatory activity patterns were similar in all mice and correlated with sleep-like rhythms under urethane anesthesia (Clement et al., 2008; Pagliardini et al., 2013).

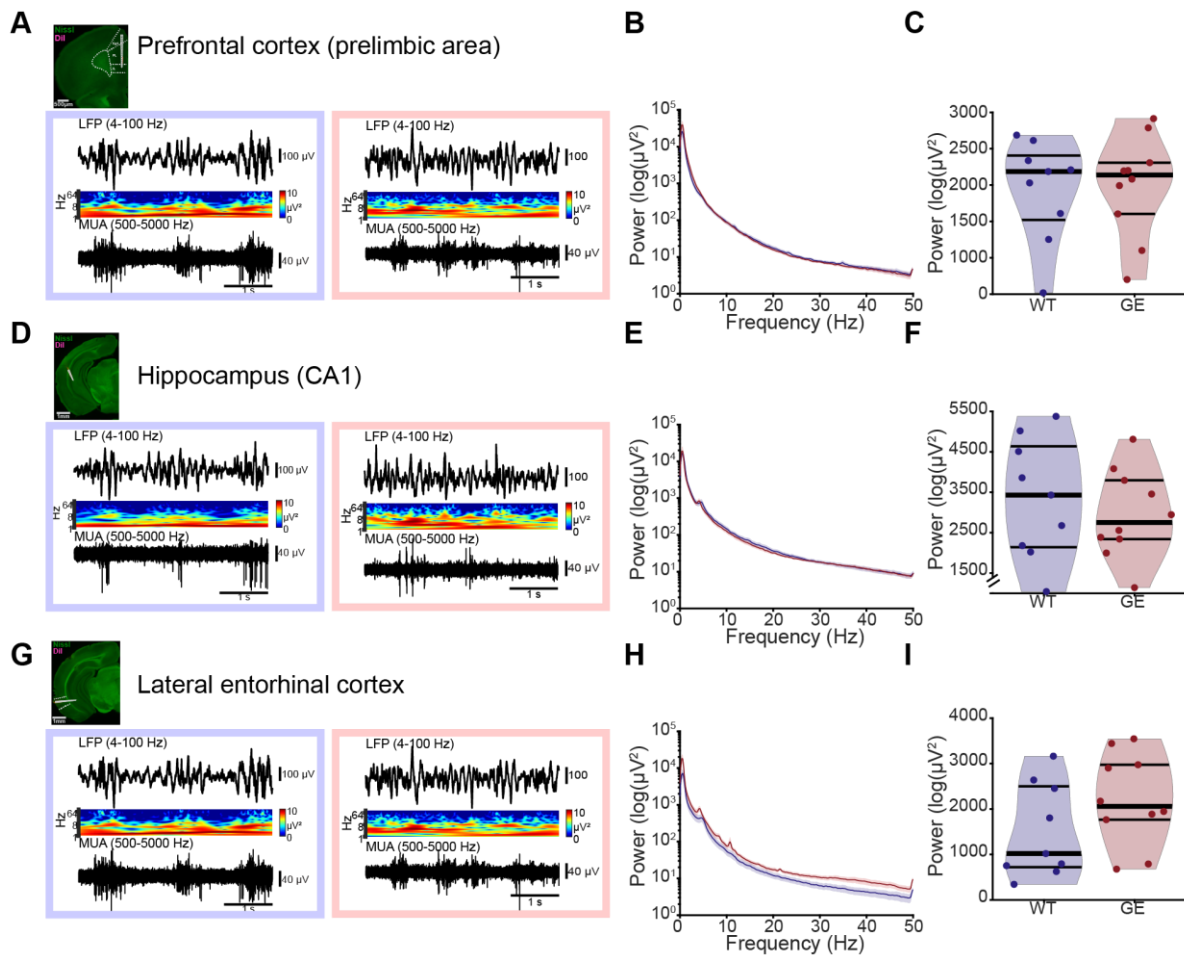


**Figure 11: Prefrontal LFP activity in juvenile GE and WT mice.** (A) Examples of recordings of LFP and MUA in the PL of one WT and one GE mouse. The LFP filtered to 4-100Hz, wavelet spectrum for 2-64 Hz and MUA filtered to 500-5000 Hz for a 5 s period are shown. (B) Power spectrum for 1-50 Hz in log scale for WT (blue,  $n=9$ ) and GE mice (red,  $n=10$ ). (C) Violin plot displaying the mean power in 4-40 Hz spectrum in WT and GE mice. (D) + (G) Same as (A) but for HP and LEC respectively. (E) + (H) Same as (B) but for HP and LEC respectively. (F) + (I) Same as (C) but for HP and LEC respectively.

In (C), (F) and (I) data are presented as median with 25<sup>th</sup> and 75<sup>th</sup> percentiles. Individual data points are shown as dots. The shaded area represents the probability distribution of the variable. \*  $p<0.05$ , \*\*  $p<0.01$ , \*\*\*  $p<0.001$ , Mann-Whitney-U test.

Electrophysiological activity patterns in the PL in WT ( $n = 9$ ) and GE mice ( $n = 10$ ) appeared to be similar to each other (Figure 11, A). Accordingly, the oscillatory broad-band power in the 1-50 Hz spectrum did not differ between the two groups (Figure 11, B). The quantitative analysis of the power spectrum at 4-40 Hz revealed no significant disparity in the oscillatory activity between WT and dual-hit GE mice ( $p = 1$ ). Similarly, the electrophysiological patterns recorded in the CA1 of WT and GE mice showed no gross differences (Figure 11, D). The power spectrum for 1-50 Hz frequencies was also similar (Figure 11, E) and the mean power quantification of the frequency range from 4-40 Hz did not show a significant difference between WT and GE mice ( $p = 0.6$ ) (Figure 11, F). As a third area, the LEC was investigated. The electrophysiological patterns appear enhanced at first glance in the dual-hit GE mice (Figure 11, G). Similarly, the power spectrum of 1-50 Hz of GE mice is slightly enhanced compared to WT mice (Figure 11, H). However, this did not reach significance levels;

accordingly, LEC power is not significantly different between the two groups in this spectrum ( $p = 0.18$ ) (Figure 11, I) or in 30-50 Hz ( $p = 0.11$ ) (not shown).

In addition to the LFP, the spiking activity provides information regarding the local network activity within a specific brain region. Similar to the LFP activity, the firing activity of the three areas assessed as multi-unit FR in spikes per second was not different in any of the areas. However, there was a trend towards an enhanced FR in the LEC (PL:  $p = 0.55$ , HP:  $p = 0.32$ , LEC superficial layers:  $p = 0.06$ , LEC deep layers:  $p = 0.06$ ) (Figure 12).

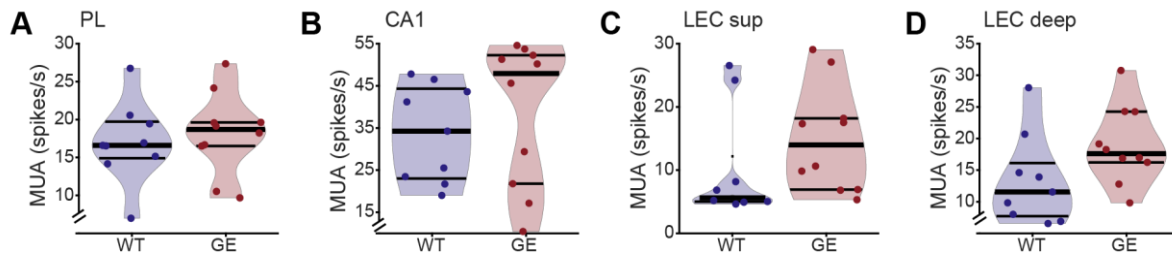


**Figure 12: Multi-unit firing activity in juvenile WT and GE mice.** (A) Violin plot displaying the MUA in the PL of WT (blue,  $n=9$ ) and GE mice (red,  $n=10$ ). (B) Violin plot displaying the MUA in the CA1 of WT (blue,  $n=9$ ) and GE mice (red,  $n=10$ ). (C) Violin plot displaying the MUA in the superficial layers of LEC of WT (blue,  $n=9$ ) and GE mice (red,  $n=10$ ). (D) Violin plot displaying the MUA in the deep layers of LEC of WT (blue,  $n=9$ ) and GE mice (red,  $n=10$ ).

Data are presented as median with 25<sup>th</sup> and 75<sup>th</sup> percentiles. Individual data points are shown as dots. The shaded area represents the probability distribution of the variable. \*  $p < 0.05$ , \*\*  $p < 0.01$ , \*\*\*  $p < 0.001$ , Mann-Whitney-U test.

These results imply that within the three areas the local electrophysiological activity is not grossly different between prejuvenile WT and dual-hit GE mice.

### 3.2.2 Synchrony between prefrontal cortex and hippocampal formation is augmented in prejuvenile GE mice

Even though the power and firing rates within each area are not different in prejuvenile GE mice to WT mice, this does not mean that the network activity is as well. Neuronal activity gives rise to oscillations. Synchronized oscillations and brain activity enable an efficient and flexible transfer of information between brain areas and thus long-range communication (Buzsáki et al., 2012; Buzsáki and Draguhn, 2004; Buzsáki and Watson, 2012). The communication and synchrony in the prefrontal-hippocampal network under entrainment of the LEC is proposed to be relevant for memory function (Colgin et al., 2009). Therefore, oscillatory synchrony between the three areas was evaluated.

Analysis of imaginary coherence between the three areas revealed an enhanced synchrony between PL-HP, PL-LEC and HP-LEC in slow frequencies of 3-8 Hz. This peak was subsequently quantified. Between the LEC and PL, prejuvenile GE mice showed an augmented imaginary coherence ( $p = 0.007$ ). In contrast, neither the imaginary coherence between the HP and PL nor between the LEC and HP is significantly different between WT and GE mice ( $p = 0.11$  and  $p = 0.72$ ) (Figure 13).

## Results

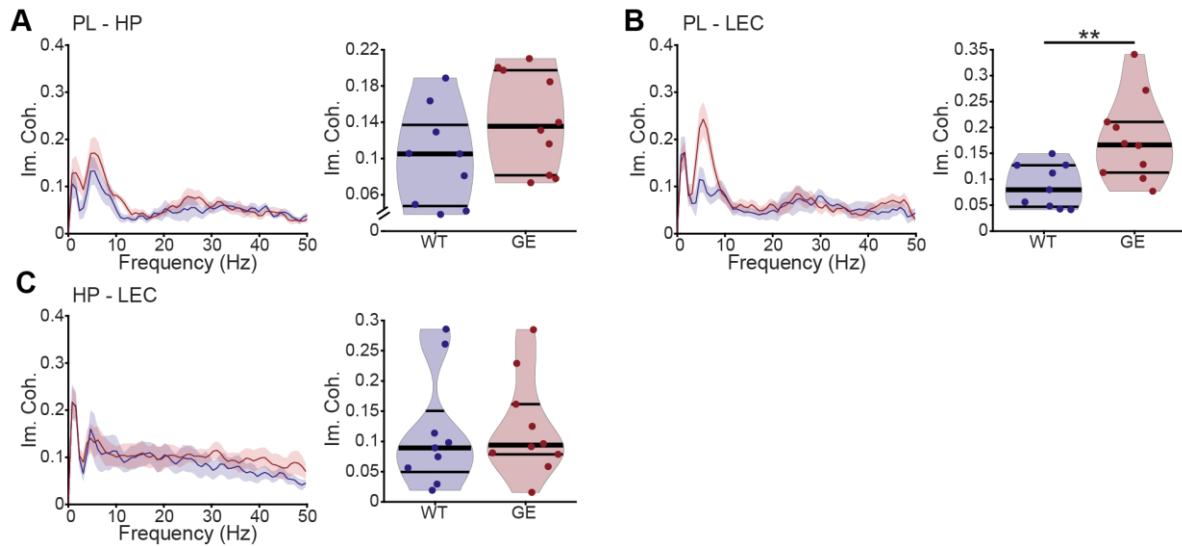


**Figure 13: Synchrony in LFPs between the PL, CA1 and LEC.** (A) Left, spectrum of imaginary coherence between the PL and CA1. Right, violin plot displaying the mean imaginary coherence in 3-8 Hz in WT (blue, n=9) and GE mice (red, n=10). (B) Left, spectrum of imaginary coherence between PL and LEC. Right, violin plot displaying the mean imaginary coherence in 3-8 Hz in WT and GE mice. (C) Left, spectrum of imaginary coherence between the CA1 and LEC. Right, violin plot displaying the mean imaginary coherence in 3-8 Hz in WT and GE mice.

In the right plots of (A), (B) and (C) data are presented as median with 25<sup>th</sup> and 75<sup>th</sup> percentiles. Individual data points are shown as dots. The shaded area represents the probability distribution of the variable. \* p<0.05, \*\* p<0.01, \*\*\* p<0.001, Mann-Whitney-U test.

As the imaginary coherence analysis revealed a peak in theta frequency between all areas and prefrontal spikes are entrained by the hippocampal theta rhythm, spike-phase synchrony by pairwise-phase consistency (PPC) was assessed in the theta frequency as a second, more in-depth synchrony measure (Siapas et al., 2005).

Prejuvenile GE mice exhibited a significantly higher locking of prefrontal spikes to hippocampal theta ( $p = 0.009$ ) as well as to entorhinal theta rhythm ( $p = 0.038$ ). However, entrainment of hippocampal spikes by entorhinal theta rhythm was not significantly different in GE mice than in WT mice ( $p = 0.6$ ) (Figure 14).

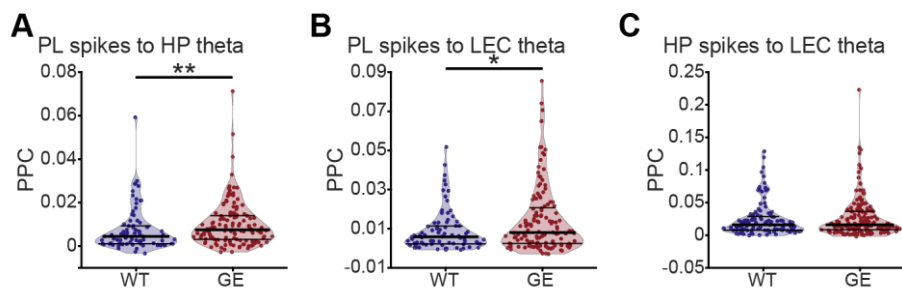


**Figure 14: Synchrony in firing and LFP across areas.** (A) PPC of prefrontal units to hippocampal theta rhythm in WT (blue, n=9) and GE mice (red, n=10). (B) PPC of prefrontal units to entorhinal theta rhythm in WT and GE mice. (C) PPC of hippocampal units to entorhinal theta rhythm in WT and GE mice.

Data are presented as median with 25<sup>th</sup> and 75<sup>th</sup> percentiles. Individual data points are shown as dots. The shaded area represents the probability distribution of the variable. \* p<0.05, \*\* p<0.01, \*\*\* p<0.001, Mann-Whitney-U test.

These findings show that entrainment of the prefrontal-hippocampal network is disturbed in prejuvenile GE mice, especially in synchrony of the HP and LEC with the PFC. This disturbed development of synchrony between the three areas could have implications for behavioral dysfunctions in neurodevelopmental disorders.

### 3.3 Establishment of delayed non-match to sample working memory task on the MobileHomeCage

Adolescence is considered a vulnerable period regarding the development of the PFC. The PFC undergoes a prolonged maturation compared to sensory and subcortical brain areas (Chini and Hanganu-Opatz, 2021; Klune et al., 2021). Alongside the reorganization in function, structure and morphology during this life period, cognitive abilities arise and progress (Klune et al., 2021). One of these abilities is working memory, which is hypothesized, to linearly increase during adolescence and is reportedly disturbed in neurodevelopmental disorders (Chini and Hanganu-Opatz, 2021; Sigurdsson and Duvarci, 2016). To investigate the development of working memory abilities and relate this to the functional development of the prefrontal-hippocampal network, attempts were made to establish a delayed non-match to sample (DNMS) T-Maze task for head-fixed adolescent mice on the MobileHomeCage.



**Figure 15: Recording procedure.** Schematic representing the recording procedure and possible movement on the MobileHomeCage.

In this system, round, carbon platforms with a diameter of 290 mm and a wall height of 15 mm for open field assessment and with a diameter of 330 mm and the same wall height for the working memory task are air-lifted. The floor is covered with a Depron foam mat to allow for better grip and therefore easier movement. The inherent characteristics of this system permit the head-fixed mice to move in any direction, thereby emulating free spatial orientation and locomotion (Figure 15).

The DNMS task for head-fixed mice is adapted from a protocol for freely-moving mice (Bitzenhofer et al., 2021; Sigurdsson et al., 2010). Here a paradigm in a Y- or T-Maze is utilized. The protocol used with the freely-moving mice is depicted in the upper row of Figure 16. In this task, the mice are placed into one arm of the maze, which is considered the start zone throughout the entire task. After a habituation phase in the maze in which the mice are allowed to explore all three arms of the Y-maze freely, they are transferred back to the start zone for the actual task. In the sample phase, one arm of the maze is closed and the mice are trained to run into the open arm, at the end of which they receive a reward. After consumption of the reward

and a short delay, they are placed back into the start zone, now with both arms open. In the test phase, a visit to the arm that was not visited in the sample phase is rewarded. After the mice successfully completed at least 7 out of 10 consecutive trials, the mice were considered to have learned the task. The criterion was reached when the correct performance of the 7 out of 10 trials was achieved on three consecutive days.

This basic protocol of a sample, delay and test phase was retained and transferred to the round T-Maze used for the head-fixed DNMS task (Figure 16).

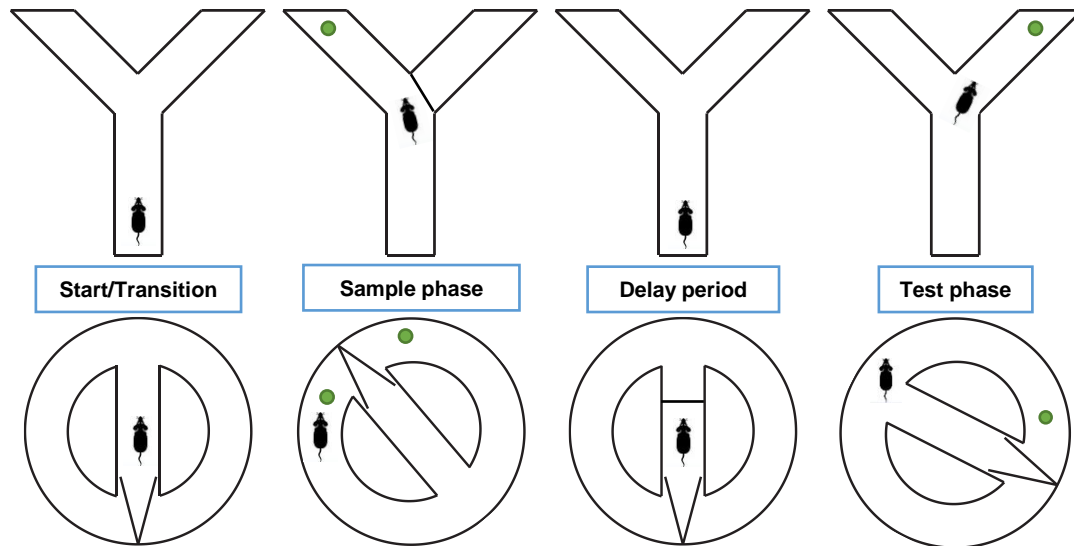


**Figure 16: Schematic representation of DNMS task.** Upper panels, representation of Y-Maze task in freely moving animals in comparison to the same task in head-fixed conditions on the MobileHomeCage in a round arena, lower panels.

The carbon maze with depron mat floor was obtained from Neurotar (Helsinki, Finland) and modified to meet the needs of the task. The original maze consisted of a round depron mat with a carbon wall at a height of 15 mm, two insets creating a maze and a swing door, which prevents mice from going back in the direction they came from. The maze was modified to include a door in the outer wall to allow a transition from the open field round maze to the T-Maze, with the mouse remaining head-fixed. Additional inner walls were also added to make it easier for the mice to swing the door open and to take away corner space in which to hide (Figure 17, A). To align the task phases, the Locomotion tracking software was customized to send TTL outputs to distinct channels of the recording amplifier depending on the position of the mouse in the maze. For this purpose, the maze was digitally divided into four distinct zones, namely the 'waiting/starting area', two 'reward zones', and the 'decision zone' (Figure 17, B). Entry into each of these zones triggered a TTL output to a distinct channel in the amplifier. Additionally, the software tracked the movement of the mouse and sent a TTL for movement to another amplifier channel.

The reward was delivered in liquid form over a lick-port fixed to the clamp system for the headplate fixation. Reward delivery was triggered manually and controlled with a syringe pump. At the same time that the reward delivery was initiated, a TTL was transmitted to the amplifier.

In addition to the tracking with the Locomotion tracking software, the mouse's behavior was

observed using a camera, which was also utilized to align the signal with the start of a new trial within the task.

The electrophysiological signal of LFP and MUA could be synchronized with the task phases, reward delivery and commencement of new trials by incorporating those additional signals. (Figure 17, C).

Generally, all experiments to establish the DNMS T-Maze task consisted of a pre-implantation phase, a pre-training after implantation and the actual training phase. In the pre-implantation phase, the mice were regularly handled by the experimenter and accustomed to the reward used in the task. The pre-training phase was conducted on the MobileHomeCage and comprised of a habituation to the head-fixed movement in the open field maze and an acclimatization to the T-Maze, both without and with the door, incorporating reward delivery in the reward zones to familiarize the mice with the lick-port and zones. As previously described, the actual training sessions consisted of the sample, delay and test phases. The delay phase was set to 30 sec and the inter-trial interval to 90 sec.

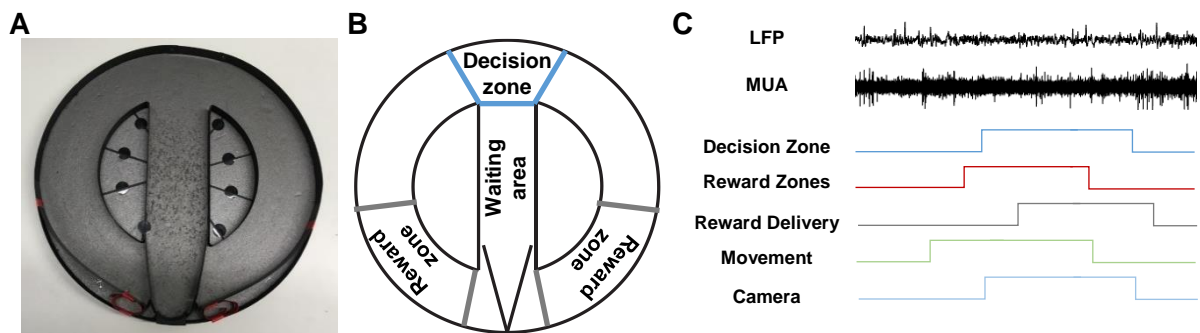


**Figure 17: T-Maze modifications and alignment with recording.** (A) Photograph of the modified T-Maze from Neurotar that was used for the experiments. (B) Schematic representation of the T-Maze with the different zones the mice enter during the task. (C) Schematic representation of alignment of the location of the mouse in the zones with the electrophysiological recording.

The first round of experiments to establish the DNMS T-Maze task on the MobileHomeCage were performed in teamwork with a lab rotation student, Magdalena Rados, who carried out the training of the mice under my supervision. As it was planned to perform the task as early as can be achieved in adolescent development, the aim was to shrink the pre-training protocol to as few days as possible. Therefore, the first two groups underwent three days of pre-training, consisting of one day of open field, T-Maze without door and T-Maze with door, respectively. Here, all experiments were carried out under food restriction with a food delivery of 2.5 g chow per mouse per day for 3 days before the training sessions. In the first two groups, condensed milk was used as a reward. In the sample phase of the actual training sessions, one arm was closed with a removable cardboard wall. The same wall was used to close the waiting area during the delay phase and the inter-trial interval. As the mice often struggled to open the swing door or refused to move for a long time, some trials were ‘helped’, meaning the T-Maze was pushed slightly to initiate movement of the mice. Trials were terminated after 3 min of the mouse not entering one of the arms in the sample and test phases. In the first group, the ratio of ‘helped’ trials was high across the training sessions, with the animals showing no learning effects (Figure 18, A). Therefore, in the second group, assistance was only given during the first days of training. However, this resulted in a high number of terminated trials and, at day

6, a mixture of terminated and ‘helped’ trials. This led to the termination of training at day 6 of this experimental group without a learning effect (Figure 18, B).

Accordingly, several adjustments were made for the third group. The age of the mice was increased to above P40, as it had been shown previously that P40 mice can learn this task in freely-moving conditions (Bitzenhofer et al., 2021). In addition, the reward was switched to sweetened condensed milk diluted in water, and habituation to the T-Maze without the door was increased to three sessions. This led to increased performance in the mice with fewer ‘helped’ trials (Figure 18, C).

As the mice showed an actual learning curve in the third group of these experiments, this protocol was used for the next approach. However, in this approach (Approach 2), no trials were ‘helped’ with the initiation of movement anymore; only the transition from the reward zone to the waiting area through the door was assisted.

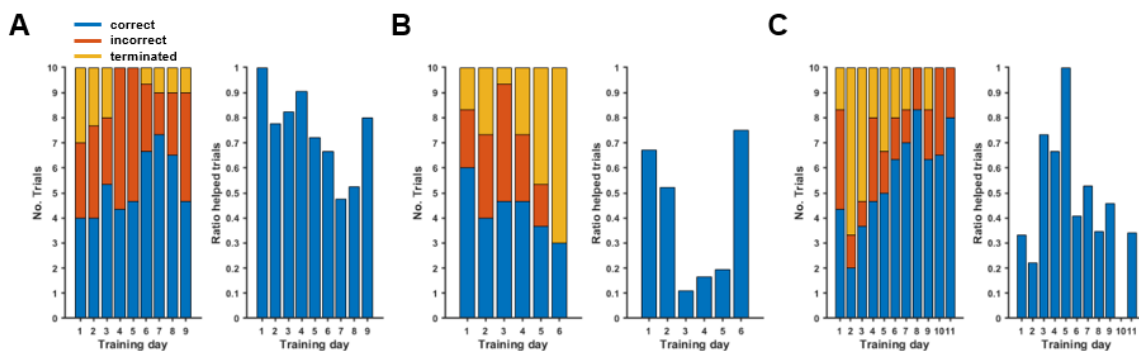


**Figure 18: First round of experiments to establish the T-Maze task.** (A) Left, number of successful (blue), unsuccessful (orange) and terminated (yellow) trials in the first pilot experimental group. Right, number of trials that were assisted through a little push to initiate movement. (B) Left, mean number of successful, unsuccessful and terminated trials in the second pilot experimental group. Right, mean number of trials that were assisted through a little push to initiate movement. (C) Left, number of successful, unsuccessful and terminated trials in the third pilot experimental group. Right, number of trials that were assisted through a little push to initiate movement.

As the mice did not reach the success criteria in the first round of T-Maze experiments, some things were amended in the previous protocol. To enhance the motivation of the mice, the restriction was switched from food restriction to citric acid water restriction, as summarized for several studies in (Barkus et al., 2022). The cardboard walls used to close one arm during the sample phase and the waiting area were switched to carbon walls to resemble the appearance of the maze. The removal of the walls was done using long forceps. In this second approach, the pre-training was gradually enhanced up to 10 open field habituations, up to three times T-Maze without the door and three times T-Maze with the door. The mice were subsequently trained for 6 to 10 days, depending on the number of terminated trials. This group exhibited no discernible learning curve when examining terminated trials as well (Figure 19, A). However, most performed trials were done correctly, with no clear bias for either side of the maze (Figure 19, B). Nonetheless, most mice had a high number of terminated trials, and the success rate was rather low (Figure 19, D). Additionally, the training time would have been suitable for late adolescent and early adult mice, but not for the younger, prejuvenile mice (P20-25).

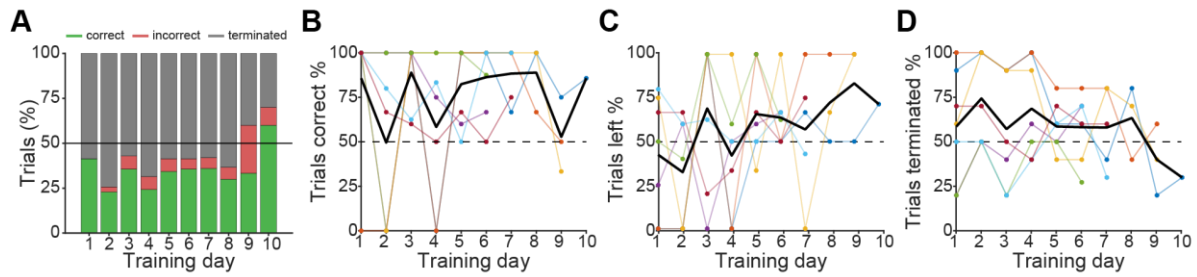


**Figure 19: Second approach to establish the T-Maze task in head-fixed conditions with experimental group 1.** (A) Bar graph displaying the mean number of successful, unsuccessful and terminated trials of the experimental group 1 (n=7). (B) Mean correct trials across training days as a learning curve. The learning curves of individual animals are displayed in different colors, the mean learning curve is displayed in black. (C) Number of trials in which the animals turned left in the test trial across training days. The curves of individual animals are displayed in different colors, the mean curve is displayed in black. (D) Number of trials that were terminated because the mice did not move within the time limit. The curves of individual animals are displayed in different colors, the mean curve is displayed in black.

As a result of the previously reported outcomes, a slight modification was made to the protocol to reduce the required number of days for training. To accomplish this, the overall number of pre-training sessions remained constant, but additional training sessions were carried out on the same day. Accordingly, the last six open field habituation sessions were performed right before the T-Maze habituation. Nevertheless, the number of terminated trials was still too high and increased across training sessions (Figure 20, A+D). The mice did not learn the task, and showed no bias for either side of the maze (Figure 20, B+C).

This suggests that the motivation of mice was too low, and the number of pre-training and training days was still too long to for young mice to perform the task.

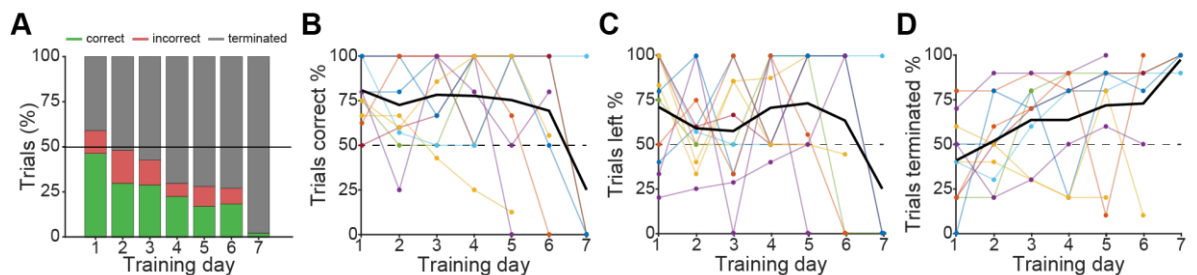


**Figure 20: Third approach to establish the T-Maze task in head-fixed conditions with experimental group 2.** (A) Bar graph displaying the mean number of successful, unsuccessful and terminated trials of the experimental group 2 (n=11). (B) Mean correct trials across training days as a learning curve. The learning curves of individual animals are displayed in different colors, the mean learning curve is displayed in black. (C) Number of trials in which the animals turned left in the test trial across training days. The curves of individual animals are displayed in different colors, the mean curve is displayed in black. (D) Number of trials that were terminated because the mice did not move within the time limit. The curves of individual animals are displayed in different colors, the mean curve is displayed in black.

To enhance the motivation of the animals, further adjustments to the protocol were implemented. After consultation with other scientists performing learning tasks in the research center, the reward was changed to corn oil without any restrictions. As a subsequent step, the experiments were performed from 3a.m. to 7a.m. to coincide with the end of the dark phase of the mouse day. The mice were housed in a 7a.m.-7p.m. 12 hr light and 7p.m.-7a.m. 12 hr dark cycle. The pre-training was performed as described in the previous approach.

This reduced the number of terminated trials (Figure 21, A+D). However, it did not enhance performance (Figure 21, B+C).

This indicates that the corn oil reward and the execution of the task in the dark phase might enable the task to be established.

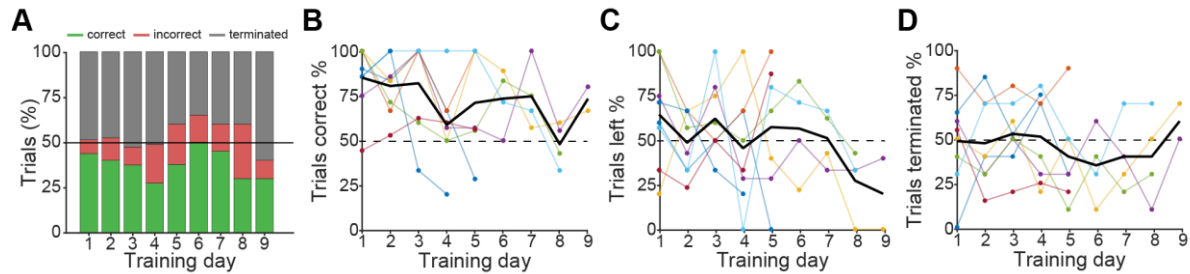


**Figure 21: Fourth approach to establish the T-Maze task in head-fixed conditions with experimental group 3.** (A) Bar graph displaying the mean number of successful, unsuccessful and terminated trials of the experimental group 3 (n=8). (B) Mean correct trials across training days as a learning curve. The learning curves of individual animals are displayed in different colors, the mean learning curve is displayed in black. (C) Number of trials in which the animals turned left in the test trial across training days. The curves of individual animals are displayed in different colors, the mean curve is displayed in black. (D) Number of trials that were terminated because the mice did not move within the time limit. The curves of individual animals are displayed in different colors, the mean curve is displayed in black.

According to the results from the previous approach, the mice were then housed in an inverted dark/light cycle. The corn oil reward with no restriction was kept. The open field habituation was shortened to fit it into fewer days, to make the test feasible for the young mice as well. The T-Maze habituation without and with door were kept as in the previous protocol, since these are more crucial habituation steps. Moreover, the number of training sessions per day was increased from 10 to 20 trials, to try to achieve higher learning.

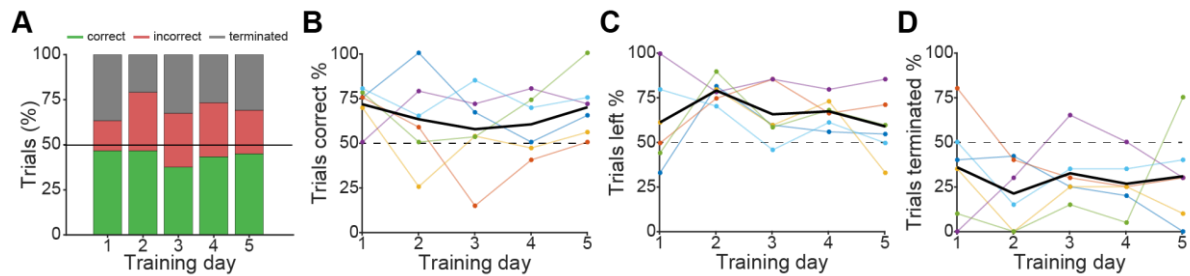


**Figure 22: Fifth approach to establish the T-Maze task in head-fixed conditions with experimental group 4.** (A) Bar graph displaying the mean number of successful, unsuccessful and terminated trials of the experimental group 4 (n=6). (B) Mean correct trials across training days as a learning curve. In colors the learning curves of individual animals are displayed, in black the mean learning curve. (C) Number of trials the animals turned left in the test trial across training days. In colors the curves of individual animals are displayed, in black the mean curve. (D) Number of trials the animals that were terminated because the mice didn't move within the time limit. In colors the curves of individual animals are displayed, in black the mean curve.

This protocol decreased the number of terminated trials, but they still made up around 25 % of trials (Figure 22, A+D). The proportion of correctly executed trials ranged from 50 to 70 %, but the criterion was not reached (Figure 22, B). The correct performance could be due to chance level, as mice in a maze tend to explore a previously unvisited, novel arms. Mice showed no clear bias for one side of the maze (Figure 22, B).

---

These results, together with experiments carried out by a colleague with the last protocol (unpublished data) to exclude the effects of the experimenter, demonstrate that the implementation of the DNMS T-Maze task on the MobileHomeCage is not feasible for young, adolescent and early adult mice.

### 3.4 Prefrontal-hippocampal network activity patterns across late development in $Df(16)A^{+/-}$ and WT mice

The PFC is considered a hub of cognitive processing and, in close connection with the hippocampus (HP) underlying working memory functions (Miller, 2000; Miller and Cohen, 2001). Dysfunctions in this cognitive domain are a core symptom of neurodevelopmental disorders (Sigurdsson and Duvarci, 2016). According to the previously described multiple hit hypothesis, the etiology of these disorders includes genetic and environmental hits during vulnerable time windows of development (Davis et al., 2016). One vulnerable time window of development is the adolescent phase. During this time, cognitive abilities emerge and mature, but on the flip side, some neurodevelopmental disorders begin to show (Chini and Hanganu-Opatz, 2021; Klune et al., 2021). However, the developmental trajectories of prefrontal-hippocampal development in the context of neurodevelopmental disorders are not fully elucidated. Therefore, simultaneous recordings of LFP and spiking activity were performed in the medial (m) PFC and intermediate/ventral (i/v) CA1 of the HP in female and male  $Df(16)A^{+/-}$  and wildtype (WT) mice from P20-60. A part of this data, namely the prefrontal single-unit spiking activity acquired in WT mice, were additionally used in another project, which aimed at deciphering how the extreme distributions of structural and functional parameters in the adult brain unfold during development ((Chini et al., 2023), currently under revision at *Cell Reports*). In the results comprising the fourth part of this thesis, the acquired data from PFC and HP were compared for effects of condition ( $Df(16)A^{+/-}$  vs. WT) across age (comparison of slopes) and in two age groups, namely early adolescent (early ado, P20-39) and late adolescent (late ado, P40-60) (Figure 23, A).

As the mice were recorded several times across the adolescent period, the data were compared and statistically analyzed using a linear mixed-effect model (LME), with mouse identity, sex and recording number as random effects, to account for nested effects in the data. ‘Age x condition’ describes a statistical effect between the developmental trajectories;  $p_{\text{early ado}}$  and  $p_{\text{late ado}}$  indicate effects between  $Df(16)A^{+/-}$  and WT mice in either early ado or late ado age;  $p_{Df(16)A^{+/-}}$  and  $p_{\text{WT}}$  describe effects between early ado and late ado age in either  $Df(16)A^{+/-}$  or WT condition. To maintain the readability of the next paragraphs, only relevant p-values are mentioned; the detailed statistics can be found in Table 2 in the Appendix.

#### 3.4.1 $Df(16)A^{+/-}$ mice show a similar weight increase to WT with implanted headplates

During the recording process of the electrophysiological activity, the mice were head-fixed to a system called the MobileHomeCage (Neurotar, Helsinki, Finland). To be able to fix the mice

---

into the system, a metal headplate was attached to the skull using a previously established surgery method suitable for prejuvenile mice of this young age (P15-20) (Pöpplau et al., 2023). In this study, it was also reported that mice with the implant increase in weight similarly to mice without implants, and that the attachment of a head-fixation device did not affect cortical thickness in prefrontal areas (Pöpplau et al., 2023). To compare whether the  $Df(16)A^{+/-}$  mice also showed undisturbed growth when implanted, the weight of the mice was monitored across the experimental period (Figure 23, A).

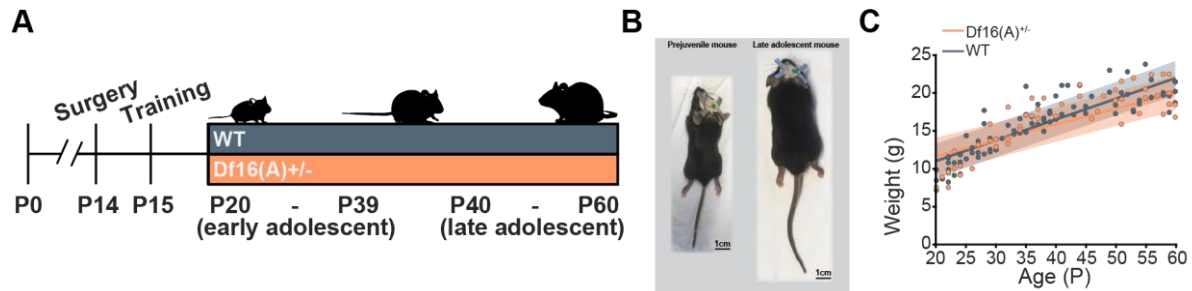


**Figure 23. Experimental timeline and increase in body size and weight across the adolescent period.** (A) Timeline illustrating the experimental design. (B) A prejuvenile mouse with implanted headplate and a late adolescent mouse with implanted headplate in comparison. The scale bars show 1cm. (C) Scatter plot illustrating the increase in weight across age in implanted  $Df(16)A^{+/-}$  (orange,  $n_{(Df(16)A^{+/-})} = 52$  recordings, 14 mice) and WT mice (blue-grey,  $n_{(WT)} = 82$  recordings, 23 mice).

Data in scatter plots are presented as individual data points and the line displays the predicted values of the linear mixed-effect models, with the shaded area representing the 95 %-confidence interval. ‘Age x condition \*’ indicates a significant difference between the slopes of the predicted values for the  $Df(16)A^{+/-}$  and WT mice, linear mixed-effect models. For detailed statistics see Table 2.

The mice significantly increased in body size across the experimental timeline (Figure 23, B). The  $Df(16)A^{+/-}$  gained weight similarly to the age-matched WT mice (LME, slopes:  $p = 0.07$ , detailed statistics in Table 2) (Figure 23, C). This eliminates confounding factors due to a different weight increase during development.

### 3.4.2 $Df(16)A^{+/-}$ mice show minor alterations in locomotor behavior

The often-reported hyperactivity in mouse models of neurodevelopmental disorders is proposed to be dependent on the mesolimbic system, a brain circuitry involving the ventral tegmental area, Nucleus accumbens, amygdala as well as the HP and PFC (Jones et al., 2011). To evaluate hyperactivity on the MobileHomeCage, the movement time as the ratio of total time during the first 5 min of recording was evaluated. The duration of time spent in the center of the maze was evaluated as a proxy for anxiety-related behavior. The movement patterns on the MobileHomeCage during the first 5 minutes of recording time were reconstructed (Figure 24, A).

## Results

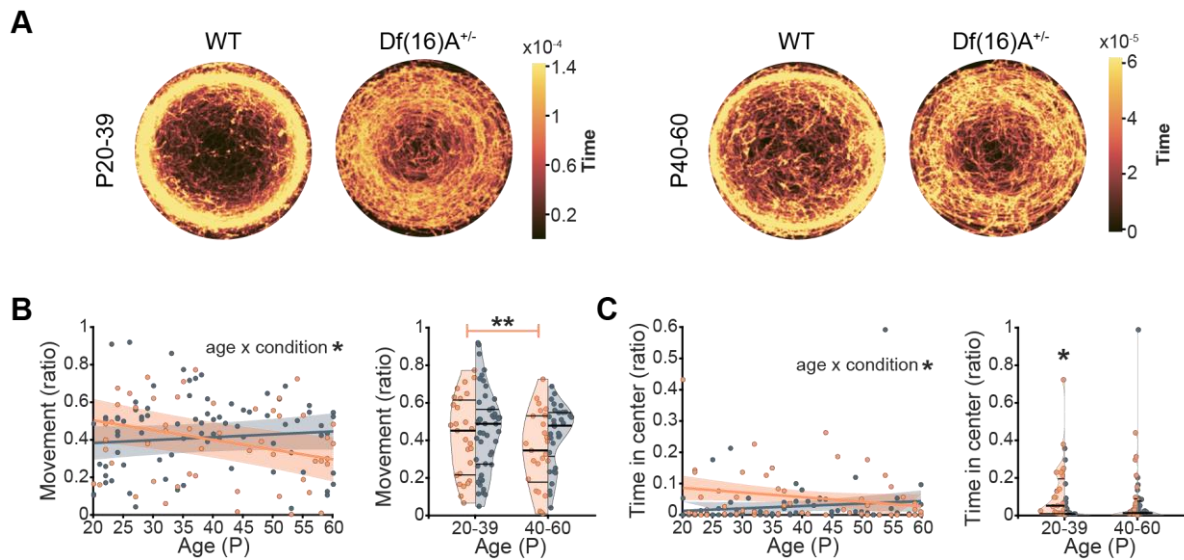


**Figure 24: Movement patterns on the MobileHomeCage in the first 5 min of the recording throughout late development in *Df(16)A<sup>+/-</sup>* and WT mice.** (A) Color-coded heatmaps of time spent in particular positions in the first 5min on the MobileHomeCage in early ado *Df(16)A<sup>+/-</sup>* and WT mice, left and right, in late ado *Df(16)A<sup>+/-</sup>* and WT mice. (B) Left, scatter plot showing the time the mice spent moving during the first 5 min of recording as the ratio of the total 5 min across age. Right, violin plot displaying the movement ratio during the first 5 min of recording in early ado and late ado *Df(16)A<sup>+/-</sup>* (orange,  $n_{Df(16)A^{+/-}} = 52$  recordings, 14 mice) and WT mice (blue-grey,  $n_{WT} = 82$  recordings, 23 mice). (C) Same as (B) but for the time spent in the center region of the platform. Data in scatter plots are presented as individual data points and the line displays the predicted values of the linear mixed-effect models, with the shaded area representing the 95 %-confidence interval. ‘Age x condition \*’ indicates a significant difference between the slopes of the predicted values for the *Df(16)A<sup>+/-</sup>* and WT mice, linear mixed-effect models. In the violin plots, data are presented with median, 25th and 75th percentiles and the shaded area represents the probability density of the variable. \* $p < 0.05$ , \*\* $p < 0.01$ , \*\*\* $p < 0.001$ , linear mixed-effect models. For detailed statistics see Table 2.

In head-fixed conditions, *Df(16)A<sup>+/-</sup>* mice showed a different developmental trajectory of locomotor activity than WT mice. This is because in *Df(16)A<sup>+/-</sup>* mice, the movement ratio in the first 5 min decreased across age, which was not observed in WT mice (‘age x condition’: LME,  $p = 0.007$ ; groups: LME,  $p_{Df(16)A^{+/-}} = 0.005$ ,  $p_{WT} = 0.226$ , detailed statistics in Table 2) (Figure 24, A). *Df(16)A<sup>+/-</sup>* mice exhibited a similar effect in anxiety-related behavior; across age, the time *Df(16)A<sup>+/-</sup>* mice spent in the center area of the carbon cage of the MobileHomeCage decreased (‘age x condition’: LME,  $p = 0.046$ ; detailed statistics in Table 2). In the early ado group, *Df(16)A<sup>+/-</sup>* mice spent more time in the center region than their age-matched controls (LME,  $p_{\text{early ado}} = 0.03$ ,  $p_{\text{late ado}} = 0.87$ , detailed statistics in Table 2) (Figure 24, B).

These results demonstrate that, during early adolescence, *Df(16)A<sup>+/-</sup>* mice exhibit an altered locomotor activity with an abnormal developmental trajectory.

The signal obtained from electrophysiological recordings was categorized into movement and resting periods by aligning the locomotor activity with the electrophysiological activity through a TTL input into the amplifier, thereby allowing for a distinct examination of the electrophysiological signal for distinct behavioral states. To test for confounding factors of differences in movement on the MobileHomeCage, the locomotor activity was also evaluated across 30 min of recording time, where a habituation is expected (Figure 25, A).

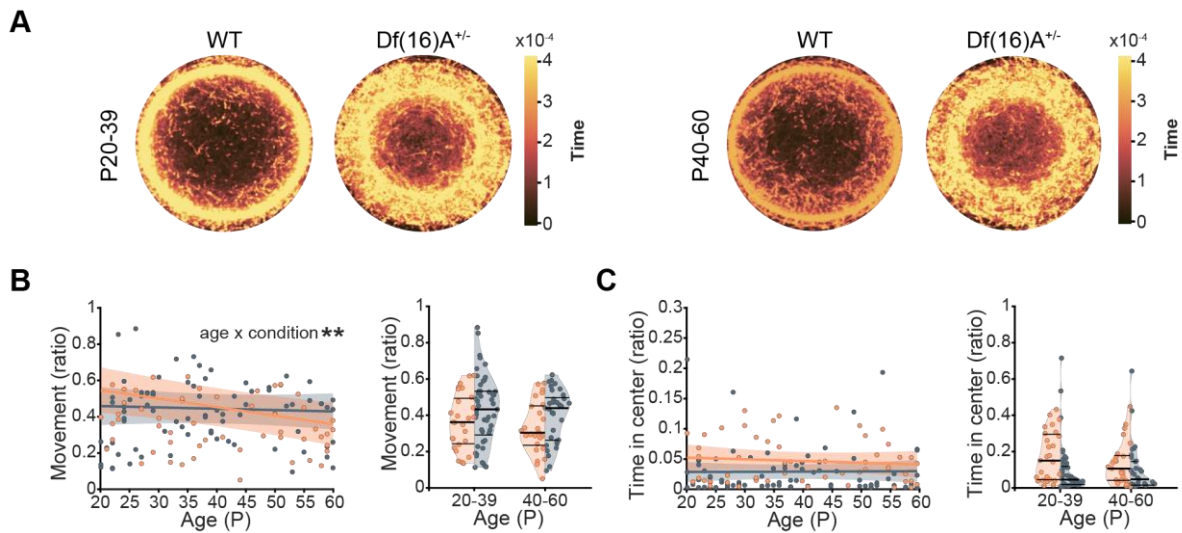


**Figure 25: Movement patterns on the MobileHomeCage in 30 min of the recording throughout late development in  $Df(16)A^{+/-}$  and WT mice.** (A) Color-coded heatmaps of time spent in particular positions in 30 min on the MobileHomeCage in early ado  $Df(16)A^{+/-}$  and WT mice, left and right, in late ado  $Df(16)A^{+/-}$  and WT mice. (B) Left, scatter plot showing the time the mice spent moving during the first 5 min of recording as the ratio of the total 30 min across age. Right, violin plot displaying the movement ratio during 30 min of recording in early ado and late ado  $Df(16)A^{+/-}$  (orange,  $n_{(Df(16)A^{+/-})} = 52$  recordings, 14 mice) and WT mice (blue-grey,  $n_{(WT)} = 82$  recordings, 23 mice). (C) Same as (B) but for the time spent in the center region of the platform.

Data in scatter plots are presented as individual data points and the line displays the predicted values of the linear mixed-effect models, with the shaded area representing the 95 %-confidence interval. ‘Age x condition \*’ indicates a significant difference between the slopes of the predicted values for the  $Df(16)A^{+/-}$  and WT mice, linear mixed-effect models. In the violin plots, data are presented with median, 25th and 75th percentiles and the shaded area represents the probability density of the variable. \* $p < 0.05$ , \*\* $p < 0.01$ , \*\*\* $p < 0.001$ , linear mixed-effect models. For detailed statistics see Table 2.

Across the 30 minutes of recording time,  $Df(16)A^{+/-}$  mice showed a different developmental trajectory of locomotor activity than WT mice, with the  $Df(16)A^{+/-}$  mice exhibiting a decreasing movement ratio across age. This was not observed in WT mice (‘age x condition’: LME,  $p = 0.007$ ; groups: LME,  $p_{Df(16)A^{+/-}} = 0.06$ ,  $p_{WT} = 0.35$ , detailed statistics in Table 2) (Figure 25, A). The time the mice spent in the center region of the carbon cage did not differ between the conditions and across age (detailed statistics in Table 2) (Figure 25, B).

Across the 30 min of recording time, locomotor activity showed only minor differences in the developmental trajectories, but not between age and condition groups. Since the movement ratio and the time spent in the center of the carbon cage were not significantly different between  $Df(16)A^{+/-}$  and WT mice, it was concluded that the electrophysiological signal can be divided into movement and resting periods without further consideration.

### 3.4.3 Developmental trajectories of prefrontal local field potential are disturbed in $Df(16)A^{+/-}$ mice

Coordinated neuronal activity patterns, the oscillations, are important for information processing between brain areas (Buzsáki et al., 2012; Buzsáki and Draguhn, 2004; Buzsáki and Watson, 2012). Oscillatory activity patterns already arise during early life stages, and a disruption of their development can result in abnormalities, possibly causing mental disorders

(Chini and Hanganu-Opatz, 2021). In order to gain insight into the development of the PFC in the context of neurodevelopmental disorders, the oscillatory and spiking activity was monitored during movement and resting periods in adolescent mice (Figure 26, A). All investigated mice showed similar patterns of oscillatory activity, with a second, less prominent peak in theta power and higher activity during movement periods (Figure 26, B). The analysis here was focused on theta and broad-band gamma-band activity. Theta activity is propagated between areas, and several studies have reported coherent theta activity between the PFC and HP in memory tasks (Adhikari et al., 2010; Jones and Wilson, 2005; O'Neill et al., 2013). The fast gamma oscillations are put in context with rhythms evoked by local synchronized networks (Buzsáki and Wang, 2012).

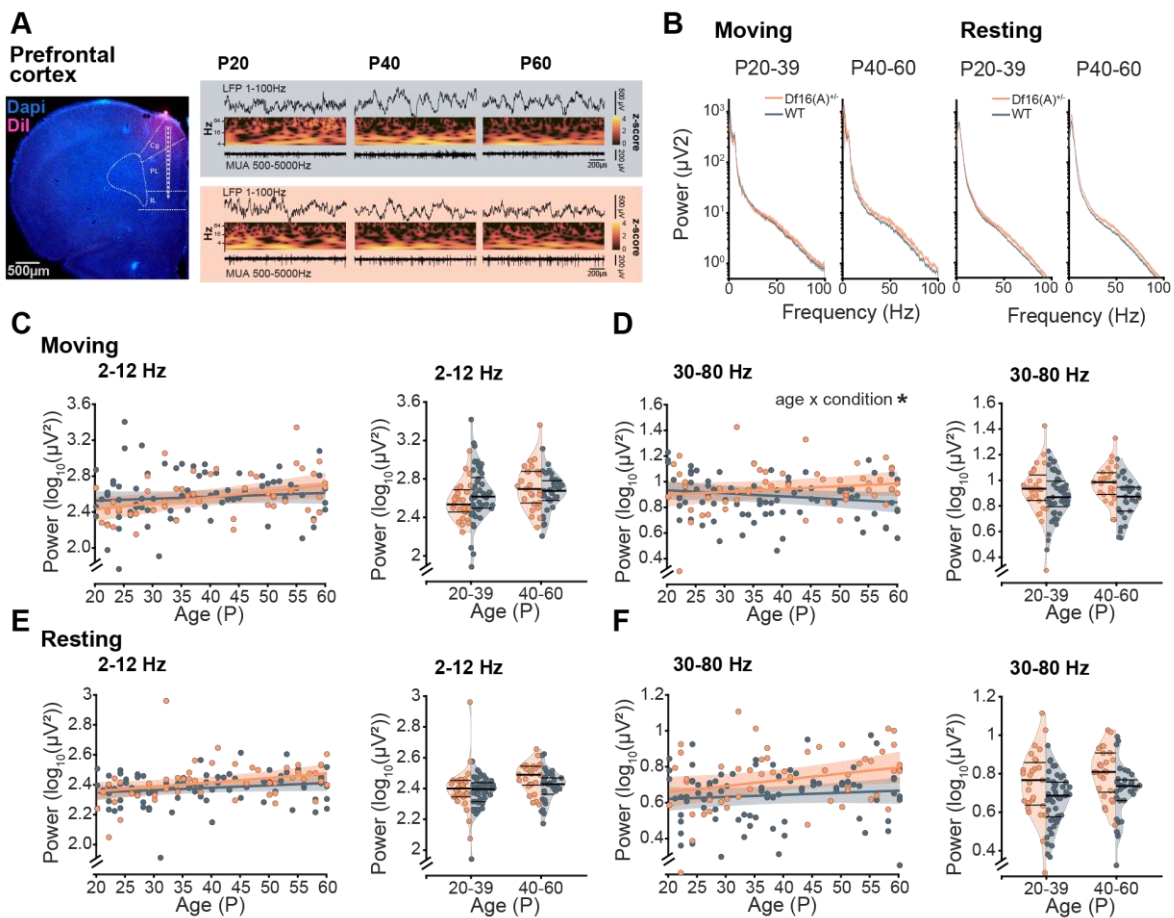


**Figure 26: Prefrontal LFP properties throughout late development in *Df(16)A<sup>+/-</sup>* and WT mice.** (A) Left, digital photomontage reconstructing the location of DiI-labeled extracellular electrodes in the mPFC. Right, examples of recordings of LFP and MUA in the PL of the PFC of *Df(16)A<sup>+/-</sup>* and WT mice at the age of P20, P40 and P60. (B) Mean power spectrum of early ado and late ado *Df(16)A<sup>+/-</sup>* (orange,  $n_{(Df(16)A^{+/-})} = 52$  recordings, 14 mice) and WT mice (blue-grey,  $n_{(WT)} = 82$  recordings, 23 mice) during movement left, and during rest, right. (C) Left, scatter plot displaying the power in 2-12 Hz theta range across age during movement. Right, violin plot showing the power in 2-12 Hz theta in early ado and late ado *Df(16)A<sup>+/-</sup>* and WT mice. (D), (E) + (F) Same as (C) but for mean power in 30-80 Hz broad-band gamma range during movement and 2-12 Hz theta and 30-80 Hz broad-band gamma during resting periods.

Data in scatter plots are presented as individual data points and the line displays the predicted values of the linear mixed-effect models, with the shaded area representing the 95 %-confidence interval. \*Age x condition\* indicates a significant difference between the slopes of the predicted values for the *Df(16)A<sup>+/-</sup>* and WT mice, linear mixed-effect models. In the violin plots, data are presented with median, 25th and 75th percentiles and the shaded area

## Results

represents the probability density of the variable. \* $p < 0.05$ , \*\* $p < 0.01$ , \*\*\* $p < 0.001$ , linear mixed-effect models. For detailed statistics see Table 2.

There was no difference in the development of prefrontal theta power between  $Df(16)A^{+/-}$  and WT mice. Neither the slopes across age were different during movement or resting periods ('age x condition': LME,  $p = 0.384$ ,  $p = 0.213$ ), nor was the theta power impaired in early or late ado  $Df(16)A^{+/-}$  mice (groups: LME,  $p_{\text{early ado}} = 0.508$ ,  $p_{\text{late ado}} = 0.566$  and  $p_{\text{early ado}} = 0.451$ ,  $p_{\text{late ado}} > 0.276$ , detailed statistics in Table 2) (Figure 26, C+E).

Analyzing the rapid oscillatory rhythms revealed a different picture. The developmental trajectories of broad-band gamma power between  $Df(16)A^{+/-}$  and WT mice were different across age during movement ('age x condition': LME,  $p = 0.046$ , detailed statistics in Table 2). However, there was no significant difference in broad-band gamma power in early ado or late ado between the  $Df(16)A^{+/-}$  and WT mice (groups: LME  $p_{\text{early ado}} = 0.901$ ,  $p_{\text{late ado}} = 0.162$  and  $p_{\text{early ado}} = 0.137$ ,  $p_{\text{late ado}} = 0.124$ , detailed statistics in Table 2).

These results indicate a transient abnormality in prefrontal fast oscillatory activity during adolescence, which normalizes towards the end of adolescence or the onset of adulthood.

The oscillatory activity at fast frequencies depends on an interplay between excitatory pyramidal and inhibitory interneurons (Buzsáki and Draguhn, 2004; Buzsáki et al., 2013). A measure for the ratio of excitation/inhibition is the 1/f slope or the decay of the power spectrum from slow frequencies to fast frequencies (Donoghue et al., 2020). Therefore, the 1/f slope across age was investigated to deepen the insight into the observed local network abnormalities in the PFC. There was no difference in the developmental trajectories of the excitation/inhibition ratio during movement or during resting periods in the  $Df(16)A^{+/-}$  mice ('age x condition': LME,  $p = 0.203$  and  $p = 0.07$ , detailed statistics in Table 2) (Figure 27). During resting periods, late ado WT mice showed a shift towards less inhibition / more excitation compared to early ado WT mice; this was not evident in the  $Df(16)A^{+/-}$  mice (groups: LME,  $p_{Df(16)A^{+/-}} = 0.232$ ,  $p_{WT} = 0.001$ , detailed statistics in Table 2). During movement periods, prefrontal activity in early ado  $Df(16)A^{+/-}$  mice showed a lower 1/f slope and therefore a shift towards less inhibition / more excitation in this developmental period (groups: LME,  $p_{\text{early ado}} = 0.029$ ,  $p_{\text{late ado}} = 0.331$ , detailed statistics in Table 2).

These results indicate a transient change in the excitation/inhibition ratio in  $Df(16)A^{+/-}$  mice in the adolescent developmental period.

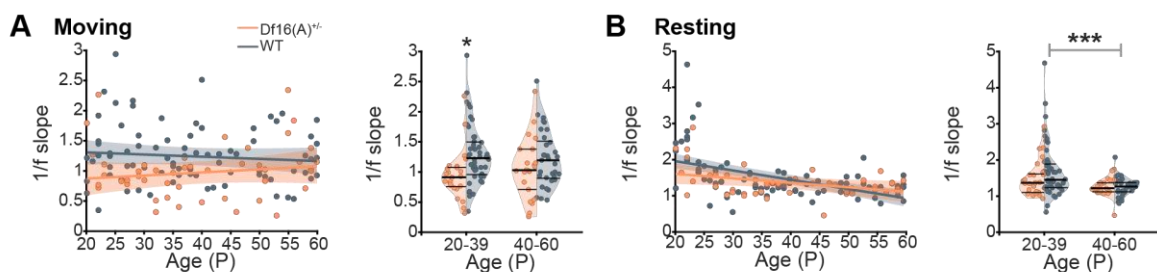


**Figure 27: Excitation/inhibition ratio illustrated by 1/f slope in the PFC of  $Df(16)A^{+/-}$  and WT mice across late development.** (A) Left, scatter plot and right, violin plot displaying the 1/f slopes calculated for 30-50 Hz range of the power spectrum across age and in early ado as well as late ado  $Df(16)A^{+/-}$  (orange,  $n_{Df(16)A^{+/-}} = 52$  recordings, 14 mice) and WT mice (blue-grey,  $n_{WT} = 82$  recordings, 23 mice) during movement periods. (B) Same as (A) but for resting periods.

## Results

Data in scatter plots are presented as individual data points and the line displays the predicted values of the linear mixed-effect models, with the shaded area representing the 95 %-confidence interval. ‘Age x condition \*’ indicates a significant difference between the slopes of the predicted values for the *Df(16)A<sup>+/-</sup>* and WT mice, linear mixed-effect models. In the violin plots, data are presented with median, 25th and 75th percentiles and the shaded area represents the probability density of the variable. \* $p < 0.05$ , \*\* $p < 0.01$ , \*\*\* $p < 0.001$ , linear mixed-effect models. For detailed statistics see Table 2.

The amplitude of gamma oscillations is modulated by the phase of the theta oscillations, which influences the synchrony between brain areas but also within one area (Sirota et al., 2008). Therefore, it was investigated whether the changes in prefrontal local network development observed in *Df(16)A<sup>+/-</sup>* mice are accompanied by changes in prefrontal synchrony. To this end, the phase-amplitude coupling (PAC) across age in *Df(16)A<sup>+/-</sup>* and WT mice was assessed. The theta phase modulated the gamma amplitude most prominently in the 70-100 Hz spectrum through lower theta frequencies (4-8 Hz) during resting periods and higher theta frequencies (8-12 Hz) during movement periods (Figure 28, A+C). There was no difference in the development of PAC across age during movement periods between *Df(16)A<sup>+/-</sup>* and WT mice (groups: LME,  $p_{\text{early ado}} = 0.177$ ,  $p_{\text{late ado}} = 0.081$ , detailed statistics in Table 2). During resting periods, the *Df(16)A<sup>+/-</sup>* mice exhibited an increasing PAC, with the PAC being significantly lower in early ado *Df(16)A<sup>+/-</sup>* than early ado WT mice (‘age x condition’: LME,  $p = 0.033$ ; groups: LME,  $p_{\text{early ado}} = 0.003$ ,  $p_{\text{late ado}} = 0.49$ , detailed statistics in Table 2) (Figure 28, B+D). These results show that the prefrontal LFP synchrony development in adolescence is abnormal in *Df(16)A<sup>+/-</sup>* mice.

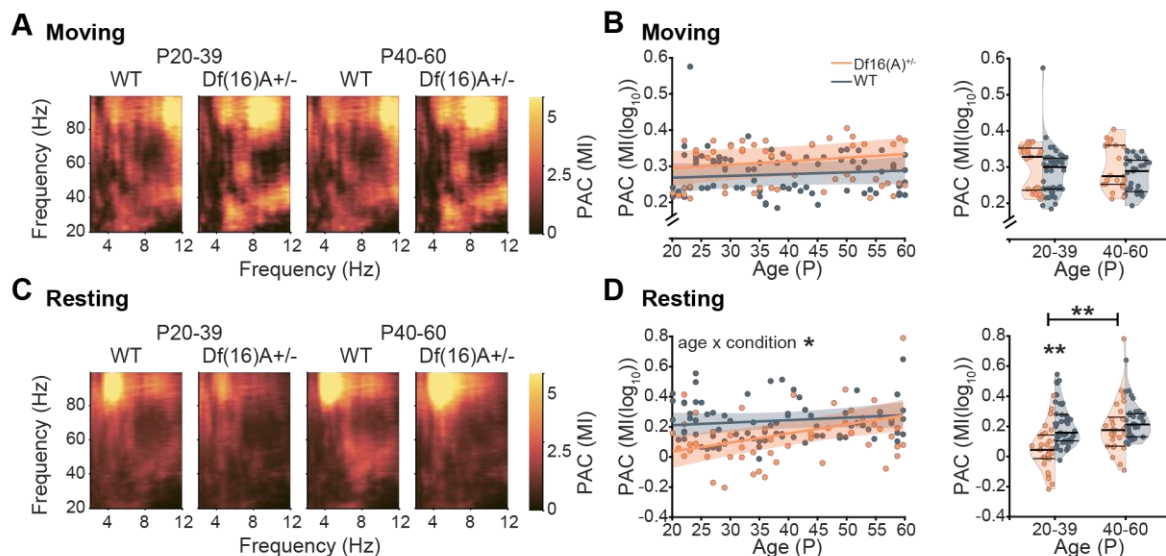


**Figure 28: Cross-frequency coupling between prefrontal theta phase and prefrontal gamma amplitude throughout late development in *Df(16)A<sup>+/-</sup>* and WT mice.** (A) Color-coded heatmaps showing the mean PAC modulation index (MI) of the theta phase of the PFC modulating the gamma amplitude in early ado and late ado *Df(16)A<sup>+/-</sup>* (orange,  $n_{(Df(16)A^{+/-})} = 52$  recordings, 14 mice) and WT mice (blue-grey,  $n_{(WT)} = 82$  recordings, 23 mice) during movement periods. (B) Left, scatter plot and right, violin plot indicating the quantified PAC MI across age and early ado and late ado *Df(16)A<sup>+/-</sup>* and WT mice. (C) Same as (A) but for resting periods. (D) Same as (B) but for resting periods.

In (B) and (D) data in scatter plots are presented as individual data points and the line displays the predicted values of the linear mixed-effect models, with the shaded area representing the 95 %-confidence interval. ‘Age x condition \*’ indicates a significant difference between the slopes of the predicted values for the *Df(16)A<sup>+/-</sup>* and WT mice, linear mixed-effect models. In the violin plots, data are presented with median, 25th and 75th percentiles and the

## Results

shaded area represents the probability density of the variable. \* $p < 0.05$ , \*\* $p < 0.01$ , \*\*\* $p < 0.001$ , linear mixed-effect models. For detailed statistics see Table 2.

When taken together, this demonstrates that the prefrontal LFP properties, particularly in fast frequencies, are disrupted in late development in  $Df(16)A^{+/-}$  mice in an activity-dependent manner. Consequently, the development of the local network activity in the PFC is abnormal in adolescent  $Df(16)A^{+/-}$  mice.

### 3.4.4 Prefrontal spiking activity is altered in a behavioral state-dependent manner in adolescent $Df(16)A^{+/-}$ mice

Local prefrontal activity, particularly gamma rhythms, is dependent on the spiking activity within the brain area, specifically a precisely timed interaction between excitatory and inhibitory interneurons (Cardin, 2016). Accordingly, the spiking activity and synchrony in the PFC were investigated.

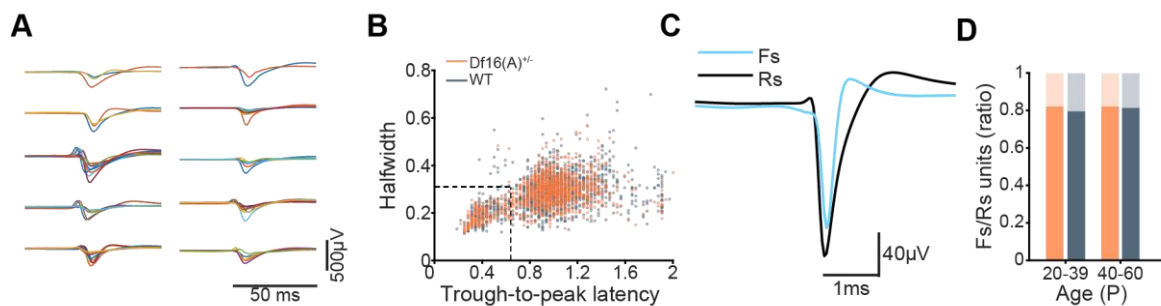


**Figure 29: Separation of single units into fast spiking, putative PV-interneurons and regular spiking, putative pyramidal neurons. (A)** Examples of clustered single units in different channels from one recording from a late ado WT mouse. **(B)** Scatter plot illustrating halfwidth as a function of trough-to-peak latency of single units recorded from both  $Df(16)A^{+/-}$  (orange,  $n_{(Df(16)A^{+/-})}$ : 1125 units, 52 recordings, 14 mice) and WT mice (blue-grey,  $n_{(WT)}$ : 1701 units, 82 recordings, 23 mice). The dotted lines correspond to the threshold used to classify the single units into fast spiking (Fs) and regular spiking (Rs) units. **(C)** Mean waveforms of Rs units (black) and Fs units (blue) of all recordings and mice in all age groups. **(D)** Bar graph showing the percentage of units that are classified as Rs (dark area) or Fs (light area) in early ado and late ado  $Df(16)A^{+/-}$  and WT mice. For detailed statistics see Table 2.

To do so on a single unit activity (SUA) level, the spiking activity from one recording was clustered and sorted into spikes arising from one putative neuron or unit (Figure 29, A). Based on their waveforms, the single units were further divided into fast-spiking (Fs), putative parvalbumin (PV) interneurons and regular-spiking (Rs), putative pyramidal neurons with a previously published protocol setting thresholds in the halfwidth and trough-to-peak latency (Bitzenhofer et al., 2020) (Figure 29, B+C). In early ado and late ado  $Df(16)A^{+/-}$  and WT mice, the ratio of detected and recorded Rs/Fs units was roughly 80/20 % with no significant difference between the groups (groups: LME,  $p_{\text{early ado}} = 0.067$ ,  $p_{\text{late ado}} = 0.977$ , detailed statistics in Table 2) (Figure 29, D).

In order to assess the functional properties of the classified single units, the FR and the ISI were investigated for Rs and Fs units separately.

## Results

There were no differences in the developmental trajectories of FR of Rs units in  $Df(16)A^{+/-}$  and WT mice ('age x condition':  $p = 0.141$ );, but early ado  $Df(16)A^{+/-}$  mice showed a lower FR than late ado  $Df(16)A^{+/-}$  mice during movement periods (groups: LME,  $p_{Df(16)A^{+/-}} = 0.008$ ,  $p_{WT} = 0.228$ , detailed statistics in Table 2) (Figure 30, A). The variance in FR, evaluated by the ISI, was higher in early ado WT mice compared to age-matched  $Df(16)A^{+/-}$  mice and to late ado WT mice ('age x condition': LME,  $p = 0.243$ , groups: LME,  $p_{early\ ado} = 0.002$  §,  $p_{late\ ado} = 0.166$ ,  $p_{Df(16)A^{+/-}} = 0.04$ ,  $p_{WT} = 0.774$ , detailed statistics in Table 2) (Figure 30, B). During resting periods, the FR and ISI as proxies of the functional properties of Rs units were not different between  $Df(16)A^{+/-}$  and WT mice (Figure 30, C+D).

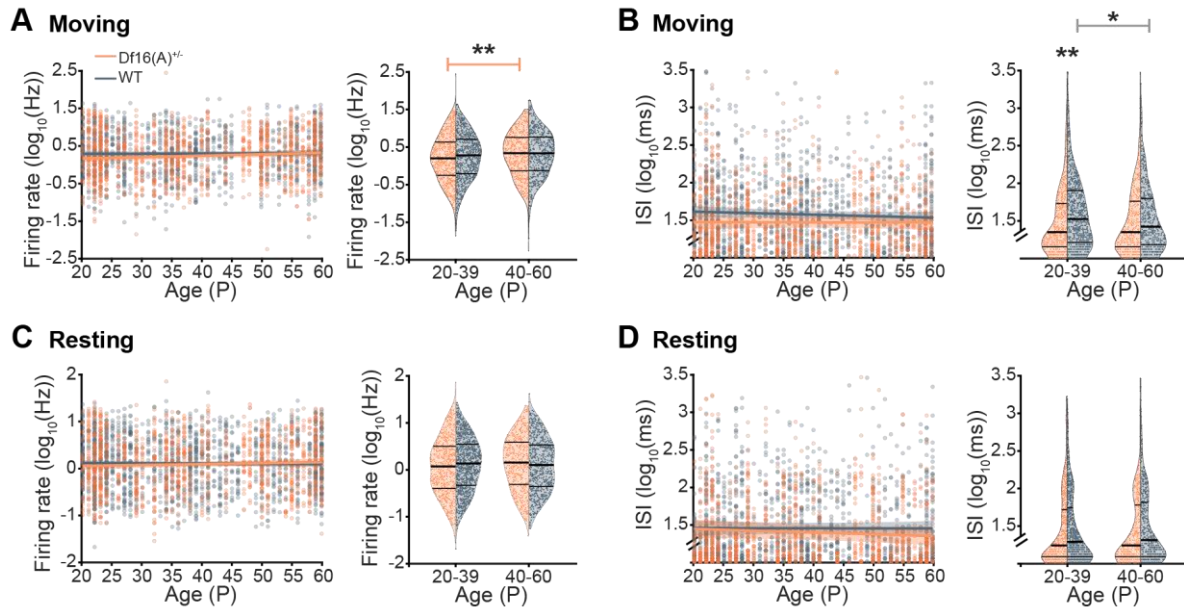


**Figure 30: Firing patterns of Rs units in the PFC of  $Df(16)A^{+/-}$  and WT mice across late development. (A)** Left, scatter plot illustrating the FR of Rs units across age and right, violin plot displaying the same in early ado and late ado  $Df(16)A^{+/-}$  (orange,  $n_{Df(16)A^{+/-}}$ : 951 Rs units, 52 recordings, 14 mice) and WT mice (blue-grey,  $n_{WT}$ : 1422 Rs units, 82 recordings, 23 mice) during movement periods. **(B)** Left, scatter plot illustrating the ISI of Rs units across age and right, violin plot displaying the same in early ado and late ado mice during movement periods. **(C)** Same as (A) but for resting periods. **(D)** Same as (B) but for resting periods.

Data in scatter plots are presented as individual data points and the line displays the predicted values of the linear mixed-effect models, with the shaded area representing the 95 %-confidence interval. 'Age x condition \*' indicates a significant difference between the slopes of the predicted values for the  $Df(16)A^{+/-}$  and WT mice, linear mixed-effect models. In the violin plots, data are presented with median, 25th and 75th percentiles and the shaded area represents the probability density of the variable. \* $p < 0.05$ , \*\* $p < 0.01$ , \*\*\* $p < 0.001$ , linear mixed-effect models. For detailed statistics see Table 2.

The functional properties of Fs units were assessed with the same methods, namely FR and ISI. The development of Fs activity across adolescence in FR and ISI was not different between  $Df(16)A^{+/-}$  and WT mice (Figure 31).

These findings indicate that the firing properties of Rs, but not Fs units show minor abnormalities during adolescent development in  $Df(16)A^{+/-}$  mice, especially in their rhythmicity of firing.

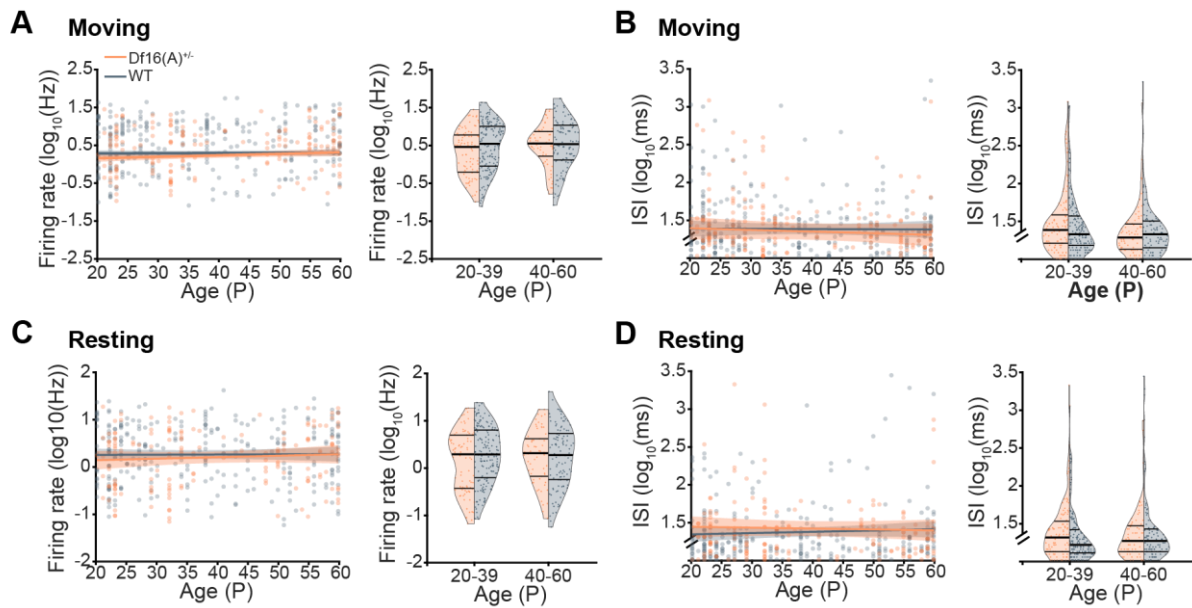


**Figure 31: Firing patterns of Fs units in the PFC of  $Df(16)A^{+/-}$  and WT mice across late development.** (A) Left, scatter plot illustrating the FR of Fs units across age and right, violin plot displaying the same in early ado and late ado  $Df(16)A^{+/-}$  (orange,  $n_{Df(16)A^{+/-}}$ : 174 Fs units, 52 recordings, 14 mice) and WT mice (blue-grey,  $n_{WT}$ : 279 Fs units, 82 recordings, 23 mice) during movement periods. (B) Left, scatter plot illustrating the ISI of Fs units across age and right, violin plot displaying the same in early ado and late ado mice during movement periods. (C) Same as (A) but for resting periods. (D) Same as (B) but for resting periods.

Data in scatter plots are presented as individual data points and the line displays the predicted values of the linear mixed-effect models, with the shaded area representing the 95 %-confidence interval. \*Age x condition \* indicates a significant difference between the slopes of the predicted values for the  $Df(16)A^{+/-}$  and WT mice, linear mixed-effect models. In the violin plots, data are presented with median, 25th and 75th percentiles and the shaded area represents the probability density of the variable. \* $p < 0.05$ , \*\* $p < 0.01$ , \*\*\* $p < 0.001$ , linear mixed-effect models. For detailed statistics see Table 2.

To assess whether these minor alterations in firing properties coincide with the alterations in gamma oscillation development, the synchrony of the spiking activity with the prefrontal gamma rhythm was assessed (Figure 32, A). Units that are significantly locked to a specific LFP rhythm fire preferentially during a specific phase of this LFP rhythm (Siapas et al., 2005). Constructed examples are shown in Figure 32, A. The blue units fire mostly in one specific phase of the LFP rhythms (upper part: in the peaks, lower part: in the troughs). The green units fire randomly in the rhythms; they are not locked.

Assessment of significant locking with the Rayleigh test for non-uniformity, showed that around 90 % of recorded units are locked to the prefrontal gamma rhythm, with no differences between conditions and early ado and late ado mice (groups: LME,  $p_{\text{early ado}} = 0.51$ ,  $p_{\text{late ado}} = 0.92$ ,  $p_{Df(16)A^{+/-}} = 0.82$ ,  $p_{WT} = 0.47$ , detailed statistics in Table 2) (Figure 32, B). The strength of locking was analyzed by calculating the PPC only for significantly locked units. The developmental trajectories of PPC of prefrontal Rs units to the prefrontal gamma rhythm decreased from early ado to late ado mice in both,  $Df(16)A^{+/-}$  and WT mice during movement and resting periods (groups: LME,  $p_{Df(16)A^{+/-}} < 0.001$ ,  $p_{WT} < 0.001$  and  $p_{Df(16)A^{+/-}} < 0.001$ ,  $p_{WT} < 0.001$ , detailed statistics in Table 2) (Figure 32, C+D).

There were no differences in the developmental trajectories of Fs units, but there was a decrease in locking strength between early ado and late ado WT mice during movement periods (groups:

## Results

LME,  $p_{Df(16)A^{+/-}} = 0.257$  and  $p_{WT} = 0.003$ , detailed statistics in Table 2). There were no differences during resting periods (Figure 32, E+F).

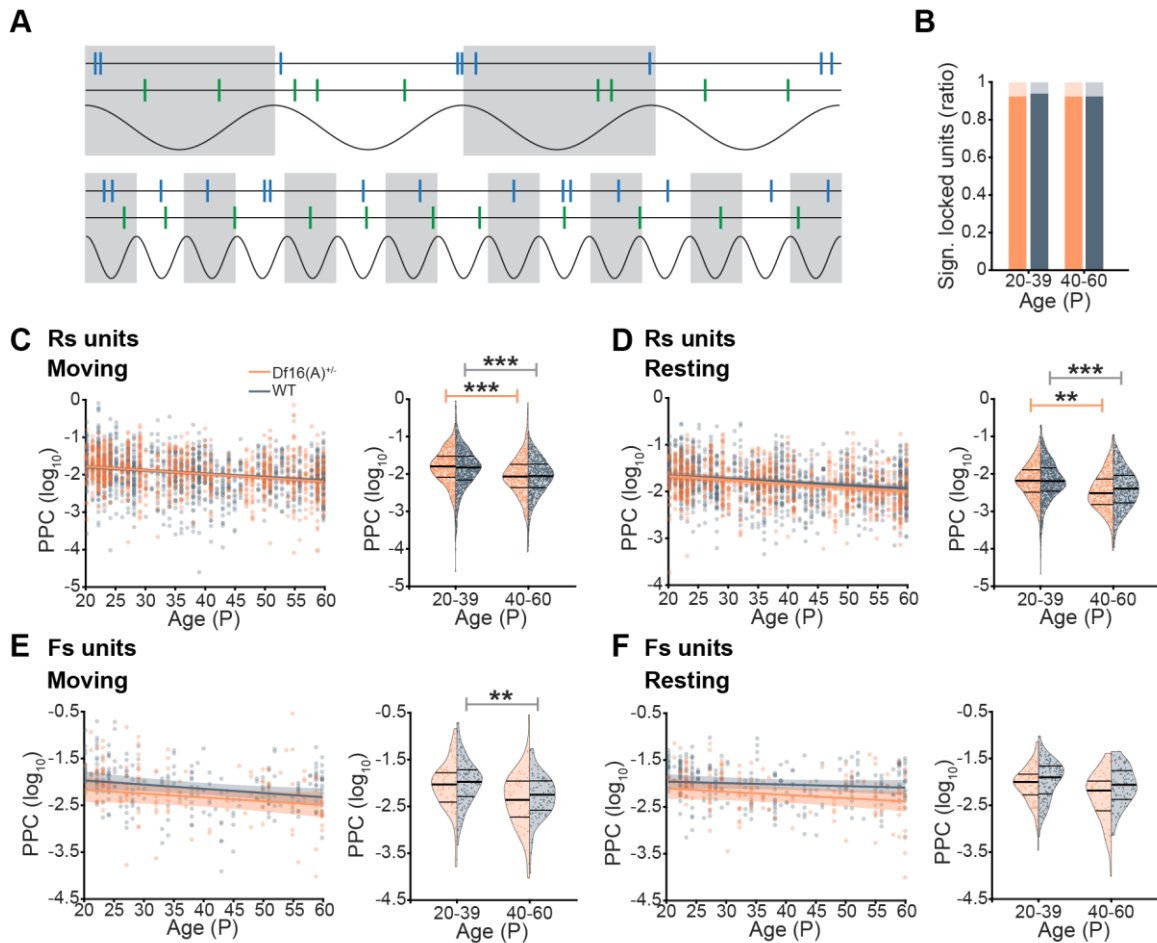


**Figure 32: Synchrony of prefrontal firing with prefrontal broadband gamma rhythm throughout late development in  $Df(16)A^{+/-}$  and WT mice.** (A) Schematic representation of evaluation process of significant locking of the firing rhythm of one unit to a specific LFP rhythm. Upper part, firing of a significantly locked (blue) and a not locked (green) unit to a slow oscillatory rhythm. Lower part, firing of a significantly locked (blue) and not locked (green) unit to a fast oscillatory rhythm. (B) Bar graph showing the number of single units, which are significantly locked (dark areas) to the broadband gamma rhythm of the PFC in early ado and late ado  $Df(16)A^{+/-}$  (orange,  $n_{(Df(16)A^{+/-})}$ : 1125 units, 52 recordings, 14 mice) and WT mice (blue-grey,  $n_{(WT)}$ : 1422 Rs units, 82 recordings, 23 mice). (C) PPC of significantly locked Rs units to the prefrontal broadband gamma rhythm during movement periods, left, displayed in a scatter plot across age and right, in a violin plot illustrating the PPC in early ado and late ado  $Df(16)A^{+/-}$  and WT mice. (D) Same as (C) but for resting periods. (E) PPC of significantly locked Fs units to the prefrontal broadband gamma rhythm during movement periods, left, displayed in a scatter plot across age and right, in a violin plot illustrating the PPC in early ado and late ado  $Df(16)A^{+/-}$  (orange,  $n_{(Df(16)A^{+/-})}$ : 174 Fs units, 52 recordings, 14 mice) and WT mice (blue-grey,  $n_{(WT)}$ : 279 Fs units, 82 recordings, 23 mice). (F) Same as (E) but for resting periods.

In (C)-(F) data in scatter plots are presented as single units and the line displays the predicted values of the linear mixed-effect models, with the shaded area representing the 95 %-confidence interval. ‘Age x condition \*’ indicates a significant difference between the slopes of the predicted values for the  $Df(16)A^{+/-}$  and WT mice, linear mixed-effect models. In the violin plots, data are presented with median, 25th and 75th percentiles and the shaded area represents the probability density of the variable. \* $p < 0.05$ , \*\* $p < 0.01$ , \*\*\* $p < 0.001$ , linear mixed-effect models. For detailed statistics see Table 2.

This suggests that the development towards a less synchronized firing to the prefrontal gamma rhythm across adolescent development is not disturbed in  $Df(16)A^{+/-}$  mice.

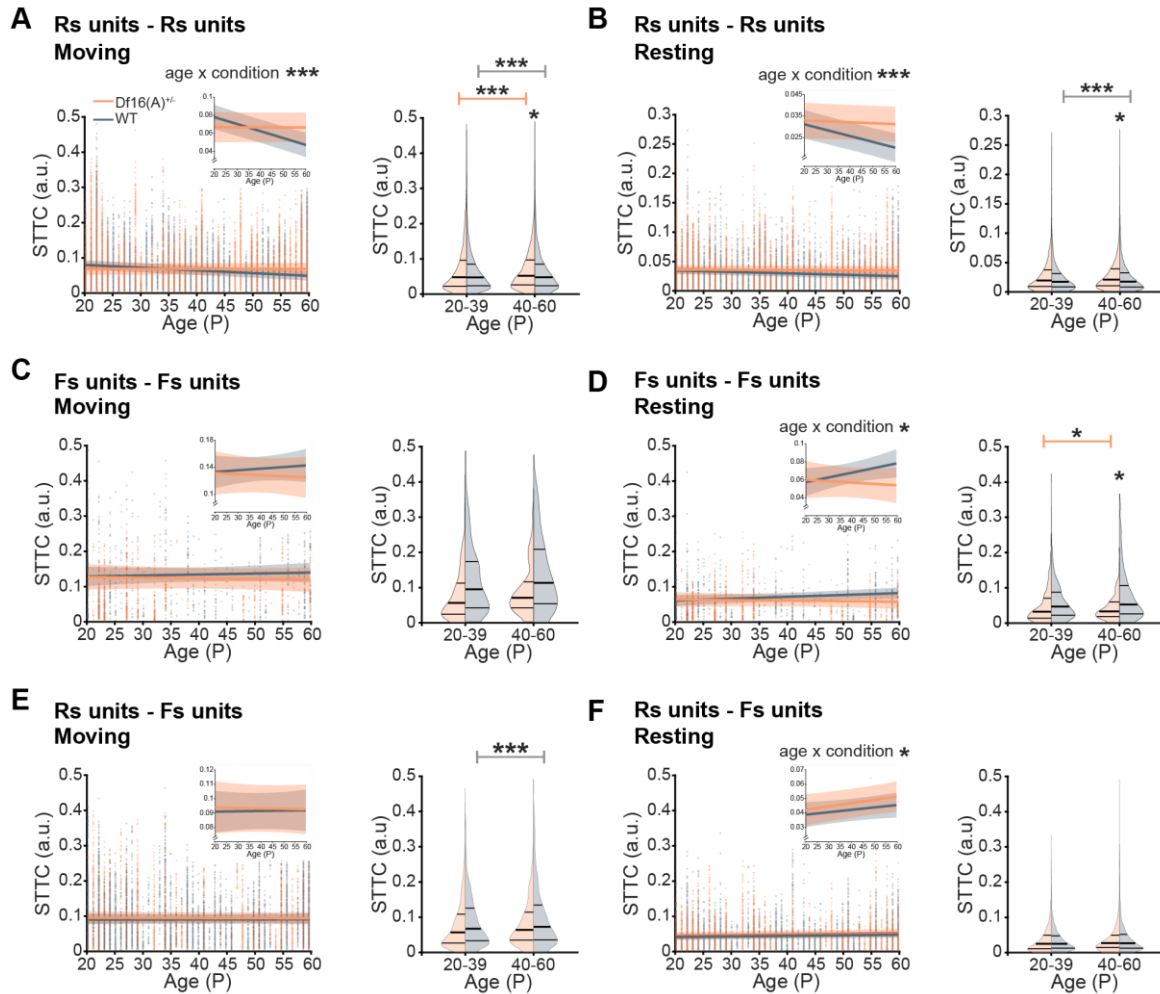


**Figure 33: Firing synchrony between single units in the PFC throughout late development in *Df(16)A<sup>+/-</sup>* and WT mice.** (A) Left, scatter plot displaying the STTC with a latency of 10 ms of prefrontal Rs units with all other Rs units during movement. The inset displays the predicted STTC values across age. Right, violin plot displaying the STTC grouped in early ado and late ado *Df(16)A<sup>+/-</sup>* (orange,  $n_{(Df(16)A^{+/-})}$ : 951 Rs units, 52 recordings, 14 mice) and WT mice (blue-grey,  $n_{(WT)}$ : 1701 units, 82 recordings, 23 mice). (B) Same as (A) but for resting periods. (C) Left, scatter plot displaying the STTC with a latency of 10 ms of prefrontal Fs units with all other Fs units during movement. The inset displays the predicted STTC values across age. Right, violin plot displaying the STTC grouped in early ado and late ado *Df(16)A<sup>+/-</sup>* (orange,  $n_{(Df(16)A^{+/-})}$ : 174 Fs units, 52 recordings, 14 mice) and WT mice (blue-grey,  $n_{(WT)}$ : 279 Fs units, 82 recordings, 23 mice). (D) Same as (C) but for resting periods. (E) Left, scatter plot displaying the STTC with a latency of 10 ms of prefrontal Rs units with all Fs units during movement. The inset displays the predicted STTC values across age. Right, violin plot displaying the STTC grouped in early ado and late ado *Df(16)A<sup>+/-</sup>* and WT mice. (F) Same as (E) but for resting periods.

Data in scatter plots are presented as single units and the line displays the predicted values of the linear mixed-effect models, with the shaded area representing the 95 %-confidence interval. ‘Age x condition \*’ indicates a significant difference between the slopes of the predicted values for the *Df(16)A<sup>+/-</sup>* and WT mice, linear mixed-effect models. In the violin plots, data are presented with median, 25th and 75th percentiles and the shaded area represents the probability density of the variable. \* $p < 0.05$ , \*\* $p < 0.01$ , \*\*\* $p < 0.001$ , linear mixed-effect models. For detailed statistics see Table 2.

As the gamma activity is dependent on the precise interaction between Rs and Fs units (Cardin, 2016), the spike time tiling coefficient (STTC) was investigated as a measure of synchrony between spike trains (Cutts and Eglén, 2014).

The spike synchrony between Rs units decreased with age in WT mice, but not in *Df(16)A<sup>+/-</sup>* mice (‘age x condition’: LME,  $p < 0.001$ , detailed statistics in Table 2). This resulted in an

---

increased synchrony between spike trains of Rs units in late ado *Df(16)A<sup>+/-</sup>* mice, observed during movement and during resting periods (groups: LME,  $p_{\text{early ado}} = 0.55$  §,  $p_{\text{late ado}} = 0.03$ , detailed statistics in Table 2) (Figure 33, A+B). The developmental trajectory of Fs units exhibited a divergent pattern and developed differently during resting periods in WT and *Df(16)A<sup>+/-</sup>* mice ('age x condition': LME,  $p = 0.01$  detailed statistics in Table 2). In late ado mice, this resulted in less synchronized firing of Fs units in *Df(16)A<sup>+/-</sup>* mice (groups: LME,  $p_{\text{early ado}} = 0.74$  §,  $p_{\text{late ado}} = 0.01$ , detailed statistics in Table 2) (Figure 33, C+D). Between spike trains of Rs units and Fs units, the developmental trajectories of synchrony were different in WT and *Df(16)A<sup>+/-</sup>* mice, but the direction of development was the same ('age x condition': LME,  $p = 0.66$  and  $p = 0.32$ , detailed statistics in Table 2). The synchrony within the age groups was not different between the conditions (Figure 33, E+F).

Collectively, these findings reveal an abnormal progression of prefrontal firing synchrony in an behavioral state-dependent and neuron type-specific manner across adolescence in *Df(16)A<sup>+/-</sup>* mice.

### 3.4.5 Developmental trajectories of hippocampal theta power are abnormal in adolescent *Df(16)A<sup>+/-</sup>* mice

Hippocampal activity tremendously influences prefrontal activity not only in adults, but also already during neonatal age (Brockmann et al., 2011; Sirota et al., 2008). Here, the hippocampal activity was recorded simultaneously with prefrontal activity (Figure 34, A). The hippocampal power spectrum, similar to the prefrontal spectrum, exhibits the typical decay from slow to high frequencies and a second prominent theta power peak during movement periods (Figure 34, B).

Theta activity is an oscillatory rhythm that is propagated between brain areas, and several studies have reported coherent theta activity between the PFC and HP in memory tasks (Adhikari et al., 2010; Jones and Wilson, 2005; O'Neill et al., 2013). Therefore, it was hypothesized that the abnormal development of local network activity in the PFC is influenced by a disturbed development of hippocampal activity. Hence, hippocampal activity was investigated to detect possible developmental abnormalities in the adolescent *Df(16)A<sup>+/-</sup>* mice.

As previously mentioned regarding the prefrontal activity, the primary focus of hippocampal power was also placed on the propagated theta and the locally generated gamma oscillations. The hippocampal theta power during movement periods in *Df(16)A<sup>+/-</sup>* mice shows an abnormal development with an increase across age, the opposite tendency in comparison to WT mice ('age x condition': LME,  $p = 0.01$ , detailed statistics in Table 2). In addition, theta power in early ado *Df(16)A<sup>+/-</sup>* mice was significantly lower than in late ado or age-matched WT mice (groups: LME,  $p_{\text{early ado}} = 0.004$ ,  $p_{\text{late ado}} = 0.26$ ,  $p_{Df(16)A^{+/-}} = 0.03$ ,  $p_{WT} = 0.14$ , detailed statistics in Table 2) (Figure 34, C). During resting periods, there was no observable difference between conditions or across age (detailed statistics in Table 2) (Figure 34, E).

There was no difference in hippocampal gamma power development in *Df(16)A<sup>+/-</sup>* mice compared to WT mice (detailed statistics in Table 2) (Figure 34, D+F).

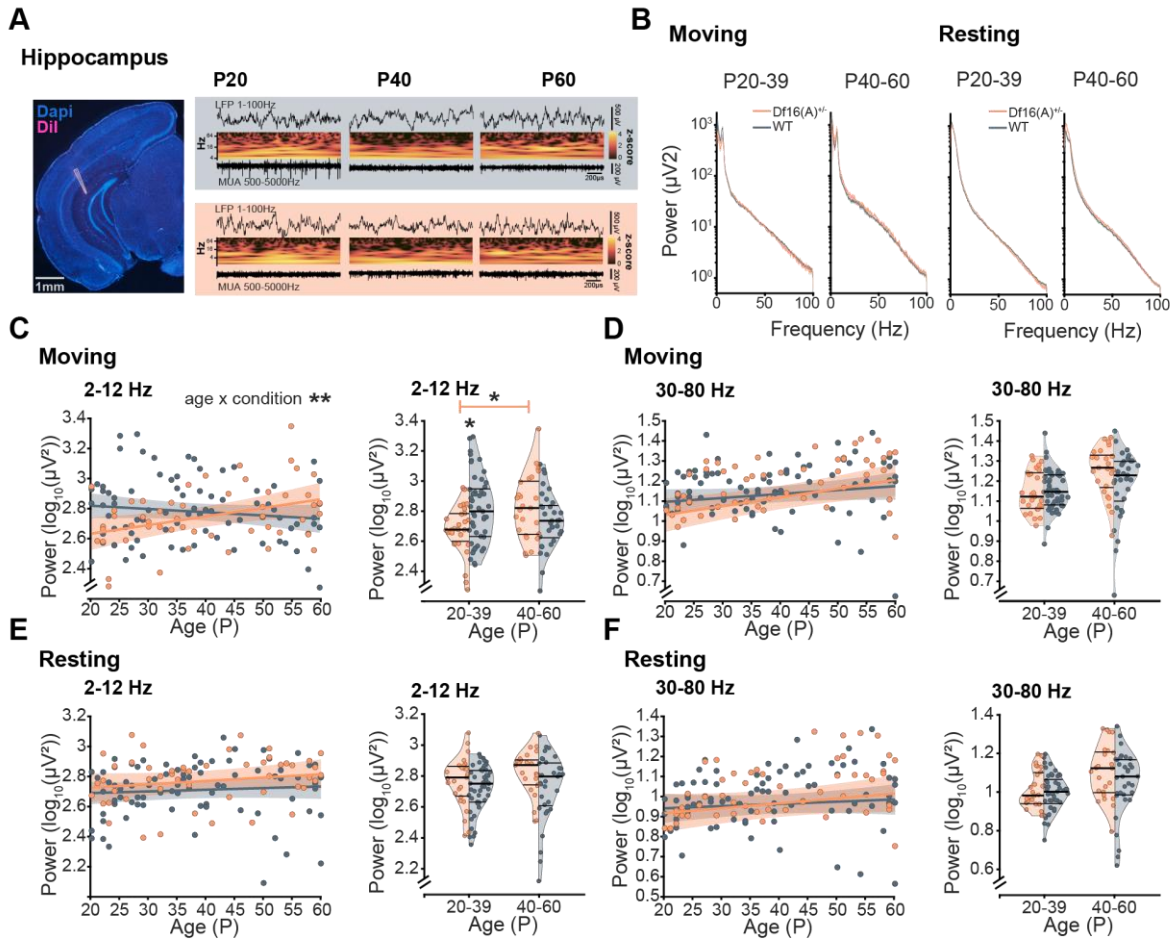


**Figure 34: Hippocampal LFP properties throughout late development in  $Df(16)A^{+/-}$  and WT mice.** (A) Left, digital photomontage reconstructing the location of DiI-labeled extracellular electrodes in the CA1. Right, examples of recordings of LFP and MUA in the CA1 of the PFC of  $Df(16)A^{+/-}$  and WT mice at the age of P20, P40 and P60. (B) Mean power spectrum of early ado and late ado  $Df(16)A^{+/-}$  (orange,  $n_{(Df(16)A^{+/-})} = 52$  recordings, 14 mice) and WT mice (blue-grey,  $n_{(WT)} = 82$  recordings, 23 mice) during movement, left, and during rest, right. (C) Left, scatter plot displaying the power in 2-12 Hz theta range across age during movement. Right, violin plot showing the power in 2-12 Hz theta in early ado and late ado  $Df(16)A^{+/-}$  and WT mice. (D), (E) + (F) Same as (C) but for mean power in 30-80 Hz broad-band gamma range during movement and 2-12 Hz theta and 30-80 Hz broad-band gamma during resting periods.

Data in scatter plots are presented as individual data points and the line displays the predicted values of the linear mixed-effect models, with the shaded area representing the 95 %-confidence interval. ‘Age x condition \*’ indicates a significant difference between the slopes of the predicted values for the  $Df(16)A^{+/-}$  and WT mice, linear mixed-effect models. In the violin plots, data are presented with median, 25th and 75th percentiles and the shaded area represents the probability density of the variable. \* $p < 0.05$ , \*\* $p < 0.01$ , \*\*\* $p < 0.001$ , linear mixed-effect models. For detailed statistics see Table 2.

These results show that the hippocampal theta rhythm, but not the gamma activity developed differently in  $Df(16)A^{+/-}$  mice in a state-dependent manner.

To further investigate possible abnormalities in hippocampal development during adolescence in the  $Df(16)A^{+/-}$  mice, firing patterns were investigated and revealed no differences in FR and ISI between  $Df(16)A^{+/-}$  and WT mice across age (detailed statistics in Table 2) (Figure 35).

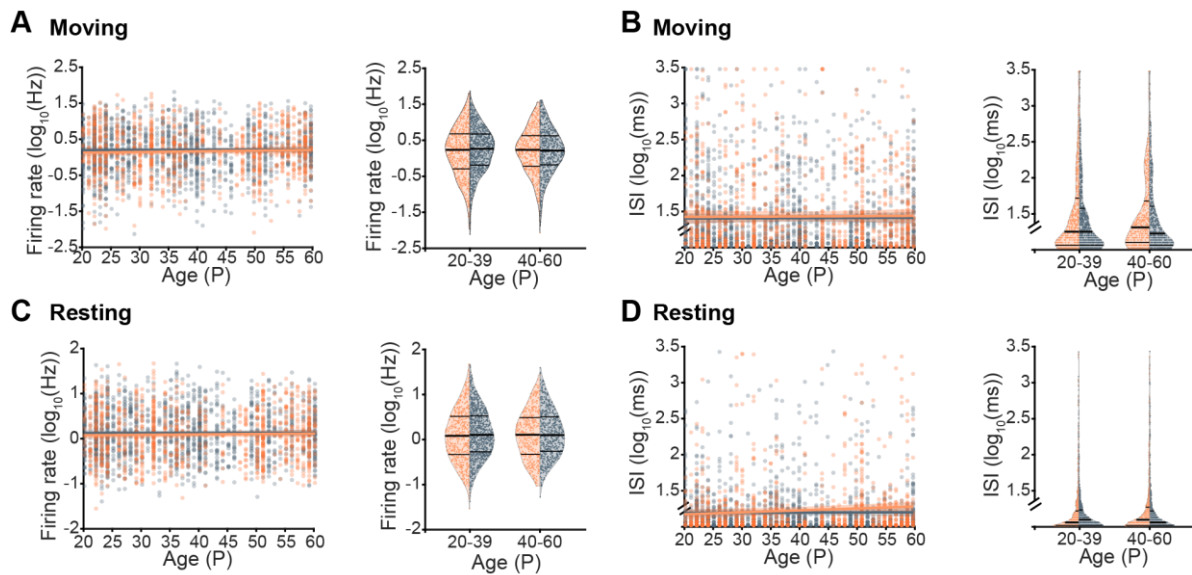


**Figure 35: Hippocampal firing properties throughout late development in  $Df(16)A^{+/-}$  and WT mice.** (A) FR of hippocampal single units during movement periods, left, displayed in a scatter plot across age and right, in a violin plot grouped in early ado and late ado  $Df(16)A^{+/-}$  (orange,  $n_{(Df(16)A^{+/-})}$ : 1041 units, 52 recordings, 14 mice) and WT mice (blue-grey,  $n_{(WT)}$ : 1529 units, 82 recordings, 23 mice). (B) Same as (A) but for resting periods. (C) ISI of hippocampal single units during movement periods, left, displayed in a scatter plot across age and right, in a violin plot grouped in early ado and late ado  $Df(16)A^{+/-}$  and WT mice. (D) Same as (C) but for resting periods. Data in scatter plots are presented as individual data points and the line displays the predicted values of the linear mixed-effect models, with the shaded area representing the 95 %-confidence interval. ‘Age x condition \*’ indicates a significant difference between the slopes of the predicted values for the  $Df(16)A^{+/-}$  and WT mice, linear mixed-effect models. In the violin plots, data are presented with median, 25th and 75th percentiles and the shaded area represents the probability density of the variable. \* $p < 0.05$ , \*\* $p < 0.01$ , \*\*\* $p < 0.001$ , linear mixed-effect models. For detailed statistics see Table 2.

Along the same lines, the synchronizations of hippocampal units with the theta rhythm and other hippocampal units were analyzed. During movement, spike-LFP interaction did not develop differently. However, the spike-spike interactions showed an increasing trend, being steeper in  $Df(16)A^{+/-}$  mice and, hence, being higher in late ado  $Df(16)A^{+/-}$  mice than during early adolescence (‘age x condition’: LME,  $p < 0.001$ ; groups: LME,  $p_{Df(16)A^{+/-}} < 0.001$ ,  $p_{WT} = 0.36$ , detailed statistics in Table 2) (Figure 36, A+B).

During resting periods, PPC values increased in both  $Df(16)A^{+/-}$  and WT mice (detailed statistics in Table 2). In contrast, spike-spike synchrony decreased in  $Df(16)A^{+/-}$  mice, but not in WT mice (‘age x condition’: LME,  $p < 0.001$ ; groups: LME,  $p_{Df(16)A^{+/-}} < 0.049$ ,  $p_{WT} = 0.08$ , detailed statistics in Table 2) (Figure 36, C+D).

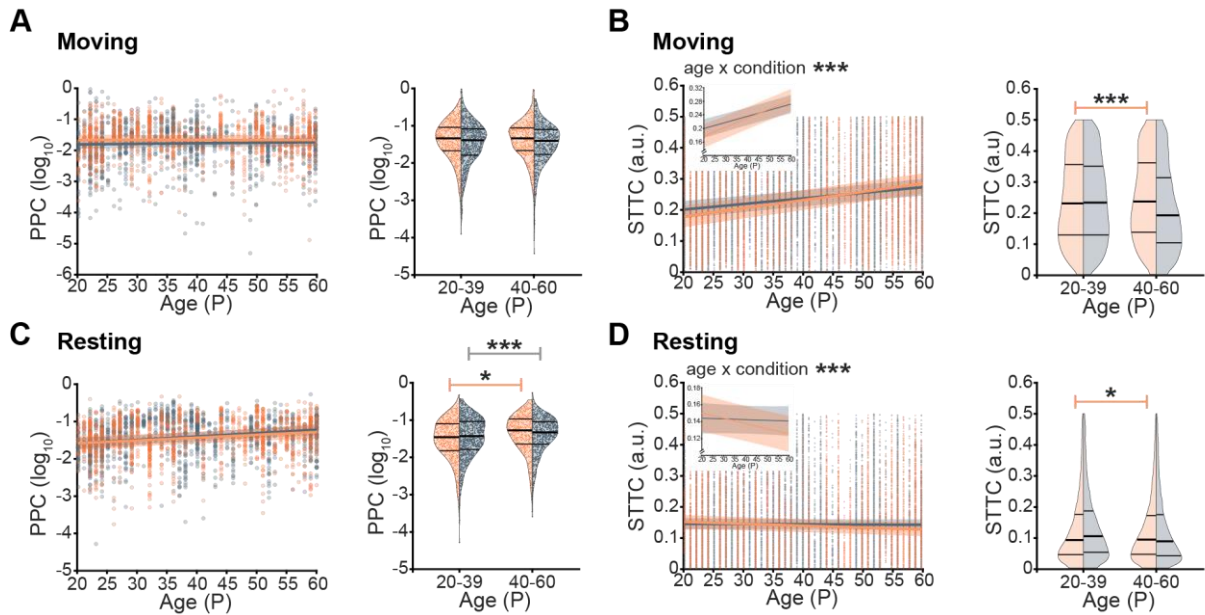


**Figure 36: Synchrony between firing and LFP and spike-spike synchrony in the HP throughout late development in  $Df(16)A^{+/-}$  and WT mice.** (A) PPC of significantly locked units to the hippocampal theta rhythm during movement periods, left, displayed in a scatter plot across age and right, in a violin plot illustrating the PPC in early ado and late ado  $Df(16)A^{+/-}$  (orange,  $n_{(Df(16)A^{+/-})}$ : 1041 units, 52 recordings, 14 mice) and WT mice (blue-grey,  $n_{(WT)}$ : 1529 units, 82 recordings, 23 mice). (B) Left, scatter plot displaying the STTC with a latency of 100 ms of hippocampal units with all other hippocampal units during movement. The inset shows the predicted STTC values across age. Right, violin plot displaying the STTC grouped in early ado and late ado  $Df(16)A^{+/-}$  and WT mice. (C) Same as (A) but for resting periods. (D) Same as (B) but for resting periods.

Data in scatter plots are presented as individual data points and the line displays the predicted values of the linear mixed-effect models, with the shaded area representing the 95 %-confidence interval. ‘Age x condition \*’ indicates a significant difference between the slopes of the predicted values for the  $Df(16)A^{+/-}$  and WT mice, linear mixed-effect models. In the violin plots, data are presented with median, 25th and 75th percentiles and the shaded area represents the probability density of the variable. \* $p < 0.05$ , \*\* $p < 0.01$ , \*\*\* $p < 0.001$ , linear mixed-effect models. For detailed statistics see Table 2.

These results indicate that hippocampal development is disrupted throughout adolescence in  $Df(16)A^{+/-}$  mice. This manifests predominantly in an increasing, but transient change in theta power during movement periods, which is the rhythm that mainly synchronizes the PFC to the HP during working memory tasks.

### 3.4.6 LFP-synchrony in $Df(16)A^{+/-}$ mice is disturbed throughout and in late adolescence

LFP-synchrony between the PFC and HP, especially in the theta activity, has been reported to be elevated in memory tasks (Adhikari et al., 2010; Jones and Wilson, 2005; O’Neill et al., 2013). Therefore, to investigate whether the disrupted hippocampal theta activity in adolescence in  $Df(16)A^{+/-}$  mice was accompanied by or underlying a disrupted LFP-synchrony between the areas, the imaginary coherence was investigated. The imaginary coherence represents the frequency-resolved synchrony and was analyzed for movement and resting periods. The coherence spectrum showed a prominent peak in the theta range, especially during movement periods (Figure 37, A+C). Therefore, the coherence of the peak located in the 2-12 Hz spectrum was quantified. This revealed that there was no difference in the developmental

trajectories of imaginary coherence (detailed statistics in Table 2). However, in late ado *Df(16)A<sup>+/-</sup>* mice, synchrony in the theta range, indicated by a significantly lower imaginary coherence, was disturbed (groups: LME,  $p_{\text{early ado}} = 0.117$ ,  $p_{\text{late ado}} = 0.015$ , detailed statistics in Table 2) (Figure 37, B+D).

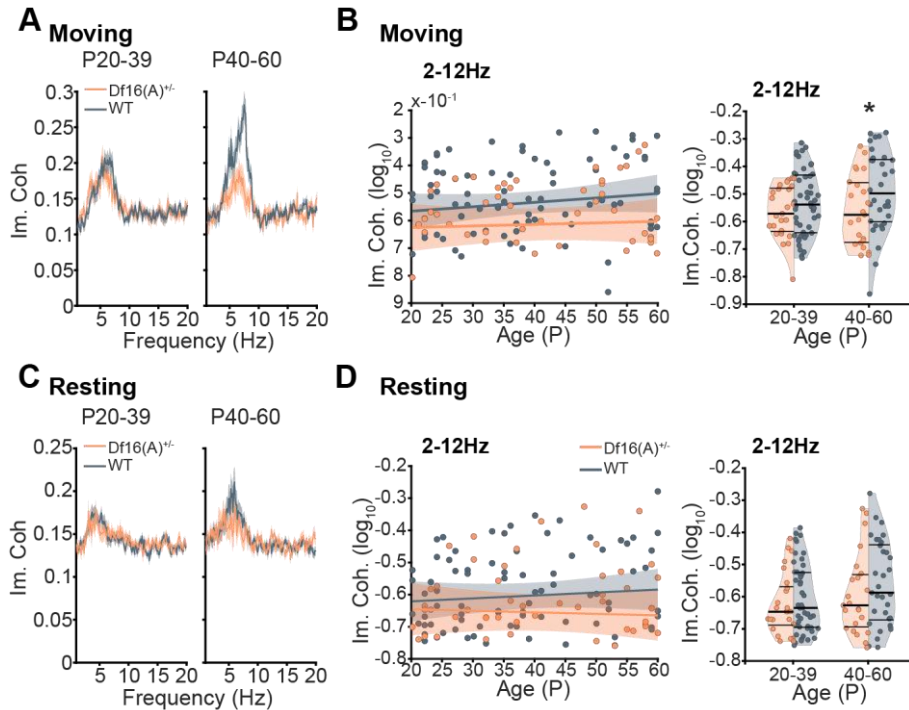


**Figure 37: Frequency-resolved synchrony of LFPs between the PFC and HP throughout late development in *Df(16)A<sup>+/-</sup>* and WT mice.** (A) Mean imaginary coherence spectra between the HP and PFC of left, early ado and right, late ado, *Df(16)A<sup>+/-</sup>* (orange,  $n_{Df(16)A^{+/-}} = 52$  recordings, 14 mice) and WT mice (blue-grey,  $n_{WT} = 82$  recordings, 23 mice) during movement. (B) Left, scatter plot displaying the imaginary coherence between HP and PFC across age and right, violin plot showing the imaginary coherence between the two areas grouped in early ado and late ado *Df(16)A<sup>+/-</sup>* and WT mice during movement. (C) Same as (A) but for resting periods. (D) Same as (B) but for resting periods.

Data in scatter plots are presented as individual data points and the line displays the predicted values of the linear mixed-effect models, with the shaded area representing the 95 %-confidence interval. ‘Age x condition \*’ indicates a significant difference between the slopes of the predicted values for the *Df(16)A<sup>+/-</sup>* and WT mice, linear mixed-effect models. In the violin plots, data are presented with median, 25th and 75th percentiles and the shaded area represents the probability density of the variable. \* $p < 0.05$ , \*\* $p < 0.01$ , \*\*\* $p < 0.001$ , linear mixed-effect models. For detailed statistics see Table 2.

In order to evaluate the directionality of the communication, the spectral dependency ratio (SDR) was assessed (Shajarisales et al., 2015). In both conditions during movement, as well as during resting periods, the hippocampal drive of the PFC was higher than the prefrontal drive of the HP (groups: signrank,  $p_{Df(16)A^{+/-}} < 0.001$ ,  $p_{WT} < 0.001$ , detailed statistics in Table 2) (Figure 38, A+C). The normalization of SDR values allowed a direct comparison of directionality strength. These normalized values showed that there were no observable differences in SDR in *Df(16)A<sup>+/-</sup>* and WT mice during both movement and resting periods (detailed statistics in Table 2) (Figure 38, B+D).

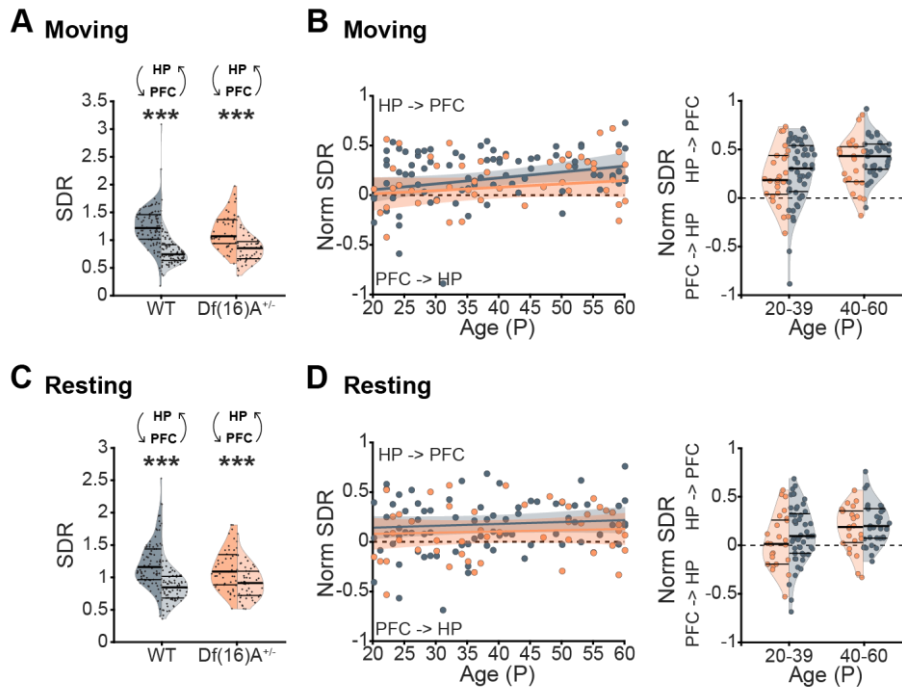


**Figure 38: Directed synchrony of LFPs between the PFC and HP throughout late development in  $Df(16)A^{+/-}$  and WT mice.** (A) Violin plot displaying the SDR between the HP and PFC. The left part of the violin indicates the directionality from the HP to the PFC and the right part the directionality from the PFC to the HP during movement periods. (B) Left, scatter plot displaying normalized SDR values across age during movement periods. Values higher than 1 indicate a higher drive from the HP, values lower than 1 indicate a higher drive from the PFC. Right, violin plot showing the same normalized SDR values grouped in early ado and late ado  $Df(16)A^{+/-}$  (orange,  $n_{(Df(16)A^{+/-})} = 52$  recordings, 14 mice) and WT mice (blue-grey,  $n_{(WT)} = 82$  recordings, 23 mice) during movement periods. (C) Same as (A) but for resting periods. (D) Same as (B) but for resting periods. Data in scatter plots are presented as individual data points and the line displays the predicted values of the linear mixed-effect models, with the shaded area representing the 95 %-confidence interval. ‘Age x condition \*’ indicates a significant difference between the slopes of the predicted values for the  $Df(16)A^{+/-}$  and WT mice, linear mixed-effect models. In the violin plots, data are presented with median, 25th and 75th percentiles and the shaded area represents the probability density of the variable. \* $p < 0.05$ , \*\* $p < 0.01$ , \*\*\* $p < 0.001$ , linear mixed-effect models. For detailed statistics see Table 2.

These results indicate that the strength of synchrony, rather than the directionality is affected in  $Df(16)A^{+/-}$  mice.

Since there was an evident disturbance in the local network development of the PFC across adolescence in  $Df(16)A^{+/-}$  mice and the hippocampal theta phase reportedly modulates prefrontal gamma amplitude (Sirota et al., 2008), the PAC between the areas was investigated (Figure 39, A+C). During movement periods, the developmental trajectories of PAC were different in  $Df(16)A^{+/-}$  and WT mice, resulting in a decreased PAC in late ado  $Df(16)A^{+/-}$  mice (‘age x condition’:  $p = 0.02$ , groups: LME,  $p_{\text{early ado}} = 0.21$ ,  $p_{\text{late ado}} = 0.02$ , detailed statistics in Table 2) (Figure 39, B). During resting periods, in both conditions, PAC increased between early ado and late ado age (groups: LME,  $p_{Df(16)A^{+/-}} = 0.044$ ,  $p_{WT} < 0.001$ , detailed statistics in Table 2) (Figure 39, D).

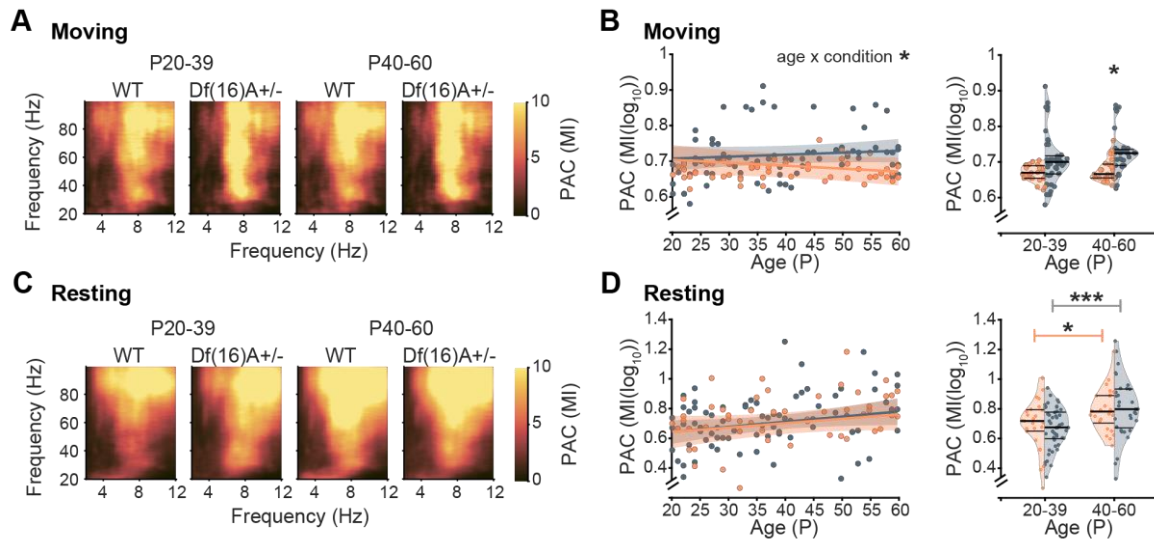


**Figure 39: Cross-frequency coupling between the hippocampal theta phase and the prefrontal gamma amplitude throughout late development in  $Df(16)A^{+/-}$  and WT mice.** (A) Color-coded heatmaps showing the mean PAC MI of the theta phase of the HP modulating the gamma amplitude of PFC in early ado and late ado  $Df(16)A^{+/-}$  (orange,  $n_{(Df(16)A^{+/-})} = 52$  recordings, 14 mice) and WT mice. (B) Left, scatter plot and right, violin plot indicating the quantified PAC MI across age and in early ado and late ado  $Df(16)A^{+/-}$  and WT (blue-grey,  $n_{(WT)} = 82$  recordings, 23 mice) mice during movement. (C) Same as (A) but for resting periods. (D) Same as (B) but for resting periods.

Data in scatter plots are presented as individual data points and the line displays the predicted values of the linear mixed-effect models, with the shaded area representing the 95 %-confidence interval. ‘Age x condition \*’ indicates a significant difference between the slopes of the predicted values for the  $Df(16)A^{+/-}$  and WT mice, linear mixed-effect models. In the violin plots, data are presented with median, 25th and 75th percentiles and the shaded area represents the probability density of the variable. \* $p < 0.05$ , \*\* $p < 0.01$ , \*\*\* $p < 0.001$ , linear mixed-effect models. For detailed statistics see Table 2.

These results indicate that, especially during movement periods, the LFP-synchrony between the HP and PFC is disturbed in late ado  $Df(16)A^{+/-}$  mice and across their adolescent development.

### 3.4.7 Synchronization of prefrontal and hippocampal units develops abnormally across adolescence in $Df(16)A^{+/-}$ mice

Since the development of prefrontal gamma amplitude modulation by the hippocampal theta phase is perturbed in  $Df(16)A^{+/-}$  mice during movement periods, the question arose whether the HP theta also abnormally entrains prefrontal spiking during adolescence. Therefore, spike-LFP synchrony with PPC of prefrontal units to hippocampal theta as well as STTC between hippocampal and prefrontal units with a lag of 100 ms was assessed.

In the first step, significant locking of prefrontal units to the hippocampal theta was investigated. The ratio of significantly locked units differed neither across age nor between conditions (detailed statistics in Table 2) (Figure 40).

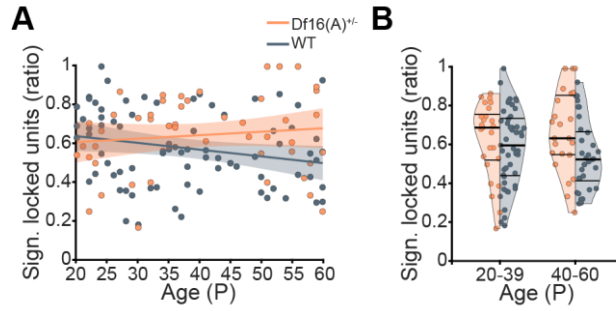


**Figure 40: Number of significantly locked prefrontal units to hippocampal theta rhythm throughout late development in  $Df(16)A^{+/-}$  and WT mice.** (A) Scatter plot displaying the ratio of prefrontal single units that are significantly locked to hippocampal theta rhythm across age. (B) Violin plot showing the ratio of prefrontal single units that are significantly locked to hippocampal theta rhythm grouped in early ado and late ado  $Df(16)A^{+/-}$  and WT mice (orange,  $n_{(Df(16)A^{+/-})}$ : 1125 units, 52 recordings, 14 mice; blue-grey,  $n_{(WT)}$ : 1701 units, 82 recordings, 23 mice).

Data in scatter plots are presented as individual data points and the line displays the predicted values of the linear mixed-effect models, with the shaded area representing the 95 %-confidence interval. ‘Age x condition \*’ indicates a significant difference between the slopes of the predicted values for the  $Df(16)A^{+/-}$  and WT mice, linear mixed-effect models. In the violin plots, data are presented with median, 25th and 75th percentiles and the shaded area represents the probability density of the variable. \* $p < 0.05$ , \*\* $p < 0.01$ , \*\*\* $p < 0.001$ , linear mixed-effect models. For detailed statistics see Table 2.

The strength of locking of Rs units during movement showed a decrease in WT mice across age, which was not evident in  $Df(16)A^{+/-}$  mice (‘age x condition’: LME,  $p = 0.048$ , groups: LME,  $p_{Df(16)A^{+/-}} = 0.81$ ,  $p_{WT} = 0.03$ , detailed statistics in Table 2) (Figure 41, A). During resting periods, there was a decrease in PPC of Rs units between early ado and late ado age in both conditions (groups: LME,  $p_{Df(16)A^{+/-}} = 0.026$ ,  $p_{WT} = 0.002$ , detailed statistics in Table 2) (Figure 41, B).

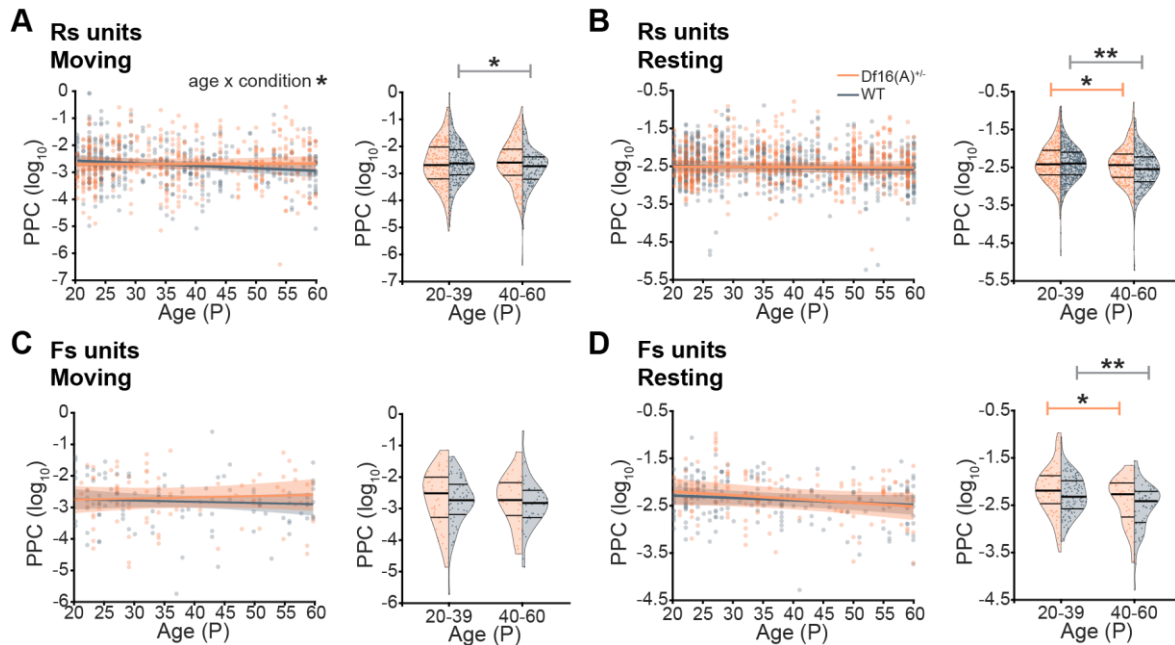


**Figure 41: Synchrony of prefrontal firing with hippocampal theta rhythm throughout late development in  $Df(16)A^{+/-}$  and WT mice.** (A) PPC of significantly locked Rs units to the hippocampal theta rhythm during movement periods, left, displayed in a scatter plot across age and right, in a violin plot illustrating the PPC in early ado and late ado  $Df(16)A^{+/-}$  (orange,  $n_{(Df(16)A^{+/-})}$ : 1125 units, 52 recordings, 14 mice) and WT mice (blue-grey,  $n_{(WT)}$ :

## Results

1422 Rs units, 82 recordings, 23 mice). **(B)** Same as (A) but for resting periods. **(C)** PPC of significantly locked Fs units to the hippocampal theta rhythm during movement periods, left, displayed in a scatter plot across age and right, in a violin plot illustrating the PPC in early ado and late ado  $Df(16)A^{+/-}$  (orange,  $n_{Df(16)A^{+/-}}$ : 174 Fs units, 52 recordings, 14 mice) and WT mice (blue-grey,  $n_{WT}$ ): 279 Fs units, 82 recordings, 23 mice). **(D)** Same as (C) but for resting periods.

Data in scatter plots are presented as single units and the line displays the predicted values of the linear mixed-effect models, with the shaded area representing the 95 %-confidence interval. ‘Age x condition \*’ indicates a significant difference between the slopes of the predicted values for the  $Df(16)A^{+/-}$  and WT mice, linear mixed-effect models. In the violin plots, data are presented with median, 25th and 75th percentiles and the shaded area represents the probability density of the variable. \* $p < 0.05$ , \*\* $p < 0.01$ , \*\*\* $p < 0.001$ , linear mixed-effect models. For detailed statistics see Table 2.

Similarly, the locking strength of Fs during rest decreased between early ado and late ado age in both conditions (groups: LME,  $p_{Df(16)A^{+/-}} = 0.013$ ,  $p_{WT} = 0.002$ , detailed statistics in Table 2), while there were no differences during movement (Figure 41, C+D). This indicated a development towards a hypersynchronization during adolescence in  $Df(16)A^{+/-}$  mice.

To test whether this is also evident in spike-spike correlations, the STTC values of hippocampal units with Rs or Fs units were analyzed, respectively.

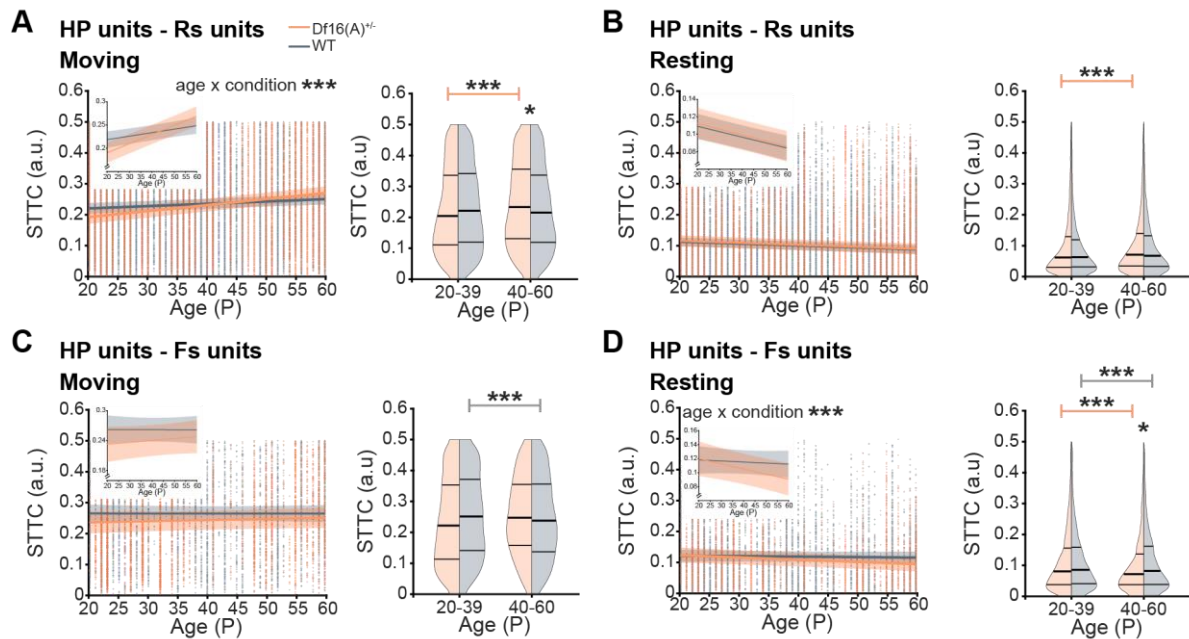


**Figure 42: Firing synchrony between prefrontal and hippocampal units throughout late development in  $Df(16)A^{+/-}$  and WT mice.** **(A)** Left, scatter plot displaying the STTC with a latency of 100 ms of hippocampal units with prefrontal Rs units during movement. The inset shows the predicted STTC values across age. Right, violin plot displaying the STTC grouped in early ado and late ado  $Df(16)A^{+/-}$  (orange,  $n_{Df(16)A^{+/-}}$ : PFC 951 Rs units + HP 1041 units, 52 recordings, 14 mice) and WT mice (blue-grey,  $n_{WT}$ ): PFC 1701 units + HP 1529 units, 82 recordings, 23 mice). **(B)** Same as (A) but for resting periods. **(C)** Left, scatter plot displaying the STTC with a latency of 100 ms of hippocampal units with prefrontal Fs units during movement. The inset shows the predicted STTC values across age. Right, violin plot displaying the STTC grouped in early ado and late ado  $Df(16)A^{+/-}$  (orange,  $n_{Df(16)A^{+/-}}$ : PFC 174 Fs units + HP 1041 units, 52 recordings, 14 mice) and WT mice (blue-grey,  $n_{WT}$ ): 279 Fs units + HP 1529 units, 82 recordings, 23 mice). **(D)** Same as (C) but for resting periods.

Data in scatter plots are presented as single units and the line displays the predicted values of the linear mixed-effect models, with the shaded area representing the 95 %-confidence interval. ‘Age x condition \*’ indicates a significant difference between the slopes of the predicted values for the  $Df(16)A^{+/-}$  and WT mice, linear mixed-effect models. In the violin plots, data are presented with median, 25th and 75th percentiles and the shaded area represents the probability density of the variable. \* $p < 0.05$ , \*\* $p < 0.01$ , \*\*\* $p < 0.001$ , linear mixed-effect models. For detailed statistics see Table 2.

STTC values between the HP and Rs units during movement were increased with age, with a steeper increase in *Df(16)A<sup>+/-</sup>* mice ('age x condition': LME,  $p < 0.001$ , detailed statistics in Table 2). This resulted in higher spike-spike synchrony in late ado *Df(16)A<sup>+/-</sup>* mice compared to age-matched WT and early ado *Df(16)A<sup>+/-</sup>* mice (groups: LME,  $p_{\text{early ado}} = 0.056$ ,  $p_{\text{late ado}} = 0.047$ ,  $p_{Df(16)A^{+/-}} < 0.001$ ,  $p_{\text{WT}} = 0.291$ , detailed statistics in Table 2) (Figure 42, A). During resting periods, spike-synchrony with Rs units in both conditions decreased across age with a significant difference between early ado and late ado *Df(16)A<sup>+/-</sup>* mice (groups: LME,  $p_{Df(16)A^{+/-}} < 0.001$ ,  $p_{\text{WT}} = 0.653$ , detailed statistics in Table 2) (Figure 42, B).

The STTC values between the HP and Fs units decreased across age in resting periods, with a steeper decline in *Df(16)A<sup>+/-</sup>* mice ('age x condition': LME,  $p < 0.001$ , detailed statistics in Table 2). This resulted in a hyposynchronization in late ado *Df(16)A<sup>+/-</sup>* mice (groups: LME,  $p_{\text{early ado}} = 0.947$ ,  $p_{\text{late ado}} = 0.026$ ,  $p_{Df(16)A^{+/-}} < 0.001$ ,  $p_{\text{WT}} < 0.001$ , detailed statistics in Table 2) (Figure 42, D). During movement periods, there was no significant difference in STTC values between *Df(16)A<sup>+/-</sup>* and WT mice, but a decrease between early ado and late ado WT mice (groups: LME,  $p_{Df(16)A^{+/-}} = 0.813$ ,  $p_{\text{WT}} < 0.001$ , detailed statistics in Table 2) (Figure 42, C).

To summarize, the synchrony between hippocampal activity and Rs units exhibited a developmental trend towards a higher correlation across adolescence in *Df(16)A<sup>+/-</sup>* mice during movement, in contrast to LFP correlations. This trend towards hypersynchronization during movement periods is contrasted by a developmental tendency towards lower synchronization during resting periods of hippocampal activity with Fs units.

## 4 Discussion

The aim of this work was to identify and analyze underlying mechanisms of prefrontal-hippocampal network activity throughout development, especially during adolescence, in the context of neurodevelopmental disorders.

The neonatal period in rodents is considered a critical developmental period (Chini and Hanganu-Opatz, 2021; Clancy et al., 2001). In a mouse model of neurodevelopmental disorders, combining a genetic predisposition (G) with an environmental stimulus (E), the discontinuous activity patterns as well as morphological features of prefrontal neurons are disorganized in neonates (Chini et al., 2020). As microglia play a central role in the shaping of neuronal circuits by engulfing synapses, the initial hypothesis was that the microglia in the PFC of neonatal dual-hit GE mice are hyperactive. The first part of this thesis demonstrated that the microglia found in the PFC of neonatal GE mice showed hyperactivity by increased engulfment of synaptic vesicle material. Therefore, it was concluded that in neonatal GE mice, the reduced number of synapses is caused by an overpruning. This phenotype of microglia was rescued by a treatment of neonatal GE mice with the antibiotic minocycline, during the critical developmental period of P1-8.

Alongside the reduction in microglia hyperactivity described in this thesis, normalizations of prefrontal activity patterns, complexity of dendritic trees and recognition memory deficits have been associated with early minocycline administration, highlighting the criticality of this life period (Chini et al., 2020). Treatment with minocycline during P9 to P16, did not rescue behavioral deficits in recency recognition (RR) tasks. Instead, GE mice treated with minocycline during this later period showed comparable deficits to untreated GE mice. This confirms that the early neonatal period is essential for the development of prefrontal activity.

However, the PFC is known to undergo a prolonged developmental period and maturational changes well into adolescent age (Chini and Hanganu-Opatz, 2021; Delevich et al., 2018). During this late developmental period, the interaction of the PFC with the hippocampal formation plays an important role (Arguello and Gogos, 2009; Klune et al., 2021; Sigurdsson and Duvarci, 2016). Previous studies have described that the prefrontal-hippocampal network activity is disturbed in GE mice during the neonatal period (Hartung et al., 2016b; Oberlander et al., 2019; Xu et al., 2021a). Here it is shown that this network synchrony between PFC and hippocampus (HP), as well as between prefrontal and lateral entorhinal cortex (LEC), was elevated in mice at a pre-pubescent age (P16-26) (Dutta and Sengupta, 2016). These results show that the prefrontal-hippocampal network activity was perturbed during the pre-adolescent stage in GE mice.

These results leave open the question of the functional relevance of this network during adolescence. One core symptom in neurodevelopmental disorders such as schizophrenia is deficits in working memory. Working memory relies on a functional prefrontal-hippocampal network. Therefore, it was attempted to establish a delayed non-match to sample (DNMS) T-Maze task in head-fixed mice to enable simultaneous electrophysiological recordings.

---

However, the mice were incapable of learning this task under these head-fixed conditions, or lacked the motivation to perform the task under the more stressful head-fixed conditions.

Open field behavior on the MobileHomeCage was normal and hence, it was possible to establish a method to record prefrontal and hippocampal activity during movement and resting periods across adolescent age. The awake, head-fixed recordings aimed to clarify the unresolved inquiry regarding the developmental trajectories throughout adolescence, with a focus on determining whether and which activity patterns are specifically altered. In chapter 4 of this thesis, a purely genetic model with a strong genetic risk factor for neurodevelopmental disorders was investigated (Karayiorgou et al., 2010; Oberlander et al., 2019). The neonatal *Df(16)A*<sup>+/-</sup> mice show network deficits that are similar to the abnormalities in the prefrontal-hippocampal network of neonatal GE mice (Oberlander et al., 2019). During adolescence, abnormal developmental trajectories of local prefrontal activity in broad-band gamma power and synchrony of spike trains were identified. Regarding the HP, an abnormal development of theta power was shown. Theta is a main rhythm of prefrontal-hippocampal synchrony (Adhikari et al., 2010; Jones and Wilson, 2005). While the synchrony in local field potentials (LFP) between the two areas displayed a development to hyposynchronization, the firing synchrony of hippocampal and prefrontal pyramidal neurons increased during development in the *Df(16)A*<sup>+/-</sup> model. Neonatal *Df(16)A*<sup>+/-</sup> mice showed a weaker coupling of prefrontal-hippocampal network activity which was not seen in early ado mice, but was apparent again in late adolescence. Together, the abnormal development of prefrontal activity and network synchrony indicates that adolescent development in neurodevelopmental disorders is not merely a continuation of preset disturbances. Adolescence is the time point of fine-tuning and reorganization of network activity (Pöpplau et al., 2023). The results here substantiate that this reorganization of the prefrontal-hippocampal network activity is perturbed in specific manners in *Df(16)A*<sup>+/-</sup> mice.

In summary, the findings from this thesis show that both neonatal time and adolescence are vulnerable developmental time points for the maturation of the prefrontal-hippocampal network in the context of neurodevelopmental disorders. Abnormalities in adolescence are not merely a continuation of preset perturbations of early development. Instead, the reorganization and fine-tuning observed in healthy development is disturbed in mouse models of neurodevelopmental disorders. This can arguably be the underlying cause for cognitive disruptions observed during and after adolescence in these disorders. In the following sections, the results will be discussed in more detail in a sequence resembling the presentation of the results.

## **4.1 Considerations of the dual-hit GE and the *Df(16)A*<sup>+/-</sup> mouse models in schizophrenia research**

Mental disorders, though they comprise a diverse variety of diseases, share an underlying cause of abnormal developmental processes in the brain. Thus, they are also termed neurodevelopmental disorders (Davis et al., 2016). Mental disorders are a considerable burden

---

on patients and societies, yet lack thorough elucidation and sufficient treatment options (Arguello and Gogos, 2009; MacKenzie et al., 2018; Panov et al., 2023). Studying these diseases in humans has its limitations due to obvious ethical considerations (Kaur and Cadenhead, 2010). Accordingly, animal models have proved to be valuable tools in biomedical research (Markram, 2013; Mukherjee et al., 2022). In neuroscience, human and animal model studies complement each other reciprocally, each guiding the direction of research of the respective other domain so the research stays relevant to the human condition (Phillips and Roth, 2019). In addition, animal models can provide an in-depth look into the biological mechanisms underlying diseases, the resulting implications for behavioral abilities and can establish a causal link between mechanisms and disease outcome (Phillips and Roth, 2019).

The quality of animal models in neuropsychiatric disorders is assessed using different criteria; typically, three validities are considered (Subramanian, 2022). These are face, construct and predictive validity, initially introduced to assess the quality of animal models in depression (Willner, 1984). However, these criteria are also valid for other psychiatric diseases (Belzung and Lemoine, 2011). Face validity refers to the resemblance of the phenotype of the human disease, i.e., do the symptoms in the animal model reflect the symptoms that manifest in patients. Construct validity reflects how well the underlying mechanisms that induce the animal model's phenotype mirror the currently understood etiology of the disease in humans; for example, genetic models are animal models with high construct validity. Predictive validity is a measure of how well a model can predict currently unknown aspects of the disease, e.g., medical treatment (Subramanian, 2022; Willner, 1984). These three classical criteria remain most widely accepted, though other proposals to extend and refine these criteria exist (Belzung and Lemoine, 2011; Denayer et al., 2014; Subramanian, 2022). In general, animal models are incapable of accurately capturing the full extent of human psychiatric disorders, hence no animal model shows perfect validity in all three classes (Belzung and Lemoine, 2011).

Common animal models for neurodevelopmental disorders are models of maternal immune activation (MIA), with either the bacterial component lipopolysaccharide (LPS) or the viral mimetic polyinosinic:polycytidylic acid (poly I:C) (Boksa, 2010; Reisinger et al., 2015). MIA triggers an inflammatory reaction with the release of specific cytokines and chemokines, some of which can pass through the placenta into the fetus and disrupt brain development after crossing the blood-brain barrier. This results in a higher susceptibility for neurodevelopmental disorders (Boksa, 2010). MIA with poly I:C shows good construct and face validity (Boksa, 2010).

Nonetheless, according to the multiple-hit hypothesis for neurodevelopmental disorders, the etiology of these disorders comprises several hits during distinct vulnerable periods of life (Davis et al., 2016). In addition to environmental hits, the risk factors for neurodevelopmental disorders can include genetic predispositions (Davis et al., 2016). In the first part of the thesis, this multiple-hit approach was used. To this end, genetically primed mice with a mutation in the *disrupted-in-schizophrenia 1* (*Disc1*) gene underwent a MIA through poly I:C injection during gestation. The DISC1 protein shows functions in neural development and brain maturation processes, being involved in neuronal proliferation, differentiation, migration, cAMP signaling and cytoskeletal formation (Soares et al., 2011). It is expressed in particularly high amounts during critical periods and near neuronal progenitors, and is therefore proposed

---

to be involved in embryonic and adult neurogenesis (Brandon et al., 2009; Le Strat et al., 2009). However, the assessment of the *Disc1* gene as a sole risk factor and being causative for schizophrenia has been revised, as it was found to be involved in many other mental disorders as well (Brandon et al., 2009). In addition, it has been argued that the *Disc1* mutation shows a general face validity for psychiatric disorders (Tomoda et al., 2016). The combination of the two hits, the genetic predisposition (G) and the environmental hit with MIA (E), can help to broaden the knowledge of the mechanisms underlying neurodevelopmental disorders (Esposito et al., 2018). Hence, the dual-hit GE mouse model was used here to investigate the prefrontal network activity in neonatal and prejuvenile development. The neonatal age in rodents roughly mirrors the second to third trimester of gestation in humans (Clancy et al., 2001). Prejuvenile age (around P14-P25) is the period when mice start to leave their nest and explore their environment, the time of weaning and gain of behavioral abilities (Dutta and Sengupta, 2016). This time in rodents' life translates to young children around 2-7 years of age in humans (Dutta and Sengupta, 2016; Khodosevich and Sellgren, 2023). Some neurodevelopmental disorders, namely autism spectrum disorders (ASD), attentional deficit hyperactivity disorder (ADHD) and global developmental delay (GDD) are usually diagnosed between 3 and 6 years of age in humans (Mintz Hemed and Melosh, 2023). The results here and from other investigations show perturbed development of prefrontal network activity during the neonatal and prejuvenile period in GE mice (Chini et al., 2020; Hartung et al., 2016b; Oberlander et al., 2019; Xu et al., 2019; Xu et al., 2021a; Xu et al., 2021b). The perturbations found at neonatal age suggest abnormal developments already take place at a very early and critical stage, manifesting as behavioral deficits at a prejuvenile age. These findings may potentially be linked to the onset of ASD, ADHD and GDD (Chini et al., 2020; Hartung et al., 2016b; Xu et al., 2021a).

However, this leaves open the question of neurodevelopmental disorders with later onset time points, such as schizophrenia, which typically only shows an onset during adolescence and early adulthood (Gogtay et al., 2011; Khodosevich and Sellgren, 2023). In schizophrenia patients, the prefrontal-hippocampal network synchrony was found to be disturbed, possibly underlying cognitive disabilities (Meyer-Lindenberg et al., 2005; Rasetti et al., 2011). The prefrontal-hippocampal network activity is involved in the information processing and working memory tasks (Bähler et al., 2015; Eichenbaum, 2017), which have been shown to be impaired in schizophrenia patients (Gold et al., 2018).

The dual-hit GE mouse model is a general model for neurodevelopmental disorders. In contrast to the *DISC1* mutation, the 22q11.2 microdeletion is regarded a genuine risk factor for schizophrenia (Brandon et al., 2009; Karayiorgou et al., 2010). The syndrome this microdeletion causes is called the DiGeorge or 22q11.2 deletion syndrome (ds). It is highly prevalent (~1 in 4000 live births), accounts for 1-2 % of sporadic schizophrenia cases and up to one third of patients develop schizophrenia later in life (Karayiorgou et al., 2010). The 22q11.2 microdeletion typically occurs at a length of 3 Mb or 1.5 Mb; the latter is modelled in mice in the *Df(16)A<sup>+/-</sup>* mouse model (Stark et al., 2008). Neonatal mice of the *Df(16)A<sup>+/-</sup>* mouse model were shown to have similar perturbations in the prefrontal-hippocampal network as dual-hit GE mice which are not present in single-hit G or single-hit E mice, suggesting that it is a stronger genetic risk model (Hartung et al., 2016b; Oberlander et al., 2019). Thus, investigations into the prefrontal-hippocampal network activity spanning the prejuvenile to early adult life

---

period across adolescence, i.e., the typical onset period for later onset neurodevelopmental disorders such as schizophrenia, were carried out using the *Df(16)A<sup>+/-</sup>* mouse model.

## **4.2 Rescue function of transient minocycline treatment in neonatal dual-hit GE mice**

### *4.2.1 Rescue of microglial function in the prefrontal cortex during neonatal development*

Neurodevelopmental disorders have a common etiology, namely disrupted maturational processes in the brain, already very early during development (Davis et al., 2016). During this time, the brain shows discontinuous activity patterns, described as bursts of electrical activity alternating with electrically silent periods (Hanganu-Opatz, 2010; Khazipov et al., 2004; Vanhatalo and Kaila, 2006; Workman et al., 2013). This has been observed in preterm babies, but also in neonatal rodents (Hanganu-Opatz, 2010; Vanhatalo and Kaila, 2006). These oscillatory activity patterns are found in various brain areas, including the PFC (Brockmann et al., 2011; Hanganu-Opatz, 2010). The PFC is an important brain area in the context of neurodevelopmental disorders, as it is involved in cognitive processing. Dysfunctions in this behavioral domain are a key symptom in neurodevelopmental disorders (Miller, 2000; Miller and Cohen, 2001). In mouse models of neurodevelopmental disorders, it has been reported that the prefrontal network activity with the HP is already perturbed at a neonatal age (Hartung et al., 2016b; Oberlander et al., 2019; Xu et al., 2021a).

One mouse model exhibiting abnormal prefrontal network activity is the dual-hit GE model. The perturbations in local prefrontal activity observed in this model manifest in disorganized activity patterns, especially in the superficial layers of the PFC (Chini et al., 2020). The pyramidal neurons of these layers show a lesser number of spines and reduced dendritic branching, which then can result in an abnormal integration of inputs in the PFC (Chini et al., 2020). This led to the hypothesis that the pruning of synapses through microglia action might be enhanced in neonatal GE mice. Along the same lines, microglia in the PFC of neonatal GE mice showed an increased distal cell volume, which is an indicator for a higher ramification.

In the adult brain, microglia exist in different states of activity, each with different morphologies. Ramified microglia constantly monitor their surroundings for potential danger signals. On the trajectory to phagocytic activity, they pass an intermediate, bushy phase, while in their active state microglia exist in an amoeboid state (Crews and Vetreno, 2016; Mosser et al., 2017). Microglia activity and inactivity is triggered by so-called ‘on’ and ‘off’-signals. ‘Off’ signals are constantly present in healthy, normally functioning brain tissue, and disappearance of these signals activates microglia. In contrast, ‘on’ signals are released on demand and trigger an immediate microglia activation (Biber et al., 2007). Under normal conditions, activated microglia remove apoptotic or dead cells, nonfunctional structures and toxic cellular waste through phagocytosis. Various ‘on’ and ‘off’ signals are released by neurons; hence neurons are not passive receivers of immune function, but can actively modulate the brain’s immune

---

system (Biber et al., 2007; Zhao et al., 2024). An overactivation of microglia can be neurotoxic and can cause reductions in gray matter, spine density and dendritic branching found in schizophrenic patients and animal models of MIA (Howes and McCutcheon, 2017; Juckel et al., 2011).

The early immune activation through MIA can activate microglial cells in early development, which in turn can affect neuronal and synaptic development and result in abnormally built neural networks (Juckel et al., 2011; Mosser et al., 2017). Microglial cells play an active role in brain development as they interact with various cell types in the brain. Microglia phagocytose neurons and neuronal precursor cells, thus shaping the formation of neuronal circuits, but also oligodendrocyte precursor cells and hence influence myelination. Additionally, they are active on a smaller scale, and sculpt and refine existing neuronal circuits through pruning of synapses (Mehl et al., 2022). In neonatal rodents, microglia migrate through the brain to their place of destination in an activated, amoeboid state. They progressively adopt a more mature ramified morphology across the neonatal period and only fully mature by the end of the second postnatal week (Mehl et al., 2022; Miyamoto et al., 2016).

Therefore, it can be argued that the more ramified phenotype, indicated by the higher distal cell volume found in neonatal GE mice, shows that the microglia in the animal model are hypermature and monitoring their surroundings, while in age-matched control mice they are still exhibiting the amoeboid, migrating phenotype. In addition, the microglia cells in the PFC of neonatal GE mice were engulfing more synaptic material, as was indicated by the higher number and volume of VGLUT1-stained inclusions in the microglia. This underpins that the microglia in GE mice are hyperactive. The higher activity of the microglia and resulting higher pruning of synapses is argued to be the underlying reason for the reduced synaptic density and dendritic branches in prefrontal pyramidal neurons.

The tetracycline antibiotic minocycline shows anti-inflammatory properties and potently inhibits microglia activity. Minocycline has been shown to have beneficial effects in various neuropsychiatric disorders, including obsessive-compulsive disorder, chronic stress, depression and schizophrenia (Dean et al., 2012). In schizophrenia patients, minocycline used as an adjunctive therapy was able to treat psychiatric symptoms and alleviate behavioral symptoms and cognitive performance (De Picker et al., 2017; Miyaoka et al., 2008). In a MIA mouse model, the treatment with minocycline rescued sensorimotor gating deficits and a decrease in neurogenesis (Mattei et al., 2014). Minocycline treatment in the GE mice during the neonatal period of P1-8 rescued the hypermature phenotype of microglial cells found in GE mice and to a lesser extent also the synaptic pruning. In further experiments, Chini et al. (2020) could show that the more amoeboid, less engulfing phenotype of microglial cells was accompanied by a rescue of the structural and functional deficits seen in superficial layer pyramidal neurons in neonatal GE mice.

#### *4.2.2 Partial rescue of recognition memory functions in prejuvenile dual-hit GE mice*

Minocycline treatment as an add-on therapy in schizophrenia patients has been shown to ameliorate behavioral symptoms and cognitive performance (De Picker et al., 2017; Miyaoka et al., 2008). Similarly, minocycline rescued neurogenesis and sensorimotor gating functions in

---

a mouse model of MIA (Mattei et al., 2014). In the dual-hit GE mice, treatment during the early neonatal period (P1-8) normalized the microglial phenotype, led to lesser engulfing and rescued functional abnormalities in the PFC (Chini et al., 2020). In addition, minocycline administration rescued behavioral deficits in recognition memory performance in prejuvenile GE mice (Chini et al., 2020).

Tasks for recognition memory require an intact memory function, as they depend on the recognition and discrimination of differences in novelty, placement and time passed since last exploration (Bevins and Besheer, 2006). The brain circuitry essential for novelty detection and temporal order memory centers on the PFC and HP and requires an intact maturation of this network (Barker and Warburton, 2011; Krüger et al., 2012; Warburton and Brown, 2015). Here, novelty detection was assessed using the novel object recognition (NOR) paradigm, and temporal order memory was tested using the recency recognition (RR) paradigm. These tasks can be conducted with young animals because the sensory and motor abilities required for novel object recognition are mature by P17 in mice (Krüger et al., 2012). Object recognition tasks are well-suited for prejuvenile mice as they require no prior training, only little habituation and no food or water restriction. In addition, they depend on the intrinsic drive of rodents to explore and investigate novel stimuli over familiar ones (Bevins and Besheer, 2006).

In rodent models of neurodevelopmental disorders, object recognition is impaired (Wolff et al., 2011). In line with this, several studies have reported that these behavioral deficits are already present during development in prejuvenile mice of the dual-hit GE model (Chini et al., 2020; Hartung et al., 2016b; Xu et al., 2019; Xu et al., 2021a; Xu et al., 2021b). In addition, it has been shown that administration of minocycline during the early neonatal period can rescue the behavioral deficits in prejuvenile mice (Chini et al., 2020). As hypermaturity and higher pruning of microglia in the PFC of GE mice has been reported here, which was also rescued through administration of minocycline, it is tempting to speculate that the effects are connected. This connection could have various underlying mechanisms.

On the one hand, during development microglia are involved in the formation of neuronal circuits as well as in the shaping and refining of these circuits (Mehl et al., 2022). Chini et al. (2020) suggest an abnormal integration of hippocampal input by the PFC, indicated by a perturbed function of pyramidal neurons in the superficial layers and an accompanying altered morphology. The superficial layers of the PFC densely project to the deep layers of the PFC, which in turn also receive inputs from the HP (Anastasiades and Carter, 2021; Jay and Witter, 1991). Together, this indicates that the microcircuits and integration of inputs within the PFC are disturbed in the GE mice. The rescue of pyramidal neuron function and morphology by less microglial pruning could also have rescued these circuits, subsequently affecting the object recognition tasks.

On the other hand, microglial cells can influence the oxidative stress level of the brain by releasing reactive oxygen species (Monji et al., 2013). Oxidative stress in turn influences the function of the N-methyl-D-aspartate (NMDA) receptor and can cause a hypofunction (Hardingham and Do, 2016). NMDA receptors play a central role in memory functioning (Li and Tsien, 2009). Thus, the rescue of the hypermature phenotype of microglia and a subsequent, potentially altered oxidative state could be another route via which minocycline can alter the

behavioral deficits seen in GE mice. The suggested mechanisms are neither necessarily exclusive, nor are they the only possible mechanisms of rescue.

However, the administration of minocycline during a later time-point of development (P9-16) did not rescue the behavioral deficits observed in GE mice. This suggests that this time window is no longer sensitive to alterations induced by minocycline. Microglia reach their mature phenotype by the end of the second postnatal week (Mehl et al., 2022). Therefore, one possibility would be that the hypermature status found in the PFC in GE mice is already set by this time and cannot be reversed by microglial inhibition through minocycline. An alternative hypothesis could be that the miswiring of the prefrontal microcircuit during this age has long-term effects on cognitive abilities even if it is only transient. Confirmation of this would require further studies, including investigations of the initial beta-gamma entrainment by the HP and the involvement of neuromodulators or receptors such as dopamine or NMDA receptors (Ahlbeck et al., 2018; Brockmann et al., 2011; Hardingham and Do, 2016; Leslie et al., 1991). This specifically highlights the early developmental period of P1-8 as a critical period in which specific patterns in brain development are irreversibly preset and cannot be rescued by this pharmacological intervention with minocycline.

On another note, the neonatal period in rodents roughly translates to human gestation in the second to third trimester (Clancy et al., 2001). Even though certain risk factors for later manifestation of neurodevelopmental disorders can be recognized during pregnancy, neurodevelopmental disorders are typically classified in childhood and adolescence (Mintz Hemed and Melosh, 2023). ASD, GDD and ADHD are usually diagnosed between 3 and 6 years of age, schizophrenia in adolescence with the onset of the first psychotic episode (Gogtay et al., 2011; Mintz Hemed and Melosh, 2023). Minocycline administration has beneficial effects in the treatment of schizophrenia and also in the treatment of fragile X syndrome when used in adolescence (De Picker et al., 2017; Leigh et al., 2013; Miyaoka et al., 2008). Nonetheless, there are case reports that application of minocycline at a young age can also have detrimental effects and a lack of beneficial effects on severe psychotic symptoms has been reported for adolescents (Brauer et al., 2019; El-Hallak et al., 2008; Ramakrishna et al., 2009). Accordingly, a more in-depth understanding of the prefrontal-hippocampal network in later development is needed to pave the way for follow-up studies. These could identify biomarkers for early identification of neurodevelopmental disorders as well as appropriate time windows for possible intervention or prevention strategies. It was previously shown that the prefrontal-hippocampal network is disrupted in prejuvenile dual-hit GE mice (Hartung et al., 2016b; Xu et al., 2019; Xu et al., 2021a). Therefore, the prefrontal-hippocampal network in combination with the LEC was investigated. The LEC is a brain area which entrains this network already early in development (Hartung et al., 2016a).

---

### 4.3 Prefrontal-hippocampal-entorhinal network activity in anesthetized prejuvenile dual-hit GE mice

The mPFC and HP are in close communication, mostly via dense direct monosynaptic projections from the cornu ammonis 1 (CA1) to the mPFC (Ferino et al., 1987; Jay and Witter, 1991). In contrast, direct feedback projections are sparse and communication directed from the mPFC to the HP mostly relies on relay areas, such as the ventromedial thalamus (VMT) or the entorhinal cortex (EC) (Rajasethupathy et al., 2015; Xu and Südhof, 2013). The lateral part of the entorhinal cortex (LEC) is critical for decoding of context and temporal information in associative recognition memory and of stimulus features (Dickerson and Eichenbaum, 2010). The LEC as a relay station between PFC and HP is of special interest in neurodevelopmental disorders, as it receives sensory input very early on, entrains the limbic circuitry in neonatal development and is involved in temporal processing in associative recognition memory. The latter was shown to be perturbed at a prejuvenile age in the dual-hit GE mouse model of mental illness (Chini et al., 2020). This is the age period shortly after eye-opening, when mice start to leave the nest and explore their environments (Dutta and Sengupta, 2016). Reportedly, during this prejuvenile time to the onset of adolescence the entorhinal circuits emerge with their specific functions and corresponding network interactions, i.e., stable firing of grid cells only has an onset after P20 (Bjerknes et al., 2015; Tan et al., 2015; Wills et al., 2012). Moreover, during this period sensory and motor abilities have matured sufficiently to ensure recognition memory (Krüger et al., 2012).

The multi-site recordings of LFP and MUA in prejuvenile GE and control mice revealed no difference in broad-band power in PFC, HP or LEC. This is in line with other findings (Hartung et al., 2016b; Xu et al., 2021b). Compared to the prominent abnormal power reported in the neonatal prefrontal-hippocampal-entorhinal network of GE mice, this indicates that the network partially compensates the abnormal power between the neonatal and prejuvenile age period (Xu et al., 2021b). However, this compensation does not counteract all activity deficits, since entorhinal and hippocampal firing rates were increased in prejuvenile GE mice, as reported elsewhere (Xu et al., 2021b), even though they did not reach significant levels here. The communication within the network is also perturbed, as shown by the augmented coherence and pairwise-phase consistency (PPC) between the PFC and HP as well as the PFC and LEC in prejuvenile GE mice, even though the augmented coherence between the PFC and HP did not reach significant levels here.

The altered communication between the PFC and LEC suggests that the anomalies observed in the activity of the prefrontal-hippocampal-entorhinal network and the deficits observed in object recognition tasks in prejuvenile GE mice cannot solely be attributed to the altered prefrontal-hippocampal activity observed at a neonatal age (Chini et al., 2020; Hartung et al., 2016b; Oberlander et al., 2019; Xu et al., 2019; Xu et al., 2021a). This is underpinned by a reduced LEC-HP communication at a neonatal age through sparser and less efficient axonal projections from the LEC to the HP (Xu et al., 2021b). In addition, in neonatal GE mice deep layer LEC neurons exhibit abnormal membrane properties (Xu et al., 2021b). Another pathway through which this network could be affected is the entrainment of the LEC by the olfactory

---

system, which is already present in early life (Chen et al., 2023; Gretenkord et al., 2019; Kostka and Hanganu-Opatz, 2023). Olfaction is among one of the first functional sensory systems in neonatal rodents (Logan et al., 2012). In line with this, olfaction and the olfactory brain network are reportedly disturbed in schizophrenia patients and at-risk youths, hence also during adolescent development (Moberg et al., 2014; Turetsky et al., 2018).

The experiments conducted here have their limitations, as the deficits in behavioral tasks can only be connected to the reported abnormal network activity on a group level, as the electrophysiological activity was assessed under urethane anesthesia. Hence, the electrophysiological recordings could not directly be linked to the behavioral task performance, as they were not done in the same animals at the same time. Urethane mimics sleep-like patterns in electrophysiological recordings and induces a sleep-like breathing rhythm (Clement et al., 2008). In adults, anesthesia has been shown to increase slow oscillations and decrease faster ones (Purdon et al., 2015). In contrast, urethane anesthesia in neonatal rodents suppresses electrophysiological activity in a non-frequency-specific manner (Chini et al., 2019). The adult-like frequency-specific suppression of activity by anesthesia emerges around P12 in rodents (Ackman et al., 2014). Apart from blocking the direct correlation of electrophysiological activity with behavioral tasks, anesthesia makes it more difficult to interpret electrophysiological data across development. These constraints necessitate the possibility of performing electrophysiological recordings in awake mice during development.

It has been previously described that the adolescent period of development is particularly relevant in the context of prefrontal maturation and neurodevelopmental disorders, yet it remains unclear how the PFC, under the influence of the HP, develops across adolescence in these contexts. One explicit significant cognitive ability is working memory as a core symptom in neurodevelopmental disorders and specifically in schizophrenia (Gogtay et al., 2011; Miller, 2000; Miller and Cohen, 2001). Therefore, a behavioral task to assess working memory was planned to be established on a system allowing head-fixation for simultaneous, stable electrophysiological recordings in prejuvenile to early adult mice, spanning 20 to 60 days of age.

#### **4.4 Establishment of awake head-fixed recordings on the MobileHomeCage in an open field movement paradigm and a working memory task**

As mentioned above, interpretation of electrophysiological data acquired under anesthesia is difficult because the anesthesia affects the measured signals differently at distinct stages of development (Chini et al., 2019; Purdon et al., 2015). Until P12, neonatal mice show limited behavioral abilities and predominantly spend time in sleep states (Rensing et al., 2018). This allows for a specific recording technique to be performed in neonatal mice up to an age of P12 (Bitzenhofer et al., 2021; Bitzenhofer et al., 2020; Chini et al., 2019). In this procedure, head bars are fixed to the skull of the neonatal mice with dental cement in an acute surgery under

---

inhalation anesthesia. The application of a local anesthetic to the incisions limits the experience of pain. After a short recovery period from the inhalation anesthetic, the mice are fixed in a stereotactic frame in the recording setup with the help of the head bars for electrophysiological measurement. The well-being of the mouse pups is ensured through a heating mat to help maintain body temperature and an artificial cotton nest surrounding the mice (Hanganu et al., 2006). This technique can also be used on older mouse pups under urethane anesthesia and was used here for the three site recordings of PFC, HP and LEC in prejuvenile mice to compare the WT and dual-hit GE model.

However, this method is unsuitable for electrophysiological recordings in awake mice of prejuvenile and older ages. Without appropriate training, young mice with emerging behavioral and sensory abilities might perceive being restrained by the fixation as stressful and threatening, which in turn can enhance the urge to move and flee from the threatening situation (Schwarz et al., 2010). To counteract this, restrainers, i.e. in the form of stable tubes or blankets are used to prevent movement, reduce stress and enhance comfort. This method requires long training periods, often combined with food and water restriction, and is thus also unsuitable for growing and developing mice (Barkus et al., 2022; Schwarz et al., 2010). Head-fixation is not the only technique that ensures stable recordings of high quality in older, awake mice; another approach is to implant an electrode chronically. However, many electrodes for chronic implantation weigh around 2-3 g and even lightweight versions weigh 1-1.2 g (França et al., 2020; Freedman et al., 2016; Voigts et al., 2020). A prejuvenile mouse weighs around 8-9 g; hence, an electrode would make up a good portion of a mouse's body weight. The lightweight versions would be suitable if only needed for one brain area, but are inadequate to cover several brain areas, as the weight would add up. In addition, most have been only introduced very recently (França et al., 2020; Pendry et al., 2023; Sun et al., 2022).

Therefore, the previously established head-fixed method, which is suitable for young and growing mice, (Pöpplau et al., 2023) was used and adapted. Here, the mice were also head-fixed, but on a movable ground. Two different versions were established in the lab (Pöpplau et al., 2023). One version utilized a custom-made spinning disc, which allows fast movement in one direction, but limits spatial navigation. The other version, the MobileHomeCage, is an airlifted platform that allows spatial navigation and therefore mimics free locomotion and orientation (Kislin et al., 2014). The surgery technique enabled the insertion of multiple electrodes, does not require week-long training and is suitable for young mice as the implanted mice gain weight similar to not-implanted ones (Pöpplau et al., 2023).

The air-lifted carbon cage with a diameter of 290 mm is well suited also for prejuvenile mice, as it is lightweight enough to be moved by the small mice of 8-9 g body weight. Between P20 and P60 there was no increase in time the mice moved on the MobileHomeCage, indicating that the mice adapted fast to the head fixation, as had also been reported for the spinning disc, and electrophysiological recordings were possible as early as five days after the surgery (Pöpplau et al., 2023).

The adolescent mice showed mean movement ratios between 30 % and 50 % of total time on the MobileHomeCage, which is in line with adult mice after extensive training on the MobileHomeCage and on a treadmill (Carlsen et al., 2022; Juczewski et al., 2020). Therefore, it was concluded that the prejuvenile mice were already well-habituated to the head fixation on

---

the MobileHomeCage 5 days after the surgery and with two days of training. All mice displayed voluntary movement and resting periods while being head-fixed on the MobileHomeCage in a round open arena.

The movement ratio was assessed on a carbon cage resembling a round open field arena. In open field tests with rodents, the time spent in the perimeter (thigmotaxis) measured against the time spent in the center was used as a measure for anxiety (La-Vu et al., 2020). In general, in an open field, mice tend to spend more time exploring the environment around the periphery in close proximity to the walls than in the center regions (Bailey, 2009). Similar behavior was observed in the WT mice tested at P20-60, as they spent more time in the periphery than in the center. Thus, the conclusion was that the adolescent mice showed normal open field and anxiety-related behavior.

To assess the working memory in the adolescent mice and to relate the test phases to electrophysiological activity, a DNMS T-Maze task was to be established on the MobileHomeCage. Working memory is defined as the capacity to store information for a brief time and the ability to retrieve it for manipulation to achieve a goal (Baddeley, 1992). Accordingly, it is essential for goal-directed behaviors and a component of higher cognitive function (Baddeley, 1992). Since it relies on a functional prefrontal-hippocampal network, it has been proposed that dysfunctions in this network are underlying causes for working memory deficits in neurodevelopmental disorders (Backus et al., 2016; Hyman et al., 2010; Sigurdsson and Duvarci, 2016).

A version of a round T-Maze for the MobileHomeCage is commercially available at Neurotar (Helsinki, Finland). With some small modifications, this maze met the requirements to carry out the task in younger mice. These modifications included decreasing the spaces in corners to prevent mice from spending the whole time in those, adding a door in the wall to be able to transfer the mice from the open field maze to the T-Maze without releasing the head fixation and adding a removable wall to restrict the mice to the starting compartment. Even though the T-Maze was larger than the open field arena, prejuvenile mice were still able to move it.

Despite all efforts and experimental trials, it was not possible to establish the DNMS T-Maze task reliably in mice in a short enough period to be able to assess working memory in prejuvenile and early ado mice. There are a number of potential explanations: one rather obvious underlying cause could be an insufficiently long habituation period to either the head fixation procedure or the maze. However, it is unlikely that the head fixation habituation is too short due to the observations mentioned above, i.e., that adolescent mice displayed similar movement ratios to adult mice on the MobileHomeCage and a treadmill system and the movement patterns resembled behavioral patterns in an open field in freely moving mice (Bailey, 2009; Carlsen et al., 2022; Juczewski et al., 2020). Similarly, the suggestion that the habituation to the T-Maze was too short can likely also be dismissed, since the mice were trained on the maze far more often than on the open field and could move it easily even though it was bigger and heavier.

However, the combination of potential aversive factors could have led to enhanced stress levels in the mice, which would hinder their performance in the working memory task. In the open field, the only potential stress factors are the head fixation and noise levels due to the pressurized air, which can be countered through habituation while keeping the mice in their

normal environment, i.e., their holding cage. In the T-Maze task, there are various additional factors: the lick-port touching their whiskers, the food/water restriction, the swing door which the mice have to cross, the forced movement through the swing door and being held in the starting compartment for the delay and inter-trial periods. In the open field maze in the MobileHomeCage, adult mice still show slightly enhanced corticosterone levels after 25 days of habituation (Juczewski et al., 2020). As previously mentioned, adolescent mice showed normal behavior in the open field maze after only a few training sessions, but the combination with other stressors may increase the corticosterone levels further. A caloric restriction in mice, which can either be achieved by directly restricting the food intake or by restricting water intake (e.g., by adding citric acid), can motivate the mice to perform complex tasks, but can also lead to a higher increase in corticosterone levels in aversive situations (Barkus et al., 2022; Pankevich et al., 2010). Food and water restriction is a double-edged sword in adolescent mice, as it needs to be restrictive enough to increase motivation levels, but not to the point of weight loss, since this has an impact on brain maturation in this life period (Berardino et al., 2022; Lin et al., 2022). On another note, high levels of stress can adversely affect cognitive performance (Atrooz et al., 2021; Kim and Kim, 2023).

Another factor contributing to the difficulty in establishing the DNMS T-Maze task might be that the spatial orientation in the carbon T-Maze under head-fixation does not resemble that in a Y-Maze with free movement. The mice do not move their body, but rather move the ground beneath them. However, the evidence for activated place cells in the HP recorded in mice moving a circular track on the MobileHomeCage would contradict this (Go et al., 2021). This is still a possibility in the setup used in this thesis, as the walls of the T-Maze are lower than in the circular track to allow tracking of the pupil and licking behavior.

Thus, it can be argued that the combination of aversive factors led to a higher level of stress. This could be counteracted with longer training periods, but these cannot be implemented due to the young age of the mice. Alternatively, the less strong spatial orientation on the MobileHomeCage could be the underlying reason why the mice cannot learn the DNMS task.

In conclusion, implementing the complex behavioral task to assess working memory in adolescent mice was not feasible. However, without an underlying complex behavior and thus additional stressors, the mice exhibited normal behavior with voluntary movement and resting periods in the round arena resembling an open field. This made it possible to investigate the prefrontal-hippocampal network with electrophysiological recordings across adolescence in the context of neurodevelopmental disorders.

## 4.5 Late developmental patterns of prefrontal-hippocampal network activity across adolescence in a 22q11.2 deletion syndrome mouse model

### 4.5.1 Developmental trajectories of prefrontal-hippocampal network activity in the 22q11.2ds mouse model

The awake, head-fixed recordings aimed to clarify the unresolved inquiry regarding the developmental trajectories throughout adolescence, with a focus on determining whether and which activity patterns are specifically altered in the 22q11.2ds mouse model. The main findings are summarized in Figure 43. These are abnormal developmental trajectories of local prefrontal activity in broad-band gamma power and synchrony of spike trains, implying a disturbed fine-tuned excitatory and inhibitory balance. In addition, an abnormally increasing hippocampal theta power across adolescence was observed. Hippocampal theta activity prominently modulates the PFC. Regarding this, a perturbed development to a less oscillatory synchronous network with an imprecise timing of firing of prefrontal and hippocampal neurons were shown.

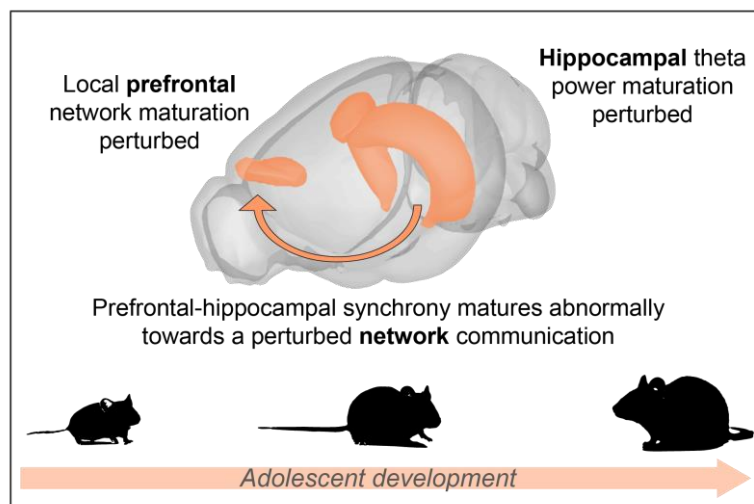


**Figure 43: Graphical summary of the perturbed developmental trajectories in the  $Df(16)A^{+/-}$  mouse model of 22q11.2ds.** This summary displays the PFC and HP located in a mouse brain with the prominent information flow from the HP to the PFC (Brainrender, (Claudi et al., 2021)) and highlights the most relevant findings across adolescent development in the  $Df(16)A^{+/-}$  mouse model.

These main findings, together with the less prominent findings, are discussed in the next chapters.

#### 4.5.1.1 Head-fixed movement patterns and movement-related activity in $Df(16)A^{+/-}$ and WT mice

As a proxy for normal development, body weight of implanted  $Df(16)A^{+/-}$  and WT mice was monitored throughout adolescence. Previous studies have shown that the experimental procedure of the headplate implantation does not influence adolescent weight gain adversely (Pöpplau et al., 2023). In general, mice show an increase in body weight from ~3-4 g in neonatal

age (P5-8) to ~10 g in prejuvenile age (P20) and ~20-25 g in early adulthood (P60) (Castelhanos-Carlos et al., 2009). Abnormal increases and decreases in body weight during development can have detrimental effects. Hence, increased as well as decreased body weight has been connected to cognitive disabilities and neurodevelopmental disorders (Georgieff et al., 2018; Isaksson et al., 2023; Miller et al., 2015; Mireku et al., 2020; Nyaradi et al., 2013; Olsen et al., 2023; Wentz et al., 2017). Here, implanted *Df(16)A*<sup>+/-</sup> and WT mice showed a similar weight gain to each other and not-implanted mice from P20 to P60, indicating that abnormalities found in the development of the prefrontal-hippocampal network cannot solely be attributed to an abnormal somatic development.

As described earlier, the movement patterns of the mice were assessed on the MobileHomeCage during recordings. It is likely that the WT mice showed normal movement patterns on the MobileHomeCage for several reasons: for one, they spent more time in the perimeter of the maze of the MobileHomeCage resembling the open field, which is typically also observed for freely moving mice in open field tasks (Bailey, 2009). Secondly, the movement patterns of adult mice trained on the MobileHomeCage for a longer period were similar to the patterns observed for the adolescent and early adult mice (Juczewski et al., 2020). And thirdly, the movement ratio of total time on the MobileHomeCage was within the same range as that of adult mice trained on the MobileHomeCage and a treadmill in head-fixed conditions (Carlsen et al., 2022; Juczewski et al., 2020).

In the *Df(16)A*<sup>+/-</sup> mice, the movement ratio developed from hyperactivity in early adolescent mice towards lower activity in early adult mice, though this did not reach significant levels in group comparisons. In open field tests in mouse models of 22q11.2ds, opposite patterns of activity have been reported. While some studies show hypolocomotion, several others show hyperlocomotion in the model mice (Saito et al., 2020; Saito et al., 2021; Stark et al., 2008; Sumitomo et al., 2018; Tripathi et al., 2020). These studies utilized a variety of animal models, mimicking either the 3 Mb or the 1.5 Mb microdeletion. However, adult *Df(16)A*<sup>+/-</sup> mice in an open field in freely moving conditions exhibit hyperlocomotion (Stark et al., 2008). The different developmental trajectories suggest that during adolescence, underlying mechanisms of locomotor behavior are disturbed in *Df(16)A*<sup>+/-</sup> mice. However, this is only reflected in adult mice or under freely moving conditions.

The heatmaps of the movement patterns as well as the enhanced time early ado *Df(16)A*<sup>+/-</sup> mice spent in the center region of the open field maze of the MobileHomeCage suggest a perturbed anxiety-related behavior in this group. The hyperactivity frequently reported in mouse models of neurodevelopmental disorders is proposed to be dependent on the mesolimbic system, a brain circuitry involving the ventral tegmental area, Nucleus accumbens, amygdala as well as the HP and PFC (Jones et al., 2011). It has been shown that the amygdala plays a particularly important role in anxiety behavior. In the open field, activation of projections from the basolateral amygdala to the central lateral amygdala and HP modulate time in the center (Felix-Ortiz et al., 2013; Tye et al., 2011). In addition, CA1 neurons enhance their firing rate in the center of the open field and the HP modulates anxiety through projections to the mPFC (Jimenez et al., 2018; Shah et al., 2004). In addition, adult *Df(16)A*<sup>+/-</sup> mice show a perturbed freezing response involving amygdala-hippocampal circuitry in a fear-conditioning task (Stark et al., 2008).

---

Taken together, these findings provide clues that during early ado development, the amygdala-hippocampal circuitry and subsequently possibly also the hippocampal input to the mPFC are subject to perturbation in *Df(16)A<sup>+/-</sup>* mice.

The open field behavior was assessed during the first five minutes on the MobileHomeCage. To align the movement to the electrophysiological recordings, the patterns were tracked for the whole duration of the recording. In this instance, a divergent trajectory of locomotor behavior was observed as well. However, neither the movement ratio nor the time in the center showed significant disparities when the groups were compared. Therefore, it was concluded that the abnormal trajectories of locomotor activity and the differences in time spent in the center during the first five minutes of the recording would not prevent segmentation of the recording into movement and resting periods. This also allowed a direct comparison of the electrophysiological signal in these periods between WT and *Df(16)A<sup>+/-</sup>* mice. The movement and resting ratio did not differ between early ado and late ado WT and *Df(16)A<sup>+/-</sup>* mice, so the same amount of electrophysiological data in movement and resting periods were investigated for WT and *Df(16)A<sup>+/-</sup>* mice.

The segmentation of the signal was performed because oscillatory activity in the HP is modulated by the behavioral state (Buzsáki, 2005). Even though results are inconclusive on the exact modulatory mechanisms, it has been reported that theta rhythm in the HP is dependent on movement behavior. It has been shown that running speed, acceleration and deceleration can influence the frequency of the most prominent theta rhythm in the HP (Geisler et al., 2007; McFarland et al., 1975; Shin and Talnov, 2001; Sławińska and Kasicki, 1998; Whishaw and Vanderwolf, 1973). Overall, these data indicate that changes in movement patterns modulate the frequency of hippocampal theta oscillations. As the hippocampal theta rhythm influences prefrontal local activity, the hippocampal and the prefrontal oscillatory activity as well as the synchrony between the two areas were investigated separately for movement and resting periods (Siapas et al., 2005; Sirota et al., 2008).

The data obtained in WT and *Df(16)A<sup>+/-</sup>* mice across adolescent development are in line with this, since both groups showed a different power spectrum regarding the slow frequencies in movement periods. In both brain areas, a second power peak in theta was present at higher frequencies, even though this was more pronounced in the HP than in the PFC.

#### *4.5.1.2 Developmental trajectories of local prefrontal network activity in the 22q11.2ds mouse model*

In the prefrontal-hippocampal network, disruptions can come from various sources. For instance, they could be attributed to local disturbances in the source brain area. In the prefrontal-hippocampal network, the flow of information primarily leads from the HP to the PFC. The HP exhibits dense monosynaptic projections to the PFC, mostly arising from the i/vCA1 (Ghoshal and Conn, 2015; Hallock et al., 2016; O'Neill et al., 2013; Wirt and Hyman, 2017). The PFC receives strong hippocampal input from CA1 in the deep layers, which is then locally integrated and transmitted to the superficial layers (Anastasiades and Carter, 2021; Ferino et al., 1987; Jay and Witter, 1991). Hence, network dysfunctions arising within the PFC could be a consequence of perturbed signal integration. Disruptions could also occur during signal transmission

between the two brain areas, either in the feed-forward or in the feedback system. The prefrontal-hippocampal network is an integral part of several complex cognitive functions, such as working memory (Miller, 2000; Miller and Cohen, 2001). To perform complex cognitive tasks, the brain needs to integrate several pieces of information at once, and it has been hypothesized that this takes place as ‘communication through coherence’ in areas of the brain (Fries, 2005). This communication can take place as a phase-phase coupling within the same frequencies or as cross-frequency coupling, e.g., between theta and gamma rhythms. Phase-phase coherence, especially in the theta frequency range, as well as phase-amplitude coupling have been proposed to be involved in working memory processes (Fell and Axmacher, 2011; Lisman and Idiart, 1995).

Furthermore, the network perturbations could result from a combination of the above, as the three factors are not necessarily mutually exclusive. Therefore, the oscillatory activity within each brain area was investigated more thoroughly, with a focus on prefrontal and network activity.

The PFC is essential for cognitive processing. Accordingly, dysfunctions in this area are a core symptom of neurodevelopmental disorders (Miller, 2000; Miller and Cohen, 2001). More recently, it has become more and more evident that abnormal development of the PFC already during early life plays a significant role in mental disorders (Chini and Hanganu-Opatz, 2021; Chini et al., 2020; Hartung et al., 2016b; Oberlander et al., 2019; Xu et al., 2019). During very early development, the brain shows distinct oscillatory patterns which can be observed in various species, including humans and rodents (Hanganu-Opatz, 2010; Khazipov et al., 2004; Vanhatalo and Kaila, 2006; Workman et al., 2013). These alternating patterns between bouts of oscillatory activity and silent periods are also observed in neonatal mice of the dual-hit GE mouse model and *Df(16)A<sup>+/-</sup>* mice of the same age (Chini et al., 2020; Hartung et al., 2016b; Oberlander et al., 2019; Xu et al., 2019). The occurrence of the oscillatory bouts is higher in *Df(16)A<sup>+/-</sup>* mice, but with a decreased power, similar to what has been observed in dual-hit GE mice (Chini et al., 2020; Hartung et al., 2016b; Oberlander et al., 2019; Xu et al., 2019).

Even though some abnormal patterns of prefrontal activity are preset at neonatal age, maturation throughout adolescence does not take place in a linear developmental trajectory (Pöpplau et al., 2023). The oscillatory activity in the PFC changes from the discontinuous patterns to continuous activity from around P11-12 (Chini and Hanganu-Opatz, 2021). After the change to continuous activity, the prefrontal activity is further refined during adolescence (Bitzenhofer et al., 2020; Pöpplau et al., 2023). Specifically, after the second postnatal week, gamma frequency accelerates from 15 Hz to the adult-like patterns at 30-80 Hz in the fourth postnatal week (Bitzenhofer et al., 2020). Nevertheless, the immature bouts of beta/low gamma already depend on drive from pyramidal neurons onto interneurons before this time (Bitzenhofer et al., 2020; Bitzenhofer et al., 2015). Hence, even though they are distinctly different, the nested gamma spindle-bursts and adult-like gamma rhythm seem to share common principles (Bitzenhofer et al., 2020; Bitzenhofer et al., 2015; Brockmann et al., 2011). Gamma power increases from prejuvenile age onward and, together with firing activity of pyramidal neurons, peaks during adolescence (Pöpplau et al., 2023). The gamma rhythm is of specific interest throughout adolescent development as it has been associated with cognitive abilities and disabilities, e.g., in neurodevelopmental disorders (Cho et al., 2015; Guan et al., 2022; Williams and Boksa,

2010). Oscillations in the classical gamma frequencies (30-80 Hz) originate from local neuronal circuits within brain areas (Atallah and Scanziani, 2009). This rhythm emerges from a fine-tuned interplay of excitatory and inhibitory neurons (Cardin, 2016).

Here, the oscillatory activity observed in both brain areas was continuous in P20 WT and *Df(16)A<sup>+/-</sup>* mice, with prefrontal gamma power showing adult-like patterns. However, the gamma power in PFC in *Df(16)A<sup>+/-</sup>* mice showed an abnormal developmental trajectory throughout adolescence, giving first hints towards a perturbed refinement of prefrontal local circuits in the model mice. The disturbed developmental trajectory of gamma power did not result in a significantly abnormal gamma power in early adulthood. In comparison, in the *LgDel<sup>+/-</sup>* mouse model, another 22q11.2ds mouse model spanning a slightly different genetic region, abnormal gamma power during development was reported as well (Mukherjee et al., 2019). In this study, elevated low gamma power was observed at P40 and P60, with reduced high gamma power at P120. This is in line with the findings here, as the developmental trend in the *Df(16)A<sup>+/-</sup>* mice also shifted towards higher gamma power in late adolescence, even though it did not reach significance here. This perturbed development of the gamma rhythm indicates an abnormal local prefrontal circuitry and signal integration in this model in adolescence. Hereby, the prefrontal activity could be influenced by inputs from the HP.

#### *4.5.1.3 Developmental trajectories of hippocampal activity in the 22q11.2ds mouse model*

Adult *Df(16)A<sup>+/-</sup>* mice show various behavioral deficits that rely on the prefrontal-hippocampal network, including a perturbed working memory (Sigurdsson et al., 2010; Stark et al., 2008). These deficits are accompanied by a reduced prefrontal-hippocampal network synchrony, but prefrontal power was reportedly not different in adult *Df(16)A<sup>+/-</sup>* mice and WT mice (Sigurdsson et al., 2010). Nonetheless, the obvious network deficits in adult age could originate from miswiring during earlier age.

The monosynaptic projections from i/vCA1 to the mPFC are already established early in development and the HP drives prefrontal oscillatory activity (Ahlbeck et al., 2018; Brockmann et al., 2011; Xu et al., 2019). Manipulation of i/vCA1 neurons entrains prefrontal activity in the prelimbic (PL) area in all frequency bands, but with a strong theta band preference in neonatal rodents (Ahlbeck et al., 2018; Xu et al., 2021a). Theta rhythm is considered a slow oscillatory rhythm arising from large networks. It mainly occurs during active exploration or rapid eye movement (REM) sleep and coordinates neuronal activity across long distances and brain areas (Buzsáki, 2002). Hippocampal theta power is perturbed in neonatal mice of the *Df(16)A<sup>+/-</sup>* and the dual-hit GE model (Hartung et al., 2016b; Oberlander et al., 2019; Xu et al., 2021a). This indicates that the HP, as the projecting area, develops abnormally in early life in addition to the local prefrontal circuits.

Throughout adolescence, the theta power development in the i/vCA1 was abnormal in *Df(16)A<sup>+/-</sup>* mice, with a significantly lower theta power in early ado transitioning towards a higher power in late ado, even though this did not reach significance. The lower power had already been observed in neonatal *Df(16)A<sup>+/-</sup>* mice (Oberlander et al., 2019). Local gamma power and firing properties did not develop differently in the HP. This leads to the suggestion that in particular the theta rhythm in the CA1 of *Df(16)A<sup>+/-</sup>* mice is perturbed, and that this perturbation changes during adolescence. Theta rhythm synchronizes the HP and PFC during

---

working memory tasks, which is impaired in schizophrenia patients (Benetti et al., 2009; Henseler et al., 2010). Working memory, similar to other cognitive abilities, matures during adolescence (Klune et al., 2021). Therefore, the switch in hippocampal theta power maturation may have an impact on the network maturation and the associated cognitive abilities. Similarly, hippocampal abnormalities have been found in adult *Df(16)A<sup>+/-</sup>* mice (Stark et al., 2008). In adult *Df(16)A<sup>+/-</sup>* mice, pyramidal neurons in the CA1 exhibit less dendritic complexity and fewer spines (Stark et al., 2008). A study in the *LgDel<sup>+/-</sup>* model shows that the reduced spine density is already present in prejuvenile mice and persists throughout adolescence (Moutin et al., 2017). Likewise, perturbations in the  $\gamma$ -Aminobutyric acid (GABA)ergic system, especially PV interneurons, are present in adolescence, and can be rescued in early adulthood (Mukherjee et al., 2019). The results from the present study complement these findings and emphasize the functional component, with disturbances in theta rhythm development, which might be essential for the maturation of the prefrontal-hippocampal network and dependent behavioral abilities.

#### *4.5.1.4 Developmental trajectories of prefrontal-hippocampal network activity in the 22q11.2ds mouse model*

Disruptions in this network can have negative implications for cognitive abilities. In humans, a functional prefrontal-hippocampal network is important for contextual information processing, fear extinction and spatial working memory paradigms (Böhner et al., 2015; Eichenbaum, 2017). In rodents, this network is involved in reward learning, anxiety and avoidance as well as working memory processing (Godsil et al., 2013).

Here, it was shown that during early adolescence, the HP already drives the mPFC to a greater extent than the mPFC drives the HP. This ratio between hippocampal drive to the PFC and prefrontal drive to the HP was not altered in the *Df(16)A<sup>+/-</sup>* mice during adolescence. However, phase-phase synchrony in theta frequency, measured through imaginary coherence, and cross-frequency synchrony, measured through PAC, were disturbed in late adolescence in *Df(16)A<sup>+/-</sup>* mice. This was not seen in early adolescent *Df(16)A<sup>+/-</sup>* mice. In neonatal *Df(16)A<sup>+/-</sup>* and dual-hit GE mice, disturbances in the hippocampal drive to the PFC in theta frequency have been reported (Hartung et al., 2016b; Oberlander et al., 2019; Xu et al., 2021a). This suggests that the prefrontal-hippocampal network is remodeled during the adolescent period until late adolescence or early adulthood. The existing network deficiencies from the neonatal period become less evident during adolescence, but lead to faulty maturation of the primed network closer to adulthood. Theta coherence within the network as well as a modulation of prefrontal gamma amplitude by the hippocampal theta phase have been shown to be relevant for cognitive functioning, especially in working memory (Adhikari et al., 2010; Fell and Axmacher, 2011; Jones and Wilson, 2005; Lisman and Idiart, 1995). A dysfunctional working memory in accordance with an abnormal theta synchrony has also been demonstrated in adult *Df(16)A<sup>+/-</sup>* mice (Sigurdsson et al., 2010). The abnormal development of the PAC indicates an abnormal influence of hippocampal activity on prefrontal local activity. In adult *Df(16)A<sup>+/-</sup>* mice, this is substantiated by a decreased phase-locking of prefrontal spikes towards hippocampal theta rhythm when the mice are performing a working memory task (Sigurdsson et al., 2010).

It is possible that this early abnormal network activity in theta frequency, which is then refined during adolescence, is the underlying cause for deficits in cognitive abilities that develop during

---

adolescence. In addition, the local prefrontal circuit activity, reflected by an abnormal gamma power development, is disturbed in this model. This activity depends on a fine-tuned balance of excitatory and inhibitory neuronal activity (Cardin, 2016). Hence, the firing patterns of prefrontal putative PV and pyramidal neurons were investigated.

In visual cortices, key players of gamma generation are PV and somatostatin-positive (SOM) interneurons. PV interneurons influence pyramidal neurons through perisomatic inhibition, and suppression of PV interneurons reduces gamma power (Cardin et al., 2009). PV interneurons mainly influence the classical gamma band, while SOM interneurons mainly act on the beta/low gamma rhythm (Chen et al., 2017). Thus, gamma rhythm depends on a precise excitation/inhibition ratio within the brain areas. Prefrontal excitatory pyramidal neurons, as well as prefrontal interneurons, receive direct projections from hippocampal neurons (Tierney et al., 2004).

To investigate this, the recorded units were functionally divided into regular spiking units, putative pyramidal neurons and fast spiking units, putative PV interneurons according to a previously published protocol used in prefrontal recordings of adolescent mice (Bitzenhofer et al., 2020). The number of recorded putative pyramidal and interneurons made up a ratio of ~80/20 %, in line with the reported values for the mammalian cortex, and did not differ across ages or between groups (Harris and Shepherd, 2015). In this case, the number of PV interneurons was quantified functionally, but not anatomically. The global number of PV-expressing interneurons appears to be comparable in mouse models of 22q11.2ds, as shown in several brain areas in the *LgDel*<sup>+/-</sup> model (Mukherjee et al., 2019). Dissecting the mPFC into its layers, the number of PV neurons in superficial, but not deep layers, was reduced in another 22q11.2ds mouse model, the *Df(h22q11)*<sup>+/+</sup> model, which also mimics the 1.5 Mb deletion and spans a slightly different genetic region than either *Df(16)A*<sup>+/-</sup> or *LgDel*<sup>+/-</sup> (Al-Absi et al., 2020). Both previously mentioned studies showed perturbed inhibitory circuitries within the PFC. The latter also indicated that the excitatory circuitry is perturbed in 22q11.2ds models, as prefrontal pyramidal neurons show less dendritic and synaptic complexity (Al-Absi et al., 2020). The former identified a time window and possible rescue mechanism via the dopaminergic system after the mice reach early adulthood (P60-75) (Mukherjee et al., 2019).

Throughout development, both synchrony of regular spiking units and synchrony of fast spiking units in the PFC showed perturbed developmental trajectories in the *Df(16)A*<sup>+/-</sup> mice. Regular spiking units developed towards a hypersynchrony independent of behavioral state, while fast spiking neurons developed towards a hyposynchronization, which was only observable during resting periods in *Df(16)A*<sup>+/-</sup> mice. The abnormal 1/f slope in early ado *Df(16)A*<sup>+/-</sup> mice indicates an imbalance in the excitation/inhibition ratio at this age. Together with the abnormal trajectory of prefrontal gamma power and the abnormal timing of firing, this indicates an abnormal fine-tuning of the excitatory/inhibitory balance across adolescence, which results in fine changes in neuronal synchronization in the mPFC.

Dysfunctional interneurons can perturb gamma rhythmicity, which in turn can lead to cognitive disabilities (Cho et al., 2015). On another note, it was shown that an inhibition of microglia during adolescence disrupts prefrontal gamma rhythm and as well cognitive functioning (Pöpplau et al., 2023). In line with the reduced dendritic and synaptic complexity in the mPFC

in a mouse model of 22q11.2ds, an altered microglial function during adolescence could be an underlying mechanistic reason for the perturbed gamma power and excitatory/inhibitory balance during later development in *Df(16)A<sup>+/-</sup>* mice (Al-Absi et al., 2020; Pöpplau et al., 2023).

Here, it was shown that the maturation of firing synchrony between hippocampal neurons and prefrontal pyramidal as well as PV interneurons is disturbed in the *Df(16)A<sup>+/-</sup>* mice during adolescent development. The precise timing of neuronal firing is crucial for the formation of neuronal ensembles, which in turn are important for information processing and storage (Andrade-Talavera et al., 2023; Buzsáki, 2010). This precise timing was disturbed across adolescent development in the *Df(16)A<sup>+/-</sup>* mice. These results lead to the hypothesis that prefrontal spikes interact with hippocampal firing, but that the coherent oscillatory rhythms cannot be generated to the same extent as in healthy development. This imprecise timing of prefrontal firing of interneurons and pyramidal neurons and the hypothetical consequently disturbed gamma rhythm could be one underlying cause for the abnormal maturation of cognitive abilities in *Df(16)A<sup>+/-</sup>* mice and possibly in 22q11.2ds patients.

This hypothesis is underpinned by studies in other 22q11.2ds mouse models (Al-Absi et al., 2020; Kahn et al., 2020; Mukherjee et al., 2019). Abnormalities in hippocampal circuit excitability underlying cognitive dysfunctions could be rescued by selectively inhibiting pyramidal cells to retune the dysregulation in the 22q11.2ds model (Kahn et al., 2020). In *LgDel<sup>+/-</sup>* mice, PV interneurons show low plasticity and a failure to inhibit pyramidal neurons. This has an onset at adult age in the mPFC, while in the CA1 it is already present in adolescence (Mukherjee et al., 2019). Two other studies showed that the NMDA receptor system in the mPFC as well as the NMDA receptor-dependent long-term potentiation (LTP) by hippocampal input is disturbed in adult *Df(h22q11)/+* mice (Didriksen et al., 2017; Tripathi et al., 2020). These results support the hypothesis that an abnormal timing of prefrontal firing in synchrony with the hippocampal firing might be the underlying cause for the disturbances in excitation/inhibition balance, which could lead to disturbed gamma rhythm development and fewer synchronous oscillatory rhythms in the mPFC and HP. These disturbed rhythms and synchrony in adolescent development could contribute to the cognitive disabilities observed in 22q11.2ds patients (Vingerhoets et al., 2020; Vorstman et al., 2015).

The results show that the refinement and rewiring during adolescence in mice modelling the 22q11.2ds syndrome does not follow the same developmental trajectory during maturation as in healthy mice. This indicates that the refinement during adolescence is not merely a continuation of preset faulty wiring, but highlights the adolescent period as a vulnerable period in this disorder, facilitating the continuous development towards a disrupted network communication and with local prefrontal circuitry as an important underlying cause.

#### *4.5.2 Translational considerations of disturbed prefrontal-hippocampal network communication throughout adolescence between the *Df(16)A<sup>+/-</sup>* model and the 22q11.2 deletion syndrome*

The *Df(16)A<sup>+/-</sup>* mouse model mimics the 1.5Mb long microdeletion found in the 22q11.2 deletion syndrome (22q11.2ds) in humans (Stark et al., 2008). This highly prevalent disease,

---

with an occurrence of 1 in 4000 births, is associated with dysfunctions in multiple organ systems, the immune and endocrine systems as well as with abnormal brain function. The neurological consequences manifest as developmental delays, cognitive deficits and neuropsychiatric disorders (McDonald-McGinn et al., 2015). 22q11.2ds patients have an about 30-fold increased risk of developing schizophrenia in their lifetime in comparison to healthy individuals (Karayiorgou et al., 2010). Cognitive deficits can be apparent before the onset of schizophrenia and the first psychotic events (Vorstman et al., 2015). Even though several patients receive their diagnosis during childhood, a number of people remain undiagnosed throughout adolescence and adulthood. This is especially problematic considering the manifestation of schizophrenia during adolescence and early adulthood. An early diagnosis can help treat or even prevent the onset of this psychiatric disorder (Fung et al., 2015). During the vulnerable period of adolescence, neuronal circuits in the brain and especially the PFC are refined and rewired, making them prone to disturbances. These in turn can result in the manifestation of neuropsychiatric disorders with cognitive disabilities (Gogtay et al., 2011; Gonzalez-Burgos and Lewis, 2008; O'Donnell, 2011; Pöppel et al., 2023). In addition, changes in neuromodulator systems, specifically the dopaminergic system, can make adolescents more prone to risk-taking behaviors, stress and drug abuse (Chambers et al., 2003; Shoval et al., 2014; Spear, 2000). Drug abuse and addiction in turn can be an additional hit in the development of schizophrenia (Davis et al., 2016; Rubino and Parolaro, 2014; Rubino et al., 2015). The plasticity of the brain and especially the PFC in this vulnerable time highlights the need for an early diagnosis and treatment of the 22q11.2ds. An early diagnosis might help prevent additional hits that could lead to the manifestation of schizophrenia, while an early treatment could start with low doses of medication and prevent side effects (Fung et al., 2015).

Animal models are valuable tools used to monitor the disease as it develops (Markram, 2013; Mukherjee et al., 2022). Mouse models of the 22q11.2ds have been used to model physical features, like the congenital cardiac anomalies. But they also mimic the abnormal brain development, with certain features of cognitive deficits relating to schizophrenic symptoms (McDonald-McGinn et al., 2015; Sigurdsson et al., 2010; Stark et al., 2008). Several genes deleted in the 22q11.2ds and *Df(16)A<sup>+/-</sup>* mouse model have been connected to brain function and development, including *Tbx1*, *Dgcr8*, *Zdhhc8*, *Prodh* and *Comt*. *Tbx1*, for instance, is involved in the brain microvascular system and has been proposed to play a role in behavioral deficits. *Zdhhc8* has effects on axonal growth and terminal arborization and hence possibly for synaptic connections and working memory. Deletion of *Dgcr8* has evoked similar effects as those in 22q11.2ds mouse models. *Comt* is involved in the dopaminergic system, and *Prodh* in the glutamatergic system (McDonald-McGinn et al., 2015). In this study, the interplay of excitation and inhibition was impaired in adolescent local prefrontal circuits due to abnormal gamma rhythm maturation and improper timing of firing of pyramidal and PV neurons. This is in line with findings in adult human patients. Altered levels of glutamate and GABA have been reported in the anterior cingulate cortex of 22q11.2ds patients performing attention and memory tasks, as well as perturbed glutamate neurotransmission in the HP of psychotic 22q11.2ds patients (da Silva Alves et al., 2011; Vingerhoets et al., 2020). In line with other studies, this implies a role of glutamate and GABA, and hence of excitation/inhibition balance in the cognitive dysfunctions in 22q11.2ds (Lewis and Moghaddam, 2006). The altered levels of

---

glutamatergic neurotransmission observed in patients of 22q11.2ds have been proposed to be associated with the gene *proline dehydrogenase (PRODH)* encoding the enzyme PRODH, which is deleted in the locus (da Silva Alves et al., 2011). This enzyme breaks down proline, which in turn is converted to glutamate (Cohen and Nadler, 1997). This gene is also deleted in mouse models mimicking the 1.5 Mb deletion, including the *Df(16)A<sup>+/-</sup>* mice (Stark et al., 2008). Accordingly, it could also have influenced the excitatory circuitry in the PFC here.

Cognitive dysfunctions, especially working memory, and local oscillatory activity in the PFC are influenced by hippocampal activity. Here, hippocampal abnormalities were found in developing *Df(16)A<sup>+/-</sup>* mice and are reportedly also present in adult *Df(16)A<sup>+/-</sup>* mice (Sigurdsson and Duvarci, 2016; Stark et al., 2008).

In comparison, in schizophrenia patients, a decreased CA1 volume has been associated with the development of psychosis (Nakahara et al., 2018). Furthermore, an abnormal hippocampal cell architecture has been proposed to underlie the functional deficits (Heckers and Konradi, 2002; Heckers and Konradi, 2010). Even though the total cell number in hippocampi of schizophrenia patients appears to be normal, the GABAergic and glutamatergic systems, especially GABA<sub>A</sub> and  $\alpha$ -amino-3-hydroxy-5-methyl-4-isoxazolepropionic acid (AMPA) receptors, are perturbed in schizophrenia patients (Heckers and Konradi, 2002). Functionally, hippocampal activity at baseline levels is increased in schizophrenic patients, but the recruitment in memory tasks is decreased (Heckers and Konradi, 2010). In 22q11.2ds patients with psychosis, higher levels of glutamate in the HP have been reported (da Silva Alves et al., 2011). Together, this indicates a disturbed excitatory/inhibitory system in schizophrenic patients with psychotic episodes (Heckers and Konradi, 2010).

Here, the hippocampal theta rhythm and with it the prefrontal-hippocampal network activity was abnormal throughout adolescence. The theta rhythm synchronizes the HP and PFC during working memory tasks and is impaired in schizophrenia patients (Benetti et al., 2009; Henseler et al., 2010). Working memory, similar to other cognitive abilities, matures during adolescence (Klune et al., 2021). Therefore, the switch in hippocampal theta power maturation may have an impact on the network maturation and the dependent cognitive abilities. Humans performing a working memory task display enhanced theta synchrony (Backus et al., 2016). In contrast, a reduced prefrontal-hippocampal synchrony has been reported in schizophrenic patients and individuals with a higher susceptibility for schizophrenia performing these tasks, highlighting a possible genetic predisposition (Benetti et al., 2009; Henseler et al., 2010). This is further supported by the manifestation of a reduced working memory and prefrontal-hippocampal theta synchrony in adult *Df(16)A<sup>+/-</sup>* mice (Sigurdsson et al., 2010). It can be hypothesized that this abnormal early network activity in theta frequency, which then develops further during adolescence, is the underlying cause for deficits in cognitive abilities maturing during adolescence.

Cognitive dysfunctions interfere with patients' personal and professional lives and are not significantly alleviated by conventional treatments of schizophrenia with antipsychotics (Arguello and Gogos, 2009; MacKenzie et al., 2018; Panov et al., 2023). 22q11.2ds patients often exhibit cognitive disabilities in combination with schizophrenia. Schizophrenia in 22q11.2ds is no different from other schizophrenia cases in terms of age at onset, course of the disease and treatment options. Schizophrenia affects the quality of life of patients negatively,

---

as they exhibit deficits in executive functioning and memory, but also weaker social and communicative abilities (Fung et al., 2015; McDonald-McGinn et al., 2015). As mentioned above, the brain overall but particularly the PFC, which is mainly involved in cognitive functions, undergo periods of remodeling and refinement during adolescence. Adolescence and early adulthood are also the time were schizophrenia typically shows an onset with the first psychotic episode (Gogtay et al., 2011; Gonzalez-Burgos and Lewis, 2008; O'Donnell, 2011; Pöppel et al., 2023). However, the higher plasticity during adolescence also makes it more susceptible to treatment aiming to prevent or attenuate psychosis. This shows the necessity of elucidating underlying developmental patterns and mechanisms of prefrontal local and long-range circuit maturation during this period (McDonald-McGinn et al., 2015; Meechan et al., 2015). Accordingly, this also puts the results presented in this thesis into greater context. Here, abnormal developmental trajectories in the local PFC and in interactions with the HP could be demonstrated. This indicates disturbed synchrony and rhythmicity of neuronal firing within the prefrontal-hippocampal network during adolescence, manifesting as miswired patterns. The identification of underlying mechanisms can contribute to the research or development of better diagnostic tools, as well as to more mechanistically and temporally matched treatment options (McDonald-McGinn et al., 2015).

## 4.6 Concluding remarks and future directions

The PFC is considered a hub of cognitive processing. It is one of the most advanced and interconnected brain areas (Miller, 2000; Miller and Cohen, 2001). Together with the hippocampal formation, it forms a network crucial for working memory function (Sigurdsson and Duvarci, 2016). Cognitive abilities, such as working memory, emerge and mature during adolescence in parallel to morphological and functional refinement of prefrontal circuits. Hence, this late developmental time is regarded as a vulnerable life period (Klune et al., 2021; Pöppel et al., 2023).

Over the last years, the understanding of early development of prefrontal local and long-range networks in physiological and pathophysiological backgrounds, especially regarding neurodevelopmental disorders, has substantially increased (Ahlbeck et al., 2018; Bitzenhofer et al., 2017; Bitzenhofer et al., 2021; Bitzenhofer et al., 2020; Bitzenhofer et al., 2015; Brockmann et al., 2011; Hartung et al., 2016a; Hartung et al., 2016b; Xu et al., 2019). However, the knowledge regarding developmental trajectories of prefrontal-hippocampal network interactions during adolescence in neurodevelopmental disorders remains sparse.

The work presented in this thesis contributes to filling these knowledge gaps by utilizing genetic and environmental mouse models of neurodevelopmental disorders. First, in the dual-hit mouse model, which combines a genetic and an environmental risk factor (GE), microglia were shown to play a key role in the perturbations in the PFC in early development. The detrimental effects of microglial overactivation could be rescued with the microglia-inhibiting antibiotic minocycline during a very specific time window. Treatment during a later time point did not show similar rescue properties and had no beneficial effect on object recognition tasks,

representing behavioral abilities depending on prefrontal-hippocampal-entorhinal interactions in prejuvenile development (Chini et al., 2020).

As the ability to discriminate novel and familiar objects arises during prejuvenile development, the activity and synchrony of this network was investigated during this time period. These investigations revealed a hypersynchronization of prefrontal-entorhinal and prefrontal-hippocampal interactions in anesthetized, prejuvenile GE mice. As these perturbations were different from those at neonatal age, the prejuvenile period in rodents, roughly translating to early childhood in humans, can also be considered vulnerable in the context of maturation of cognitive abilities.

To further inspect this, a working memory task allowing simultaneous electrophysiological recordings was supposed to be established. It transpired that the chosen setup to allow movement of the mice was sufficient for innate behaviors, but not for complex tasks. The head-fixed recordings on the MobileHomeCage allowed the investigation of open field behavior and to segment the behavioral states into movement and resting periods. However, due to technical limitations, implementation and conduction of the working memory task in these head-fixed conditions was not possible.

Nevertheless, the aim continued to be to elucidate the developmental trajectories of the prefrontal-hippocampal network across late development in the context of neurodevelopmental disorders. To this end, the prefrontal-hippocampal network was investigated from P20-60 in a purely genetic 22q11.2ds mouse model, with a greater similarity to late onset neurodevelopmental disorders such as schizophrenia. Here, it was shown that the prefrontal gamma rhythm develops abnormally in *Df(16)A<sup>+/-</sup>* mice, together with perturbed firing synchronies of pyramidal neurons and PV interneurons in a behavioral state-dependent manner. This implies an abnormal fine-tuning of the excitation/inhibition balance in the local prefrontal circuits. In the HP, the theta rhythm, which synchronizes the PFC and HP during working memory tasks, developed abnormally in the *Df(16)A<sup>+/-</sup>* mice. Regarding the network interactions, the precise timing of prefrontal pyramidal neurons as well as PV interneurons to hippocampal spike timing matured in a disrupted behavioral state-dependent manner. This could imply that prefrontal spikes interact with hippocampal firing, but that the coherent oscillatory rhythms cannot be generated as they are during healthy development. These results suggest that the imprecise timing of firing, the less coherent oscillatory rhythm and the abnormal prefrontal gamma rhythm might be the underlying causes for the insufficient maturation of cognitive abilities in 22q11.2ds mouse models and possibly patients.

Taken together, the findings presented in this thesis contribute to identifying mechanisms and time windows for possible biomarkers or interventions in neurodevelopmental disorders already before and especially during adolescence. Even though several open questions remain, the work presented here establishes a foundation for follow-up research, especially regarding the 22q11.2ds (Box 1). Future research based on this study can follow various path in two main categories, namely staying in animal models of 22q11.2ds or taking a step to humans and follow-up with translational research. Studies in animal models could follow a more mechanistic pathway and dive deeper into underlying cellular and molecular components of the perturbed development, correlate the identified perturbed development to cognitive disabilities or go in the direction of possible rescue mechanisms. One approach for the latter is described

---

in more detail in the next paragraph. Translational research could aim at identifying these perturbed developmental trajectories of the prefrontal-hippocampal network with electroencephalogram (EEG) or functional magnetic resonance imaging (fMRI) measurements as an add-on for diagnosis. One other pathway to explore could be to use these developmental trajectories to pinpoint optimal treatment time points and to use a potentially restored network activity to monitor the efficacy of treatment.

**Box 1: Outstanding questions:**

- **Questions to explore in animal models of neurodevelopmental disorders:**
  - How do altered developmental trajectories in animal models of 22q11.2ds manifest behaviorally, and what is the aberrant timeline of cognitive development within these models? Can the mechanisms of perturbed development identified here be correlated with cognitive disabilities?
  - What are the underlying cellular and molecular mechanisms responsible for the perturbed developmental trajectories observed in 22q11.2ds models?
  - Can non-invasive techniques, such as environmental enrichment, rescue the abnormal maturation of the prefrontal-hippocampal network in mouse models of neurodevelopmental disorders? If successful, are the mechanisms identified here underlying this rescue? Can the rescue lead to amelioration of cognitive disabilities?
- **Possible future paths in translational research:**
  - Can the behavioral state-dependent disturbed prefrontal-hippocampal network communication be identified with EEG or fMRI measurements and used as an add-on for diagnosis of 22q11.2ds before the first psychotic events?
  - Can insights from abnormal developmental trajectories be used to pinpoint optimal treatment windows and monitor treatment success in 22q11.2ds patients?

Adolescence is a period in which preset circuits are rewired and fine-tuned (Klune et al., 2021). The observed changes and disturbances during this time are less prominent than those observed during the neonatal period (Ahlbeck et al., 2018; Bitzenhofer et al., 2021; Bitzenhofer et al., 2020; Chini et al., 2020; Hartung et al., 2016b; Krüger et al., 2012; Pöppelau et al., 2023; Xu et al., 2019; Xu et al., 2021a). The neonatal period of rodents translates to the second to third gestational trimester of human pregnancy (Clancy et al., 2001). Neurodevelopmental disorders are typically diagnosed between 3 and 6 years of age for early onset disorders, such as ASD and ADHD, and during adolescence or early adulthood for late onset disorders, such as schizophrenia (Gogtay et al., 2011; Mintz Hemed and Melosh, 2023). Treatment during the neonatal period makes a helpful contribution to the identification of mechanisms underlying the disturbed brain development in these disorders (Chini et al., 2020). However, it cannot easily be translated to humans for treatment or prevention of these disorders. Therefore, the prejuvenile period from around P14 in rodents to early adulthood around P60 is a more suitable choice when investigating interventions that can be translated to human patients (Dutta and Sengupta, 2016). Administration of drugs across longer periods during development, especially minocycline, is one potential option, as it is approved for human use and was shown to have beneficial effects in adults with schizophrenia (Panizzutti et al., 2023). However, this administration may also have detrimental effects, as shown in some case reports for

minocycline administration in childhood and adolescence (El-Hallak et al., 2008; Ramakrishna et al., 2009). In addition, it has been reported that minocycline administration in adolescents did not have a protective effect against severe psychiatric symptoms (Brauer et al., 2019). This opens up questions regarding more specifically timed interventions and regarding non-invasive rescue techniques. One possibility of a non-invasive technique is the enrichment of the living environment. For rodents, an enriched environment (EE) can be achieved by adding stimuli for visual, motor, somatosensory and cognitive inputs to the housing cage (Nithianantharajah and Hannan, 2006). For humans, an enrichment of the living environment can be assessed by evaluation of lifestyle habits, including cognitive and physical activity, social interactions and sensorial stimulation (Colavitta et al., 2023; Flores-Ramos et al., 2022). In wildtype rodents, EE promotes dendritic branching, spine density and adult neurogenesis (Nithianantharajah and Hannan, 2006). In an ASD mouse model, early EE, before weaning, prevented cognitive deficits and rescued spine density in the CA1 (Chen et al., 2022). Hence, it could be investigated whether EE can also rescue the developmental abnormalities in the prefrontal-hippocampal network interaction in 22q11.2ds mouse models and if this can be applied to young humans, i.e., children and adolescents.

Even though there are arguments questioning the successful modelling of neurodevelopmental disorders in animal models and promoting human studies (Khodosevich and Sellgren, 2023; Zhao and Bhattacharyya, 2018), the findings presented in this thesis contribute to understanding the progression of neurodevelopmental disorders throughout adolescence and can contribute to the identification of possible biomarkers or mechanisms and time windows for interference for treatment or prevention of these disorders.

---

## References

- Ackman, J.B., Burbridge, T.J., and Crair, M.C. (2012). Retinal waves coordinate patterned activity throughout the developing visual system. *Nature* 490, 219-225.
- Ackman, J.B., Zeng, H., and Crair, M.C. (2014). Structured dynamics of neural activity across developing neocortex. *bioRxiv*, 012237.
- Adhikari, A., Topiwala, M.A., and Gordon, J.A. (2010). Synchronized activity between the ventral hippocampus and the medial prefrontal cortex during anxiety. *Neuron* 65, 257-269.
- Agster, K.L., and Burwell, R.D. (2009). Cortical efferents of the perirhinal, postrhinal, and entorhinal cortices of the rat. *Hippocampus* 19, 1159-1186.
- Ahlbeck, J., Song, L., Chini, M., Bitzenhofer, S.H., and Hanganu-Opatz, I.L. (2018). Glutamatergic drive along the septo-temporal axis of hippocampus boosts prelimbic oscillations in the neonatal mouse. *eLife* 7, e33158.
- Al-Absi, A.-R., Qvist, P., Okujeni, S., Khan, A.R., Glerup, S., Sanchez, C., and Nyengaard, J.R. (2020). Layers II/III of Prefrontal Cortex in Df(h22q11)+ Mouse Model of the 22q11.2 Deletion Display Loss of Parvalbumin Interneurons and Modulation of Neuronal Morphology and Excitability. *Molecular Neurobiology* 57, 4978-4988.
- Amaral, D.G., and Witter, M.P. (1989). The three-dimensional organization of the hippocampal formation: A review of anatomical data. *Neuroscience* 31, 571-591.
- An, S., Kilb, W., and Luhmann, H.J. (2014). Sensory-Evoked and Spontaneous Gamma and Spindle Bursts in Neonatal Rat Motor Cortex. *The Journal of Neuroscience* 34, 10870-10883.
- Anastasiades, P.G., Boada, C., and Carter, A.G. (2019). Cell-Type-Specific D1 Dopamine Receptor Modulation of Projection Neurons and Interneurons in the Prefrontal Cortex. *Cereb Cortex* 29, 3224-3242.
- Anastasiades, P.G., and Carter, A.G. (2021). Circuit organization of the rodent medial prefrontal cortex. *Trends Neurosci* 44, 550-563.
- Andrade-Talavera, Y., Fisahn, A., and Rodríguez-Moreno, A. (2023). Timing to be precise? An overview of spike timing-dependent plasticity, brain rhythmicity, and glial cells interplay within neuronal circuits. *Molecular Psychiatry* 28, 2177-2188.
- Andreou, C., Leicht, G., Nolte, G., Polomac, N., Moritz, S., Karow, A., Hanganu-Opatz, I.L., Engel, A.K., and Mulert, C. (2015). Resting-state theta-band connectivity and verbal memory in schizophrenia and in the high-risk state. *Schizophrenia research* 161, 299-307.
- Antón-Bolaños, N., Sempere-Ferrández, A., Guillamón-Vivancos, T., Martini, F.J., Pérez-Saiz, L., Gezelius, H., Filipchuk, A., Valdeolmillos, M., and López-Bendito, G. (2019). Prenatal activity from thalamic neurons governs the emergence of functional cortical maps in mice. *Science* 364, 987-990.
- Arguello, P.A., and Gogos, J.A. (2009). Cognition in Mouse Models of Schizophrenia Susceptibility Genes. *Schizophrenia bulletin* 36, 289-300.
- Atallah, B.V., and Scanziani, M. (2009). Instantaneous modulation of gamma oscillation frequency by balancing excitation with inhibition. *Neuron* 62, 566-577.
- Atrooz, F., Alkadhi, K.A., and Salim, S. (2021). Understanding stress: Insights from rodent models. *Current Research in Neurobiology* 2, 100013.
- Au - Kislin, M., Au - Mugantseva, E., Au - Molotkov, D., Au - Kuleskaya, N., Au - Khirug, S., Au - Kirilkin, I., Au - Pryazhnikov, E., Au - Kolikova, J., Au - Toptunov, D., Au - Yuryev, M., *et al.* (2014). Flat-floored Air-lifted Platform: A New Method for Combining Behavior with Microscopy or Electrophysiology on Awake Freely Moving Rodents. *JoVE*, e51869.
- Backus, A.R., Schoffelen, J.M., Szebényi, S., Hanslmayr, S., and Doeller, C.F. (2016). Hippocampal-Prefrontal Theta Oscillations Support Memory Integration. *Curr Biol* 26, 450-457.
- Baddeley, A. (1992). Working Memory. *Science* 255, 556-559.
- Bähner, F., Demanuele, C., Schweiger, J., Gerchen, M.F., Zamoscik, V., Ueltzhöffer, K., Hahn, T., Meyer, P., Flor, H., Durstewitz, D., *et al.* (2015). Hippocampal-Dorsolateral Prefrontal Coupling as a Species-Conserved Cognitive Mechanism: A Human Translational Imaging Study. *Neuropsychopharmacology* 40, 1674-1681.
- Bailey, K.C., JN (2009). Anxiety-Related Behaviors in Mice. In *Methods of Behavior Analysis in Neuroscience*, B. JJ, ed. (Boca Raton (FL): CRC Press/Taylor & Francis).
-

## References

---

- Barker, G.R., and Warburton, E.C. (2011). When is the hippocampus involved in recognition memory? *J Neurosci* 31, 10721-10731.
- Barkus, C., Bergmann, C., Branco, T., Carandini, M., Chadderton, P.T., Galiñanes, G.L., Gilmour, G., Huber, D., Huxter, J.R., Khan, A.G., *et al.* (2022). Refinements to rodent head fixation and fluid/food control for neuroscience. *Journal of Neuroscience Methods* 381, 109705.
- Basu, J., Zaremba, J.D., Cheung, S.K., Hitti, F.L., Zemelman, B.V., Losonczy, A., and Siegelbaum, S.A. (2016). Gating of hippocampal activity, plasticity, and memory by entorhinal cortex long-range inhibition. *Science* 351, aaa5694.
- Bates, D., Mächler, M., Bolker, B., and Walker, S. (2014). Fitting linear mixed-effects models using lme4. *arXiv preprint arXiv:14065823*.
- Belzung, C., and Lemoine, M. (2011). Criteria of validity for animal models of psychiatric disorders: focus on anxiety disorders and depression. *Biology of mood & anxiety disorders* 1, 9.
- Benes, F.M., and Berretta, S. (2001). GABAergic Interneurons: Implications for Understanding Schizophrenia and Bipolar Disorder. *Neuropsychopharmacology* 25, 1-27.
- Benetti, S., Mechelli, A., Picchioni, M., Broome, M., Williams, S., and McGuire, P. (2009). Functional integration between the posterior hippocampus and prefrontal cortex is impaired in both first episode schizophrenia and the at risk mental state. *Brain* 132, 2426-2436.
- Berardino, B.G., Ballarini, F., Chertoff, M., Igaz, L.M., and Cánepa, E.T. (2022). Nutritional stress timing differentially programs cognitive abilities in young adult male mice. *Nutritional neuroscience* 25, 286-298.
- Bevins, R.A., and Besheer, J. (2006). Object recognition in rats and mice: a one-trial non-matching-to-sample learning task to study 'recognition memory'. *Nature Protocols* 1, 1306-1311.
- Biber, K., Neumann, H., Inoue, K., and Boddeke, H.W.G.M. (2007). Neuronal 'On' and 'Off' signals control microglia. *Trends in Neurosciences* 30, 596-602.
- Bitzenhofer, S.H., Ahlbeck, J., Wolff, A., Wiegert, J.S., Gee, C.E., Oertner, T.G., and Hanganu-Opatz, I.L. (2017). Layer-specific optogenetic activation of pyramidal neurons causes beta-gamma entrainment of neonatal networks. *Nat Commun* 8, 14563.
- Bitzenhofer, S.H., Popplau, J.A., Chini, M., Marquardt, A., and Hanganu-Opatz, I.L. (2021). A transient developmental increase in prefrontal activity alters network maturation and causes cognitive dysfunction in adult mice. *Neuron* 109, 1350-1364 e1356.
- Bitzenhofer, S.H., Popplau, J.A., and Hanganu-Opatz, I. (2020). Gamma activity accelerates during prefrontal development. *Elife* 9.
- Bitzenhofer, S.H., Sieben, K., Siebert, K.D., Spehr, M., and Hanganu-Opatz, I.L. (2015). Oscillatory activity in developing prefrontal networks results from theta-gamma-modulated synaptic inputs. *Cell Rep* 11, 486-497.
- Bjerknes, T.L., Langston, R.F., Kruge, I.U., Moser, E.I., and Moser, M.B. (2015). Coherence among head direction cells before eye opening in rat pups. *Curr Biol* 25, 103-108.
- Boksa, P. (2010). Effects of prenatal infection on brain development and behavior: a review of findings from animal models. *Brain, behavior, and immunity* 24, 881-897.
- Bourgeron, T. (2015). What Do We Know about Early Onset Neurodevelopmental Disorders? In *Translational Neuroscience: Toward New Therapies*, S.H. K. Nikolic, ed. (Cambridge (MA): MIT Press).
- Brandon, N.J., Millar, J.K., Korth, C., Sive, H., Singh, K.K., and Sawa, A. (2009). Understanding the role of DISC1 in psychiatric disease and during normal development. *J Neurosci* 29, 12768-12775.
- Brauer, R., Herrero-Zazo, M., Barlow, D.J., Gaughran, F., Taylor, D., and Howard, L.M. (2019). Minocycline and the risk of acute psychiatric events in adolescence: A self-controlled case series. *Journal of psychopharmacology (Oxford, England)* 33, 466-471.
- Brockmann, M.D., Pöschel, B., Cichon, N., and Hanganu-Opatz, I.L. (2011). Coupled oscillations mediate directed interactions between prefrontal cortex and hippocampus of the neonatal rat. *Neuron* 71, 332-347.
- Brust, V., Schindler, P.M., and Lewejohann, L. (2015). Lifetime development of behavioural phenotype in the house mouse (*Mus musculus*). *Frontiers in Zoology* 12, S17.
- Buzsáki, G. (1986). Hippocampal sharp waves: their origin and significance. *Brain Res* 398, 242-252.
- Buzsáki, G. (2002). Theta Oscillations in the Hippocampus. *Neuron* 33, 325-340.
-

## References

---

- Buzsáki, G. (2005). Theta rhythm of navigation: Link between path integration and landmark navigation, episodic and semantic memory. *Hippocampus* 15, 827-840.
- Buzsáki, G. (2010). Neural syntax: cell assemblies, synapsembles, and readers. *Neuron* 68, 362-385.
- Buzsáki, G. (2015). Hippocampal sharp wave-ripple: A cognitive biomarker for episodic memory and planning. *Hippocampus* 25, 1073-1188.
- Buzsáki, G., Anastassiou, C.A., and Koch, C. (2012). The origin of extracellular fields and currents — EEG, ECoG, LFP and spikes. *Nature Reviews Neuroscience* 13, 407-420.
- Buzsáki, G., and Draguhn, A. (2004). Neuronal oscillations in cortical networks. *Science* 304, 1926-1929.
- Buzsáki, G., Leung, L.W., and Vanderwolf, C.H. (1983). Cellular bases of hippocampal EEG in the behaving rat. *Brain Res* 287, 139-171.
- Buzsáki, G., Logothetis, N., and Singer, W. (2013). Scaling brain size, keeping timing: evolutionary preservation of brain rhythms. *Neuron* 80, 751-764.
- Buzsáki, G., and Silva, F.L. (2012). High frequency oscillations in the intact brain. *Prog Neurobiol* 98, 241-249.
- Buzsáki, G., and Wang, X.J. (2012). Mechanisms of gamma oscillations. *Annual review of neuroscience* 35, 203-225.
- Buzsáki, G., and Watson, B.O. (2012). Brain rhythms and neural syntax: implications for efficient coding of cognitive content and neuropsychiatric disease. *Dialogues in clinical neuroscience* 14, 345-367.
- Caballero, A., Flores-Barrera, E., Cass, D.K., and Tseng, K.Y. (2014a). Differential regulation of parvalbumin and calretinin interneurons in the prefrontal cortex during adolescence. *Brain Struct Funct* 219, 395-406.
- Caballero, A., Thomases, D.R., Flores-Barrera, E., Cass, D.K., and Tseng, K.Y. (2014b). Emergence of GABAergic-dependent regulation of input-specific plasticity in the adult rat prefrontal cortex during adolescence. *Psychopharmacology* 231, 1789-1796.
- Carbon, M., and Correll, C.U. (2014). Thinking and acting beyond the positive: the role of the cognitive and negative symptoms in schizophrenia. *CNS spectrums* 19 Suppl 1, 38-52; quiz 35-37, 53.
- Cardin, J.A. (2016). Snapshots of the Brain in Action: Local Circuit Operations through the Lens of  $\gamma$  Oscillations. *J Neurosci* 36, 10496-10504.
- Cardin, J.A., Carlén, M., Meletis, K., Knoblich, U., Zhang, F., Deisseroth, K., Tsai, L.H., and Moore, C.I. (2009). Driving fast-spiking cells induces gamma rhythm and controls sensory responses. *Nature* 459, 663-667.
- Carlén, M. (2017). What constitutes the prefrontal cortex? *Science* 358, 478-482.
- Carlsen, E.M.M., Nedergaard, M., and Rasmussen, R.N. (2022). Versatile treadmill system for measuring locomotion and neural activity in head-fixed mice. *STAR Protocols* 3, 101701.
- Carpenter, W.T., Jr., Heinrichs, D.W., and Wagman, A.M. (1988). Deficit and nondeficit forms of schizophrenia: the concept. *The American journal of psychiatry* 145, 578-583.
- Castelhano-Carlos, M., Sousa, N., Ohl, F., and Baumans, V. (2009). Identification methods in newborn C57BL/6 mice: A developmental and behavioural evaluation. *Laboratory animals* 44, 88-103.
- Chambers, A.R., Tylor, J.R., and Potenza, M.N. (2003). Developmental Neurocircuitry of Motivation in Adolescence: A Critical Period of Addiction Vulnerability. *American Journal of Psychiatry* 160, 1041-1052.
- Chao, H.T., Chen, H., Samaco, R.C., Xue, M., Chahrour, M., Yoo, J., Neul, J.L., Gong, S., Lu, H.C., Heintz, N., *et al.* (2010). Dysfunction in GABA signalling mediates autism-like stereotypies and Rett syndrome phenotypes. *Nature* 468, 263-269.
- Chen, G., Zhang, Y., Li, X., Zhao, X., Ye, Q., Lin, Y., Tao, H.W., Rasch, M.J., and Zhang, X. (2017). Distinct Inhibitory Circuits Orchestrate Cortical beta and gamma Band Oscillations. *Neuron* 96, 1403-1418.e1406.
- Chen, Y.-s., Zhang, S.-m., Yue, C.-x., Xiang, P., Li, J.-q., Wei, Z., Xu, L., and Zeng, Y. (2022). Early environmental enrichment for autism spectrum disorder Fmr1 mice models has positive behavioral and molecular effects. *Experimental Neurology* 352, 114033.
- Chen, Y.N., Kostka, J.K., Bitzenhofer, S.H., and Hanganu-Opatz, I.L. (2023). Olfactory bulb activity shapes the development of entorhinal-hippocampal coupling and associated cognitive abilities. *Curr Biol* 33, 4353-4366.e4355.
-

## References

---

- Chini, M., Gretenkord, S., Kostka, J.K., Pöpplau, J.A., Cornelissen, L., Berde, C.B., Hanganu-Opatz, I.L., and Bitzenhofer, S.H. (2019). Neural Correlates of Anesthesia in Newborn Mice and Humans. *Frontiers in Neural Circuits* 13.
- Chini, M., and Hanganu-Opatz, I.L. (2021). Prefrontal Cortex Development in Health and Disease: Lessons from Rodents and Humans. *Trends Neurosci* 44, 227-240.
- Chini, M., Hnida, M., Kostka, J.K., Chen, Y.-N., and Hanganu-Opatz, I.L. (2023). Extreme distributions in the preconfigured developing brain. *bioRxiv*, 2023.2011.2013.566810.
- Chini, M., Pöpplau, J.A., Lindemann, C., Carol-Perdiguer, L., Hnida, M., Oberländer, V., Xu, X., Ahlbeck, J., Bitzenhofer, S.H., Mulert, C., and Hanganu-Opatz, I.L. (2020). Resolving and Rescuing Developmental Miswiring in a Mouse Model of Cognitive Impairment. *Neuron* 105, 60-74.e67.
- Cho, K.K., Hoch, R., Lee, A.T., Patel, T., Rubenstein, J.L., and Sohal, V.S. (2015). Gamma rhythms link prefrontal interneuron dysfunction with cognitive inflexibility in *Dlx5/6(+/-)* mice. *Neuron* 85, 1332-1343.
- Clancy, B., Darlington, R.B., and Finlay, B.L. (2001). Translating developmental time across mammalian species. *Neuroscience* 105, 7-17.
- Claudi, F., Tyson, A.L., Petrucco, L., Margrie, T.W., Portugues, R., and Branco, T. (2021). Visualizing anatomically registered data with brainrender. *Elife* 10.
- Clement, E.A., Richard, A., Thwaites, M., Ailon, J., Peters, S., and Dickson, C.T. (2008). Cyclic and sleep-like spontaneous alternations of brain state under urethane anaesthesia. *PLoS One* 3, e2004.
- Cohen, S.M., and Nadler, J.V. (1997). Proline-induced potentiation of glutamate transmission. *Brain Research* 761, 271-282.
- Colavitta, M.F., Grasso, L., and Barrantes, F.J. (2023). Environmental Enrichment in Murine Models and Its Translation to Human Factors Improving Conditions in Alzheimer Disease. *The Journal of Prevention of Alzheimer's Disease* 10, 287-300.
- Colgin, L.L. (2011). Oscillations and hippocampal-prefrontal synchrony. *Current opinion in neurobiology* 21, 467-474.
- Colgin, L.L., Denninger, T., Fyhn, M., Hafting, T., Bonnevie, T., Jensen, O., Moser, M.B., and Moser, E.I. (2009). Frequency of gamma oscillations routes flow of information in the hippocampus. *Nature* 462, 353-357.
- Collins, D.P., Anastasiades, P.G., Marlin, J.J., and Carter, A.G. (2018). Reciprocal Circuits Linking the Prefrontal Cortex with Dorsal and Ventral Thalamic Nuclei. *Neuron* 98, 366-379.e364.
- Colonnese, M., and Khazipov, R. (2012). Spontaneous activity in developing sensory circuits: Implications for resting state fMRI. *NeuroImage* 62, 2212-2221.
- Crépel, V., Aronov, D., Jorquera, I., Represa, A., Ben-Ari, Y., and Cossart, R. (2007). A parturition-associated nonsynaptic coherent activity pattern in the developing hippocampus. *Neuron* 54, 105-120.
- Crews, F.T., and Vetreno, R.P. (2016). Mechanisms of neuroimmune gene induction in alcoholism. *Psychopharmacology (Berl)* 233, 1543-1557.
- Cutts, C.S., and Eglén, S.J. (2014). Detecting Pairwise Correlations in Spike Trains: An Objective Comparison of Methods and Application to the Study of Retinal Waves. *The Journal of Neuroscience* 34, 14288-14303.
- d'Isa, R., Comi, G., and Leocani, L. (2021). Apparatus design and behavioural testing protocol for the evaluation of spatial working memory in mice through the spontaneous alternation T-maze. *Sci Rep* 11, 21177.
- da Silva Alves, F., Boot, E., Schmitz, N., Nederveen, A., Vorstman, J., Lavini, C., Pouwels, P.J., de Haan, L., Linszen, D., and van Amelsvoort, T. (2011). Proton magnetic resonance spectroscopy in 22q11 deletion syndrome. *PLoS One* 6, e21685.
- Dansie, L.E., Phommahaxay, K., Okusanya, A.G., Uwadia, J., Huang, M., Rotschafer, S.E., Razak, K.A., Ethell, D.W., and Ethell, I.M. (2013). Long-lasting effects of minocycline on behavior in young but not adult Fragile X mice. *Neuroscience* 246, 186-198.
- Datta, D., Arion, D., and Lewis, D.A. (2014). Developmental Expression Patterns of GABAA Receptor Subunits in Layer 3 and 5 Pyramidal Cells of Monkey Prefrontal Cortex. *Cerebral Cortex* 25, 2295-2305.
- Davis, J., Eyre, H., Jacka, F.N., Dodd, S., Dean, O., McEwen, S., Debnath, M., McGrath, J., Maes, M., Amminger, P., *et al.* (2016). A review of vulnerability and risks for schizophrenia: Beyond the two hit hypothesis. *Neurosci Biobehav Rev* 65, 185-194.
-

## References

---

- de Almeida, J., Jourdan, I., Murer, M.G., and Belforte, J.E. (2013). Refinement of Neuronal Synchronization with Gamma Oscillations in the Medial Prefrontal Cortex after Adolescence. *PLOS ONE* 8, e62978.
- De Picker, L.J., Morrens, M., Chance, S.A., and Boche, D. (2017). Microglia and brain plasticity in acute psychosis and schizophrenia illness course: A meta-review. *Frontiers in psychiatry* 8.
- Dean, O.M., Data-Franco, J., Giorlando, F., and Berk, M. (2012). Minocycline. *CNS Drugs* 26, 391-401.
- Deininger, M.H., Meyermann, R., and Schluesener, H.J. (2002). The allograft inflammatory factor-1 family of proteins. *FEBS letters* 514, 115-121.
- Delevich, K., Thomas, A.W., and Wilbrecht, L. (2018). Adolescence and "Late Blooming" Synapses of the Prefrontal Cortex. *Cold Spring Harb Symp Quant Biol* 83, 37-43.
- Denayer, T., Stöhr, T., and Van Roy, M. (2014). Animal models in translational medicine: Validation and prediction. *New Horizons in Translational Medicine* 2, 5-11.
- Dickerson, B.C., and Eichenbaum, H. (2010). The episodic memory system: neurocircuitry and disorders. *Neuropsychopharmacology* 35, 86-104.
- Didriksen, M., Fejgin, K., Nilsson, S.R., Birknow, M.R., Grayton, H.M., Larsen, P.H., Lauridsen, J.B., Nielsen, V., Celada, P., Santana, N., *et al.* (2017). Persistent gating deficit and increased sensitivity to NMDA receptor antagonism after puberty in a new mouse model of the human 22q11.2 microdeletion syndrome: a study in male mice. *Journal of psychiatry & neuroscience : JPN* 42, 48-58.
- Donoghue, T., Haller, M., Peterson, E.J., Varma, P., Sebastian, P., Gao, R., Noto, T., Lara, A.H., Wallis, J.D., Knight, R.T., *et al.* (2020). Parameterizing neural power spectra into periodic and aperiodic components. *Nature Neuroscience* 23, 1655-1665.
- Douaud, G., Mackay, C., Andersson, J., James, S., Quested, D., Ray, M.K., Connell, J., Roberts, N., Crow, T.J., Matthews, P.M., *et al.* (2009). Schizophrenia delays and alters maturation of the brain in adolescence. *Brain* 132, 2437-2448.
- Drzewiecki, C.M., Willing, J., and Juraska, J.M. (2016). Synaptic number changes in the medial prefrontal cortex across adolescence in male and female rats: A role for pubertal onset. *Synapse* 70, 361-368.
- Du, Q., de la Morena, M.T., and van Oers, N.S.C. (2020). The Genetics and Epigenetics of 22q11.2 Deletion Syndrome. *Frontiers in Genetics* 10.
- Dutta, S., and Sengupta, P. (2016). Men and mice: Relating their ages. *Life Sciences* 152, 244-248.
- Egorov, A.V., and Draguhn, A. (2013). Development of coherent neuronal activity patterns in mammalian cortical networks: common principles and local heterogeneity. *Mechanisms of development* 130, 412-423.
- Eichenbaum, H. (2017). Prefrontal–hippocampal interactions in episodic memory. *Nature Reviews Neuroscience* 18, 547-558.
- El-Hallak, M., Giani, T., Yeniay, B.S., Jacobs, K.E., Kim, S., Sundel, R.P., and Dedeoglu, F. (2008). Chronic Minocycline-Induced Autoimmunity in Children. *The Journal of Pediatrics* 153, 314-319.
- Engel, A.K., Fries, P., and Singer, W. (2001). Dynamic predictions: Oscillations and synchrony in top-down processing. *Nature Reviews Neuroscience* 2, 704-716.
- Eryilmaz, H., Tanner, A.S., Ho, N.F., Nitenson, A.Z., Silverstein, N.J., Petruzzini, L.J., Goff, D.C., Manoach, D.S., and Roffman, J.L. (2016). Disrupted Working Memory Circuitry in Schizophrenia: Disentangling fMRI Markers of Core Pathology vs Other Aspects of Impaired Performance. *Neuropsychopharmacology* 41, 2411-2420.
- Eşposito, G., Azhari, N., and Borelli, J. (2018). Gene × Environment Interaction in Developmental Disorders: Where Do We Stand and What's Next? *Frontiers in Psychology* 9, 2036.
- Felix-Ortiz, A.C., Beyeler, A., Seo, C., Leppla, C.A., Wildes, C.P., and Tye, K.M. (2013). BLA to vHPC inputs modulate anxiety-related behaviors. *Neuron* 79, 658-664.
- Fell, J., and Axmacher, N. (2011). The role of phase synchronization in memory processes. *Nature Reviews Neuroscience* 12, 105-118.
- Ferino, F., Thierry, A.M., and Glowinski, J. (1987). Anatomical and electrophysiological evidence for a direct projection from Ammon's horn to the medial prefrontal cortex in the rat. *Experimental brain research* 65, 421-426.
- Ferrier, D. (1890). The Croonian Lectures on Cerebral Localisation. *British medical journal* 1, 1349-1355.
-

## References

---

- Fields, R.D., Araque, A., Johansen-Berg, H., Lim, S.S., Lynch, G., Nave, K.A., Nedergaard, M., Perez, R., Sejnowski, T., and Wake, H. (2014). Glial biology in learning and cognition. *The Neuroscientist : a review journal bringing neurobiology, neurology and psychiatry* 20, 426-431.
- Flores-Barrera, E., Thomases, D.R., Heng, L.-J., Cass, D.K., Caballero, A., and Tseng, K.Y. (2014). Late Adolescent Expression of GluN2B Transmission in the Prefrontal Cortex Is Input-Specific and Requires Postsynaptic Protein Kinase A and D1 Dopamine Receptor Signaling. *Biological Psychiatry* 75, 508-516.
- Flores-Ramos, M., Yoldi-Negrete, M., Guiza-Zayas, R., Ramírez-Rodríguez, G.-B., Montes-Castrejón, A., and Fresán, A. (2022). An Indicator of environmental enrichment to measure physical, social and cognitive activities in human daily life. *BMC Psychiatry* 22, 295.
- França, A.S.C., van Hulten, J.A., and Cohen, M.X. (2020). Low-cost and versatile electrodes for extracellular chronic recordings in rodents. *Heliyon* 6, e04867.
- Freedman, D.S., Schroeder, J.B., Telian, G.I., Zhang, Z., Sunil, S., and Ritt, J.T. (2016). OptoZIF Drive: a 3D printed implant and assembly tool package for neural recording and optical stimulation in freely moving mice. *Journal of neural engineering* 13, 066013.
- Freund, T.F., and Antal, M. (1988). GABA-containing neurons in the septum control inhibitory interneurons in the hippocampus. *Nature* 336, 170-173.
- Fries, P. (2005). A mechanism for cognitive dynamics: neuronal communication through neuronal coherence. *Trends Cogn Sci* 9, 474-480.
- Fries, P. (2015). Rhythms for Cognition: Communication through Coherence. *Neuron* 88, 220-235.
- Fung, W.L.A., Butcher, N.J., Costain, G., Andrade, D.M., Boot, E., Chow, E.W.C., Chung, B., Cytrynbaum, C., Faghfoury, H., Fishman, L., *et al.* (2015). Practical guidelines for managing adults with 22q11.2 deletion syndrome. *Genetics in Medicine* 17, 599-609.
- Fuster, J.M. (2000). Executive frontal functions. *Experimental brain research* 133, 66-70.
- Fuster, J.M. (2001). Prefrontal Cortex. In *International Encyclopedia of the Social & Behavioral Sciences*, N.J. Smelser, and P.B. Baltes, eds. (Oxford: Pergamon), pp. 11969-11976.
- Fyhn, M., Molden, S., Witter, M.P., Moser, E.I., and Moser, M.B. (2004). Spatial representation in the entorhinal cortex. *Science* 305, 1258-1264.
- Garrido-Mesa, N., Zarzuelo, A., and Gálvez, J. (2013). Minocycline: far beyond an antibiotic. *British journal of pharmacology* 169, 337-352.
- Geisler, C., Robbe, D., Zugaro, M., Sirota, A., and Buzsáki, G. (2007). Hippocampal place cell assemblies are speed-controlled oscillators. *Proc Natl Acad Sci U S A* 104, 8149-8154.
- George, M., Maheshwari, S., Chandran, S., Manohar, J.S., and Sathyanarayana Rao, T.S. (2017). Understanding the schizophrenia prodrome. *Indian journal of psychiatry* 59, 505-509.
- Georgieff, M.K., Ramel, S.E., and Cusick, S.E. (2018). Nutritional influences on brain development. *Acta paediatrica (Oslo, Norway : 1992)* 107, 1310-1321.
- Ghoshal, A., and Conn, P.J. (2015). The hippocampo-prefrontal pathway: a possible therapeutic target for negative and cognitive symptoms of schizophrenia. *Future neurology* 10, 115-128.
- Giedd, J.N. (2004). Structural magnetic resonance imaging of the adolescent brain. *Ann N Y Acad Sci* 1021, 77-85.
- Giedd, J.N., Blumenthal, J., Jeffries, N.O., Castellanos, F.X., Liu, H., Zijdenbos, A., Paus, T., Evans, A.C., and Rapoport, J.L. (1999). Brain development during childhood and adolescence: a longitudinal MRI study. *Nat Neurosci* 2, 861-863.
- Go, M.A., Rogers, J., Gava, G.P., Davey, C.E., Prado, S., Liu, Y., and Schultz, S.R. (2021). Place Cells in Head-Fixed Mice Navigating a Floating Real-World Environment. *Front Cell Neurosci* 15, 618658.
- Godsil, B.P., Kiss, J.P., Spedding, M., and Jay, T.M. (2013). The hippocampal-prefrontal pathway: The weak link in psychiatric disorders? *European Neuropsychopharmacology* 23, 1165-1181.
- Gogtay, N., Giedd, J.N., Lusk, L., Hayashi, K.M., Greenstein, D., Vaituzis, A.C., Nugent, T.F., 3rd, Herman, D.H., Clasen, L.S., Toga, A.W., *et al.* (2004). Dynamic mapping of human cortical development during childhood through early adulthood. *Proc Natl Acad Sci U S A* 101, 8174-8179.
- Gogtay, N., Vyas, N.S., Testa, R., Wood, S.J., and Pantelis, C. (2011). Age of onset of schizophrenia: perspectives from structural neuroimaging studies. *Schizophrenia bulletin* 37, 504-513.
- Gold, J.M., Barch, D.M., Feuerstahler, L.M., Carter, C.S., MacDonald, A.W., III, Ragland, J.D., Silverstein, S.M., Strauss, M.E., and Luck, S.J. (2018). Working Memory Impairment Across Psychotic disorders. *Schizophrenia bulletin* 45, 804-812.
-

## References

---

- Gonzalez-Burgos, G., and Lewis, D.A. (2008). GABA neurons and the mechanisms of network oscillations: implications for understanding cortical dysfunction in schizophrenia. *Schizophrenia bulletin* 34, 944-961.
- Goutagny, R., Jackson, J., and Williams, S. (2009). Self-generated theta oscillations in the hippocampus. *Nat Neurosci* 12, 1491-1493.
- Gretenkord, S., Kostka, J.K., Hartung, H., Watznauer, K., Fleck, D., Minier-Toribio, A., Spehr, M., and Hanganu-Opatz, I.L. (2019). Coordinated electrical activity in the olfactory bulb gates the oscillatory entrainment of entorhinal networks in neonatal mice. *PLOS Biology* 17, e2006994.
- Guan, A., Wang, S., Huang, A., Qiu, C., Li, Y., Li, X., Wang, J., Wang, Q., and Deng, B. (2022). The role of gamma oscillations in central nervous system diseases: Mechanism and treatment. *Front Cell Neurosci* 16, 962957.
- Haddad, P.M., and Correll, C.U. (2018). The acute efficacy of antipsychotics in schizophrenia: a review of recent meta-analyses. *Therapeutic advances in psychopharmacology* 8, 303-318.
- Häfner, H., Maurer, K., Löffler, W., an der Heiden, W., Munk-Jørgensen, P., Hambrecht, M., and Riecher-Rössler, A. (1998). The ABC Schizophrenia Study: a preliminary overview of the results. *Social psychiatry and psychiatric epidemiology* 33, 380-386.
- Hafting, T., Fyhn, M., Molden, S., Moser, M.-B., and Moser, E.I. (2005). Microstructure of a spatial map in the entorhinal cortex. *Nature* 436, 801-806.
- Hallock, H.L., Wang, A., and Griffin, A.L. (2016). Ventral Midline Thalamus Is Critical for Hippocampal-Prefrontal Synchrony and Spatial Working Memory. *J Neurosci* 36, 8372-8389.
- Hammond, T.R., Robinton, D., and Stevens, B. (2018). Microglia and the Brain: Complementary Partners in Development and Disease. *Annual Review of Cell and Developmental Biology* 34, 523-544.
- Han, W., and Sestan, N. (2013). Cortical projection neurons: sprung from the same root. *Neuron* 80, 1103-1105.
- Hanganu-Opatz, I.L. (2010). Between molecules and experience: role of early patterns of coordinated activity for the development of cortical maps and sensory abilities. *Brain research reviews* 64, 160-176.
- Hanganu, I.L., Ben-Ari, Y., and Khazipov, R. (2006). Retinal Waves Trigger Spindle Bursts in the Neonatal Rat Visual Cortex. *The Journal of Neuroscience* 26, 6728-6736.
- Hardingham, G.E., and Do, K.Q. (2016). Linking early-life NMDAR hypofunction and oxidative stress in schizophrenia pathogenesis. *Nat Rev Neurosci* 17, 125-134.
- Harris, K.D., and Shepherd, G.M. (2015). The neocortical circuit: themes and variations. *Nat Neurosci* 18, 170-181.
- Hartung, H., Brockmann, M.D., Pöschel, B., De Feo, V., and Hanganu-Opatz, I.L. (2016a). Thalamic and Entorhinal Network Activity Differently Modulates the Functional Development of Prefrontal-Hippocampal Interactions. *J Neurosci* 36, 3676-3690.
- Hartung, H., Cichon, N., De Feo, V., Riemann, S., Schildt, S., Lindemann, C., Mulert, C., Gogos, J.A., and Hanganu-Opatz, I.L. (2016b). From Shortage to Surge: A Developmental Switch in Hippocampal-Prefrontal Coupling in a Gene-Environment Model of Neuropsychiatric Disorders. *Cereb Cortex* 26, 4265-4281.
- Heckers, S., and Konradi, C. (2002). Hippocampal neurons in schizophrenia. *Journal of neural transmission (Vienna, Austria : 1996)* 109, 891-905.
- Heckers, S., and Konradi, C. (2010). Hippocampal pathology in schizophrenia. *Behavioral neurobiology of schizophrenia and its treatment*, 529-553.
- Henseler, I., Falkai, P., and Gruber, O. (2010). Disturbed functional connectivity within brain networks subserving domain-specific subcomponents of working memory in schizophrenia: relation to performance and clinical symptoms. *Journal of psychiatric research* 44, 364-372.
- Howes, O.D., and McCutcheon, R. (2017). Inflammation and the neural diathesis-stress hypothesis of schizophrenia: a reconceptualization. *Transl Psychiatry* 7, e1024.
- Hyman, J.M., Zilli, E.A., Paley, A.M., and Hasselmo, M.E. (2010). Working Memory Performance Correlates with Prefrontal-Hippocampal Theta Interactions but not with Prefrontal Neuron Firing Rates. *Frontiers in integrative neuroscience* 4, 2.
- Isaksson, J., Ruchkin, V., Ljungström, T., and Bölte, S. (2023). Evaluation of Birth Weight and Neurodevelopmental Conditions Among Monozygotic and Dizygotic Twins. *JAMA Network Open* 6, e2321165-e2321165.
- Jauhar, S., Johnstone, M., and McKenna, P.J. (2022). Schizophrenia. *The Lancet* 399, 473-486.
-

## References

---

- Jay, T.M., and Witter, M.P. (1991). Distribution of hippocampal CA1 and subicular efferents in the prefrontal cortex of the rat studied by means of anterograde transport of Phaseolus vulgaris-leucoagglutinin. *The Journal of comparative neurology* 313, 574-586.
- Jimenez, J.C., Su, K., Goldberg, A.R., Luna, V.M., Biane, J.S., Ordek, G., Zhou, P., Ong, S.K., Wright, M.A., Zweifel, L., *et al.* (2018). Anxiety Cells in a Hippocampal-Hypothalamic Circuit. *Neuron* 97, 670-683.e676.
- Jones, B.F., and Witter, M.P. (2007). Cingulate cortex projections to the parahippocampal region and hippocampal formation in the rat. *Hippocampus* 17, 957-976.
- Jones, C.A., Watson, D.J., and Fone, K.C. (2011). Animal models of schizophrenia. *Br J Pharmacol* 164, 1162-1194.
- Jones, M.W., and Wilson, M.A. (2005). Theta Rhythms Coordinate Hippocampal–Prefrontal Interactions in a Spatial Memory Task. *PLOS Biology* 3, e402.
- Juckel, G., Manitz, M.P., Brüne, M., Friebe, A., Heneka, M.T., and Wolf, R.J. (2011). Microglial activation in a neuroinflammatory animal model of schizophrenia—a pilot study. *Schizophrenia research* 131, 96-100.
- Juczewski, K., Koussa, J.A., Kesner, A.J., Lee, J.O., and Lovinger, D.M. (2020). Stress and behavioral correlates in the head-fixed method: stress measurements, habituation dynamics, locomotion, and motor-skill learning in mice. *Scientific Reports* 10, 12245.
- Kadakia, A., Catillon, M., Fan, Q., Williams, G.R., Marden, J.R., Anderson, A., Kirson, N., and Dembek, C. (2022). The Economic Burden of Schizophrenia in the United States. *The Journal of clinical psychiatry* 83.
- Kahn, J.B., Port, R.G., Anderson, S.A., and Coulter, D.A. (2020). Modular, Circuit-Based Interventions Rescue Hippocampal-Dependent Social and Spatial Memory in a 22q11.2 Deletion Syndrome Mouse Model. *Biol Psychiatry* 88, 710-718.
- Karayorgou, M., and Gogos, J.A. (2004). The molecular genetics of the 22q11-associated schizophrenia. *Brain research Molecular brain research* 132, 95-104.
- Karayorgou, M., Simon, T.J., and Gogos, J.A. (2010). 22q11.2 microdeletions: linking DNA structural variation to brain dysfunction and schizophrenia. *Nat Rev Neurosci* 11, 402-416.
- Katz, L.C., and Shatz, C.J. (1996). Synaptic activity and the construction of cortical circuits. *Science* 274, 1133-1138.
- Kaur, T., and Cadenhead, K.S. (2010). Treatment implications of the schizophrenia prodrome. *Current topics in behavioral neurosciences* 4, 97-121.
- Keshavan, M.S., Tandon, R., Boutros, N.N., and Nasrallah, H.A. (2008). Schizophrenia, "just the facts": what we know in 2008 Part 3: neurobiology. *Schizophrenia research* 106, 89-107.
- Khazipov, R., and Luhmann, H.J. (2006). Early patterns of electrical activity in the developing cerebral cortex of humans and rodents. *Trends in Neurosciences* 29, 414-418.
- Khazipov, R., Sirota, A., Leinekugel, X., Holmes, G.L., Ben-Ari, Y., and Buzsáki, G. (2004). Early motor activity drives spindle bursts in the developing somatosensory cortex. *Nature* 432, 758-761.
- Khodosevich, K., and Sellgren, C.M. (2023). Neurodevelopmental disorders—high-resolution rethinking of disease modeling. *Molecular Psychiatry* 28, 34-43.
- Kim, E.J., and Kim, J.J. (2023). Neurocognitive effects of stress: a metaparadigm perspective. *Molecular Psychiatry* 28, 2750-2763.
- Kislin, M., Mugantseva, E., Molotkov, D., Kuleskaya, N., Khirug, S., Kirilkin, I., Pryazhnikov, E., Kolikova, J., Toptunov, D., Yuryev, M., *et al.* (2014). Flat-floored air-lifted platform: a new method for combining behavior with microscopy or electrophysiology on awake freely moving rodents. *Journal of visualized experiments : JoVE*, e51869.
- Klune, C.B., Jin, B., and DeNardo, L.A. (2021). Linking mPFC circuit maturation to the developmental regulation of emotional memory and cognitive flexibility. *Elife* 10.
- Koike, H., Arguello, P.A., Kvajo, M., Karayorgou, M., and Gogos, J.A. (2006). *Disc1* is mutated in the 129S6/SvEv strain and modulates working memory in mice. *Proc Natl Acad Sci U S A* 103, 3693-3697.
- Konstantoudaki, X., Chalkiadaki, K., Vasileiou, E., Kalemaki, K., Karagogeos, D., and Sidiropoulou, K. (2018). Prefrontal cortical-specific differences in behavior and synaptic plasticity between adolescent and adult mice. *J Neurophysiol* 119, 822-833.
- Kostka, J.K., and Hanganu-Opatz, I.L. (2023). Olfactory-driven beta band entrainment of limbic circuitry during neonatal development. *The Journal of physiology* 601, 3605-3630.
-

## References

---

- Krüger, H.-S., Brockmann, M.D., Salamon, J., Itrich, H., and Hanganu-Opatz, I.L. (2012). Neonatal hippocampal lesion alters the functional maturation of the prefrontal cortex and the early cognitive development in pre-juvenile rats. *Neurobiology of Learning and Memory* 97, 470-481.
- Kuznetsova, A., Brockhoff, P.B., and Christensen, R.H.B. (2017). lmerTest Package: Tests in Linear Mixed Effects Models. *Journal of Statistical Software* 82, 1 - 26.
- Kvajo, M., McKellar, H., Arguello, P.A., Drew, L.J., Moore, H., MacDermott, A.B., Karayiorgou, M., and Gogos, J.A. (2008). A mutation in mouse *Disc1* that models a schizophrenia risk allele leads to specific alterations in neuronal architecture and cognition. *Proc Natl Acad Sci U S A* 105, 7076-7081.
- La-Vu, M., Tobias, B.C., Schuette, P.J., and Adhikari, A. (2020). To Approach or Avoid: An Introductory Overview of the Study of Anxiety Using Rodent Assays. *Frontiers in Behavioral Neuroscience* 14.
- Laviola, G., Macri, S., Morley-Fletcher, S., and Adriani, W. (2003). Risk-taking behavior in adolescent mice: psychobiological determinants and early epigenetic influence. *Neuroscience & Biobehavioral Reviews* 27, 19-31.
- Le Strat, Y., Ramoz, N., and Gorwood, P. (2009). The role of genes involved in neuroplasticity and neurogenesis in the observation of a gene-environment interaction (GxE) in schizophrenia. *Current molecular medicine* 9, 506-518.
- Leigh, M.J., Nguyen, D.V., Mu, Y., Winarni, T.I., Schneider, A., Chechi, T., Polussa, J., Doucet, P., Tassone, F., Rivera, S.M., *et al.* (2013). A randomized double-blind, placebo-controlled trial of minocycline in children and adolescents with fragile x syndrome. *Journal of developmental and behavioral pediatrics : JDBP* 34, 147-155.
- Leinekugel, X., Khazipov, R., Cannon, R., Hirase, H., Ben-Ari, Y., and Buzsáki, G. (2002). Correlated bursts of activity in the neonatal hippocampus in vivo. *Science* 296, 2049-2052.
- Leslie, C.A., Robertson, M.W., Cutler, A.J., and Bennett Jr, J.P. (1991). Postnatal development of D 1 dopamine receptors in the medial prefrontal cortex, striatum and nucleus accumbens of normal and neonatal 6-hydroxydopamine treated rats: a quantitative autoradiographic analysis. *Developmental Brain Research* 62, 109-114.
- Lewis, D.A., and Moghaddam, B. (2006). Cognitive dysfunction in schizophrenia: convergence of gamma-aminobutyric acid and glutamate alterations. *Archives of neurology* 63, 1372-1376.
- Li, F., and Tsien, J.Z. (2009). Memory and the NMDA receptors. *The New England journal of medicine* 361, 302-303.
- Lin, W.C., Liu, C., Kosillo, P., Tai, L.-H., Galarce, E., Bateup, H.S., Lammel, S., and Wilbrecht, L. (2022). Transient food insecurity during the juvenile-adolescent period affects adult weight, cognitive flexibility, and dopamine neurobiology. *Current Biology* 32, 3690-3703.e3695.
- Lisman, J.E., and Idiart, M.A. (1995). Storage of 7 +/- 2 short-term memories in oscillatory subcycles. *Science* 267, 1512-1515.
- Logan, D.W., Brunet, L.J., Webb, W.R., Cutforth, T., Ngai, J., and Stowers, L. (2012). Learned recognition of maternal signature odors mediates the first suckling episode in mice. *Curr Biol* 22, 1998-2007.
- Luhmann, H.J., Kilb, W., and Hanganu-Opatz, I.L. (2009). Subplate cells: amplifiers of neuronal activity in the developing cerebral cortex. *Frontiers in neuroanatomy* 3, 19.
- Luzi, P., Abraham, R.M., Rafi, M.A., Curtis, M., Hooper, D.C., and Wenger, D.A. (2009). Effects of treatments on inflammatory and apoptotic markers in the CNS of mice with globoid cell leukodystrophy. *Brain research* 1300, 146-158.
- MacKenzie, N.E., Kowalchuk, C., Agarwal, S.M., Costa-Dookhan, K.A., Caravaggio, F., Gerretsen, P., Chintoh, A., Remington, G.J., Taylor, V.H., Müller, D.J., *et al.* (2018). Antipsychotics, Metabolic Adverse Effects, and Cognitive Function in Schizophrenia. *Frontiers in psychiatry* 9, 622.
- Maingret, N., Girardeau, G., Todorova, R., Goutierre, M., and Zugaro, M. (2016). Hippocampo-cortical coupling mediates memory consolidation during sleep. *Nature Neuroscience* 19, 959-964.
- Mäki, P., Veijola, J., Jones, P.B., Murray, G.K., Koponen, H., Tienari, P., Miettunen, J., Tanskanen, P., Wahlberg, K.-E., Koskinen, J., *et al.* (2005). Predictors of schizophrenia—a review. *British Medical Bulletin* 73-74, 1-15.
- Malik, R., Li, Y., Schamiloglu, S., and Sohal, V.S. (2022). Top-down control of hippocampal signal-to-noise by prefrontal long-range inhibition. *Cell* 185, 1602-1617.e1617.
- Mallya, A.P., Wang, H.D., Lee, H.N.R., and Deutch, A.Y. (2019). Microglial Pruning of Synapses in the Prefrontal Cortex During Adolescence. *Cereb Cortex* 29, 1634-1643.
-

## References

---

- Marder, S.R., and Umbricht, D. (2023). Negative symptoms in schizophrenia: Newly emerging measurements, pathways, and treatments. *Schizophrenia research* 258, 71-77.
- Marek, S., Tervo-Clemmens, B., Klein, N., Foran, W., Ghuman, A.S., and Luna, B. (2018). Adolescent development of cortical oscillations: Power, phase, and support of cognitive maturation. *PLoS Biol* 16, e2004188.
- Markram, H. (2013). Seven challenges for neuroscience. *Functional neurology* 28, 145-151.
- Massrali, A., Adhya, D., Srivastava, D.P., Baron-Cohen, S., and Kotter, M.R. (2022). Virus-Induced Maternal Immune Activation as an Environmental Factor in the Etiology of Autism and Schizophrenia. *Front Neurosci* 16, 834058.
- Mattei, D., Djodari-Irani, A., Hadar, R., Pelz, A., de Cossío, L.F., Goetz, T., Matyash, M., Kettenmann, H., Winter, C., and Wolf, S.A. (2014). Minocycline rescues decrease in neurogenesis, increase in microglia cytokines and deficits in sensorimotor gating in an animal model of schizophrenia. *Brain, behavior, and immunity* 38, 175-184.
- McConnell, S.K., Ghosh, A., and Shatz, C.J. (1989). Subplate neurons pioneer the first axon pathway from the cerebral cortex. *Science* 245, 978-982.
- McDonald-McGinn, D.M., Sullivan, K.E., Marino, B., Philip, N., Swillen, A., Vorstman, J.A.S., Zackai, E.H., Emanuel, B.S., Vermeesch, J.R., Morrow, B.E., *et al.* (2015). 22q11.2 deletion syndrome. *Nature Reviews Disease Primers* 1, 15071.
- McFarland, W.L., Teitelbaum, H., and Hedges, E.K. (1975). Relationship between hippocampal theta activity and running speed in the rat. *Journal of comparative and physiological psychology* 88, 324-328.
- McGarry, L.M., and Carter, A.G. (2017). Prefrontal Cortex Drives Distinct Projection Neurons in the Basolateral Amygdala. *Cell Rep* 21, 1426-1433.
- McGrath, J.J., Féron, F.P., Burne, T.H., Mackay-Sim, A., and Eyles, D.W. (2003). The neurodevelopmental hypothesis of schizophrenia: a review of recent developments. *Annals of medicine* 35, 86-93.
- McLaughlin, K.A., Fox, N.A., Zeanah, C.H., Sheridan, M.A., Marshall, P., and Nelson, C.A. (2010). Delayed maturation in brain electrical activity partially explains the association between early environmental deprivation and symptoms of attention-deficit/hyperactivity disorder. *Biological Psychiatry* 68, 329-336.
- Meehan, D.W., Maynard, T.M., Tucker, E.S., Fernandez, A., Karpinski, B.A., Rothblat, L.A., and LaMantia, A.S. (2015). Modeling a model: Mouse genetics, 22q11.2 Deletion Syndrome, and disorders of cortical circuit development. *Prog Neurobiol* 130, 1-28.
- Mehl, L.C., Manjally, A.V., Bouadi, O., Gibson, E.M., and Tay, T.L. (2022). Microglia in brain development and regeneration. *Development (Cambridge, England)* 149.
- Melzer, S., and Monyer, H. (2020). Diversity and function of corticopetal and corticofugal GABAergic projection neurons. *Nat Rev Neurosci* 21, 499-515.
- Meyer-Lindenberg, A.S., Olsen, R.K., Kohn, P.D., Brown, T., Egan, M.F., Weinberger, D.R., and Berman, K.F. (2005). Regionally specific disturbance of dorsolateral prefrontal-hippocampal functional connectivity in schizophrenia. *Archives of general psychiatry* 62, 379-386.
- Millar, J.K., Wilson-Annan, J.C., Anderson, S., Christie, S., Taylor, M.S., Semple, C.A., Devon, R.S., St Clair, D.M., Muir, W.J., Blackwood, D.H., and Porteous, D.J. (2000). Disruption of two novel genes by a translocation co-segregating with schizophrenia. *Human molecular genetics* 9, 1415-1423.
- Miller, A.L., Lee, H.J., and Lumeng, J.C. (2015). Obesity-associated biomarkers and executive function in children. *Pediatric research* 77, 143-147.
- Miller, E.K. (2000). The prefrontal cortex and cognitive control. *Nat Rev Neurosci* 1, 59-65.
- Miller, E.K., and Cohen, J.D. (2001). An integrative theory of prefrontal cortex function. *Annual review of neuroscience* 24, 167-202.
- Miller, G.A. (1956). The magical number seven plus or minus two: some limits on our capacity for processing information. *Psychological review* 63, 81-97.
- Mintz Hemed, N., and Melosh, N.A. (2023). An integrated perspective for the diagnosis and therapy of neurodevelopmental disorders – From an engineering point of view. *Advanced Drug Delivery Reviews* 194, 114723.
- Mireku, M.O., Cot, M., Massougbodji, A., and Bodeau-Livinec, F. (2020). Relationship between Stunting, Wasting, Underweight and Geophagy and Cognitive Function of Children. *Journal of tropical pediatrics* 66, 517-527.
-

## References

---

- Miyamoto, A., Wake, H., Ishikawa, A.W., Eto, K., Shibata, K., Murakoshi, H., Koizumi, S., Moorhouse, A.J., Yoshimura, Y., and Nabekura, J. (2016). Microglia contact induces synapse formation in developing somatosensory cortex. *Nature Communications* 7, 12540.
- Miyaoka, T., Yasukawa, R., Yasuda, H., Hayashida, M., Inagaki, T., and Horiguchi, J. (2008). Minocycline as Adjunctive Therapy for Schizophrenia: An Open-Label Study. *Clinical Neuropharmacology* 31, 287-292.
- Moberg, P.J., Kamath, V., Marchetto, D.M., Calkins, M.E., Doty, R.L., Hahn, C.G., Borgmann-Winter, K.E., Kohler, C.G., Gur, R.E., and Turetsky, B.I. (2014). Meta-analysis of olfactory function in schizophrenia, first-degree family members, and youths at-risk for psychosis. *Schizophrenia bulletin* 40, 50-59.
- Modinos, G., Allen, P., Grace, A.A., and McGuire, P. (2015). Translating the MAM model of psychosis to humans. *Trends in neurosciences* 38, 129-138.
- Mölle, M., Yeshenko, O., Marshall, L., Sara, S.J., and Born, J. (2006). Hippocampal sharp wave-ripples linked to slow oscillations in rat slow-wave sleep. *J Neurophysiol* 96, 62-70.
- Monji, A., Kato, T.A., Mizoguchi, Y., Horikawa, H., Seki, Y., Kasai, M., Yamauchi, Y., Yamada, S., and Kanba, S. (2013). Neuroinflammation in schizophrenia especially focused on the role of microglia. *Progress in Neuro-Psychopharmacology and Biological Psychiatry* 42, 115-121.
- Morris-Rosendahl, D.J., and Crocq, M.A. (2020). Neurodevelopmental disorders-the history and future of a diagnostic concept. *Dialogues in clinical neuroscience* 22, 65-72.
- Morrow, B.E., McDonald-McGinn, D.M., Emanuel, B.S., Vermeesch, J.R., and Scambler, P.J. (2018). Molecular genetics of 22q11.2 deletion syndrome. *American journal of medical genetics Part A* 176, 2070-2081.
- Mosser, C.A., Baptista, S., Arnoux, I., and Audinat, E. (2017). Microglia in CNS development: Shaping the brain for the future. *Prog Neurobiol* 149-150, 1-20.
- Moutin, E., Nikonenko, I., Stefanelli, T., Wirth, A., Ponimaskin, E., De Roo, M., and Muller, D. (2017). Palmitoylation of cdc42 Promotes Spine Stabilization and Rescues Spine Density Deficit in a Mouse Model of 22q11.2 Deletion Syndrome. *Cereb Cortex* 27, 3618-3629.
- Mukherjee, A., Carvalho, F., Eliez, S., and Caroni, P. (2019). Long-Lasting Rescue of Network and Cognitive Dysfunction in a Genetic Schizophrenia Model. *Cell* 178, 1387-1402.e1314.
- Mukherjee, P., Roy, S., Ghosh, D., and Nandi, S.K. (2022). Role of animal models in biomedical research: a review. *Laboratory Animal Research* 38, 18.
- Murlanova, K., and Pletnikov, M.V. (2023). Modeling psychotic disorders: Environment x environment interaction. *Neuroscience & Biobehavioral Reviews* 152, 105310.
- Nadarajah, B., and Parnavelas, J.G. (2002). Modes of neuronal migration in the developing cerebral cortex. *Nature Reviews Neuroscience* 3, 423-432.
- Nakahara, S., Matsumoto, M., and van Erp, T.G.M. (2018). Hippocampal subregion abnormalities in schizophrenia: A systematic review of structural and physiological imaging studies. *Neuropsychopharmacology reports* 38, 156-166.
- Nave, K.-A., and Ehrenreich, H. (2014). Myelination and oligodendrocyte functions in psychiatric diseases. *JAMA psychiatry* 71, 582-584.
- Nithianantharajah, J., and Hannan, A.J. (2006). Enriched environments, experience-dependent plasticity and disorders of the nervous system. *Nature Reviews Neuroscience* 7, 697-709.
- Nolte, G., Bai, O., Wheaton, L., Mari, Z., Vorbach, S., and Hallett, M. (2004). Identifying true brain interaction from EEG data using the imaginary part of coherency. *Clinical neurophysiology : official journal of the International Federation of Clinical Neurophysiology* 115, 2292-2307.
- Nyaradi, A., Li, J., Hickling, S., Foster, J., and Oddy, W. (2013). The role of nutrition in children's neurocognitive development, from pregnancy through childhood. *Frontiers in Human Neuroscience* 7.
- O'Donnell, P. (2011). Adolescent onset of cortical disinhibition in schizophrenia: insights from animal models. *Schizophrenia bulletin* 37, 484-492.
- O'Neill, P.K., Gordon, J.A., and Sigurdsson, T. (2013). Theta oscillations in the medial prefrontal cortex are modulated by spatial working memory and synchronize with the hippocampus through its ventral subregion. *J Neurosci* 33, 14211-14224.
- Oberlander, V.C., Xu, X., Chini, M., and Hanganu-Opatz, I.L. (2019). Developmental dysfunction of prefrontal-hippocampal networks in mouse models of mental illness. *European Journal of Neuroscience* 50, 3072-3084.
-

## References

---

- Olsen, E.M., Nilsson, K.K., Wright, C.M., Michaelsen, K.F., and Skovgaard, A.M. (2023). Infancy weight faltering and childhood neurodevelopmental disorders: a general population birth-cohort study. *European child & adolescent psychiatry* 32, 1179-1188.
- Oni-Orisan, A., Kristiansen, L.V., Haroutunian, V., Meador-Woodruff, J.H., and McCullumsmith, R.E. (2008). Altered vesicular glutamate transporter expression in the anterior cingulate cortex in schizophrenia. *Biol Psychiatry* 63, 766-775.
- Onslow, A.C.E., Bogacz, R., and Jones, M.W. (2011). Quantifying phase–amplitude coupling in neuronal network oscillations. *Progress in Biophysics and Molecular Biology* 105, 49-57.
- Owen, M.J., O'Donovan, M.C., Thapar, A., and Craddock, N. (2011). Neurodevelopmental hypothesis of schizophrenia. *The British journal of psychiatry : the journal of mental science* 198, 173-175.
- Pagliardini, S., Gosgnach, S., and Dickson, C.T. (2013). Spontaneous sleep-like brain state alternations and breathing characteristics in urethane anesthetized mice. *PLoS One* 8, e70411.
- Panizzutti, B., Skvarc, D., Lin, S., Croce, S., Meehan, A., Bortolasci, C.C., Marx, W., Walker, A.J., Hasebe, K., Kavanagh, B.E., *et al.* (2023). Minocycline as Treatment for Psychiatric and Neurological Conditions: A Systematic Review and Meta-Analysis. *International journal of molecular sciences* 24.
- Pankevich, D.E., Teegarden, S.L., Hedin, A.D., Jensen, C.L., and Bale, T.L. (2010). Caloric restriction experience reprograms stress and orexigenic pathways and promotes binge eating. *J Neurosci* 30, 16399-16407.
- Panov, G., Dyulgerova, S., and Panova, P. (2023). Cognition in Patients with Schizophrenia: Interplay between Working Memory, Disorganized Symptoms, Dissociation, and the Onset and Duration of Psychosis, as Well as Resistance to Treatment. *Biomedicines* 11.
- Pendry, R.J., Quigley, L.D., Volk, L.J., and Pfeiffer, B.E. (2023). A Lightweight Drive Implant for Chronic Tetrode Recordings in Juvenile Mice. *Journal of visualized experiments : JoVE*.
- Phillips, N.L.H., and Roth, T.L. (2019). Animal Models and Their Contribution to Our Understanding of the Relationship Between Environments, Epigenetic Modifications, and Behavior. *Genes* 10.
- Pöpplau, J.A., Schwarze, T., Dorofeikova, M., Pochinok, I., Günther, A., Marquardt, A., and Hanganu-Opatz, I.L. (2023). Reorganization of adolescent prefrontal cortex circuitry is required for mouse cognitive maturation. *Neuron*.
- Preuss, T.M. (1995). Do rats have prefrontal cortex? The rose-woolsey-akert program reconsidered. *Journal of cognitive neuroscience* 7, 1-24.
- Preuss, T.M., and Wise, S.P. (2022). Evolution of prefrontal cortex. *Neuropsychopharmacology* 47, 3-19.
- Purdon, P.L., Sampson, A., Pavone, K.J., and Brown, E.N. (2015). Clinical Electroencephalography for Anesthesiologists: Part I: Background and Basic Signatures. *Anesthesiology* 123, 937-960.
- Rajasethupathy, P., Sankaran, S., Marshel, J.H., Kim, C.K., Ferenczi, E., Lee, S.Y., Berndt, A., Ramakrishnan, C., Jaffe, A., Lo, M., *et al.* (2015). Projections from neocortex mediate top-down control of memory retrieval. *Nature* 526, 653-659.
- Ramakrishna, J., Johnson, A.R., and Banner, B.F. (2009). Long-term minocycline use for acne in healthy adolescents can cause severe autoimmune hepatitis. *Journal of clinical gastroenterology* 43, 787-790.
- Rasetti, R., Sambataro, F., Chen, Q., Callicott, J.H., Mattay, V.S., and Weinberger, D.R. (2011). Altered cortical network dynamics: a potential intermediate phenotype for schizophrenia and association with ZNF804A. *Archives of general psychiatry* 68, 1207-1217.
- Reisinger, S., Khan, D., Kong, E., Berger, A., Pollak, A., and Pollak, D.D. (2015). The Poly(I:C)-induced maternal immune activation model in preclinical neuropsychiatric drug discovery. *Pharmacology & Therapeutics* 149, 213-226.
- Rensing, N., Moy, B., Friedman, J.L., Galindo, R., and Wong, M. (2018). Longitudinal analysis of developmental changes in electroencephalography patterns and sleep-wake states of the neonatal mouse. *PLOS ONE* 13, e0207031.
- Robinson, J., Manseau, F., Ducharme, G., Amilhon, B., Vigneault, E., El Mestikawy, S., and Williams, S. (2016). Optogenetic Activation of Septal Glutamatergic Neurons Drive Hippocampal Theta Rhythms. *J Neurosci* 36, 3016-3023.
- Rodriguez, J., and Paule, M. (2009). Working Memory Delayed Response Tasks in Monkeys. In *Methods of Behavior Analysis in Neuroscience* 2nd edition, B. JJ, ed. (Boca Raton (FL): CRC Press/Taylor & Francis).
-

## References

---

- Rose, J.E., and Woolsey, C.N. (1948). The orbitofrontal cortex and its connections with the mediodorsal nucleus in rabbit, sheep and cat. *Research publications - Association for Research in Nervous and Mental Disease* 27 (1 vol.), 210-232.
- Rossant, C., Kadir, S.N., Goodman, D.F.M., Schulman, J., Hunter, M.L.D., Saleem, A.B., Grosmark, A., Belluscio, M., Denfield, G.H., Ecker, A.S., *et al.* (2016). Spike sorting for large, dense electrode arrays. *Nature Neuroscience* 19, 634-641.
- Rubino, T., and Parolaro, D. (2014). Cannabis abuse in adolescence and the risk of psychosis: a brief review of the preclinical evidence. *Progress in neuro-psychopharmacology & biological psychiatry* 52, 41-44.
- Rubino, T., Prini, P., Piscitelli, F., Zamberletti, E., Trusel, M., Melis, M., Sagheddu, C., Ligresti, A., Tonini, R., Di Marzo, V., and Parolaro, D. (2015). Adolescent exposure to THC in female rats disrupts developmental changes in the prefrontal cortex. *Neurobiology of disease* 73, 60-69.
- Sachs, N.A., Sawa, A., Holmes, S.E., Ross, C.A., DeLisi, L.E., and Margolis, R.L. (2005). A frameshift mutation in Disrupted in Schizophrenia 1 in an American family with schizophrenia and schizoaffective disorder. *Mol Psychiatry* 10, 758-764.
- Saito, R., Koebis, M., Nagai, T., Shimizu, K., Liao, J., Wulaer, B., Sugaya, Y., Nagahama, K., Uesaka, N., Kushima, I., *et al.* (2020). Comprehensive analysis of a novel mouse model of the 22q11.2 deletion syndrome: a model with the most common 3.0-Mb deletion at the human 22q11.2 locus. *Transl Psychiatry* 10, 35.
- Saito, R., Miyoshi, C., Koebis, M., Kushima, I., Nakao, K., Mori, D., Ozaki, N., Funato, H., Yanagisawa, M., and Aiba, A. (2021). Two novel mouse models mimicking minor deletions in 22q11.2 deletion syndrome revealed the contribution of each deleted region to psychiatric disorders. *Molecular Brain* 14, 68.
- Sakurai, T., and Gamo, N.J. (2019). Cognitive functions associated with developing prefrontal cortex during adolescence and developmental neuropsychiatric disorders. *Neurobiology of disease* 131, 104322.
- Scattolin, M.A.d.A., Resegue, R.M., and Rosário, M.C.d. (2022). The impact of the environment on neurodevelopmental disorders in early childhood. *Jornal de Pediatria* 98, S66-S72.
- Schwarz, C., Hentschke, H., Butovas, S., Haiss, F., Stüttgen, M.C., Gerdjikov, T.V., Bergner, C.G., and Waiblinger, C. (2010). The head-fixed behaving rat--procedures and pitfalls. *Somatosensory & motor research* 27, 131-148.
- Searle, S.R., Speed, F.M., and Milliken, G.A. (1980). Population Marginal Means in the Linear Model: An Alternative to Least Squares Means. *The American Statistician* 34, 216-221.
- Selemon, L.D., and Zecevic, N. (2015). Schizophrenia: a tale of two critical periods for prefrontal cortical development. *Transl Psychiatry* 5, e623.
- Sellgren, C.M., Gracias, J., Watmuff, B., Biag, J.D., Thanos, J.M., Whittredge, P.B., Fu, T., Worringer, K., Brown, H.E., Wang, J., *et al.* (2019). Increased synapse elimination by microglia in schizophrenia patient-derived models of synaptic pruning. *Nature Neuroscience* 22, 374-385.
- Shah, A.A., Sjovold, T., and Treit, D. (2004). Inactivation of the medial prefrontal cortex with the GABAA receptor agonist muscimol increases open-arm activity in the elevated plus-maze and attenuates shock-probe burying in rats. *Brain Res* 1028, 112-115.
- Shajarisales, N., Janzing, D., Schölkopf, B., and Besserve, M. (2015). Telling cause from effect in deterministic linear dynamical systems. In *International Conference on Machine Learning (PMLR)*, pp. 285-294.
- Shin, J., and Talnov, A. (2001). A single trial analysis of hippocampal theta frequency during nonsteady wheel running in rats. *Brain Research* 897, 217-221.
- Shoval, G., Bar-Shira, O., Zalsman, G., John Mann, J., and Chechik, G. (2014). Transitions in the transcriptome of the serotonergic and dopaminergic systems in the human brain during adolescence. *European neuropsychopharmacology : the journal of the European College of Neuropsychopharmacology* 24, 1123-1132.
- Siapas, A.G., Lubenov, E.V., and Wilson, M.A. (2005). Prefrontal Phase Locking to Hippocampal Theta Oscillations. *Neuron* 46, 141-151.
- Siapas, A.G., and Wilson, M.A. (1998). Coordinated interactions between hippocampal ripples and cortical spindles during slow-wave sleep. *Neuron* 21, 1123-1128.
- Sigurdsson, T., and Duvarci, S. (2016). Hippocampal-Prefrontal Interactions in Cognition, Behavior and Psychiatric Disease. *Frontiers in Systems Neuroscience* 9.
-

## References

---

- Sigurdsson, T., Stark, K.L., Karayiorgou, M., Gogos, J.A., and Gordon, J.A. (2010). Impaired hippocampal-prefrontal synchrony in a genetic mouse model of schizophrenia. *Nature* 464, 763-767.
- Sirota, A., Montgomery, S., Fujisawa, S., Isomura, Y., Zugaro, M., and Buzsáki, G. (2008). Entrainment of neocortical neurons and gamma oscillations by the hippocampal theta rhythm. *Neuron* 60, 683-697.
- Sisk, C.L., and Foster, D.L. (2004). The neural basis of puberty and adolescence. *Nat Neurosci* 7, 1040-1047.
- Ślawińska, U., and Kasicki, S. (1998). The frequency of rat's hippocampal theta rhythm is related to the speed of locomotion. *Brain Research* 796, 327-331.
- Small, S.A., Schobel, S.A., Buxton, R.B., Witter, M.P., and Barnes, C.A. (2011). A pathophysiological framework of hippocampal dysfunction in ageing and disease. *Nature Reviews Neuroscience* 12, 585-601.
- Soares, D.C., Carlyle, B.C., Bradshaw, N.J., and Porteous, D.J. (2011). DISC1: Structure, Function, and Therapeutic Potential for Major Mental Illness. *ACS chemical neuroscience* 2, 609-632.
- Sokolova, E., Oerlemans, A.M., Rommelse, N.N., Groot, P., Hartman, C.A., Glennon, J.C., Claassen, T., Heskens, T., and Buitelaar, J.K. (2017). A Causal and Mediation Analysis of the Comorbidity Between Attention Deficit Hyperactivity Disorder (ADHD) and Autism Spectrum Disorder (ASD). *Journal of autism and developmental disorders* 47, 1595-1604.
- Spear, L.P. (2000). The adolescent brain and age-related behavioral manifestations. *Neurosci Biobehav Rev* 24, 417-463.
- Spencer-Smith, M., and Anderson, V. (2009). Healthy and abnormal development of the prefrontal cortex. *Developmental neurorehabilitation* 12, 279-297.
- Spratt, P.W.E., Ben-Shalom, R., Keeshen, C.M., Burke, K.J., Jr., Clarkson, R.L., Sanders, S.J., and Bender, K.J. (2019). The Autism-Associated Gene *Scn2a* Contributes to Dendritic Excitability and Synaptic Function in the Prefrontal Cortex. *Neuron* 103, 673-685.e675.
- Stark, K.L., Xu, B., Bagchi, A., Lai, W.-S., Liu, H., Hsu, R., Wan, X., Pavlidis, P., Mills, A.A., Karayiorgou, M., and Gogos, J.A. (2008). Altered brain microRNA biogenesis contributes to phenotypic deficits in a 22q11.2-deletion mouse model. *Nature Genetics* 40, 751-760.
- Stephenson, G., and Craig, J.M. (2022). Chapter 35 - Environmental risk factors for neurodevelopmental disorders: Evidence from twin studies. In *Twin Research for Everyone*, A. Tarnoki, D. Tarnoki, J. Harris, and N. Segal, eds. (Academic Press), pp. 625-648.
- Stiles, J., and Jernigan, T.L. (2010). The basics of brain development. *Neuropsychology review* 20, 327-348.
- Subramanian, U. (2022). Validation of Animal Models. In *Introduction to Basics of Pharmacology and Toxicology: Volume 3 : Experimental Pharmacology : Research Methodology and Biostatistics*, M. Lakshmanan, D.G. Shewade, and G.M. Raj, eds. (Singapore: Springer Nature Singapore), pp. 157-170.
- Sumitomo, A., Horike, K., Hirai, K., Butcher, N., Boot, E., Sakurai, T., Nucifora, F.C., Jr., Bassett, A.S., Sawa, A., and Tomoda, T. (2018). A mouse model of 22q11.2 deletions: Molecular and behavioral signatures of Parkinson's disease and schizophrenia. *Sci Adv* 4, eaar6637.
- Sun, C., Cao, Y., Huang, J., Huang, K., Lu, Y., and Zhong, C. (2022). Low-cost and easy-fabrication lightweight drivable electrode array for multiple-regions electrophysiological recording in free-moving mice. *Journal of neural engineering* 19.
- Supèr, H., and Soriano, E. (1994). The organization of the embryonic and early postnatal murine hippocampus. II. Development of entorhinal, commissural, and septal connections studied with the lipophilic tracer DiI. *The Journal of comparative neurology* 344, 101-120.
- Tan, H.M., Bassett, J.P., O'Keefe, J., Cacucci, F., and Wills, T.J. (2015). The development of the head direction system before eye opening in the rat. *Curr Biol* 25, 479-483.
- Tandon, R., Nasrallah, H.A., and Keshavan, M.S. (2009). Schizophrenia, "just the facts" 4. Clinical features and conceptualization. *Schizophrenia research* 110, 1-23.
- Thiebaut de Schotten, M., and Forkel, S.J. (2022). The emergent properties of the connected brain. *Science* 378, 505-510.
- Tierney, P.L., Dégenétais, E., Thierry, A.-M., Glowinski, J., and Gioanni, Y. (2004). Influence of the hippocampus on interneurons of the rat prefrontal cortex. *European Journal of Neuroscience* 20, 514-524.
- Tolner, E.A., Sheikh, A., Yukin, A.Y., Kaila, K., and Kanold, P.O. (2012). Subplate neurons promote spindle bursts and thalamocortical patterning in the neonatal rat somatosensory cortex. *J Neurosci* 32, 692-702.
-

## References

---

- Tomoda, T., Sumitomo, A., Jaaro-Peled, H., and Sawa, A. (2016). Utility and validity of DISC1 mouse models in biological psychiatry. *Neuroscience* 321, 99-107.
- Tripathi, A., Spedding, M., Schenker, E., Didriksen, M., Cressant, A., and Jay, T.M. (2020). Cognition- and circuit-based dysfunction in a mouse model of 22q11.2 microdeletion syndrome: effects of stress. *Transl Psychiatry* 10, 41.
- Turetsky, B.I., Moberg, P.J., Quarmley, M., Dress, E., Calkins, M.E., Ruparel, K., Prabhakaran, K., Gur, R.E., and Roalf, D.R. (2018). Structural anomalies of the peripheral olfactory system in psychosis high-risk subjects. *Schizophrenia research* 195, 197-205.
- Tye, K.M., Prakash, R., Kim, S.Y., Fenno, L.E., Grosenick, L., Zarabi, H., Thompson, K.R., Gradinaru, V., Ramakrishnan, C., and Deisseroth, K. (2011). Amygdala circuitry mediating reversible and bidirectional control of anxiety. *Nature* 471, 358-362.
- Uhlhaas, P.J., and Singer, W. (2015). Oscillations and neuronal dynamics in schizophrenia: The search for basic symptoms and translational opportunities. *Biological Psychiatry* 77, 1001-1009.
- Uylings, H.B., Groenewegen, H.J., and Kolb, B. (2003). Do rats have a prefrontal cortex? *Behavioural brain research* 146, 3-17.
- Valeeva, G., Janackova, S., Nasretdinov, A., Rychkova, V., Makarov, R., Holmes, G.L., Khazipov, R., and Lenck-Santini, P.-P. (2018). Emergence of Coordinated Activity in the Developing Entorhinal–Hippocampal Network. *Cerebral Cortex* 29, 906-920.
- Van De Werd, H.J., Rajkowska, G., Evers, P., and Uylings, H.B. (2010). Cytoarchitectonic and chemoarchitectonic characterization of the prefrontal cortical areas in the mouse. *Brain Struct Funct* 214, 339-353.
- van Strien, N.M., Cappaert, N.L.M., and Witter, M.P. (2009). The anatomy of memory: an interactive overview of the parahippocampal–hippocampal network. *Nature Reviews Neuroscience* 10, 272-282.
- Vanhatalo, S., and Kaila, K. (2006). Development of neonatal EEG activity: From phenomenology to physiology. *Seminars in Fetal and Neonatal Medicine* 11, 471-478.
- Vanhatalo, S., Palva, J.M., Andersson, S., Rivera, C., Voipio, J., and Kaila, K. (2005). Slow endogenous activity transients and developmental expression of K<sup>+</sup>–Cl<sup>–</sup> cotransporter 2 in the immature human cortex. *European Journal of Neuroscience* 22, 2799-2804.
- Vinck, M., van Wingerden, M., Womelsdorf, T., Fries, P., and Pennartz, C.M. (2010). The pairwise phase consistency: a bias-free measure of rhythmic neuronal synchronization. *Neuroimage* 51, 112-122.
- Vingerhoets, C., Tse, D.H., van Oudenaren, M., Hernaes, D., van Duin, E., Zinkstok, J., Ramaekers, J.G., Jansen, J.F., McAlonan, G., and van Amelsvoort, T. (2020). Glutamatergic and GABAergic reactivity and cognition in 22q11.2 deletion syndrome and healthy volunteers: A randomized double-blind 7-Tesla pharmacological MRS study. *Journal of psychopharmacology (Oxford, England)* 34, 856-863.
- Voigts, J., Newman, J.P., Wilson, M.A., and Harnett, M.T. (2020). An easy-to-assemble, robust, and lightweight drive implant for chronic tetrode recordings in freely moving animals. *Journal of neural engineering* 17, 026044.
- Vorstman, J.A., Breetvelt, E.J., Duijff, S.N., Eliez, S., Schneider, M., Jalbrzikowski, M., Armando, M., Vicari, S., Shashi, V., Hooper, S.R., *et al.* (2015). Cognitive decline preceding the onset of psychosis in patients with 22q11.2 deletion syndrome. *JAMA Psychiatry* 72, 377-385.
- Walshe, T.M. (2016). 43On the Sacred Disease: Hippocrates. In *Neurological Concepts in Ancient Greek Medicine*, T.M. Walshe, ed. (Oxford University Press), p. 0.
- Wang, H.C., Lin, C.C., Chong, R., Zhang-Hooks, Y., Agarwal, A., Ellis-Davies, G., Rock, J., and Bergles, D.E. (2015). Spontaneous Activity of Cochlear Hair Cells Triggered by Fluid Secretion Mechanism in Adjacent Support Cells. *Cell* 163, 1348-1359.
- Warburton, E.C., and Brown, M.W. (2015). Neural circuitry for rat recognition memory. *Behavioural brain research* 285, 131-139.
- Weinberger, D.R. (1987). Implications of normal brain development for the pathogenesis of schizophrenia. *Archives of general psychiatry* 44, 660-669.
- Weinberger, D.R., Elvevåg, B., Giedd, J., and National Campaign to Prevent Teen, P. (2005). *The adolescent brain : a work in progress* (Washington, DC.: National Campaign to Prevent Teen Pregnancy Washington, DC.).
- Wentz, E., Björk, A., and Dahlgren, J. (2017). Neurodevelopmental disorders are highly over-represented in children with obesity: A cross-sectional study. *Obesity (Silver Spring, Md)* 25, 178-184.
-

## References

---

- Whishaw, I.Q., and Vanderwolf, C.H. (1973). Hippocampal EEG and behavior: Change in amplitude and frequency of RSA (Theta rhythm) associated with spontaneous and learned movement patterns in rats and cats. *Behavioral Biology* 8, 461-484.
- Wierzynski, C.M., Lubenov, E.V., Gu, M., and Siapas, A.G. (2009). State-dependent spike-timing relationships between hippocampal and prefrontal circuits during sleep. *Neuron* 61, 587-596.
- Williams, S., and Boksa, P. (2010). Gamma oscillations and schizophrenia. *Journal of psychiatry & neuroscience : JPN* 35, 75-77.
- Willner, P. (1984). The validity of animal models of depression. *Psychopharmacology (Berl)* 83, 1-16.
- Wills, T.J., Barry, C., and Cacucci, F. (2012). The abrupt development of adult-like grid cell firing in the medial entorhinal cortex. *Front Neural Circuits* 6, 21.
- Wirt, R., and Hyman, J. (2017). Integrating Spatial Working Memory and Remote Memory: Interactions between the Medial Prefrontal Cortex and Hippocampus. *Brain sciences* 7.
- Witter, M.P., Wouterlood, F.G., Naber, P.A., and Van Haefen, T. (2000). Anatomical organization of the parahippocampal-hippocampal network. *Ann N Y Acad Sci* 911, 1-24.
- Wolff, A.R., Cheyne, K.R., and Bilkey, D.K. (2011). Behavioural deficits associated with maternal immune activation in the rat model of schizophrenia. *Behavioural brain research* 225, 382-387.
- Workman, A.D., Charvet, C.J., Clancy, B., Darlington, R.B., and Finlay, B.L. (2013). Modeling Transformations of Neurodevelopmental Sequences across Mammalian Species. *The Journal of Neuroscience* 33, 7368-7383.
- WorldHealthOrganisation (2024). Adolescent health.
- Xu, W., and Südhof, T.C. (2013). A neural circuit for memory specificity and generalization. *Science* 339, 1290-1295.
- Xu, X., Chini, M., Bitzenhofer, S.H., and Hanganu-Opatz, I.L. (2019). Transient Knock-Down of Prefrontal DISC1 in Immune-Challenged Mice Causes Abnormal Long-Range Coupling and Cognitive Dysfunction throughout Development. *J Neurosci* 39, 1222-1235.
- Xu, X., Song, L., and Hanganu-Opatz, I.L. (2021a). Knock-Down of Hippocampal DISC1 in Immune-Challenged Mice Impairs the Prefrontal-Hippocampal Coupling and the Cognitive Performance Throughout Development. *Cereb Cortex* 31, 1240-1258.
- Xu, X., Song, L., Kringel, R., and Hanganu-Opatz, I.L. (2021b). Developmental decrease of entorhinal-hippocampal communication in immune-challenged DISC1 knockdown mice. *Nat Commun* 12, 6810.
- Zhang, L., Zheng, H., Wu, R., Zhu, F., Kosten, T.R., Zhang, X.-Y., and Zhao, J. (2018). Minocycline adjunctive treatment to risperidone for negative symptoms in schizophrenia: Association with pro-inflammatory cytokine levels. *Progress in Neuro-Psychopharmacology and Biological Psychiatry* 85, 69-76.
- Zhao, S., Umpierre, A.D., and Wu, L.-J. (2024). Tuning neural circuits and behaviors by microglia in the adult brain. *Trends in Neurosciences*.
- Zhao, X., and Bhattacharyya, A. (2018). Human Models Are Needed for Studying Human Neurodevelopmental Disorders. *The American Journal of Human Genetics* 103, 829-857.

---

## List of Figures

|            |  |    |
|------------|--|----|
| Figure 1:  | Surgical procedure of headplate implantation for head fixation during recordings.  | 22 |
| Figure 2:  | Training and recording procedure on the MobileHomeCage setup.  | 23 |
| Figure 3:  | Representation of microglia engulfment analysis.   | 32 |
| Figure 4:  | Examples of 3D reconstructed microglial cells with inclusions of VGLUT puncta in the three conditions.   | 32 |
| Figure 5:  | Phagocytic activity of microglial cells in GE mice, GE mice treated with minocycline and control mice.   | 33 |
| Figure 6:  | Object Recognition Paradigms.  | 34 |
| Figure 7:  | Interaction with the objects in the NOR.   | 34 |
| Figure 8:  | NOR in WT and GE mice treated with minocycline during P9 to P16.   | 34 |
| Figure 9:  | Interaction with the objects in the RR.  | 35 |
| Figure 10: | RR in WT and GE minocycline treated mice during P9 to P16.   | 36 |
| Figure 11: | Prefrontal LFP activity in juvenile GE and WT mice.  | 37 |
| Figure 12: | Multi-unit firing activity in juvenile WT and GE mice.   | 38 |
| Figure 13: | Synchrony in LFPs between the PL, CA1 and LEC.   | 39 |
| Figure 14: | Synchrony in firing and LFP across areas.  | 39 |
| Figure 15: | Recording procedure.   | 40 |
| Figure 16: | Schematic representation of DNMS task.   | 41 |
| Figure 17: | T-Maze modifications and alignment with recording.   | 42 |
| Figure 18: | First round of experiments to establish the T-Maze task.   | 43 |
| Figure 19: | Second approach to establish the T-Maze task in head-fixed conditions with experimental group 1.   | 44 |
| Figure 20: | Third approach to establish the T-Maze task in head-fixed conditions with experimental group 2.  | 44 |
| Figure 21: | Fourth approach to establish the T-Maze task in head-fixed conditions with experimental group 3.   | 45 |
| Figure 22: | Fifth approach to establish the T-Maze task in head-fixed conditions with experimental group 4.  | 45 |
| Figure 23: | Experimental timeline and increase in body size and weight across the adolescent period.   | 47 |
| Figure 24: | Movement patterns on the MobileHomeCage in the first 5 min of the recording throughout late development in <i>Df(16)A<sup>+/-</sup></i> and WT mice. | 48 |
| Figure 25: | Movement patterns on the MobileHomeCage in 30 min of the recording throughout late development in <i>Df(16)A<sup>+/-</sup></i> and WT mice.          | 49 |
| Figure 26: | Prefrontal LFP properties throughout late development in <i>Df(16)A<sup>+/-</sup></i> and WT mice.   | 50 |
| Figure 27: | Excitation/inhibition ratio illustrated by 1/f slope in the PFC of <i>Df(16)A<sup>+/-</sup></i> and WT mice across late development.                 | 51 |

---

## List of Tables

---

|   |    |
|---|----|
| Figure 28: Cross-frequency coupling between prefrontal theta phase and prefrontal gamma amplitude throughout late development in <i>Df(16)A<sup>+/-</sup></i> and WT mice.....          | 52 |
| Figure 29: Separation of single units into fast spiking, putative PV-interneurons and regular spiking, putative pyramidal neurons. ....   | 53 |
| Figure 30: Firing patterns of Rs units in the PFC of <i>Df(16)A<sup>+/-</sup></i> and WT mice across late development. ....   | 54 |
| Figure 31: Firing patterns of Fs units in the PFC of <i>Df(16)A<sup>+/-</sup></i> and WT mice across late development. ....   | 55 |
| Figure 32: Synchrony of prefrontal firing with prefrontal broad-band gamma rhythm throughout late development in <i>Df(16)A<sup>+/-</sup></i> and WT mice.....                          | 56 |
| Figure 33: Firing synchrony between single units in the PFC throughout late development in <i>Df(16)A<sup>+/-</sup></i> and WT mice.....  | 57 |
| Figure 34: Hippocampal LFP properties throughout late development in <i>Df(16)A<sup>+/-</sup></i> and WT mice. ....   | 59 |
| Figure 35: Hippocampal firing properties throughout late development in <i>Df(16)A<sup>+/-</sup></i> and WT mice. ....  | 60 |
| Figure 36: Synchrony between firing and LFP and spike-spike synchrony in the HP throughout late development in <i>Df(16)A<sup>+/-</sup></i> and WT mice. ....                           | 61 |
| Figure 37: Frequency-resolved synchrony of LFPs between the PFC and HP throughout late development in <i>Df(16)A<sup>+/-</sup></i> and WT mice. ....                                    | 62 |
| Figure 38: Directed synchrony of LFPs between the PFC and HP throughout late development in <i>Df(16)A<sup>+/-</sup></i> and WT mice.....   | 63 |
| Figure 39: Cross-frequency coupling between the hippocampal theta phase and the prefrontal gamma amplitude throughout late development in <i>Df(16)A<sup>+/-</sup></i> and WT mice..... | 64 |
| Figure 40: Number of significantly locked prefrontal units to hippocampal theta rhythm throughout late development in <i>Df(16)A<sup>+/-</sup></i> and WT mice.....                     | 65 |
| Figure 41: Synchrony of prefrontal firing with hippocampal theta rhythm throughout late development in <i>Df(16)A<sup>+/-</sup></i> and WT mice.....                                    | 65 |
| Figure 42: Firing synchrony between prefrontal and hippocampal units throughout late development in <i>Df(16)A<sup>+/-</sup></i> and WT mice.....                                       | 66 |
| Figure 43: Graphical summary of the perturbed developmental trajectories in the <i>Df(16)A<sup>+/-</sup></i> mouse model of 22q11.2ds.....  | 81 |

## List of Tables

|   |     |
|---|-----|
| Table 1: List of materials, equipment and software used in the experiments..... | 113 |
| Table 2: Detailed statistics for Figures 23-42.....                             | 115 |

# Appendix

## List of materials, equipment and software

**Table 1:** List of materials, equipment and software used in the experiments.

| <b>Experiment models: organisms / strains</b>   |  |
|---|--|
| Mouse: C57BL/6J (control, WT)   | Animal facility, Universitätsklinikum Hamburg-Eppendorf  |
| Mouse: <i>Disc1</i> (B6.129S6-Disc1tm1Kara, MGI: 3623218)   | J. Gogos, Zuckerman Institute, Columbia, NY, USA         |
| Mouse: <i>Df(16)A<sup>+/-</sup></i> (Del(16Dgcr2-Hira)3Aam) (MGI:3798957)                               | J. Gogos, Zuckerman Institute, Columbia, NY, USA         |
| <b>Primers</b>  |  |
| <i>Disc1</i><br>5'-TAGCCACTCTCATTGTCAGC-3'<br>5'-CCTCATCCCTTCCACTCAGC-3'                                | metabion international AG, Planegg/Steinkirchen, Germany |
| <i>Df(16)A<sup>+/-</sup></i><br>5'-ATTCCCCATGGACTAATTATGGACAGG-3'<br>5'-GGTATCTCCATAAGACAGAATGCTATGC-3' | metabion international AG, Planegg/Steinkirchen, Germany |
| <b>Software</b>   |  |
| Adobe Acrobat Reader DC   | Adobe, San Jose, CA, USA                                 |
| Adobe Illustrator CS6   | Adobe, San Jose, CA, USA                                 |
| Anaconda 1.9.6  | Anaconda Inc, Austin, TX, USA                            |
| Cheetah   | Digital Lynx SX; Neuralynx, Bozeman, MO, USA             |
| Endnote X8  | Clarivate, Jersey, UK                                    |
| ImageJ 1.52c  | Wayne Rasband National Institute of Health, USA          |
| klusta  | Cortex lab, University College London, London, UK        |
| MATLAB2017b   | Mathworks, Portola Valley, MA, USA                       |
| Microsoft Office 2016   | Microsoft Corporation, Redmond, WA, USA                  |
| MobileHomeCage® Locomotion tracking software v.2.2.1  | Neurotar, Helsinki, Finland                              |
| phy   | Cortex lab, University College London, London, UK        |
| R Statistical Software  | R Project for Statistical Computing, Salzburg, Austria   |
| uEye cockpit  | iDS Imaging, Aachen, Germany                             |
| Video Mot2 software   | TSE Systems GmbH, Berlin, Germany                        |
| <b>Laboratory and technical equipment</b>   |  |
| Amplifier   | Digital Lynx SX; Neuralynx, Bozeman, MO, USA             |
| Binocular microscope Olympus SZ51   | Olympus, Hamburg, Germany                                |
| Carbon T-Maze for MobileHomeCage®   | Neurotar, Helsinki, Finland                              |
| CCD camera  | VIDEOR TECHNICAL E. Hartig GmbH, Rödermark, Germany      |
| Confocal microscope Olympus FX-100  | Olympus, Hamburg, Germany                                |
| Harvard Apparatus Anesthetic Vaporizers   | Harvard Apparatus, Holliston, MA, USA                    |
| Head-stage  | Neuralynx, Bozeman, MO, USA                              |
| Hot Bead Sterilizer   | Fine Science Tools, Heidelberg, Germany                  |
| IKA®MS 3 basic shakers  | Sigma-Aldrich, St Louis, MO, USA                         |
| MobileHomeCage®   | Neurotar, Helsinki, Finland                              |
| Motorized arm Scientifica IVM Triple  | Scientifica, Uckfield, UK                                |

## Appendix

|  |  |
|--|--|
| Objective/lens LMZ45T3   | Kowa Optimed Deutschland, Düsseldorf, Germany            |
| Olympus KL 1500 microscopic lamp                                     | Olympus, Hamburg, Germany                                |
| Pipettes   | Gilson, Middleton, WI, USA                               |
| Stereotactic frames  | World Precision Instruments, Friedberg, Germany          |
| uEye+ camera U3-31F0CP Rev.2.2                                       | iDS Imaging Development Systems GmbH, Obersulm, Germany  |
| Vibratom VT1000S   | Leica, Wetzlar, Germany                                  |
| <b>Chemicals and consumables</b>                                     |  |
| Alexa Fluor-488 goat anti-guinea pig                                 | Molecular Probes, Eugene, OR, USA                        |
| Alexa Fluor-568 donkey anti-rabbit                                   | Life Technologies, Carlsbad, CA, USA                     |
| Betaisodona (PovidonIod)   | MundiPharma, Frankfurt a.M., Germany                     |
| Bovine serum albumine  | Jackson Immuno Research, West Grove, PA, USA             |
| Bupivacaine/Lidocaine (self-produced)                                | Apotheke am UKE, Hamburg, Germany                        |
| Cannulas   | B. Braun Melsungen AG, Melsungen, Germany                |
| Condensed milk   | Bärenmarke, Vertriebsgesellschaft mbH, Thalfang, Germany |
| Corn oil   | Mazola, Elmshorn, Germany                                |
| 1,1'-Dioctadecyl-3,3',3'-<br>Tetramethylindocarbocyanine Perchlorate | Invitrogen, Life Technologies GmbH, Darmstadt, Germany   |
| Eye ointment Bepanthen   | Bayer, Leverkusen, Germany                               |
| Fluoromount-G  | BIOZOL Diagnostica Vertrieb GmbH, Eching, Germany        |
| Histofix   | Carl Roth, Karlsruhe, Germany                            |
| Isoflurane (Sedoconda)   | SedanaMedical AB, Danderyd, Sweden                       |
| Ketamine   | aniMedica, Senden, Germany                               |
| Kwik-Cast sealant  | World Precision Instruments, Friedberg, Germany          |
| Kwik-Sil sealant   | World Precision Instruments, Friedberg, Germany          |
| lick-port  | Neurotar, Helsinki, Finland                              |
| Stainless steel headplate model 9                                    | Neurotar, Helsinki, Finland                              |
| Metacam (Meloxicam)  | Boehringer-Ingelheim, Ingelheim, Germany                 |
| Minocycline  | Sigma-Aldrich, St Louis, MO, USA                         |
| Paladur (acrylic resin for prosthesis)                               | Henry Schein Dental Deutschland GmbH, Langen, Germany    |
| Physiological NaCl solution  | B. Braun Melsungen AG, Melsungen, Germany                |
| Pipette tips   | Sarstedt, Nümbrecht, Germany                             |
| Polyclonal guinea-pig antibody against<br>VGLUT1                     | Synaptic Systems, Göttingen, Germany                     |
| polyinosinic:polycytidylic acid sodium salt $\gamma$ -<br>irradiated | Sigma-Aldrich, St Louis, MO, USA                         |
| Rabbit monoclonal primary antibody against<br>IBA-1                  | Wako, Neuss, Germany                                     |
| Recording electrode (1 shank, 16 channels),<br>A1x16-5mm-100-703 LP  | NeuroNexus, Ann Arbor, MI, USA                           |
| Recording electrode (1 shank, 16 channels),<br>A1x16-5mm-50-703 LP   | NeuroNexus, Ann Arbor, MI, USA                           |
| ROTI®Mount FluorCare DAPI  | Carl Roth GmbH + Co. KG, Karlsruhe, Germany              |
| Super-Bond C & B (dental cement)                                     | Hentschel-Dental, Teningen, Germany                      |
| Superglue  | UHU, Bühl, Deutschland                                   |
| Sweetened condensed milk   | DOVGAN GmbH, Hamburg, Germany                            |
| Syringe (1ml, 5ml, 50ml)   | B. Braun Melsungen AG, Melsungen, Germany                |
| TritonX-100  | Sigma-Aldrich, St Louis, MO, USA                         |
| Urethane   | Sigma-Aldrich, St Louis, MO, USA                         |
| VECTASHIELD®   | Vector Laboratories, Newark, CA, USA                     |
| Xylazine   | WDT eG, Garbsen, Germany                                 |

## Detailed statistics for Results 3.4

Table 2: Detailed statistics for Figures 23-42

| Figure      | Test                      | n  | Factors                | Groups                                     | df      | [lower.CL upper.CL] | p-value |
|-------------|---------------------------|--|------------------------|--|---------|---------------------|---------|
| 23C         | Linear mixed-effect model | $n_{(WT)} = 82$ recordings, 23 mice<br>$n_{(Df(16)A+/+)} = 52$ recordings, 14 mice   | age                    |  | 70.32   |                     |         |
|             |                           |  | condition              |  | 104.55  |                     |         |
|             |                           |  | age-condition (slopes) | WT P20-60                                  | 81.60   | [0.205 0.295]       | 0.0702  |
|             |                           |  |                        | Df(16)A+/- P20-60                          | 107.10  | [0.155 0.257]       |         |
| 24B (left)  | Linear mixed-effect model | $n_{(WT)} = 82$ recordings, 23 mice<br>$n_{(Df(16)A+/+)} = 52$ recordings, 14 mice   | age                    |  | 89.60   |                     | 0.780   |
|             |                           |  | condition              |  | 111.40  |                     | 0.015   |
|             |                           |  | age-condition (slopes) | WT P20-60                                  | 89.20   | [-0.00494 0.00373]  | 0.007   |
|             |                           |  |                        | Df(16)A+/- P20-60                          | 120.20  | [-0.01130 -0.00219] |         |
| 24B (right) | Linear mixed-effect model | $n_{(WT, \text{early ado})} = 49$ recordings, 18 mice<br>$n_{(WT, \text{late ado})} = 33$ recordings, 14 mice<br>$n_{(Df(16)A+/, \text{early ado})} = 27$ recordings, 12 mice<br>$n_{(Df(16)A+/, \text{late ado})} = 25$ recordings, 10 mice | age                    | WT early ado / WT late ado                 | 72.80   |                     | 0.226   |
|             |                           |  | condition              | Df(16)A+/- early ado / Df(16)A+/- late ado | 85.10   |                     | 0.005   |
|             |                           |  |                        | Df(16)A+/- early ado / WT early ado        | 42.90   |                     | 0.236   |
|             |                           |  |                        | Df(16)A+/- late ado / WT late ado          | 50.30   |                     | 0.186   |
| 24C (left)  | Linear mixed-effect model | $n_{(WT)} = 82$ recordings, 23 mice<br>$n_{(Df(16)A+/+)} = 52$ recordings, 14 mice   | age                    |  | 128.00  |                     | 0.665   |
|             |                           |  | condition              |  | 128.00  |                     | 0.007   |
|             |                           |  | age-condition (slopes) | WT P20-60                                  | 108.00  | [-0.00130 2.02e-03] | 0.046   |
|             |                           |  |                        | Df(16)A+/- P20-60                          | 104.00  | [-0.00375 5.47e-05] |         |
| 24C (right) | Linear mixed-effect model | $n_{(WT, \text{early ado})} = 49$ recordings, 18 mice<br>$n_{(WT, \text{late ado})} = 33$ recordings, 14 mice<br>$n_{(Df(16)A+/, \text{early ado})} = 27$ recordings, 12 mice<br>$n_{(Df(16)A+/, \text{late ado})} = 25$ recordings, 10 mice | age                    | WT early ado / WT late ado                 | 95.50   |                     | 0.253   |
|             |                           |  | condition              | Df(16)A+/- early ado / Df(16)A+/- late ado | 85.20   |                     | 0.262   |
|             |                           |  |                        | Df(16)A+/- early ado / WT early ado        | 42.30   |                     | 0.030   |
|             |                           |  |                        | Df(16)A+/- late ado / WT late ado          | 51.80   |                     | 0.868   |
| 25B (left)  | Linear mixed-effect model | $n_{(WT)} = 82$ recordings, 23 mice<br>$n_{(Df(16)A+/+)} = 52$ recordings, 14 mice   | age                    |  | 101.10  |                     | 0.645   |
|             |                           |  | condition              |  | 93.31   |                     | 0.030   |
|             |                           |  | age-condition (slopes) | WT P20-60                                  | 112.00  | [-0.00396 0.00248]  | 0.007   |
|             |                           |  |                        | Df(16)A+/- P20-60                          | 108.00  | [-0.00788 -0.00150] |         |
| 25B (right) | Linear mixed-effect model | $n_{(WT, \text{early ado})} = 49$ recordings, 18 mice<br>$n_{(WT, \text{late ado})} = 33$ recordings, 14 mice<br>$n_{(Df(16)A+/, \text{early ado})} = 27$ recordings, 12 mice<br>$n_{(Df(16)A+/, \text{late ado})} = 25$ recordings, 10 mice | age                    | WT early ado / WT late ado                 | 66.20   |                     | 0.353   |
|             |                           |  | condition              | Df(16)A+/- early ado / Df(16)A+/- late ado | 68.50   |                     | 0.059   |
|             |                           |  |                        | Df(16)A+/- early ado / WT early ado        | 39.60   |                     | 0.485   |
|             |                           |  |                        | Df(16)A+/- late ado / WT late ado          | 44.30   |                     | 0.515   |
| 25C (left)  | Linear mixed-effect model | $n_{(WT)} = 82$ recordings, 23 mice<br>$n_{(Df(16)A+/+)} = 52$ recordings, 14 mice   | age                    |  | 95.77   |                     | 0.630   |
|             |                           |  | condition              |  | 120.00  |                     | 0.179   |
|             |                           |  | age-condition (slopes) | WT P20-60                                  | 96.00   | [-0.00111 0.000676] | 0.582   |
|             |                           |  |                        | Df(16)A+/- P20-60                          | 112.00  | [-0.00152 0.000493] |         |
| 25C (right) | Linear mixed-effect model | $n_{(WT, \text{early ado})} = 49$ recordings, 18 mice<br>$n_{(WT, \text{late ado})} = 33$ recordings, 14 mice<br>$n_{(Df(16)A+/, \text{early ado})} = 27$ recordings, 12 mice<br>$n_{(Df(16)A+/, \text{late ado})} = 25$ recordings, 10 mice | age                    | WT early ado / WT late ado                 | 85.80   |                     | 0.855   |
|             |                           |  | condition              | Df(16)A+/- early ado / Df(16)A+/- late ado | 82.60   |                     | 0.537   |
|             |                           |  |                        | Df(16)A+/- early ado / WT early ado        | 46.50   |                     | 0.094   |
|             |                           |  |                        | Df(16)A+/- late ado / WT late ado          | 53.60   |                     | 0.343   |
| 26C (left)  | Linear mixed-effect model | $n_{(WT)} = 82$ recordings, 23 mice<br>$n_{(Df(16)A+/+)} = 52$ recordings, 14 mice   | age                    |  | 102.381 |                     | 0.078   |
|             |                           |  | condition              |  | 121.42  |                     | 0.762   |
|             |                           |  | age-condition (slopes) | WT P20-60                                  | 99.5    | [-0.000276 0.00479] | 0.384   |
|             |                           |  |                        | Df(16)A+/- P20-60                          | 110.2   | [0.000751 0.00652]  |         |
| 26C (right) | Linear mixed-effect model | $n_{(WT, \text{early ado})} = 49$ recordings, 18 mice<br>$n_{(WT, \text{late ado})} = 33$ recordings, 14 mice<br>$n_{(Df(16)A+/, \text{early ado})} = 27$ recordings, 12 mice<br>$n_{(Df(16)A+/, \text{late ado})} = 25$ recordings, 10 mice | age                    | WT early ado / WT late ado                 | 86.00   |                     | 0.737   |
|             |                           |  | condition              | Df(16)A+/- early ado / Df(16)A+/- late ado | 85.00   |                     | 0.082   |
|             |                           |  |                        | Df(16)A+/- early ado / WT early ado        | 46.60   |                     | 0.508   |
|             |                           |  |                        | Df(16)A+/- late ado / WT late ado          | 53.50   |                     | 0.566   |
| 26D (left)  | Linear mixed-effect model | $n_{(WT)} = 82$ recordings, 23 mice<br>$n_{(Df(16)A+/+)} = 52$ recordings, 14 mice   | age                    |  | 85.60   |                     | 0.271   |
|             |                           |  | condition              |  | 116.31  |                     | 0.165   |
|             |                           |  | age-condition (slopes) | WT P20-60                                  | 89.90   | [-0.00576 0.00166]  | 0.046   |
|             |                           |  |                        | Df(16)A+/- P20-60                          | 116.20  | [-0.00187 0.00629]  |         |
| 26D (right) | Linear mixed-effect model | $n_{(WT, \text{early ado})} = 49$ recordings, 18 mice<br>$n_{(WT, \text{late ado})} = 33$ recordings, 14 mice<br>$n_{(Df(16)A+/, \text{early ado})} = 27$ recordings, 12 mice<br>$n_{(Df(16)A+/, \text{late ado})} = 25$ recordings, 10 mice | age                    | WT early ado / WT late ado                 | 80.10   |                     | 0.355   |
|             |                           |  | condition              | Df(16)A+/- early ado / Df(16)A+/- late ado | 90.80   |                     | 0.341   |
|             |                           |  |                        | Df(16)A+/- early ado / WT early ado        | 47.80   |                     | 0.901   |
|             |                           |  |                        | Df(16)A+/- late ado / WT late ado          | 57.10   |                     | 0.162   |
| 26E (left)  | Linear mixed-effect model | $n_{(WT)} = 82$ recordings, 23 mice<br>$n_{(Df(16)A+/+)} = 52$ recordings, 14 mice   | age                    |  | 96.51   |                     | 0.453   |
|             |                           |  | condition              |  | 120.30  |                     | 0.212   |
|             |                           |  | age-condition (slopes) | WT P20-60                                  | 95.50   | [-3.56e-03 0.00785] | 0.213   |
|             |                           |  |                        | Df(16)A+/- P20-60                          | 112.50  | [4.54e-05 0.01293]  |         |
| 26E (right) | Linear mixed-effect model | $n_{(WT, \text{early ado})} = 49$ recordings, 18 mice<br>$n_{(WT, \text{late ado})} = 33$ recordings, 14 mice<br>$n_{(Df(16)A+/, \text{early ado})} = 27$ recordings, 12 mice<br>$n_{(Df(16)A+/, \text{late ado})} = 25$ recordings, 10 mice | age                    | WT early ado / WT late ado                 | 89      |                     | 0.130   |
|             |                           |  | condition              | Df(16)A+/- early ado / Df(16)A+/- late ado | 84      |                     | 0.090   |
|             |                           |  |                        | Df(16)A+/- early ado / WT early ado        | 46.5    |                     | 0.451   |
|             |                           |  |                        | Df(16)A+/- late ado / WT late ado          | 53.4    |                     | 0.276   |
| 26F (left)  | Linear mixed-effect model | $n_{(WT)} = 82$ recordings, 23 mice<br>$n_{(Df(16)A+/+)} = 52$ recordings, 14 mice   | age                    |  | 90.04   |                     | 0.983   |
|             |                           |  | condition              |  | 118.40  |                     | 0.929   |
|             |                           |  | age-condition (slopes) | WT P20-60                                  | 93.00   | [-0.00350 0.00343]  | 0.288   |
|             |                           |  |                        | Df(16)A+/- P20-60                          | 114.00  | [-0.00172 0.00605]  |         |
| 26F (right) | Linear mixed-effect model | $n_{(WT, \text{early ado})} = 49$ recordings, 18 mice<br>$n_{(WT, \text{late ado})} = 33$ recordings, 14 mice<br>$n_{(Df(16)A+/, \text{early ado})} = 27$ recordings, 12 mice<br>$n_{(Df(16)A+/, \text{late ado})} = 25$ recordings, 10 mice | age                    | WT early ado / WT late ado                 | 87.4    |                     | 0.260   |
|             |                           |  | condition              | Df(16)A+/- early ado / Df(16)A+/- late ado | 99.6    |                     | 0.249   |
|             |                           |  |                        | Df(16)A+/- early ado / WT early ado        | 47.9    |                     | 0.137   |
|             |                           |  |                        | Df(16)A+/- late ado / WT late ado          | 55.1    |                     | 0.124   |
| 27A (left)  | Linear mixed-effect model | $n_{(WT)} = 82$ recordings, 23 mice<br>$n_{(Df(16)A+/+)} = 52$ recordings, 14 mice   | age                    |  | 87.03   |                     | 0.156   |
|             |                           |  | condition              |  | 111.96  |                     | 0.050   |
|             |                           |  | age-condition (slopes) | WT P20-60                                  | 89.90   | [-0.00303 0.0181]   | 0.203   |
|             |                           |  |                        | Df(16)A+/- P20-60                          | 99.70   | [-0.01398 0.0116]   |         |
| 27A (right) | Linear mixed-effect model | $n_{(WT, \text{early ado})} = 49$ recordings, 18 mice<br>$n_{(WT, \text{late ado})} = 33$ recordings, 14 mice<br>$n_{(Df(16)A+/, \text{early ado})} = 27$ recordings, 12 mice<br>$n_{(Df(16)A+/, \text{late ado})} = 25$ recordings, 10 mice | age                    | WT early ado / WT late ado                 | 79.80   |                     | 0.577   |
|             |                           |  | condition              | Df(16)A+/- early ado / Df(16)A+/- late ado | 90.60   |                     | 0.315   |
|             |                           |  |                        | Df(16)A+/- early ado / WT early ado        | 44.10   |                     | 0.029   |
|             |                           |  |                        | Df(16)A+/- late ado / WT late ado          | 56.80   |                     | 0.331   |
| 27B (left)  | Linear mixed-effect model | $n_{(WT)} = 82$ recordings, 23 mice<br>$n_{(Df(16)A+/+)} = 52$ recordings, 14 mice   | age                    |  | 95.43   |                     | 0.000   |
|             |                           |  | condition              |  | 112.81  |                     | 0.047   |
|             |                           |  | age-condition (slopes) | WT P20-60                                  | 95.80   | [0.01261 0.0354]    | 0.071   |
|             |                           |  |                        | Df(16)A+/- P20-60                          | 98.30   | [-0.00373 0.0239]   |         |

# Appendix

|                    |                    |  |               |  |        |                     |       |
|--------------------|--------------------|--|---------------|--|--------|---------------------|-------|
| <b>27B (right)</b> | Linear             | $n_{(WT, \text{early ado})} = 49$ recordings, 18 mice                | age           | WT early ado / WT late ado                 | 88.30  |                     | 0.001 |
|                    | mixed-effect model | $n_{(WT, \text{late ado})} = 33$ recordings, 14 mice                 | condition     | Df(16)A+/- early ado / Df(16)A+/- late ado | 103.20 |                     | 0.232 |
|                    |                    | $n_{(Df(16)A+/-, \text{early ado})} = 27$ recordings, 12 mice        |               | Df(16)A+/- early ado / WT early ado        | 39.00  |                     | 0.201 |
|                    |                    | $n_{(Df(16)A+/-, \text{late ado})} = 25$ recordings, 10 mice         |               | Df(16)A+/- late ado / WT late ado          | 56.50  |                     | 0.832 |
| <b>28B (left)</b>  | Linear             |  | age           |  | 101.00 |                     | 0.428 |
|                    | mixed-effect model |  | condition     |  | 92.64  |                     | 0.573 |
|                    |                    | $n_{(WT)} = 82$ recordings, 23 mice                                  | age-condition | WT P20-60                                  | 101.00 | [-0.000750 0.00173] | 0.386 |
|                    |                    | $n_{(Df(16)A+/-)} = 52$ recordings, 14 mice                          | (slopes)      | Df(16)A+/- P20-60                          | 125.00 | [-0.000253 0.00220] |       |
| <b>28B (right)</b> | Linear             | $n_{(WT, \text{early ado})} = 49$ recordings, 18 mice                | age           | WT early ado / WT late ado                 | 78.50  |                     | 0.329 |
|                    | mixed-effect model | $n_{(WT, \text{late ado})} = 33$ recordings, 14 mice                 | condition     | Df(16)A+/- early ado / Df(16)A+/- late ado | 96.10  |                     | 0.090 |
|                    |                    | $n_{(Df(16)A+/-, \text{early ado})} = 27$ recordings, 12 mice        |               | Df(16)A+/- early ado / WT early ado        | 39.30  |                     | 0.177 |
|                    |                    | $n_{(Df(16)A+/-, \text{late ado})} = 25$ recordings, 10 mice         |               | Df(16)A+/- late ado / WT late ado          | 43.80  |                     | 0.081 |
| <b>28D (left)</b>  | Linear             |  | age           |  | 91.99  |                     | 0.320 |
|                    | mixed-effect model |  | condition     |  | 118.86 |                     | 0.003 |
|                    |                    | $n_{(WT)} = 82$ recordings, 23 mice                                  | age-condition | WT P20-60                                  | 95.20  | [-0.00167 0.00501]  | 0.033 |
|                    |                    | $n_{(Df(16)A+/-)} = 52$ recordings, 14 mice                          | (slopes)      | Df(16)A+/- P20-60                          | 112.70 | [0.00227 0.00982]   |       |
| <b>28D (right)</b> | Linear             | $n_{(WT, \text{early ado})} = 49$ recordings, 18 mice                | age           | WT early ado / WT late ado                 | 88.00  |                     | 0.253 |
|                    | mixed-effect model | $n_{(WT, \text{late ado})} = 33$ recordings, 14 mice                 | condition     | Df(16)A+/- early ado / Df(16)A+/- late ado | 93.30  |                     | 0.001 |
|                    |                    | $n_{(Df(16)A+/-, \text{early ado})} = 27$ recordings, 12 mice        |               | Df(16)A+/- early ado / WT early ado        | 46.80  |                     | 0.003 |
|                    |                    | $n_{(Df(16)A+/-, \text{late ado})} = 25$ recordings, 10 mice         |               | Df(16)A+/- late ado / WT late ado          | 53.00  |                     | 0.490 |
| <b>29D (right)</b> | Linear             |  | age           | WT early ado / WT late ado                 | 88.00  |                     | 0.082 |
|                    | mixed-effect model | $n_{(WT)} = 1422$ rs units, 82 rec, 23 mice                          | condition     | Df(16)A+/- early ado / Df(16)A+/- late ado | 104.00 |                     | 0.553 |
|                    |                    | $n_{(Df(16)A+/-)} = 951$ rs units, 52 rec, 14 mice                   |               | Df(16)A+/- early ado / WT early ado        | 50.00  |                     | 0.067 |
|                    |                    |  |               | Df(16)A+/- late ado / WT late ado          | 56.70  |                     | 0.977 |
| <b>30A (left)</b>  | Linear             |  | age           |  | 71.50  |                     | 0.635 |
|                    | mixed-effect model |  | condition     |  | 116.20 |                     | 0.042 |
|                    |                    | $n_{(WT)} = 1422$ rs units, 82 rec, 23 mice                          | age-condition | WT P20-60                                  | 83.80  | [-0.002901 0.00471] | 0.141 |
|                    |                    | $n_{(Df(16)A+/-)} = 951$ rs units, 52 rec, 14 mice                   | (slopes)      | Df(16)A+/- P20-60                          | 117.70 | [-0.000242 0.00896] |       |
| <b>30A (right)</b> | Linear             | $n_{(WT, \text{early ado})} = 860$ rs units, 49 rec, 18 mice         | age           | WT early ado / WT late ado                 | 140.00 |                     | 0.228 |
|                    | mixed-effect model | $n_{(WT, \text{late ado})} = 562$ rs units, 33 rec, 14 mice          | condition     | Df(16)A+/- early ado / Df(16)A+/- late ado | 172.00 |                     | 0.008 |
|                    |                    | $n_{(Df(16)A+/-, \text{early ado})} = 537$ rs units, 27 rec, 12 mice |               | Df(16)A+/- early ado / WT early ado        | 34.10  |                     | 0.135 |
|                    |                    | $n_{(Df(16)A+/-, \text{late ado})} = 414$ rs units, 25 rec, 10 mice  |               | Df(16)A+/- late ado / WT late ado          | 44.20  |                     | 0.849 |
| <b>30B (left)</b>  | Linear             |  | age           |  | 89.04  |                     | 0.155 |
|                    | mixed-effect model |  | condition     |  | 155.14 |                     | 0.015 |
|                    |                    | $n_{(WT)} = 1422$ rs units, 82 rec, 23 mice                          | age-condition | WT P20-60                                  | 96.20  | [-0.00503 0.000829] | 0.243 |
|                    |                    | $n_{(Df(16)A+/-)} = 951$ rs units, 52 rec, 14 mice                   | (slopes)      | Df(16)A+/- P20-60                          | 158.60 | [-0.00340 0.003328] |       |
| <b>30B (right)</b> | Linear             | $n_{(WT, \text{early ado})} = 860$ rs units, 49 rec, 18 mice         | age           | WT early ado / WT late ado                 | 143.00 |                     | 0.040 |
|                    | mixed-effect model | $n_{(WT, \text{late ado})} = 562$ rs units, 33 rec, 14 mice          | condition     | Df(16)A+/- early ado / Df(16)A+/- late ado | 119.00 |                     | 0.774 |
|                    |                    | $n_{(Df(16)A+/-, \text{early ado})} = 537$ rs units, 27 rec, 12 mice |               | Df(16)A+/- early ado / WT early ado        | 44.00  |                     | 0.002 |
|                    |                    | $n_{(Df(16)A+/-, \text{late ado})} = 414$ rs units, 25 rec, 10 mice  |               | Df(16)A+/- late ado / WT late ado          | 56.80  |                     | 0.166 |
| <b>30C (left)</b>  | Linear             |  | age           |  | 72.13  |                     | 0.397 |
|                    | mixed-effect model |  | condition     |  | 104.40 |                     | 0.056 |
|                    |                    | $n_{(WT)} = 1422$ rs units, 82 rec, 23 mice                          | age-condition | WT P20-60                                  | 85.90  | [-0.00486 0.00196]  | 0.093 |
|                    |                    | $n_{(Df(16)A+/-)} = 951$ rs units, 52 rec, 14 mice                   | (slopes)      | Df(16)A+/- P20-60                          | 107.90 | [-0.00197 0.00635]  |       |
| <b>30C (right)</b> | Linear             | $n_{(WT, \text{early ado})} = 860$ rs units, 49 rec, 18 mice         | age           | WT early ado / WT late ado                 | 143.00 |                     | 0.913 |
|                    | mixed-effect model | $n_{(WT, \text{late ado})} = 562$ rs units, 33 rec, 14 mice          | condition     | Df(16)A+/- early ado / Df(16)A+/- late ado | 175.00 |                     | 0.033 |
|                    |                    | $n_{(Df(16)A+/-, \text{early ado})} = 537$ rs units, 27 rec, 12 mice |               | Df(16)A+/- early ado / WT early ado        | 32.70  |                     | 0.134 |
|                    |                    | $n_{(Df(16)A+/-, \text{late ado})} = 414$ rs units, 25 rec, 10 mice  |               | Df(16)A+/- late ado / WT late ado          | 44.00  |                     | 0.664 |
| <b>30D (left)</b>  | Linear             |  | age           |  | 91.66  |                     | 0.946 |
|                    | mixed-effect model |  | condition     |  | 149.60 |                     | 0.674 |
|                    |                    | $n_{(WT)} = 1422$ rs units, 82 rec, 23 mice                          | age-condition | WT P20-60                                  | 99.20  | [-0.00364 0.0034]   | 0.220 |
|                    |                    | $n_{(Df(16)A+/-)} = 951$ rs units, 52 rec, 14 mice                   | (slopes)      | Df(16)A+/- P20-60                          | 203.60 | [-0.00623 0.0014]   |       |
| <b>30D (right)</b> | Linear             | $n_{(WT, \text{early ado})} = 860$ rs units, 49 rec, 18 mice         | age           | WT early ado / WT late ado                 | 108.00 |                     | 0.301 |
|                    | mixed-effect model | $n_{(WT, \text{late ado})} = 562$ rs units, 33 rec, 14 mice          | condition     | Df(16)A+/- early ado / Df(16)A+/- late ado | 156.00 |                     | 0.547 |
|                    |                    | $n_{(Df(16)A+/-, \text{early ado})} = 537$ rs units, 27 rec, 12 mice |               | Df(16)A+/- early ado / WT early ado        | 42.50  |                     | 0.481 |
|                    |                    | $n_{(Df(16)A+/-, \text{late ado})} = 414$ rs units, 25 rec, 10 mice  |               | Df(16)A+/- late ado / WT late ado          | 51.20  |                     | 0.109 |
| <b>31A (left)</b>  | Linear             |  | age           |  | 69.75  |                     | 0.363 |
|                    | mixed-effect model |  | condition     |  | 71.16  |                     | 0.476 |
|                    |                    | $n_{(WT)} = 279$ fs units, 82 rec, 23 mice                           | age-condition | WT P20-60                                  | 76.30  | [-0.00416 0.0111]   | 0.784 |
|                    |                    | $n_{(Df(16)A+/-)} = 174$ fs units, 52 rec, 14 mice                   | (slopes)      | Df(16)A+/- P20-60                          | 70.20  | [-0.00458 0.0143]   |       |
| <b>31A (right)</b> | Linear             | $n_{(WT, \text{early ado})} = 167$ fs units, 49 rec, 18 mice         | age           | WT early ado / WT late ado                 | 97.90  |                     | 0.660 |
|                    | mixed-effect model | $n_{(WT, \text{late ado})} = 112$ fs units, 33 rec, 14 mice          | condition     | Df(16)A+/- early ado / Df(16)A+/- late ado | 98.90  |                     | 0.399 |
|                    |                    | $n_{(Df(16)A+/-, \text{early ado})} = 107$ fs units, 27 rec, 12 mice |               | Df(16)A+/- early ado / WT early ado        | 29.40  |                     | 0.350 |
|                    |                    | $n_{(Df(16)A+/-, \text{late ado})} = 67$ fs units, 25 rec, 10 mice   |               | Df(16)A+/- late ado / WT late ado          | 35.30  |                     | 0.749 |
| <b>31B (left)</b>  | Linear             |  | age           |  | 89.77  |                     | 0.863 |
|                    | mixed-effect model |  | condition     |  | 94.77  |                     | 0.799 |
|                    |                    | $n_{(WT)} = 279$ fs units, 82 rec, 23 mice                           | age-condition | WT P20-60                                  | 84.90  | [-0.00496 0.00418]  | 0.567 |
|                    |                    | $n_{(Df(16)A+/-)} = 174$ fs units, 52 rec, 14 mice                   | (slopes)      | Df(16)A+/- P20-60                          | 83.90  | [-0.00756 0.00335]  |       |
| <b>31B (right)</b> | Linear             | $n_{(WT, \text{early ado})} = 167$ fs units, 49 rec, 18 mice         | age           | WT early ado / WT late ado                 | 94.20  |                     | 0.495 |
|                    | mixed-effect model | $n_{(WT, \text{late ado})} = 112$ fs units, 33 rec, 14 mice          | condition     | Df(16)A+/- early ado / Df(16)A+/- late ado | 96.80  |                     | 0.342 |
|                    |                    | $n_{(Df(16)A+/-, \text{early ado})} = 107$ fs units, 27 rec, 12 mice |               | Df(16)A+/- early ado / WT early ado        | 33.70  |                     | 0.752 |
|                    |                    | $n_{(Df(16)A+/-, \text{late ado})} = 67$ fs units, 25 rec, 10 mice   |               | Df(16)A+/- late ado / WT late ado          | 58.20  |                     | 0.499 |
| <b>31C (left)</b>  | Linear             |  | age           |  | 66.08  |                     | 0.797 |
|                    | mixed-effect model |  | condition     |  | 70.33  |                     | 0.555 |
|                    |                    | $n_{(WT)} = 279$ fs units, 82 rec, 23 mice                           | age-condition | WT P20-60                                  | 76.10  | [-0.00858 0.00663]  | 0.594 |
|                    |                    | $n_{(Df(16)A+/-)} = 174$ fs units, 52 rec, 14 mice                   | (slopes)      | Df(16)A+/- P20-60                          | 72.40  | [-0.00769 0.01117]  |       |
| <b>31C (right)</b> | Linear             | $n_{(WT, \text{early ado})} = 167$ fs units, 49 rec, 18 mice         | age           | WT early ado / WT late ado                 | 87.70  |                     | 0.741 |
|                    | mixed-effect model | $n_{(WT, \text{late ado})} = 112$ fs units, 33 rec, 14 mice          | condition     | Df(16)A+/- early ado / Df(16)A+/- late ado | 86.90  |                     | 0.676 |
|                    |                    | $n_{(Df(16)A+/-, \text{early ado})} = 107$ fs units, 27 rec, 12 mice |               | Df(16)A+/- early ado / WT early ado        | 33.00  |                     | 0.539 |
|                    |                    | $n_{(Df(16)A+/-, \text{late ado})} = 67$ fs units, 25 rec, 10 mice   |               | Df(16)A+/- late ado / WT late ado          | 38.30  |                     | 0.951 |
| <b>31D (left)</b>  | Linear             |  | age           |  | 448.00 |                     | 0.434 |
|                    | mixed-effect model |  | condition     |  | 448.00 |                     | 0.166 |
|                    |                    | $n_{(WT)} = 279$ fs units, 82 rec, 23 mice                           | age-condition | WT P20-60                                  | 86.60  | [-0.00266 0.00600]  | 0.326 |
|                    |                    | $n_{(Df(16)A+/-)} = 174$ fs units, 52 rec, 14 mice                   | (slopes)      | Df(16)A+/- P20-60                          | 78.70  | [-0.00633 0.00399]  |       |
| <b>31D (right)</b> | Linear             | $n_{(WT, \text{early ado})} = 167$ fs units, 49 rec, 18 mice         | age           | WT early ado / WT late ado                 | 93.80  |                     | 0.232 |
|                    | mixed-effect model | $n_{(WT, \text{late ado})} = 112$ fs units, 33 rec, 14 mice          | condition     | Df(16)A+/- early ado / Df(16)A+/- late ado | 84.00  |                     | 0.484 |
|                    |                    | $n_{(Df(16)A+/-, \text{early ado})} = 107$ fs units, 27 rec, 12 mice |               | Df(16)A+/- early ado / WT early ado        | 24.50  |                     | 0.288 |
|                    |                    | $n_{(Df(16)A+/-, \text{late ado})} = 67$ fs units, 25 rec, 10 mice   |               | Df(16)A+/- late ado / WT late ado          | 37.00  |                     | 0.555 |

# Appendix

|                    |                    |   |               |  |         |                       |        |
|--------------------|--------------------|---|---------------|--|---------|-----------------------|--------|
| <b>32B (left)</b>  | Linear             |   | age           | WT early ado / WT late ado                 | 87.20   |                       | 0.471  |
|                    | mixed-effect model |   | condition     | Df(16)A+/- early ado / Df(16)A+/- late ado | 92.80   |                       | 0.816  |
|                    |                    | $n_{WT}$ : 1422 rs units, 82 rec, 23 mice                   | age-condition | Df(16)A+/- early ado / WT early ado        | 49.10   |                       | 0.505  |
|                    |                    | $n_{Df(16)A+/-}$ : 951 rs units, 52 rec, 14 mice            | (slopes)      | Df(16)A+/- late ado / WT late ado          | 55.70   |                       | 0.924  |
| <b>32C (left)</b>  | Linear             |   | age           |  | 78.63   |                       | 0.000  |
|                    | mixed-effect model |   | condition     |  | 131.60  |                       | 0.557  |
|                    |                    | $n_{WT}$ : 1422 rs units, 82 rec, 23 mice                   | age-condition | WT P20-60                                  | 90.70   | [-0.0117 -0.00499]    | 0.661  |
|                    |                    | $n_{Df(16)A+/-}$ : 951 rs units, 52 rec, 14 mice            | (slopes)      | Df(16)A+/- P20-60                          | 152.80  | [-0.0132 -0.00536]    |        |
| <b>32C (right)</b> | Linear             | $n_{WT, early ado}$ : 860 rs units, 49 rec, 18 mice         | age           | WT early ado / WT late ado                 | 241.00  |                       | <.0001 |
|                    | mixed-effect model | $n_{WT, late ado}$ : 562 rs units, 33 rec, 14 mice          | condition     | Df(16)A+/- early ado / Df(16)A+/- late ado | 445.00  |                       | 0.000  |
|                    |                    | $n_{Df(16)A+/-, early ado}$ : 537 rs units, 27 rec, 12 mice |               | Df(16)A+/- early ado / WT early ado        | 43.20   |                       | 0.656  |
|                    |                    | $n_{Df(16)A+/-, late ado}$ : 414 rs units, 25 rec, 10 mice  |               | Df(16)A+/- late ado / WT late ado          | 58.60   |                       | 0.759  |
| <b>32D (left)</b>  | Linear             |   | age           |  | 86.11   |                       | 0.000  |
|                    | mixed-effect model |   | condition     |  | 149.45  |                       | 0.822  |
|                    |                    | $n_{WT}$ : 1422 rs units, 82 rec, 23 mice                   | age-condition | WT P20-60                                  | 95.10   | [-0.00971 -0.00382]   | 0.362  |
|                    |                    | $n_{Df(16)A+/-}$ : 951 rs units, 52 rec, 14 mice            | (slopes)      | Df(16)A+/- P20-60                          | 187.50  | [-0.01152 -0.00501]   |        |
| <b>32D (right)</b> | Linear             | $n_{WT, early ado}$ : 860 rs units, 49 rec, 18 mice         | age           | WT early ado / WT late ado                 | 290.00  |                       | 0.000  |
|                    | mixed-effect model | $n_{WT, late ado}$ : 562 rs units, 33 rec, 14 mice          | condition     | Df(16)A+/- early ado / Df(16)A+/- late ado | 557.00  |                       | 0.002  |
|                    |                    | $n_{Df(16)A+/-, early ado}$ : 537 rs units, 27 rec, 12 mice |               | Df(16)A+/- early ado / WT early ado        | 42.40   |                       | 0.323  |
|                    |                    | $n_{Df(16)A+/-, late ado}$ : 414 rs units, 25 rec, 10 mice  |               | Df(16)A+/- late ado / WT late ado          | 53.70   |                       | 0.496  |
| <b>32E (left)</b>  | Linear             |   | age           |  | 58.51   |                       | 0.015  |
|                    | mixed-effect model |   | condition     |  | 82.88   |                       | 0.268  |
|                    |                    | $n_{WT}$ : 279 fs units, 82 rec, 23 mice                    | age-condition | WT P20-60                                  | 69.50   | [-0.0162 -0.00171]    | 0.862  |
|                    |                    | $n_{Df(16)A+/-}$ : 174 fs units, 52 rec, 14 mice            | (slopes)      | Df(16)A+/- P20-60                          | 83.10   | [-0.0172 0.00088]     |        |
| <b>32E (right)</b> | Linear             | $n_{WT, early ado}$ : 167 fs units, 49 rec, 18 mice         | age           | WT early ado / WT late ado                 | 103.00  |                       | 0.003  |
|                    | mixed-effect model | $n_{WT, late ado}$ : 112 fs units, 33 rec, 14 mice          | condition     | Df(16)A+/- early ado / Df(16)A+/- late ado | 131.00  |                       | 0.254  |
|                    |                    | $n_{Df(16)A+/-, early ado}$ : 107 fs units, 27 rec, 12 mice |               | Df(16)A+/- early ado / WT early ado        | 38.40   |                       | 0.055  |
|                    |                    | $n_{Df(16)A+/-, late ado}$ : 67 fs units, 25 rec, 10 mice   |               | Df(16)A+/- late ado / WT late ado          | 56.80   |                       | 0.519  |
| <b>32F (left)</b>  | Linear             |   | age           |  | 57.29   |                       | 0.293  |
|                    | mixed-effect model |   | condition     |  | 101.08  |                       | 0.627  |
|                    |                    | $n_{WT}$ : 279 fs units, 82 rec, 23 mice                    | age-condition | WT P20-60                                  | 74.20   | [-0.00921 0.002849]   | 0.309  |
|                    |                    | $n_{Df(16)A+/-}$ : 174 fs units, 52 rec, 14 mice            | (slopes)      | Df(16)A+/- P20-60                          | 106.90  | [-0.01405 0.000308]   |        |
| <b>32F (right)</b> | Linear             | $n_{WT, early ado}$ : 167 fs units, 49 rec, 18 mice         | age           | WT early ado / WT late ado                 | 102.00  |                       | 0.319  |
|                    | mixed-effect model | $n_{WT, late ado}$ : 112 fs units, 33 rec, 14 mice          | condition     | Df(16)A+/- early ado / Df(16)A+/- late ado | 126.00  |                       | 0.390  |
|                    |                    | $n_{Df(16)A+/-, early ado}$ : 107 fs units, 27 rec, 12 mice |               | Df(16)A+/- early ado / WT early ado        | 33.00   |                       | 0.058  |
|                    |                    | $n_{Df(16)A+/-, late ado}$ : 67 fs units, 25 rec, 10 mice   |               | Df(16)A+/- late ado / WT late ado          | 37.60   |                       | 0.094  |
| <b>33A (left)</b>  | Linear             |   | age           |  | 3344.00 |                       | 0.000  |
|                    | mixed-effect model |   | condition     |  | 38.02   |                       | 0.004  |
|                    |                    | $n_{WT}$ : 1422 rs units, 82 rec, 23 mice                   | age-condition | WT P20-60                                  | >3000   | [-0.000970 -0.000577] | <.0001 |
|                    |                    | $n_{Df(16)A+/-}$ : 951 rs units, 52 rec, 14 mice            | (slopes)      | Df(16)A+/- P20-60                          | >3000   | [-0.000185 0.000174]  |        |
| <b>33A (right)</b> | Linear             | $n_{WT, early ado}$ : 860 rs units, 49 rec, 18 mice         | age           | WT early ado / WT late ado                 | >3000   |                       | <.0001 |
|                    | mixed-effect model | $n_{WT, late ado}$ : 562 rs units, 33 rec, 14 mice          | condition     | Df(16)A+/- early ado / Df(16)A+/- late ado | >3000   |                       | <.0001 |
|                    |                    | $n_{Df(16)A+/-, early ado}$ : 537 rs units, 27 rec, 12 mice |               | Df(16)A+/- early ado / WT early ado        | >3000   |                       | 0.545  |
|                    |                    | $n_{Df(16)A+/-, late ado}$ : 414 rs units, 25 rec, 10 mice  |               | Df(16)A+/- late ado / WT late ado          | >3000   |                       | 0.028  |
| <b>33B (left)</b>  | Linear             |   | age           |  | 3985.00 |                       | 0.000  |
|                    | mixed-effect model |   | condition     |  | 37.18   |                       | 0.511  |
|                    |                    | $n_{WT}$ : 1422 rs units, 82 rec, 23 mice                   | age-condition | WT P20-60                                  | >3000   | [-0.000328 -1.61e-04] | <.0001 |
|                    |                    | $n_{Df(16)A+/-}$ : 951 rs units, 52 rec, 14 mice            | (slopes)      | Df(16)A+/- P20-60                          | >3000   | [-0.000114 3.75e-05]  |        |
| <b>33B (right)</b> | Linear             | $n_{WT, early ado}$ : 860 rs units, 49 rec, 18 mice         | age           | WT early ado / WT late ado                 | >3000   |                       | <.0001 |
|                    | mixed-effect model | $n_{WT, late ado}$ : 562 rs units, 33 rec, 14 mice          | condition     | Df(16)A+/- early ado / Df(16)A+/- late ado | >3000   |                       | 0.257  |
|                    |                    | $n_{Df(16)A+/-, early ado}$ : 537 rs units, 27 rec, 12 mice |               | Df(16)A+/- early ado / WT early ado        | >3000   |                       | 0.284  |
|                    |                    | $n_{Df(16)A+/-, late ado}$ : 414 rs units, 25 rec, 10 mice  |               | Df(16)A+/- late ado / WT late ado          | >3000   |                       | 0.033  |
| <b>33C (left)</b>  | Linear             |   | age           |  | 66.25   |                       | 0.571  |
|                    | mixed-effect model |   | condition     |  | 112.30  |                       | 0.731  |
|                    |                    | $n_{WT}$ : 279 fs units, 82 rec, 23 mice                    | age-condition | WT P20-60                                  | 68.80   | [-0.000683 0.001219]  | 0.311  |
|                    |                    | $n_{Df(16)A+/-}$ : 174 fs units, 52 rec, 14 mice            | (slopes)      | Df(16)A+/- P20-60                          | 87.60   | [-0.001225 0.000848]  |        |
| <b>33C (right)</b> | Linear             | $n_{WT, early ado}$ : 167 fs units, 49 rec, 18 mice         | age           | WT early ado / WT late ado                 | 110.80  |                       | 0.416  |
|                    | mixed-effect model | $n_{WT, late ado}$ : 112 fs units, 33 rec, 14 mice          | condition     | Df(16)A+/- early ado / Df(16)A+/- late ado | 71.50   |                       | 0.121  |
|                    |                    | $n_{Df(16)A+/-, early ado}$ : 107 fs units, 27 rec, 12 mice |               | Df(16)A+/- early ado / WT early ado        | 36.30   |                       | 0.785  |
|                    |                    | $n_{Df(16)A+/-, late ado}$ : 67 fs units, 25 rec, 10 mice   |               | Df(16)A+/- late ado / WT late ado          | 53.20   |                       | 0.326  |
| <b>33D (left)</b>  | Linear             |   | age           |  | 61.75   |                       | 0.061  |
|                    | mixed-effect model |   | condition     |  | 111.80  |                       | 0.187  |
|                    |                    | $n_{WT}$ : 279 fs units, 82 rec, 23 mice                    | age-condition | WT P20-60                                  | 64.80   | [-3.18e-05 0.001081]  | 0.011  |
|                    |                    | $n_{Df(16)A+/-}$ : 174 fs units, 52 rec, 14 mice            | (slopes)      | Df(16)A+/- P20-60                          | 90.00   | [-7.56e-04 0.000442]  |        |
| <b>33D (right)</b> | Linear             | $n_{WT, early ado}$ : 167 fs units, 49 rec, 18 mice         | age           | WT early ado / WT late ado                 | 117.90  |                       | 0.555  |
|                    | mixed-effect model | $n_{WT, late ado}$ : 112 fs units, 33 rec, 14 mice          | condition     | Df(16)A+/- early ado / Df(16)A+/- late ado | 83.10   |                       | 0.019  |
|                    |                    | $n_{Df(16)A+/-, early ado}$ : 107 fs units, 27 rec, 12 mice |               | Df(16)A+/- early ado / WT early ado        | 30.80   |                       | 0.736  |
|                    |                    | $n_{Df(16)A+/-, late ado}$ : 67 fs units, 25 rec, 10 mice   |               | Df(16)A+/- late ado / WT late ado          | 41.40   |                       | 0.015  |
| <b>33E (left)</b>  | Linear             |   | age           |  | 302.80  |                       | 0.899  |
|                    | mixed-effect model |   | condition     |  | 55.35   |                       | 0.672  |
|                    |                    | $n_{WT}$ : 1701 units, 82 rec, 23 mice                      | age-condition | WT P20-60                                  | >3000   | [-0.000333 0.000379]  | 0.659  |
|                    |                    | $n_{Df(16)A+/-}$ : 1125 units, 52 rec, 14 mice              | (slopes)      | Df(16)A+/- P20-60                          | >3000   | [-0.000401 0.000336]  |        |
| <b>33E (right)</b> | Linear             | $n_{WT, early ado}$ : 1027 units, 49 rec, 18 mice           | age           | WT early ado / WT late ado                 | >3000   |                       | 0.022  |
|                    | mixed-effect model | $n_{WT, late ado}$ : 674 units, 33 rec, 14 mice             | condition     | Df(16)A+/- early ado / Df(16)A+/- late ado | >3000   |                       | 0.259  |
|                    |                    | $n_{Df(16)A+/-, early ado}$ : 644 units, 27 rec, 12 mice    |               | Df(16)A+/- early ado / WT early ado        | >3000   |                       | 0.853  |
|                    |                    | $n_{Df(16)A+/-, late ado}$ : 481 units, 25 rec, 10 mice     |               | Df(16)A+/- late ado / WT late ado          | >3000   |                       | 0.596  |
| <b>33F (left)</b>  | Linear             |   | age           |  | 485.60  |                       | 0.088  |
|                    | mixed-effect model |   | condition     |  | 47.11   |                       | 0.711  |
|                    |                    | $n_{WT}$ : 1701 units, 82 rec, 23 mice                      | age-condition | WT P20-60                                  | >3000   | [-2.44e-05 0.000359]  | 0.323  |
|                    |                    | $n_{Df(16)A+/-}$ : 1125 units, 52 rec, 14 mice              | (slopes)      | Df(16)A+/- P20-60                          | >3000   | [-3.62e-05 0.000426]  |        |
| <b>33F (right)</b> | Linear             | $n_{WT, early ado}$ : 1027 units, 49 rec, 18 mice           | age           | WT early ado / WT late ado                 | >3000   |                       | 0.212  |
|                    | mixed-effect model | $n_{WT, late ado}$ : 674 units, 33 rec, 14 mice             | condition     | Df(16)A+/- early ado / Df(16)A+/- late ado | >3000   |                       | 0.299  |
|                    |                    | $n_{Df(16)A+/-, early ado}$ : 644 units, 27 rec, 12 mice    |               | Df(16)A+/- early ado / WT early ado        | >3000   |                       | 0.477  |
|                    |                    | $n_{Df(16)A+/-, late ado}$ : 481 units, 25 rec, 10 mice     |               | Df(16)A+/- late ado / WT late ado          | >3000   |                       | 0.480  |

## Appendix

|                |              |   |                           |  |                  |  |                  |
|----------------|--------------|---|---------------------------|--|------------------|--|------------------|
| 34C<br>(left)  | Linear       |   | age                       |  | 104.02           |  | 0.385            |
|                | mixed-effect |   | condition                 |  | 121.79           |  | 0.005            |
|                | model        | $n_{(WT)} = 82$ recordings, 23 mice<br>$n_{(Df(16)A+/-)} = 52$ recordings, 14 mice  | age-condition<br>(slopes) | WT P20-60<br>Df(16)A+/- P20-60   | 100.00<br>110.00 | [-0.006518 0.00256]<br>[0.000776 0.01114]  | 0.006            |
| 34C<br>(right) | Linear       | $n_{(WT, \text{early ado})} = 49$ recordings, 18 mice   | age                       | WT early ado / WT late ado   | 102.00           |  | 0.139            |
|                | mixed-effect | $n_{(WT, \text{late ado})} = 33$ recordings, 14 mice  |                           | Df(16)A+/- early ado / Df(16)A+/- late ado                               | 117.00           |  | 0.026            |
|                | model        | $n_{(Df(16)A+/-, \text{early ado})} = 27$ recordings, 12 mice<br>$n_{(Df(16)A+/-, \text{late ado})} = 25$ recordings, 10 mice         | condition                 | Df(16)A+/- early ado / WT early ado<br>Df(16)A+/- late ado / WT late ado | 46.70<br>52.30   |  | 0.042<br>0.263   |
| 34D<br>(left)  | Linear       |   | age                       |  | 103.07           |  | 0.141            |
|                | mixed-effect |   | condition                 |  | 121.58           |  | 0.103            |
|                | model        | $n_{(WT)} = 82$ recordings, 23 mice<br>$n_{(Df(16)A+/-)} = 52$ recordings, 14 mice  | age-condition<br>(slopes) | WT P20-60<br>Df(16)A+/- P20-60   | 99.80<br>110.10  | [-0.000685 0.00460]<br>[0.001355 0.00738]  | 0.147            |
| 34D<br>(right) | Linear       | $n_{(WT, \text{early ado})} = 49$ recordings, 18 mice   | age                       | WT early ado / WT late ado   | 125.00           |  | 0.509            |
|                | mixed-effect | $n_{(WT, \text{late ado})} = 33$ recordings, 14 mice  |                           | Df(16)A+/- early ado / Df(16)A+/- late ado                               | 128.00           |  | 0.026            |
|                | model        | $n_{(Df(16)A+/-, \text{early ado})} = 27$ recordings, 12 mice<br>$n_{(Df(16)A+/-, \text{late ado})} = 25$ recordings, 10 mice         | condition                 | Df(16)A+/- early ado / WT early ado<br>Df(16)A+/- late ado / WT late ado | 53.60<br>61.60   |  | 0.224<br>0.641   |
| 34E<br>(left)  | Linear       |   | age                       |  | 93.66            |  | 0.272            |
|                | mixed-effect |   | condition                 |  | 119.54           |  | 0.880            |
|                | model        | $n_{(WT)} = 82$ recordings, 23 mice<br>$n_{(Df(16)A+/-)} = 52$ recordings, 14 mice  | age-condition<br>(slopes) | WT P20-60<br>Df(16)A+/- P20-60   | 91.80<br>114.80  | [-0.00175 0.00607]<br>[-0.00104 0.00768]   | 0.614            |
| 34E<br>(right) | Linear       | $n_{(WT, \text{early ado})} = 49$ recordings, 18 mice   | age                       | WT early ado / WT late ado   | 81.6             |  | 0.5937           |
|                | mixed-effect | $n_{(WT, \text{late ado})} = 33$ recordings, 14 mice  |                           | Df(16)A+/- early ado / Df(16)A+/- late ado                               | 82.6             |  | 0.1509           |
|                | model        | $n_{(Df(16)A+/-, \text{early ado})} = 27$ recordings, 12 mice<br>$n_{(Df(16)A+/-, \text{late ado})} = 25$ recordings, 10 mice         | condition                 | Df(16)A+/- early ado / WT early ado<br>Df(16)A+/- late ado / WT late ado | 45.9<br>53.2     |  | 0.5232<br>0.1839 |
| 34F<br>(left)  | Linear       |   | age                       |  | 89.34            |  | 0.443            |
|                | mixed-effect |   | condition                 |  | 99.55            |  | 0.496            |
|                | model        | $n_{(WT)} = 82$ recordings, 23 mice<br>$n_{(Df(16)A+/-)} = 52$ recordings, 14 mice  | age-condition<br>(slopes) | WT P20-60<br>Df(16)A+/- P20-60   | 94.50<br>113.10  | [-0.001761 0.00396]<br>[-0.000792 0.00565] | 0.443            |
| 34F<br>(right) | Linear       | $n_{(WT, \text{early ado})} = 49$ recordings, 18 mice   | age                       | WT early ado / WT late ado   | 106.00           |  | 0.327            |
|                | mixed-effect | $n_{(WT, \text{late ado})} = 33$ recordings, 14 mice  |                           | Df(16)A+/- early ado / Df(16)A+/- late ado                               | 120.00           |  | 0.107            |
|                | model        | $n_{(Df(16)A+/-, \text{early ado})} = 27$ recordings, 12 mice<br>$n_{(Df(16)A+/-, \text{late ado})} = 25$ recordings, 10 mice         | condition                 | Df(16)A+/- early ado / WT early ado<br>Df(16)A+/- late ado / WT late ado | 51.00<br>60.00   |  | 0.822<br>0.633   |
| 35A<br>(left)  | Linear       |   | age                       |  | 86.90            |  | 0.562            |
|                | mixed-effect |   | condition                 |  | 168.12           |  | 0.310            |
|                | model        | $n_{(WT)} = 1529$ units, 82 rec, 23 mice<br>$n_{(Df(16)A+/-)} = 1041$ units, 52 rec, 14 mice  | age-condition<br>(slopes) | WT P20-60<br>Df(16)A+/- P20-60   | 98.80<br>162.70  | [-0.00294 0.00536]<br>[-0.00184 0.00749]   | 0.498            |
| 35A<br>(right) | Linear       | $n_{(WT, \text{early ado})} = 912$ units, 49 rec, 18 mice   | age                       | WT early ado / WT late ado   | 122.20           |  | 0.318            |
|                | mixed-effect | $n_{(WT, \text{late ado})} = 617$ units, 33 rec, 14 mice  |                           | Df(16)A+/- early ado / Df(16)A+/- late ado                               | 95.20            |  | 0.160            |
|                | model        | $n_{(Df(16)A+/-, \text{early ado})} = 551$ units, 27 rec, 12 mice<br>$n_{(Df(16)A+/-, \text{late ado})} = 490$ units, 25 rec, 10 mice | condition                 | Df(16)A+/- early ado / WT early ado<br>Df(16)A+/- late ado / WT late ado | 45.00<br>57.80   |  | 0.177<br>0.744   |
| 35B<br>(left)  | Linear       |   | age                       |  | 125.50           |  | 0.846            |
|                | mixed-effect |   | condition                 |  | 235.10           |  | 0.970            |
|                | model        | $n_{(WT)} = 1529$ units, 82 rec, 23 mice<br>$n_{(Df(16)A+/-)} = 1041$ units, 52 rec, 14 mice  | age-condition<br>(slopes) | WT P20-60<br>Df(16)A+/- P20-60   | 120.00<br>147.00 | [-0.00338 0.00278]<br>[-0.00316 0.00385]   | 0.731            |
| 35B<br>(right) | Linear       | $n_{(WT, \text{early ado})} = 912$ units, 49 rec, 18 mice   | age                       | WT early ado / WT late ado   | 143.80           |  | 0.775            |
|                | mixed-effect | $n_{(WT, \text{late ado})} = 617$ units, 33 rec, 14 mice  |                           | Df(16)A+/- early ado / Df(16)A+/- late ado                               | 78.90            |  | 0.718            |
|                | model        | $n_{(Df(16)A+/-, \text{early ado})} = 551$ units, 27 rec, 12 mice<br>$n_{(Df(16)A+/-, \text{late ado})} = 490$ units, 25 rec, 10 mice | condition                 | Df(16)A+/- early ado / WT early ado<br>Df(16)A+/- late ado / WT late ado | 51.90<br>64.30   |  | 0.356<br>0.454   |
| 35C<br>(left)  | Linear       |   | age                       |  | 84.86            |  | 0.526            |
|                | mixed-effect |   | condition                 |  | 163.70           |  | 0.469            |
|                | model        | $n_{(WT)} = 1529$ units, 82 rec, 23 mice<br>$n_{(Df(16)A+/-)} = 1041$ units, 52 rec, 14 mice  | age-condition<br>(slopes) | WT P20-60<br>Df(16)A+/- P20-60   | 103.00<br>155.00 | [-0.00442 0.00228]<br>[-0.00411 0.00348]   | 0.704            |
| 35C<br>(right) | Linear       | $n_{(WT, \text{early ado})} = 912$ units, 49 rec, 18 mice   | age                       | WT early ado / WT late ado   | 113.00           |  | 0.432            |
|                | mixed-effect | $n_{(WT, \text{late ado})} = 617$ units, 33 rec, 14 mice  |                           | Df(16)A+/- early ado / Df(16)A+/- late ado                               | 121.00           |  | 0.431            |
|                | model        | $n_{(Df(16)A+/-, \text{early ado})} = 551$ units, 27 rec, 12 mice<br>$n_{(Df(16)A+/-, \text{late ado})} = 490$ units, 25 rec, 10 mice | condition                 | Df(16)A+/- early ado / WT early ado<br>Df(16)A+/- late ado / WT late ado | 47.00<br>60.00   |  | 0.238<br>0.960   |
| 35D<br>(left)  | Linear       |   | age                       |  | 107.50           |  | 0.839            |
|                | mixed-effect |   | condition                 |  | 207.40           |  | 0.188            |
|                | model        | $n_{(WT)} = 1529$ units, 82 rec, 23 mice<br>$n_{(Df(16)A+/-)} = 1041$ units, 52 rec, 14 mice  | age-condition<br>(slopes) | WT P20-60<br>Df(16)A+/- P20-60   | 114.00<br>150.00 | [-0.001908 0.00234]<br>[0.000303 0.00512]  | 0.052            |
| 35D<br>(right) | Linear       | $n_{(WT, \text{early ado})} = 912$ units, 49 rec, 18 mice   | age                       | WT early ado / WT late ado   | 159.00           |  | 0.918            |
|                | mixed-effect | $n_{(WT, \text{late ado})} = 617$ units, 33 rec, 14 mice  |                           | Df(16)A+/- early ado / Df(16)A+/- late ado                               | 234.00           |  | 0.184            |
|                | model        | $n_{(Df(16)A+/-, \text{early ado})} = 551$ units, 27 rec, 12 mice<br>$n_{(Df(16)A+/-, \text{late ado})} = 490$ units, 25 rec, 10 mice | condition                 | Df(16)A+/- early ado / WT early ado<br>Df(16)A+/- late ado / WT late ado | 48.40<br>58.80   |  | 0.721<br>0.163   |
| 36A<br>(left)  | Linear       |   | age                       |  | 107.80           |  | 0.286            |
|                | mixed-effect |   | condition                 |  | 94.66            |  | 0.183            |
|                | model        | $n_{(WT)} = 1529$ units, 82 rec, 23 mice<br>$n_{(Df(16)A+/-)} = 1041$ units, 52 rec, 14 mice  | age-condition<br>(slopes) | WT P20-60<br>Df(16)A+/- P20-60   | 129.00<br>219.00 | [-0.00291 0.00961]<br>[-0.00513 0.00782]   | 0.465            |
| 36A<br>(right) | Linear       | $n_{(WT, \text{early ado})} = 912$ units, 49 rec, 18 mice   | age                       | WT early ado / WT late ado   | 124.00           |  | 0.159            |
|                | mixed-effect | $n_{(WT, \text{late ado})} = 617$ units, 33 rec, 14 mice  |                           | Df(16)A+/- early ado / Df(16)A+/- late ado                               | 204.00           |  | 0.757            |
|                | model        | $n_{(Df(16)A+/-, \text{early ado})} = 551$ units, 27 rec, 12 mice<br>$n_{(Df(16)A+/-, \text{late ado})} = 490$ units, 25 rec, 10 mice | condition                 | Df(16)A+/- early ado / WT early ado<br>Df(16)A+/- late ado / WT late ado | 38.50<br>42.60   |  | 0.209<br>0.474   |
| 36B<br>(left)  | Linear       |   | age                       |  | 1662.00          |  | 0.000            |
|                | mixed-effect |   | condition                 |  | 37.66            |  | 0.029            |
|                | model        | $n_{(WT)} = 1529$ units, 82 rec, 23 mice<br>$n_{(Df(16)A+/-)} = 1041$ units, 52 rec, 14 mice  | age-condition<br>(slopes) | WT P20-60<br>Df(16)A+/- P20-60   | >3000<br>>3000   | [0.00134 0.00226]<br>[0.00220 0.00309]     | <0.001           |
| 36B<br>(right) | Linear       | $n_{(WT, \text{early ado})} = 912$ units, 49 rec, 18 mice   | age                       | WT early ado / WT late ado   | >3000            |  | 0.364            |
|                | mixed-effect | $n_{(WT, \text{late ado})} = 617$ units, 33 rec, 14 mice  |                           | Df(16)A+/- early ado / Df(16)A+/- late ado                               | >3000            |  | <0.001           |
|                | model        | $n_{(Df(16)A+/-, \text{early ado})} = 551$ units, 27 rec, 12 mice<br>$n_{(Df(16)A+/-, \text{late ado})} = 490$ units, 25 rec, 10 mice | condition                 | Df(16)A+/- early ado / WT early ado<br>Df(16)A+/- late ado / WT late ado | >3000<br>>3000   |  | 0.162<br>0.110   |
| 36C<br>(left)  | Linear       |   | age                       |  | 146.60           |  | 0.000            |
|                | mixed-effect |   | condition                 |  | 100.70           |  | 0.772            |
|                | model        | $n_{(WT)} = 1529$ units, 82 rec, 23 mice<br>$n_{(Df(16)A+/-)} = 1041$ units, 52 rec, 14 mice  | age-condition<br>(slopes) | WT P20-60<br>Df(16)A+/- P20-60   | 147.00<br>262.00 | [0.00451 0.0135]<br>[0.00292 0.0121]       | 0.426            |
| 36C<br>(right) | Linear       | $n_{(WT, \text{early ado})} = 912$ units, 49 rec, 18 mice   | age                       | WT early ado / WT late ado   | 423.00           |  | <0.0001          |
|                | mixed-effect | $n_{(WT, \text{late ado})} = 617$ units, 33 rec, 14 mice  |                           | Df(16)A+/- early ado / Df(16)A+/- late ado                               | 750.00           |  | 0.021            |
|                | model        | $n_{(Df(16)A+/-, \text{early ado})} = 551$ units, 27 rec, 12 mice<br>$n_{(Df(16)A+/-, \text{late ado})} = 490$ units, 25 rec, 10 mice | condition                 | Df(16)A+/- early ado / WT early ado<br>Df(16)A+/- late ado / WT late ado | 37.50<br>41.60   |  | 0.995<br>0.419   |

# Appendix

|                |                           |  |                        |                                |  |   |                |
|----------------|---------------------------|--|------------------------|--------------------------------|--|---|----------------|
| 36D<br>(left)  | Linear mixed-effect model |  | age                    |                                | 1027.00                                    |   | 0.629          |
|                |                           |  | condition              |                                | 42.30                                      |   | 0.152          |
|                |                           | $n_{(WT)}$ : 1529 units, 82 rec, 23 mice<br>$n_{(Df(16)A+/+)}$ : 1041 units, 52 rec, 14 mice   | age-condition (slopes) | WT P20-60<br>Df(16)A+/+ P20-60 | >3000<br>>3000                             | [-0.000426 0.000257]<br>[-0.000942 -0.000278] | <.0001         |
| 36D<br>(right) | Linear mixed-effect model |  | age                    |                                | WT early ado / WT late ado                 |   | 0.076          |
|                |                           |  | condition              |                                | Df(16)A+/+ early ado / Df(16)A+/+ late ado |   | 0.049          |
|                |                           | $n_{(WT, \text{early ado})}$ : 912 units, 49 rec, 18 mice<br>$n_{(WT, \text{late ado})}$ : 617 units, 33 rec, 14 mice<br>$n_{(Df(16)A+/+, \text{early ado})}$ : 551 units, 27 rec, 12 mice<br>$n_{(Df(16)A+/+, \text{late ado})}$ : 490 units, 25 rec, 10 mice             | age-condition (slopes) | WT P20-60<br>Df(16)A+/+ P20-60 | >3000<br>>3000                             |   | 0.790<br>0.724 |
| 37B<br>(right) | Linear mixed-effect model |  | age                    |                                | 101.15                                     |   | 0.238          |
|                |                           |  | condition              |                                | 115.81                                     |   | 0.587          |
|                |                           | $n_{(WT)}$ : 82 recordings, 23 mice<br>$n_{(Df(16)A+/+)}$ : 52 recordings, 14 mice   | age-condition (slopes) | WT P20-60<br>Df(16)A+/+ P20-60 | 97.90<br>104.90                            | [-0.00109 0.00428]<br>[-0.00256 0.00367]      | 0.550          |
| 37B<br>(left)  | Linear mixed-effect model |  | age                    |                                | WT early ado / WT late ado                 |   | 0.146          |
|                |                           |  | condition              |                                | Df(16)A+/+ early ado / Df(16)A+/+ late ado |   | 0.996          |
|                |                           | $n_{(WT, \text{early ado})}$ : 49 recordings, 18 mice<br>$n_{(WT, \text{late ado})}$ : 33 recordings, 14 mice<br>$n_{(Df(16)A+/+, \text{early ado})}$ : 27 recordings, 12 mice<br>$n_{(Df(16)A+/+, \text{late ado})}$ : 25 recordings, 10 mice                             | age-condition (slopes) | WT P20-60<br>Df(16)A+/+ P20-60 | 85.60<br>89.20                             |   | 0.117<br>0.105 |
| 37D<br>(right) | Linear mixed-effect model |  | age                    |                                | 88.53                                      |   | 0.468          |
|                |                           |  | condition              |                                | 112.50                                     |   | 0.966          |
|                |                           | $n_{(WT)}$ : 82 recordings, 23 mice<br>$n_{(Df(16)A+/+)}$ : 52 recordings, 14 mice   | age-condition (slopes) | WT P20-60<br>Df(16)A+/+ P20-60 | 94.10<br>123.00                            | [-0.00159 0.00341]<br>[-0.00335 0.00239]      | 0.378          |
| 37D<br>(left)  | Linear mixed-effect model |  | age                    |                                | WT early ado / WT late ado                 |   | 0.050          |
|                |                           |  | condition              |                                | Df(16)A+/+ early ado / Df(16)A+/+ late ado |   | 0.456          |
|                |                           | $n_{(WT, \text{early ado})}$ : 49 recordings, 18 mice<br>$n_{(WT, \text{late ado})}$ : 33 recordings, 14 mice<br>$n_{(Df(16)A+/+, \text{early ado})}$ : 27 recordings, 12 mice<br>$n_{(Df(16)A+/+, \text{late ado})}$ : 25 recordings, 10 mice                             | age-condition (slopes) | WT P20-60<br>Df(16)A+/+ P20-60 | 81.70<br>88.30                             |   | 0.226<br>0.075 |
| 38A            | signrank                  |  | Directionality         |                                | WT P20-60<br>Df(16)A+/+ P20-60             |   | 0.000<br>0.000 |
|                | Linear mixed-effect model |  | age                    |                                | 129.00                                     |   | 0.056          |
|                |                           | $n_{(WT)}$ : 82 recordings, 23 mice<br>$n_{(Df(16)A+/+)}$ : 52 recordings, 14 mice   | age-condition (slopes) | WT P20-60<br>Df(16)A+/+ P20-60 | 103.20<br>93.20                            | [-0.000301 0.0136]<br>[-0.004358 0.0118]      | 0.526          |
| 38B<br>(left)  | Linear mixed-effect model |  | age                    |                                | WT early ado / WT late ado                 |   | 0.051          |
|                |                           |  | condition              |                                | Df(16)A+/+ early ado / Df(16)A+/+ late ado |   | 0.216          |
|                |                           | $n_{(WT, \text{early ado})}$ : 49 recordings, 18 mice<br>$n_{(WT, \text{late ado})}$ : 33 recordings, 14 mice<br>$n_{(Df(16)A+/+, \text{early ado})}$ : 27 recordings, 12 mice<br>$n_{(Df(16)A+/+, \text{late ado})}$ : 25 recordings, 10 mice                             | age-condition (slopes) | WT P20-60<br>Df(16)A+/+ P20-60 | 90.10<br>94.60                             |   | 0.459<br>0.353 |
| 38C            | signrank                  |  | Directionality         |                                | WT P20-60<br>Df(16)A+/+ P20-60             |   | 0.000<br>0.000 |
|                | Linear mixed-effect model |  | age                    |                                | 86.71                                      |   | 0.944          |
|                |                           | $n_{(WT)}$ : 82 recordings, 23 mice<br>$n_{(Df(16)A+/+)}$ : 52 recordings, 14 mice   | age-condition (slopes) | WT P20-60<br>Df(16)A+/+ P20-60 | 113.00<br>115.00                           | [-0.00596 0.00639]<br>[-0.00681 0.00720]      | 0.472<br>0.995 |
| 38D<br>(right) | Linear mixed-effect model |  | age                    |                                | WT early ado / WT late ado                 |   | 0.198          |
|                |                           |  | condition              |                                | Df(16)A+/+ early ado / Df(16)A+/+ late ado |   | 0.220          |
|                |                           | $n_{(WT, \text{early ado})}$ : 49 recordings, 18 mice<br>$n_{(WT, \text{late ado})}$ : 33 recordings, 14 mice<br>$n_{(Df(16)A+/+, \text{early ado})}$ : 27 recordings, 12 mice<br>$n_{(Df(16)A+/+, \text{late ado})}$ : 25 recordings, 10 mice                             | age-condition (slopes) | WT P20-60<br>Df(16)A+/+ P20-60 | 82.40<br>104.10                            |   | 0.316<br>0.450 |
| 39B<br>(right) | Linear mixed-effect model |  | age                    |                                | 91.57                                      |   | 0.334          |
|                |                           |  | condition              |                                | 107.80                                     |   | 0.379          |
|                |                           | $n_{(WT)}$ : 82 recordings, 23 mice<br>$n_{(Df(16)A+/+)}$ : 52 recordings, 14 mice   | age-condition (slopes) | WT P20-60<br>Df(16)A+/+ P20-60 | 91.00<br>121.00                            | [-0.00059 0.001692]<br>[-0.00200 0.000356]    | 0.017          |
| 39B<br>(left)  | Linear mixed-effect model |  | age                    |                                | WT early ado / WT late ado                 |   | 0.092          |
|                |                           |  | condition              |                                | Df(16)A+/+ early ado / Df(16)A+/+ late ado |   | 0.739          |
|                |                           | $n_{(WT, \text{early ado})}$ : 49 recordings, 18 mice<br>$n_{(WT, \text{late ado})}$ : 33 recordings, 14 mice<br>$n_{(Df(16)A+/+, \text{early ado})}$ : 27 recordings, 12 mice<br>$n_{(Df(16)A+/+, \text{late ado})}$ : 25 recordings, 10 mice                             | age-condition (slopes) | WT P20-60<br>Df(16)A+/+ P20-60 | 80.30<br>97.60                             |   | 0.208<br>0.025 |
| 39D<br>(right) | Linear mixed-effect model |  | age                    |                                | 107.70                                     |   | 0.055          |
|                |                           |  | condition              |                                | 121.90                                     |   | 0.913          |
|                |                           | $n_{(WT)}$ : 82 recordings, 23 mice<br>$n_{(Df(16)A+/+)}$ : 52 recordings, 14 mice   | age-condition (slopes) | WT P20-60<br>Df(16)A+/+ P20-60 | 106.00<br>107.00                           | [-0.00011 0.00701]<br>[-0.00114 0.00703]      | 0.827          |
| 39D<br>(left)  | Linear mixed-effect model |  | age                    |                                | WT early ado / WT late ado                 |   | 0.000          |
|                |                           |  | condition              |                                | Df(16)A+/+ early ado / Df(16)A+/+ late ado |   | 0.044          |
|                |                           | $n_{(WT, \text{early ado})}$ : 49 recordings, 18 mice<br>$n_{(WT, \text{late ado})}$ : 33 recordings, 14 mice<br>$n_{(Df(16)A+/+, \text{early ado})}$ : 27 recordings, 12 mice<br>$n_{(Df(16)A+/+, \text{late ado})}$ : 25 recordings, 10 mice                             | age-condition (slopes) | WT P20-60<br>Df(16)A+/+ P20-60 | 91.90<br>84.90                             |   | 0.897<br>0.463 |
| 40A            | Linear mixed-effect model |  | age                    |                                | 100.71                                     |   | 0.298          |
|                |                           |  | condition              |                                | 114.73                                     |   | 0.223          |
|                |                           | $n_{(WT)}$ : 1701 units, 82 rec, 23 mice<br>$n_{(Df(16)A+/+)}$ : 1125 units, 52 rec, 14 mice   | age-condition (slopes) | WT P20-60<br>Df(16)A+/+ P20-60 | 101.00<br>102.00                           | [-0.00651 0.00204]<br>[-0.00211 0.00785]      | 0.071          |
| 40B            | Linear mixed-effect model |  | age                    |                                | WT early ado / WT late ado                 |   | 0.202          |
|                |                           |  | condition              |                                | Df(16)A+/+ early ado / Df(16)A+/+ late ado |   | 0.565          |
|                |                           | $n_{(WT, \text{early ado})}$ : 1027 units, 49 recs, 18 mice<br>$n_{(WT, \text{late ado})}$ : 674 units, 33 rec, 14 mice<br>$n_{(Df(16)A+/+, \text{early ado})}$ : 644 units, 27 rec, 12 mice<br>$n_{(Df(16)A+/+, \text{late ado})}$ : 481 units, 25 rec, 10 mice           | age-condition (slopes) | WT P20-60<br>Df(16)A+/+ P20-60 | 88.90<br>90.10                             |   | 0.654<br>0.070 |
| 41A<br>(left)  | Linear mixed-effect model |  | age                    |                                | 106.30                                     |   | 0.036          |
|                |                           |  | condition              |                                | 138.30                                     |   | 0.119          |
|                |                           | $n_{(WT)}$ : 1422 rs units, 82 rec, 23 mice<br>$n_{(Df(16)A+/+)}$ : 951 rs units, 52 rec, 14 mice  | age-condition (slopes) | WT P20-60<br>Df(16)A+/+ P20-60 | 112.00<br>136.00                           | [-0.01806 -0.000563]<br>[-0.00869 0.010095]   | 0.048          |
| 41A<br>(right) | Linear mixed-effect model |  | age                    |                                | WT early ado / WT late ado                 |   | 0.026          |
|                |                           |  | condition              |                                | Df(16)A+/+ early ado / Df(16)A+/+ late ado |   | 0.808          |
|                |                           | $n_{(WT, \text{early ado})}$ : 860 rs units, 49 rec, 18 mice<br>$n_{(WT, \text{late ado})}$ : 562 rs units, 33 rec, 14 mice<br>$n_{(Df(16)A+/+, \text{early ado})}$ : 537 rs units, 27 rec, 12 mice<br>$n_{(Df(16)A+/+, \text{late ado})}$ : 414 rs units, 25 rec, 10 mice | age-condition (slopes) | WT P20-60<br>Df(16)A+/+ P20-60 | 165.00<br>169.00                           |   | 0.590<br>0.169 |
| 41B<br>(left)  | Linear mixed-effect model |  | age                    |                                | 101.02                                     |   | 0.404          |
|                |                           |  | condition              |                                | 128.97                                     |   | 0.707          |
|                |                           | $n_{(WT)}$ : 1422 rs units, 82 rec, 23 mice<br>$n_{(Df(16)A+/+)}$ : 951 rs units, 52 rec, 14 mice  | age-condition (slopes) | WT P20-60<br>Df(16)A+/+ P20-60 | 111.00<br>224.00                           | [-0.00714 0.00293]<br>[-0.00586 0.00462]      | 0.551          |
| 41B<br>(right) | Linear mixed-effect model |  | age                    |                                | WT early ado / WT late ado                 |   | 0.002          |
|                |                           |  | condition              |                                | Df(16)A+/+ early ado / Df(16)A+/+ late ado |   | 0.026          |
|                |                           | $n_{(WT, \text{early ado})}$ : 860 rs units, 49 rec, 18 mice<br>$n_{(WT, \text{late ado})}$ : 562 rs units, 33 rec, 14 mice<br>$n_{(Df(16)A+/+, \text{early ado})}$ : 537 rs units, 27 rec, 12 mice<br>$n_{(Df(16)A+/+, \text{late ado})}$ : 414 rs units, 25 rec, 10 mice | age-condition (slopes) | WT P20-60<br>Df(16)A+/+ P20-60 | 191.00<br>316.00                           |   | 0.749<br>0.444 |
| 41C<br>(left)  | Linear mixed-effect model |  | age                    |                                | 183.00                                     |   | 0.597          |
|                |                           |  | condition              |                                | 183.00                                     |   | 0.660          |
|                |                           | $n_{(WT)}$ : 279 fs units, 82 rec, 23 mice<br>$n_{(Df(16)A+/+)}$ : 174 fs units, 52 rec, 14 mice   | age-condition (slopes) | WT P20-60<br>Df(16)A+/+ P20-60 | 85.20<br>65.50                             | [-0.0184 0.0108]<br>[-0.0136 0.0211]          | 0.430          |

## Appendix

|                    |                    |  |               |  |         |                       |        |
|--------------------|--------------------|--|---------------|--|---------|-----------------------|--------|
| <b>41C (right)</b> | Linear             | $\eta_{WT, \text{early ado}}$ : 167 fs units, 49 rec, 18 mice                  | age           | WT early ado / WT late ado                 | 100.50  |                       | 0.809  |
|                    | mixed-effect model | $\eta_{WT, \text{late ado}}$ : 112 fs units, 33 rec, 14 mice                   | condition     | Df(16)A+/- early ado / Df(16)A+/- late ado | 48.50   |                       | 0.760  |
|                    |                    | $\eta_{Df(16)A+/-, \text{early ado}}$ : 107 fs units, 27 rec, 12 mice          |               | Df(16)A+/- early ado / WT early ado        | 17.00   |                       | 0.782  |
|                    |                    | $\eta_{Df(16)A+/-, \text{late ado}}$ : 67 fs units, 25 rec, 10 mice            |               | Df(16)A+/- late ado / WT late ado          | 14.40   |                       | 0.557  |
| <b>41D (left)</b>  | Linear             |  | age           |  | 60.33   |                       | 0.195  |
|                    | mixed-effect model |  | age-condition |  | 127.95  |                       | 0.458  |
|                    |                    | $\eta_{WT}$ : 279 fs units, 82 rec, 23 mice                                    |               | WT P20-60                                  | 61.60   | [-0.0125 0.00267]     | 0.521  |
|                    |                    | $\eta_{Df(16)A+/-}$ : 174 fs units, 52 rec, 14 mice                            |               | Df(16)A+/- P20-60                          | 106.10  | [-0.0171 0.00140]     |        |
| <b>41D (right)</b> | Linear             | $\eta_{WT, \text{early ado}}$ : 167 fs units, 49 rec, 18 mice                  | age           | WT early ado / WT late ado                 | 102.70  |                       | 0.002  |
|                    | mixed-effect model | $\eta_{WT, \text{late ado}}$ : 112 fs units, 33 rec, 14 mice                   | condition     | Df(16)A+/- early ado / Df(16)A+/- late ado | 75.70   |                       | 0.013  |
|                    |                    | $\eta_{Df(16)A+/-, \text{early ado}}$ : 107 fs units, 27 rec, 12 mice          |               | Df(16)A+/- early ado / WT early ado        | 24.20   |                       | 0.660  |
|                    |                    | $\eta_{Df(16)A+/-, \text{late ado}}$ : 67 fs units, 25 rec, 10 mice            |               | Df(16)A+/- late ado / WT late ado          | 24.40   |                       | 0.735  |
| <b>42A (left)</b>  | Linear             |  | age           |  | 1194.00 |                       | 0.000  |
|                    | mixed-effect model |  | age-condition |  | 46.20   |                       | 0.000  |
|                    |                    | $\eta_{WT}$ : 1422 rs + 1529 HP units, 82 rec, 23 mice                         |               | WT P20-60                                  | >3000   | [0.000418 0.00108]    | <.0001 |
|                    |                    | $\eta_{Df(16)A+/-}$ : 951 rs + 1041 HP units, 52 rec, 14 mice                  |               | Df(16)A+/- P20-60                          | >3000   | [0.001641 0.00226]    |        |
| <b>42A (right)</b> | Linear             | $\eta_{WT, \text{early ado}}$ : 860 rs + 912 HP units, 49 rec, 18 mice         | age           | WT early ado / WT late ado                 | >3000   |                       | 0.291  |
|                    | mixed-effect model | $\eta_{WT, \text{late ado}}$ : 562 rs + 617 HP units, 33 rec, 14 mice          | condition     | Df(16)A+/- early ado / Df(16)A+/- late ado | >3000   |                       | <.0001 |
|                    |                    | $\eta_{Df(16)A+/-, \text{early ado}}$ : 537 rs + 551 HP units, 27 rec, 12 mice |               | Df(16)A+/- early ado / WT early ado        | >3000   |                       | 0.056  |
|                    |                    | $\eta_{Df(16)A+/-, \text{late ado}}$ : 414 rs + 490 HP units, 25 rec, 10 mice  |               | Df(16)A+/- late ado / WT late ado          | >3000   |                       | 0.047  |
| <b>42B (left)</b>  | Linear             |  | age           |  | 2601.00 |                       | 0.000  |
|                    | mixed-effect model |  | age-condition |  | 39.99   |                       | 0.665  |
|                    |                    | $\eta_{WT}$ : 1422 rs + 1529 HP units, 82 rec, 23 mice                         |               | WT P20-60                                  | >3000   | [-0.000845 -0.000397] | 0.653  |
|                    |                    | $\eta_{Df(16)A+/-}$ : 951 rs + 1041 HP units, 52 rec, 14 mice                  |               | Df(16)A+/- P20-60                          | >3000   | [-0.000863 -0.000446] |        |
| <b>42B (right)</b> | Linear             | $\eta_{WT, \text{early ado}}$ : 860 rs + 912 HP units, 49 rec, 18 mice         | age           | WT early ado / WT late ado                 | >3000   |                       | 0.653  |
|                    | mixed-effect model | $\eta_{WT, \text{late ado}}$ : 562 rs + 617 HP units, 33 rec, 14 mice          | condition     | Df(16)A+/- early ado / Df(16)A+/- late ado | >3000   |                       | <.0001 |
|                    |                    | $\eta_{Df(16)A+/-, \text{early ado}}$ : 537 rs + 551 HP units, 27 rec, 12 mice |               | Df(16)A+/- early ado / WT early ado        | >3000   |                       | 0.421  |
|                    |                    | $\eta_{Df(16)A+/-, \text{late ado}}$ : 414 rs + 490 HP units, 25 rec, 10 mice  |               | Df(16)A+/- late ado / WT late ado          | >3000   |                       | 0.726  |
| <b>42C (left)</b>  | Linear             |  | age           |  | 222.00  |                       | 0.975  |
|                    | mixed-effect model |  | age-condition |  | 59.09   |                       | 0.040  |
|                    |                    | $\eta_{WT}$ : 279 fs + 1529 HP units, 82 rec, 23 mice                          |               | WT P20-60                                  | >3000   | [-0.000752 0.000729]  | 0.108  |
|                    |                    | $\eta_{Df(16)A+/-}$ : 174 fs + 1041 HP units, 52 rec, 14 mice                  |               | Df(16)A+/- P20-60                          | >3000   | [-0.000341 0.001109]  |        |
| <b>42C (right)</b> | Linear             | $\eta_{WT, \text{early ado}}$ : 167 fs + 912 HP units, 49 rec, 18 mice         | age           | WT early ado / WT late ado                 | >3000   |                       | <.0001 |
|                    | mixed-effect model | $\eta_{WT, \text{late ado}}$ : 112 fs + 617 HP units, 33 rec, 14 mice          | condition     | Df(16)A+/- early ado / Df(16)A+/- late ado | >3000   |                       | 0.813  |
|                    |                    | $\eta_{Df(16)A+/-, \text{early ado}}$ : 107 fs + 551 HP units, 27 rec, 12 mice |               | Df(16)A+/- early ado / WT early ado        | >3000   |                       | 0.098  |
|                    |                    | $\eta_{Df(16)A+/-, \text{late ado}}$ : 67 fs + 490 HP units, 25 rec, 10 mice   |               | Df(16)A+/- late ado / WT late ado          | >3000   |                       | 0.785  |
| <b>42D (left)</b>  | Linear             |  | age           |  | 295.10  |                       | 0.541  |
|                    | mixed-effect model |  | age-condition |  | 55.65   |                       | 0.294  |
|                    |                    | $\eta_{WT}$ : 279 fs + 1529 HP units, 82 rec, 23 mice                          |               | WT P20-60                                  | >3000   | [-0.000641 0.000336]  | 0.000  |
|                    |                    | $\eta_{Df(16)A+/-}$ : 174 fs + 1041 HP units, 52 rec, 14 mice                  |               | Df(16)A+/- P20-60                          | >3000   | [-0.001222 -0.000241] |        |
| <b>42D (right)</b> | Linear             | $\eta_{WT, \text{early ado}}$ : 167 fs + 912 HP units, 49 rec, 18 mice         | age           | WT early ado / WT late ado                 | >3000   |                       | <.0001 |
|                    | mixed-effect model | $\eta_{WT, \text{late ado}}$ : 112 fs + 617 HP units, 33 rec, 14 mice          | condition     | Df(16)A+/- early ado / Df(16)A+/- late ado | >3000   |                       | <.0001 |
|                    |                    | $\eta_{Df(16)A+/-, \text{early ado}}$ : 107 fs + 551 HP units, 27 rec, 12 mice |               | Df(16)A+/- early ado / WT early ado        | >3000   |                       | 0.947  |
|                    |                    | $\eta_{Df(16)A+/-, \text{late ado}}$ : 67 fs + 490 HP units, 25 rec, 10 mice   |               | Df(16)A+/- late ado / WT late ado          | >3000   |                       | 0.026  |

## List of Publications

Parts of the experiments carried out in the scope of this thesis are published. Given the experiments and analyses included in these studies, only those personally performed by myself are presented in this thesis.

Chini, M., Pöpplau, J.A., Lindemann, C., Carol-Perdiguer, L., **Hnida, M.**, Oberländer, V., Xu, X., Ahlbeck, J., Bitzenhofer, S.H., Mulert, C., and Hanganu-Opatz, I.L. (2020). Resolving and Rescuing Developmental Miswiring in a Mouse Model of Cognitive Impairment. *Neuron* 105, 60-74.e67. DOI: 10.1016/j.neuron.2019.09.042

Chini, M., **Hnida, M.**, Kostka, J.K., Chen, Y.-N., and Hanganu-Opatz, I.L. (2023). Extreme distributions in the preconfigured developing brain. *bioRxiv*, 2023.2011.2013.566810. DOI: <https://doi.org/10.1101/2023.11.13.566810> (currently under revision in *Cell Reports*)

## Acknowledgements

This work would not have come to fruition without the incredible support and guidance from so many people. I want to express my heartfelt thanks to all of them for being part of this unforgettable journey. Their help, advice, feedback, criticism and the scientific and non-scientific backing have truly made all the difference in bringing this thesis to life.

First and foremost, I would like to thank my supervisor Ileana Hanganu-Opatz for giving me the opportunity to perform the work behind this thesis in her institute and for her continuous support, supervision and helpful advice. I am grateful for her encouragement and the freedom to pursue my own research interest and ideas. This support contributed to both my scientific and personal growth.

I would like to thank the current and former members of the Institute of Developmental Neurophysiology for invaluable support, great feedback, good advice and practical help. In particular, many thanks to Jastyn Pöplau, Anne Günther, Mattia Chini, Johanna Kostka, Sebastian Bitzenhofer and Irina Pochinok for helpful and interesting scientific and casual discussions and enjoyable time spent together inside and outside the lab.

Further, I would like to thank Peggy Putthoff, Annette Marquardt and Achim Dahlmann for excellent technical support and assistance. Many thanks also go to Torsten Renz and Fritz Kutschera for their technical help with implementing also challenging ideas and their patience, reliability and great ideas.

Finally, I would like to thank my family and friends for always having my back and making this possible. Thank you, Madeleine Hamley, especially for your linguistic expertise and proof reading. Thank you, Sally and Jana for always having an open ear and great moments and memories. I am grateful to Anita, Ralf, Kathrin, Kai, Wilfried and Elisabeth for unconditionally being there and helping me pursue my own personal and scientific journey. Special thanks to Hendrik for bringing me back to earth, always being there and loving support.